UNIVERSITE DE LILLE - SCIENCES ET TECHNOLOGIES
Ecole doctorale Science de la Matière, du Rayonnement et de l'Environnement

THESE DE DOCTORAT

Spécialité : Biotechnologies agroalimentaire, sciences de l'aliment, physiologie

Présentée et soutenue par

Weiji LIU

Pour l'obtention du grade de

DOCTEUR DE L'UNIVERSITE DE LILLE

Role of casein micelle on the thermal denaturation of whey protein solutions and fouling mechanisms

Rôle de la micelle de caséine sur la dénaturation thermique des solutions de protéines de lactosérum et les mécanismes d'encrassement

---

Unité Matériaux et Transformations

Équipe : Processus aux Interfaces et Hygiène des Matériaux (INRAE)

Soutenue le 22 avril 2022 devant le jury composé de :

Président
Maude Jimenez : *Professeure de Université de Lille, UMET, UMR 8207, Lille (France)*

Rapporteurs
Karine Loubiere : *Directrice de recherche CNRS, LGC, UMR 5503 Toulouse (France)*
Luc Fillaudeau : *Directeur de recherche INRAE, LISBP, UMR INSA/INRAE, Toulouse (France)*

Examinateurs
Sandro Machietto : *Professeur Imperial College of London, Londre (Royaume-Uni)*
Romain Jeantet : *Professeur Institut Agro*, STLO, *UMR 1253 STLO, Rennes (France)*

Invités et co-encadrants
Christophe André : *Professeur JUNIA, HEI, Université Catholique, Lille (France)*

Co-Directeur de thèse
Xiao Dong Chen : *Professeur, Soochow University (Chine)*

Directeur de thèse
Guillaume Delaplace : *Directeur de recherche, INRAE – UMET, UMR 8207, Lille (France)*

Preface/Acknowledgments

"*Good scientist is wrong 90% of the time, but a really good scientist is wrong 99% of the time*" said professor Michael Levitt, the Noble prize winner in 2013. I would have never understood this phrase correctly until my PhD project started. Not at that time I could realize how many difficulties I was about to encounter and how much fun I would obtain by solving them. While, fortunately, I was not fighting alone.

My closest alliances, undoubtedly, are both of my supervisors, Prof. Guillaume Delaplace and Prof. Xiao Dong Chen. Of course, without them, this project would never be initialized. The present work was carried out under the frame of an International Associated Laboratory FOODPRINT gathering Agrocampus Ouest, INRAE and Soochow University. This "sandwich" program associated to this PhD project makes it possible for me to stay half of my PhD period in France (Lille) and half in China (Suzhou). Special thanks to my french supervisor Guillaume for his warm welcoming and help during my first stay in Lille. His enthusiasm for the project, his patience and fruitful discussions are all greatly appreciated. I would also like to address my thanks to my co-supervisor Dr. Christophe André for his help with my articles and valuable discussions concerning kinetic models.

I also want to thank Prof. Luc Fillaudeau and Prof. Karine Loubiere for their interest in my work and for dedicating their time and expertise to the examination of this manuscript. I am also very grateful to Prof. Maude Jimenez from Université de Lille (France), Prof. Romain Jeantet from Institut Agro (Rennes, France), and Prof. Sandro Machietto from Imperial College of London (UK) for accepting to be a part of my defense jury.

My appreciation also goes to my colleagues in UMET lab for the friendly working atmosphere and their help with my thesis: Luisa Scudeller with HPLC and electrophoresis, Thierry Six with the pilot plant plate heat exchanger unit, Laurent Wauquier with custom-built devices, Severine Bellayer with EPMA imaging and Marwan Abdallah with discussions of casein structures. I am deeply grateful to every one of them and all the other members of PIHM team as I could not have completed this work without their precious help.

Finally, I wish to express my heartfelt gratitude to my parents whose continuous encouragement was critical in completing this thesis. For my love, Tia, we are just beyond the relationship that

needs to express “thank you”. Your quitting job and following me to France is such romantic self-sacrificing. I love you to to the moon and back.

Weiji Liu. Lille, March, 2022.

Abstract

The present work is a contribution to better understanding the influence of casein micelles on the fouling of serum whey protein solutions. In particular, various experimental and numerical approaches have been carried out both at laboratory and pilot scales (meanwhile new tools have been progressively set up, for instance, development of a new kinetic model describing thermal denaturation of β-lactoglobulin (BLG), installation of a laboratory-scale fouling device and a kinetic-based 3D fouling model based on computational fluid dynamics (CFD)) to describe denaturation phenomena and better understand the role of casein micelle and calcium in fouling mechanisms.

Precisely, the role of casein micelle on the whey protein fouling was investigated in a pilot-scale plate heat exchanger (PHE) and also in a custom-built laboratory-scale device. In the pilot plant, the total fouling deposit mass dropped significantly with the addition of casein, resulting in a minimum value located at casein/whey mass ratio of 0.2. Exceeding this critical ratio, fouling deposit increased with elevated casein concentrations. However, in the bench-scale device, the fouling was suppressed and maintained at a low extent even at high casein/whey mass ratios (up to 4). These fouling results were obtained without any pH modifications such that the pH of the fouling solutions increased with elevated casein/whey ratios. When the pH of the fouling solutions was fixed at 6.6, casein lost its fouling-mitigating ability, especially at high casein/whey ratios. To obtain deeper insight into fouling, the fouling deposit was characterized using Electron-Probe Micro Analysis (EPMA) and electrophoresis. A rennenting-based technique was also applied to evaluate the molecular status of casein proteins (dissociated form *vs* casein micelle) and to reveal the interactions between caseins and whey proteins. Gathering all pieces of evidence obtained, it was hypothesized that at low casein concentrations, the pre-existed colloidal calcium phosphate (CCP) nanoclusters (in casein powder) when introduced into the whey protein solutions, might act as nucleation points facilitating the precipitation of Ca^{2+} around the CCP clusters (induced by higher temperature), decreasing the Ca^{2+} level in the serum phase, and consequently suppress the fouling build-up. Whilst at higher casein concentrations, most caseins existed as casein micelles. Despite this, a larger proportion of caseins dissociated from the micelles, particularly at neutral pH. These dissociated caseins could express chaperone-like functions to prevent the thermal denaturation of BLG. Regarding the minerals, casein micelles are capable to transfer ionic

calciums into CCP during heating. However, this ability is weaker at lower pH, resulting in higher Ca^{2+} levels at pH 6.6, and consequently induces more significant fouling at pH 6.6.

In parallel, the effect of casein on the thermal denaturation of BLG was examined at a molecular level by performing kinetic experiments. The data were initially fitted using an overall one-step reaction model, widely admitted in the literature. This model can hardly provide detailed information on the BLG denaturation pathway, therefore, it was decided to develop a new kinetic model. The developed model interprets mathematically the break-slope behavior in the Arrhenius plot and provides detailed thermodynamic information for both unfolding and aggregation processes. It was first applied to investigate the role of ionic calcium on the thermal denaturation behavior of BLG. Results confirmed that ionic calcium has a protective role on the thermal unfolding of BLG at low temperatures. In contrast, at higher temperatures, calcium promotes aggregation and the formation of unfolded BLG species. The developed model was also used to re-evaluated those kinetic results obtained initially using the one-step model. Based on this model, casein presents contrary effects compared to Ca^{2+}: increasing casein concentrations favor the unfolding of BLG while prohibiting the aggregation of BLG. These results are in line with the chaperone-like functions of caseins.

This denaturation kinetic model was also utilized to evaluate the denaturation behavior of BLG in the microchannel of the laboratory-scale fouling device. The thermal denaturation of BLG and its fouling behavior was numerically simulated using CFD in a 3D environment. Results showed a linear relationship between the pre-exponential factor of deposition reaction and calcium concentration, suggesting the fouling is built in such a pattern that only one calcium ion per BLG molecule is involved. Calcium was confirmed to be essential to fouling growth with significant effects both on the thermal denaturation and deposition processes.

These results permit us to conclude that casein micelle mitigates whey protein fouling by acting as a natural calcium chelator during thermal processing. These fouling mitigation effects could be enhanced particularly at higher pH conditions, resulting in more dissociated caseins that are released from the casein micelle to prohibit BLG denaturation as well as fouling through their chaperone-like functions.

Table of Contents

Nomenclature

Symbols		
$\hat{A}$	**[-]**	Emitted light collection fraction
A	[m^2]	Area or plate heat exchanger area
Bi	**[-]**	Biot number
C_i	[$kg \cdot m^{-3}$]	Concentration of species *i*
C_S	[$kg \cdot m^{-3}$]	Soluble BLG concentration
C_{S0}	[$kg \cdot m^{-3}$]	Initial BLG concentration
C_p	[$J \cdot kg^{-1} \cdot K^{-1}$]	Specific heat capacity
d_i	[m]	Particle diameter of species *i* (m)
D_i	[$m^2 \cdot s^{-1}$]	Diffusion coefficient of species *i*
D_h	[m]	Hydraulic diameter
Ea_i	[$J \cdot mol^{-1}$]	Activation energy of process *i*
e	[m]	Flow gap between plates
$\boldsymbol{F}$	[$N \cdot m^{-3}$]	Volume force vector
h	[$W \cdot m^{-2} \cdot K^{-1}$]	Convective heat transfer coefficient
$\hat{h}$	[J·s]	Plank constant (≈6.62×10^{-34} J·s)
$\boldsymbol{I}$	**[-]**	Unit vector
I_0	**[-]**	Excitation light intensity
I_{flu}	**[-]**	Fluorescence intensity
J_f	[$g \cdot m^{-2} \cdot s^{-1}$]	Fouling rate
k	[$W \cdot m^{-1} \cdot K^{-1}$]	Thermal conductivity
k_f	[$g^{1-n} \cdot L^{n-1} \cdot s^{-1}$]	Reaction rate constant in one-step model, depending on reaction order n
k_i	[$g^{1-n} \cdot L^{n-1} \cdot s^{-1}$]	Reaction rate constant of process *i* depending on reaction order n
k_{f0}	[$g^{1-n} \cdot L^{n-1} \cdot s^{-1}$]	Pre-exponential factor in one-step model, depending on reaction order n
k_{0i}	[$g^{1-n} \cdot L^{n-1} \cdot s^{-1}$]	Pre-exponential factor for process *i* depending on reaction order n
k_B	[$J \cdot K^{-1}$]	Boltzman constant (≈1.38×10^{-23} $J \cdot K^{-1}$)
k_D	[$g \cdot m^{-2} \cdot s^{-1}$]	Deposition rate
K_c	**[-]**	Equilibrium constant
l	[m]	Plate width
$\dot{m}_d$	[$g \cdot s^{-1}$]	Deposition growth rate
$\dot{m}_r$	[$g \cdot s^{-1}$]	Deposition removal rate
m_h	[$kg \cdot s^{-1}$]	Mass flow rate of fouling fluid
m_f	[$kg \cdot m^{-2}$]	Fouling mass coverage
n	**[-]**	Reaction order
$\boldsymbol{N}_i$	[$kg \cdot m^{-2} \cdot s^{-1}$]	Mass flux of species *i*
N_{AV}	[mol^{-1}]	Avogadro constant ($6.023 \cdot 10^{23}$ mol^{-1})
p	[Pa]	Pressure
$\boldsymbol{Q}$	[$W \cdot m^{-3}$]	Heat sources

$\mathbf{q}$	[W·m^{-2}]	Heat flux
R	[J·mol^{-1}·K^{-1}]	Universal gas constant (8.314 J·mol^{-1}·K^{-1})
R_f	[m^2·K·W^{-1}]	Thermal resistance of fouling layer
R_i	[kg·m^{-3}·s^{-1}]	Reaction rate expression
r_D	[g·m^{-2}·s^{-1}]	Deposition rate
S	[m^2]	Surface area of different plate geometries
T	[K]	Temperature
T_c	[K]	Critical temperature
T_d	[K]	Denaturation temperature
$\boldsymbol{u}$	[m·s^{-1}]	Velocity vector
$\boldsymbol{v}$	[m·s^{-1}]	Fluid velocity
U_f	[W·K^{-1}·m^{-2}]	Overall heat transfer coefficient
V_i	[mol·m^{-3}]	Molar volume of the particles *i*
$\hat{V}_i$	[m^{-3}]	Volume of fluid processed
ΔH	[J·mol^{-1}]	Enthalpy
ΔS	[J·mol^{-1}·K^{-1}]	Entropy
ΔG	[J·mol^{-1}]	Gibbs energy
ΔC_i	[kg·m^{-3}]	native BLG concentration difference between inlet and outlet of a channel in PHE
ΔT_{LMTD}	[K]	Logarithmic mean temperature difference

Greek letters

α	**[-]**	Unfolding ratio
β	**[-]**	Proportionality constant
δ	[m]	Thickness
ε	**[**m^2·mol^{-1}**]**	Extinction coefficient of the dye
λ	[W·m^{-1}·K^{-1}]	Thermal conductivity
μ	[Pa·s]	Fluid viscosity
ν	[m·s^{-1}**]**	Fluid velocity
τ_w	**[**Pa**]**	Wall shear stress
ρ	[kg·m^{-3}]	Density
φ	**[-]**	Proportion factor
Φ	**[-]**	Quantum yield of the dye

Subscripts

A	Aggregated BLG
Al	Aluminum
d	Deposit
D	Deposition of BLG
f	Fouling process
flu	Fluorescence
in	Inlet
L	Longitudinal mean value

N	native BLG
p	Product
p,i	Process fluid inlet
p,o	Process fluid outlet
S	Soluble BLG
sd	Steel-deposit interface
SS	Stainless steel
U	Unfolded BLG
w	Water (hot medium)
w,i	Hot water inlet
w,o	Hot water outlet
ws	Water-steel interface

Abbreviations

A	Aggregated BLG
AAS	Atomic Absorption Spectrometry
ACP	Amorphous Calcium Phosphate
AFM	Atomic Force Microscopy
α-La	α-Lactalbumin
BLG	β-Lactoglobulin
BSA	Bovine Serum Albumin
Ca-ISE	Calcium Ion Selective Electrode
CCP	Colloidal Calcium Phosphate
CD	Circular Dichroism
CFD	Computational Fluid Dynamics
CI	Confident Interval
CIP	Cleaning-In-Place
CLSM	Confocal Laser Scanning Microscopy
CMP	Caseinomacropeptide
DA	Dimensional analysis
DCPD	Dicalcium Phosphate Dihydrate
DLC	Diamond-Like Carbon
DSC	Differential Scanning Calorimetry
DSI	Direct Steam Injector
DTT	1,4-dithiothreitol
EDS	Energy Dispersive Spectroscopy
EDTA	Ethylenediamine Tetraacetic Acid
EPMA	Electron-Probe Micro Analysis
FAO	Food and Agriculture Organization
FPLC	Fast Protein Liquid Chromatography
FTIR	Fourier Transform Infrared
GPC	Gel Permeation Chromatography
GuHCl	Guanidinium Hydrochloride.
HAP	Hydroxyapatite
HCA	Hydrophobic Cluster Analysis
HPLC	High-Performance Liquid Chromatography

HTST	High-Temperature-Short-Time
IgG	Immunoglobulin-G
IMCU	International Milk Clotting Unit
IMFs	Infant milk formulas
M	Molten-globule state
N	Native BLG
OCP	Octacalcium Phosphate
OVA	Ovalbumin
PAGE	Polyacrylamide Gel Electrophoresis
PDB	Protein Data Bank
PCP	Primary Casein Particles
PHE	Plate Heat Exchanger
PMMA	Polymethyl Methacrylate
PM556	Pyrromethene 556
QCM	Quartz Crystal Microbalance
R	Reversible-state BLG
Re	Reynolds number
RhB	Rhodamine B
RP-HPLC	Reversed-Phase HPLC
RSS	Residual Sum of Squares
S	Soluble BLG
SAXS	Small Angle X-ray Spectroscopy
SD	Standard Deviations
SDS-PAGE	Sodium Dodecyl Sulphate-PAGE
SEC	Size-Exclusive Chromatography
SEM	Scanning Electron Microscopy
sHsp	small Heat-Shock proteins
SS	Stainless steel
TCP	Tricalcium Phosphate
TEM	Transmission Electron Microscopy
TFA	Trifluoroacetic Acid
ThT	Thioflavin T
THE	Tubular Heat Exchanger
TICT	Twisted Intramolecular Charge-Transfer
ToF-SIMS	Time-of-Flight Secondary Ion Mass Spectrometry
U	Unfolded BLG
UHT	Ultra-High-Temperature
WFM	Wide-field Fluorescence Microscopy
WPI	Whey Protein Isolate

General Introduction

Global demand for milk and dairy products has increased dramatically in recent decades, and it will inevitably continue to increase through a combination of global population growth, increased lifespan and improved economic prosperity in the developing world (Salter, 2016). According to The Food and Agriculture Organization (FAO), the world population will soon reach 9.1 billion by 2050 when food production will have to increase by 70% to meet the demand for adequate nutrition. This will drive stronger demand for dairy proteins and therefore larger milk production in a global scale.

Indeed, milk and dairy-derived products are indispensable components of the food supply chain which present numerous nutritional and functional properties. Since decades, dairy fractions were employed as added-value ingredients to boost functional properties of foodstuffs. A remarkable number of highly transformed dairy products are readily consumed by virtually all population groups (*e.g*. infants, children, teenagers, middle-aged and the elderly). For example, in 2010, dairy-based functional foods (*e.g*. with added probiotics, omega-3, phytosterols) already accounted for 43% of a $ 16 billion market (ÖZer and Kirmaci, 2010). More recently, according to the International Dairy Federation (IDF) World Dairy Situation Report 2020, the global dairy consumption has reached 114.7 kg per capita (IDF, 2020). Even if this average value is blind to reveal the great disparity existing between the different regions of the world (ranging from 42 kg in Africa to approx. 275 kg in Europe and North America) and cannot depict external factors influencing this local consumption per inhabitant, such as trade-off between habit and access level to milk supply, the continuous upward trend accompanying the increase of population is unambiguous.

To supply this demand, the global milk production keeps increasing and reached a total annual worldwide milk production of 881 million tonnes in 2019, with a steady growth trend of 2.2% close to the average over the last decade (2.4%; IDF, 2020). For all milk species produced, cow's milk represents the main portion (84%) of the total milk production and most of it will be sold as a heat-treated product (*e.g*. pasteurized, high-pasteurized or Ultra-High-Temperature, UHT) or converted to dairy products such as cheese, cultured milk, yogurts or milk powders (Arvanitoyannis and Kassaveti, 2009).

Thermal processing of milk is mandatory to ensure the microbiological harmlessness of dairy products as well as to extend their shelf-life. In fact, every dairy product is heated at least once where pasteurization being the most common way of treatment (Lewis and Deeth, 2008). In most production lines, thermal processing of milk is performed in a plate heat exchanger (PHE) where the milk is heated by heat transfer through stainless steel from hot water. However, the unwanted formation of fouling deposits formed upon the stainless steel surface during thermal processing seems unavoidable and remains an unresolved issue. This deposit burdens heat processes both financially through oversizing, production loss and cleaning cost as well as environmentally by drastically increasing energy consumption and abundant uses of water and harsh chemicals (Tamime, 2009; Zouaghi et al., 2019). As a result of fouling, there is a possibility of deterioration in product quality because the processed fluid cannot be heated up to the required temperature. In fact, in the dairy industry, the cost due to the interruption in production can be dominant compared with the cost of the reduction in performance efficiency (Georgiadis et al., 1998b). According to Van Asselt et al. (2005), about 80% of the total production costs in the dairy industry can be attributed to fouling and cleaning of the process equipment. Thus, a better understanding of the underlying fouling mechanism is crucial to reducing dairy production costs and environmental impact. This PhD manuscript aims at contributing to this general purpose.

Dairy fouling issue has been vastly studied since the 1960s, allowing to demystify two dominant mechanisms namely: i) heat-induced denaturation of proteins and ii) mineral precipitations. It was also established that, β-lactoglobulin (BLG), the major component of whey proteins, is the key protein that drives fouling. Consequently, most fouling experiments were studied with whey protein fractions which are most of the time casein-free. Unfortunately, the influence of casein, which is another major protein component over whey proteins in milk (~80% of milk protein), is not so well covered in the literature and; has never been studied exhaustively to investigate its role in fouling of whey protein solutions. Therefore, one the of main objectives of this thesis is to partially fill this gap by studying the role of casein on whey protein fouling behavior in a pilot plant PHE.

In parallel, as the thermal denaturation of BLG has been recognized to play a key role in fouling occurrence (whatever the presence of casein), the development of a chemical reaction model concerning thermal denaturation of BLG is therefore of vital importance to bridge this bulk

reaction with surface deposition. Inspection of the state-of-art reveals that the thermal denaturation pathway of BLG can be simplified to follow a two-step successive reaction scheme, *i.e*. unfolding and aggregation. Despite this, a conventional overall one-step reaction model was generally used to mathematically describe the thermal denaturation of BLG. Even though this model provides an overview on the thermal denaturation behavior of BLG which helps to gain a better understanding of the thermodynamic parameters important in the reaction process, its lack of ability to quantify the amount of different BLG species (*e.g.* native BLG, unfolded BLG and aggregated BLG) limits itself to establish a causal link between bulk BLG denaturation reactions and the severity of surface deposition reactions. This is mainly because the unfolded BLG specie has been widely accepted to be the fouling precursor.

Another shortcoming of the overall one-step reaction model is its failure to provide a mathematical interpretation of the break-slope phenomenon in the Arrhenius plot. This abnormal behavior is generally attributed to the competition of the two subreactions at different temperatures. Particularly, the unfolding step of BLG is always considered as a simple straightforward reaction and is the rate-limited step at low temperatures. A close inspection of the literature permits us to find accumulative pieces of evidence that point out a contrary: the thermal unfolding of BLG is unlikely to be a rate-limited step at any temperatures. As a matter of fact, as in the realm of biology, the thermal damage of protein typically occurs in a time scale of milliseconds. Therefore, the second objective of this thesis is to develop a novel reaction model describing the thermal denaturation pathway of BLG with a biological basis. This model is expected to be a new tool providing the correlation between thermal denaturations in the bulk and the deposition reactions, particularly in the presence of caseins.

As aforementioned, most fouling experiments were performed in industry-like systems such as those in pilot plant PHEs. The complexities of the fluid mechanics and the configuration itself in the PHEs make it hard to investigate the surface reaction kinetics concerning fouling growth. To this end, the third objective of the present thesis is to design and build a bench-scale device that mimics PHEs to obtain deposition kinetics. With a simplified configuration, realistic 3D simulation of thermal denaturation of proteins in the bulk, as well as deposition in the microchannel in the device, can be achieved using computational fluid dynamics (CFD). Particularly, the thermal denaturation of BLG in the bulk is solved using our developed reaction model as mentioned

previously. To compare between two fouling systems (*i.e.* PHE vs benchtop fouling device), the final objective of this thesis is to study the effect of casein on the thermal denaturation of whey proteins and fouling behavior in the custom-built bench-scale fouling system. This attempts to investigate the effect of two different flow regimes on the fouling behavior (*i.e.* turbulence in PHEs and laminar in bench-scale fouling device).

This manuscript, therefore, organizes into five chapters. Chapter One contains the state-of-art about fouling mechanisms and impacting factors. Chapter Two will present a comprehensive study regarding the effect of casein/whey mass ratio on the BLG denaturation and fouling behavior in a pilot plant PHE. A novel reaction model concerning thermal denaturation of BLG will be detailed in Chapter Three. The design of the benchtop fouling device, as well as a realistic 3D CFD modeling combined with experimental fouling runs, will be shown in Chapter Four. After that, the effect of casein on the BLG denaturation and fouling behavior in the custom-built laboratory-scale fouling device will be displayed in Chapter Five. The general conclusion and outlooks will be presented at the end of this manuscript.

Chapter One. State of the art on dairy fouling mechanisms and impacting factors

In this chapter, the necessity of thermal processing of milk is firstly introduced followed by its consequential fouling issues. Next, a historical investigation of fouling composition is presented, revealing two dominant fouling mechanisms, *i.e*. thermal denaturation of whey proteins and mineral precipitations. These two mechanisms are subsequently described in order: the BLG-based thermal denaturation mechanism and its derived kinetic reaction model are depicted. Caseins, particularly, their chaperone-like functions and their potential role on fouling are discussed. After that, the role of minerals, *e.g*. their precipitation due to high temperature as well as impacts on the thermal denaturation of proteins are shown. With these two main mechanisms are formally described, an overall fouling mechanism including its influencing factors are summarized. Other contributions on fouling such as the establishment of computational models and the development of laboratory-scale fouling devices are also outlined. Finally, the cleaning of dairy fouling is briefly introduced as it is beyond the scope of this thesis.

1.1 Thermal processing of milk and related issues

Milk is one of the best food endowed to human beings which contains most nutrients and also acts as an energy source. However, as being rich in an array of nutrients, it serves as an excellent medium for growth of bacteria. Therefore, processing of raw milk is essential to achieve food safety (microbiological quality to requisite standards) as well as food quality (aesthetics, nutrition, texture/rheological aspects, shelf value, preservation value) of milk (Borad et al., 2017). Up to date, thermal processing is omnipresent in dairy manufacturing to ensure food safety by elimination of spoilage and pathogenic micro-organisms.

There are several types of thermal treatments depending on the processing temperature and time. For example, for traditional pasteurization, it is a relatively mild process that consists of low heating temperature (60 °C) with long time (20 minutes). While a more classical pasteurization involves temperature around 72-76 °C and 15 to 20 s durations. More recently, known as High-Temperature-Short-Time (HTST) pasteurization process requires higher temperatures (80-90 °C) and shorter exposure times (~5 s) (Hammer and idf, 2004). These pasteurization processes were confirmed to be adequate for destroying almost all yeasts, molds, common spoilage as well as ensuring adequate destruction of common pathogenic, heat-resistant organisms. With these processes, pasteurized milk typically can have a refrigerated shelf life of up to three weeks. To further kill spores and extend shelf life, sterilization is applied with much higher temperatures and

much shorter time. For example, typical sterilization allows the processed fluid to reach 115 °C for 15 minutes. Further increases the temperature up to 150 °C with extremely short time (1-2 s), known as Ultra-High-Temperature (UHT) treatment can achieve a much longer shelf life of up to several months even without cold chain management (Rasane et al., 2020).

This increased shelf life of UHT without refrigeration has gained widespread acceptance and popularity by many consumers, although UHT milk has not been accepted by all because of the perceived 'cooked' taste of the product. Consequently, the need for extending the shelf life of pasteurized milk, without detectable changes to the flavor profile is sought and has proven to be an engineering challenge (Chandrapala and Zisu, 2016). For this reason, there is an increasing trend for developing new processing methods for milk with thermal treatments such as electrical resistive heating (McMahon et al., 2011) or non-thermal techniques including microfiltration (Schmidt et al., 2012), pulsed electric field (Griffiths, 2010), high pressure processing (Chawla et al., 2011), ultrasound (Chandrapala et al., 2012a) or combined use of them (Chandrapala et al., 2012b; Fernández García and Riera Rodríguez, 2014; Walkling-Ribeiro et al., 2011). These alternative techniques although offer minimal detrimental effect on milk quality (*e.g.* aroma, flavor, appearance and nutritional value), are still under investigation and therefore, yet to be implemented commercially. Currently, pasteurized milk remains preferred in many countries such as UK, Austria or Netherland (Lewis and Deeth, 2008).

Nevertheless, milk and its derived products tend to foul upon plate heat exchanger (PHE) during thermal processing has become a ubiquitous problem since PHEs were introduced for pasteurization and sterilization of milk in the 1930s (Visser and Jeurnink, 1997). These unwanted deposits generated upon the surface (typically on stainless steel) time-by-time during processing burden the process as it retards heat transfer efficiency (Mahdi et al., 2009), enhances the pressure-drop (Grijspeerdt et al., 2004) and also increases the possibility of biocontamination due to insufficient cleaning (Fryer et al., 2006). In fact, milk fouling is so rapid that heat exchangers need to be cleaned every day to maintain production capability and efficiency to meet strict hygiene standards. This frequency seems more serious when compared to other PHE processing plants such as petroleum, petrochemical which usually need to be cleaned only once or twice a year (Bansal and Chen, 2006). Operating costs are therefore increased due to frequent shutdowns on the production line for cleaning as well as corresponding use of excessive water and erosive chemicals

(Gillham et al., 1999; Tamime, 2009). According to Georgiadis et al. (1998b), the costs due to interruption in production can be dominating compared to the cost due to reduction in performance efficiency. In fact, around 80% of the total production costs are attributed to fouling (Van Asselt et al., 2005). From a recent review (Goode et al., 2013), the economic penalties of fouling in heat exchangers as discussed by Müller-Steinhagen et al. (2011) can be summarized:

(i) **Capital expenditure**, due to:

(a) *Excess heat transfer surface area compensating for the occurrence of fouling*.

(b) *Higher transport and installation costs for bigger and heavier equipment*.

(c) *Cleaning systems, including their installation and maintenance costs*.

(ii) **Fuel cost** (*If extra energy such as steam is required to keep the fouled heat exchanger operating for the required performance*).

(iii) **Maintenance cost** (*of the heat exchanger, cleaning system and any ancillary equipment in the process loop, for example, chemical tank level probes, flow meters, interface probes*)

(iv) **Production loss** (*cost of continuous production without shut-down for cleaning and maintenance as compared to the actual production cost*)

Consequently, a better understanding on the fouling mechanism will definitely help to diminish fouling which allows progressively toward a more eco-efficient and environmental-friendly process. There have been enormous research efforts to elucidate the fouling mechanism as well as corresponding impacting facts in the past few decades. Hence, the following sections of this chapter will focus on the historical development and state-of-art concerning dairy fouling issues.

1.2 Composition of milk and fouling deposits

The complexities of dairy fouling issues can be mainly attributed to the complexity of milk itself. Milk is a complicated bio-emulsion that contains mostly water (~87.5%) with around 4.8% lactose, 3.9% fat and 3.4% proteins (Bansal and Chen, 2006). More details of milk components are summarized in Figure 1.1. Inspection on the composition of fouling deposits provides a first glance at the underlying fouling mechanisms. The composition of fouling deposits can vary widely depending on processing conditions such as temperature, flow velocity and heat treatment methods or product factors, including compositions, or pH of the milk. A detailed historical literature review on the fouling deposit compositions can be seen in Table 1.1.

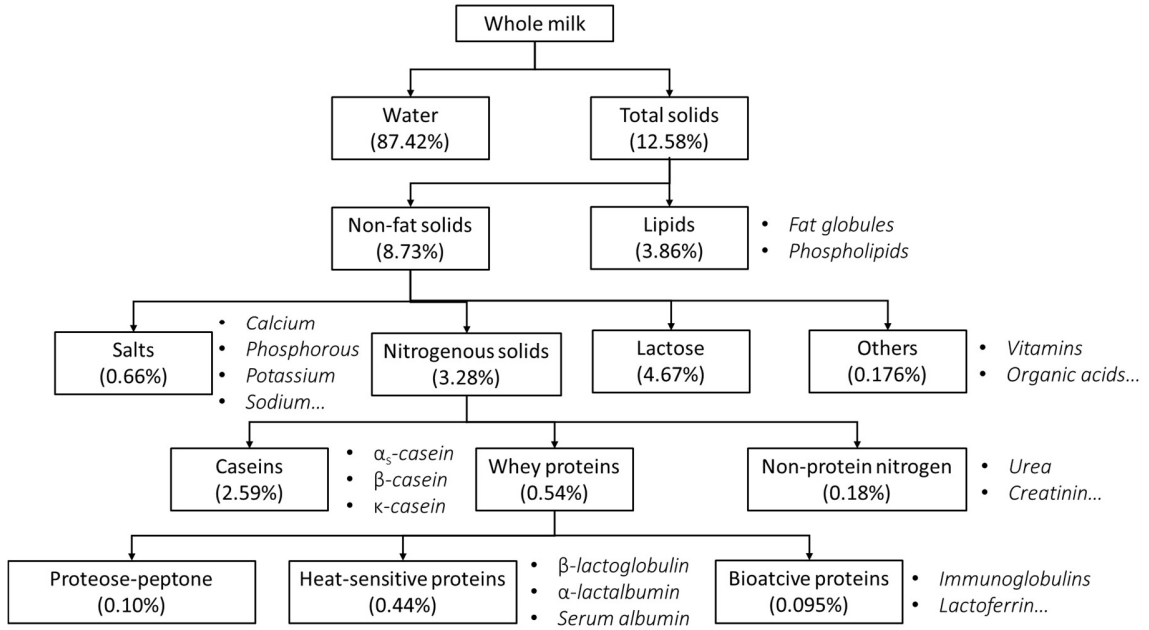

Figure 1.1. Typical distribution of the components in milk. This figure is simplified and adapted from Sadeghinezhad et al. (2013).

Table 1.1. Composition of dairy fouling deposits from literature.

Reference	Milk type	Temperature (°C)	Equipment	Composition in deposits (% dry basis)		
				Proteins	Minerals	Fat
Lyster (1965)	Whole milk	85	PHE*	60	25	12
		137.8	PHE	19	71	3
Skudder et al. (1981)	Whole milk	80-110	PHE	55	27	ND

		110-140		21	62	ND
Delsing and Hiddink (1983)	Skim milk	76	THE*	78	17	ND†
Lalande et al. (1984)	Whole milk	65-120	PHE	47	42	0.5
		120-138		14	74	2
Tissier (1984)	Whole milk	72	Pasteuriser	50	15	25
		90	Steriliser	50	40	1
		138		12	75	3
Skudder et al. (1986)	Whole milk	80-110	PHE	51	20	6
		110-140		20	63	5
Grandison (1988)	Whole milk	110-140	PHE	20-45	58-28	1-28
Yoon and Lund (1989)	Whole milk	88	PHE	43	45	ND
		120		45	40	ND
Jeurnink and Dekruif (1995)	Skim milk	85	PHE	44.4	45	0.4
Calvo and Derafael (1995)	Whole milk	80	PHE	52	9	23
Truong et al. (2002)	Whole milk	4-90	THE	32	5	50
		105	DSI*	62	20	3
		110		39	8	40
Truong et al. (2017)	Whole milk	75-95	DSI	40	5	40

*PHE, THE, and DSI refer to Plate Heat Exchanger, Tubular heat exchanger, Direct steam injector, respectively.
†ND refers to Non-Detected values

In general, fouling deposits were clarified into two main categories as firstly proposed by Burton (1968):

- Type A: found typically under 100 °C with a spongy and soft white morphology. This type of deposit is usually noted as proteinaceous deposit as it has a high protein content (50-60%), half of which being β-lactoglobulin, as well as 30-35% minerals (essentially calcium and phosphate) and around 5% lipids (Belmar-Beiny et al., 1993; Daufin et al., 1987).
- Type B: formed at higher temperatures with grey color and brittle structure, often referred as milk stone. It is predominantly minerals (70-80%) with less protein content (15-20%) and 5% lipids (Davies et al., 1997; Fryer et al., 2006; Lyster, 1965).

Based on these results, two dominant mechanisms are recognized for milk-based fouling, named

i) *heat-induced denaturation of proteins*

ii) *mineral precipitations*

Further efforts are subsequently paid to elucidate these fouling mechanisms. For example, by looking deeper, Tissier (1984) revealed the dominant contribution of β-lactoglobulin (BLG, a major component of whey proteins) on fouling as it accounts for more than 50% in the type A deposit despite it constitutes less than 5% of the milk solids. Calvo and Derafael (1995) also detailed those milk proteins of the deposit obtained from raw milk after a pasteurization process (heated to 80 °C), and they found 34.4% β-lactoglobulin, 18.6% α-lactalbumin (αLa) with 47.1% casein proteins inside the deposit. Since then, thermal denaturation of BLG has received tremendous attention and it is nowadays widely recognized to be the key that drives fouling. On the other hand, other major components such as casein proteins, sugars or fats were not considered to have significant contributions to fouling due to their little content in deposits (Jeurnink et al., 1996b). In particular, the effect of caseins, the major milk proteins (≥80%) on fouling was always neglected due to their relatively high thermostability. Nevertheless, recently, caseins have been noted to act as molecular chaperones which prevent the denaturation and aggregation of BLG, and therefore its role in fouling behavior can not be ignored. The next section of this chapter will review the whey proteins-based fouling machanisms as well as several important impacting factors, esepcially, the caseins which is the key in this thesis.

1.3 Thermal denaturation of whey proteins

The whey proteins are typical globular proteins with well-defined secondary and tertiary structures. These proteins retain their native conformations only within relatively limited temperatures. Once exposed to extremes of temperatures, heat-induced denaturation and aggregation occur. As aforementioned, thermal denaturation of whey proteins has been noted as a key that drives fouling. Indeed, whey proteins are the most thermosensitive dairy proteins. Among them, α-lactalbumin (αLa) has the lowest denaturation temperature, followed by bovine serum albumin (BSA), immunoglobulin-G (IgG) and finally β-lactoglobulin (BLG) as summarized in Table 1.2. Despite its relatively higher denaturation temperature compared to other whey proteins, BLG has been recognized to play a predominant role in protein denaturation and its subsequent fouling behaviors. Ever since the 1990s, researchers were trying to correlate BLG denaturation and fouling growth (Changani et al., 1997; Dalgleish, 1990; Jeurnink et al., 1996a; Karlsson et al., 1996). Predictive fouling models based on BLG denaturation and aggregation were therefore developed (De Jong, 1996; Fryer, 1989; Lalande et al., 1984; Visser and Jeurnink, 1997). More recent advances concerning fouling models will be presented in the later section (section 1.6).

Table 1.2. Composition and biological functions of whey proteins in bovine milk. Several important physical properties are also included. (Bernal and Jelen, 1985; de Wit, 1998; deWit and Klarenbeek, 1984; Moore et al., 1997; Sreedhara et al., 2010).

Whey proteins	Weight contribution (g/L in milk)	Molecular weight (kDa)	Disulphide bonds/molecule	Free thiol group/molecule	T_d† (°C)	Biological function
BLG*	3.2	18.4	2	1	72-74	Transfer
αLa*	1.2	14.2	4	0	61-62	Lactose synthesis
BSA*	0.4	66	17	1	64-72	Fatty acid transfer
IgG*	0.8	160	4	0.2	72	Passive immunity
Lactoferrin	0.03-0.1	80	17	0	70	Bacteriostatic agents

*BLG, α-La, BSA and IgG represent β-lactoglobulin, α-lactalbumin, bovine serum albumin and Immunoglobulin-G, respectively.
†T_d refers to denaturation temperature.

1.3.1 β-lactoglobulin (BLG)

BLG is one of the major components of whey proteins. It is a globular protein that is extremely acid-stable. It normally exists as a dimer with a subunit molecular weight of 18.4 kDa. The structure of native BLG is now well-known from both X-ray crystallographic studies (Brownlow et al., 1997; Qin et al., 1999) and high-resolution nuclear magnetic resonance studies (Fogolari et al., 1998; Kuwata et al., 1999; Uhrínová et al., 1998). Each BLG monomer comprises 162 amino acids, with one free cysteine and two disulfide bridges as shown in the three-dimensional structure in Figure 1.2 (Brownlow et al., 1997). Its secondary structure consists of 10-15% α-helix, ~50% β-sheets with turns accounting for 20% and the remaining 15% representing amino acid residues in a random non-repetitive arrangement without well-defined structures (Boye et al., 2009; Creamer et al., 1983). The quaternary structure of BLG greatly depends on environmental conditions such as temperature, ionic strength or pH that have individual and collective effects on the protein association state (Verheul et al., 1999). In physiological conditions, the dimeric form is predominant, but BLG can also be found in tetrameric, octameric or multimeric states (Gottschalk et al., 2003; Kumosins.Tf and Timashef.Sn, 1966).

In its nature, BLG is capable of irreversibly adsorption upon stainless steel surface to form monolayers even at room temperature. For example, Sakiyama et al. (1999) investigated the adsorption behavior of BLG as well as its peptides obtained by tryptic digestion at room temperature. The primary structures of these peptides from BLG were identified, and it was shown that most peptides that can be strongly adsorbed onto stainless steel surfaces have at least one acidic amino acid residue. In particular, the key peptide fragment as noted as T5 (Thr-Pro-Glu-Val-Asp-Asp-Glu-Ala-Leu-Glu-Lys, sequences in BLG ranges from 125 to 135) has been found as they showed an adsorption behavior almost identical to that of native BLG molecule (Imamura et al., 2003; Sakiyama et al., 1999). At higher temperature (typically ≥65 °C), the amount of BLG adsorbed upon stainless steel surface increase steeply (Itoh et al., 1995). However, if BLG is preheated or its sulfhydryl group was carboxymethylated (from –SH to $–SCH_2COOH$) the adsorption behavior of BLG was significantly suppressed. Based on these findings, an important role of thermal denaturation of BLG protein on its adsorption behavior has been recognized. A schematic representation of how the thermal denaturation of BLG affects its adsorption process is shown in Figure 1.3.

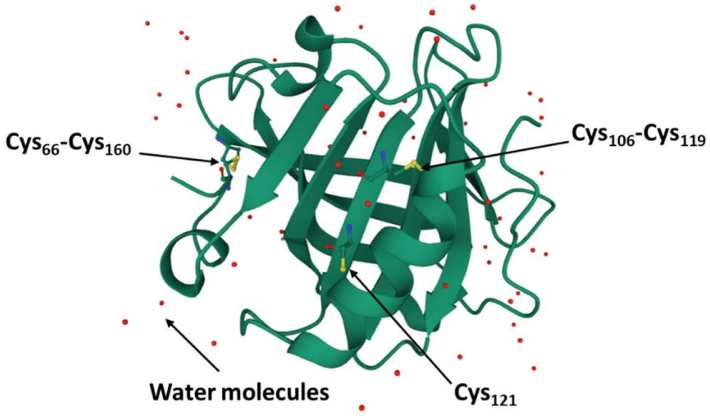

Figure 1.2. Schematic representation of the three-dimensional structure of β-lactoglobulin. The structure was illustrated on the basis of Protein Data Bank (PBD coordinates (1BSY) (Qin et al., 1998). Five cysteine residues are shown in Ball & Stick type in yellow, where two disulfide bonds at Cys_{66}-Cys_{160} and Cys_{106}-Cys_{119} can be found. One free thiol group located at Cys_{121} is buried inside the hydrophobic pocket. Red dots represent water molecules showing the accessibility of water for BLG.

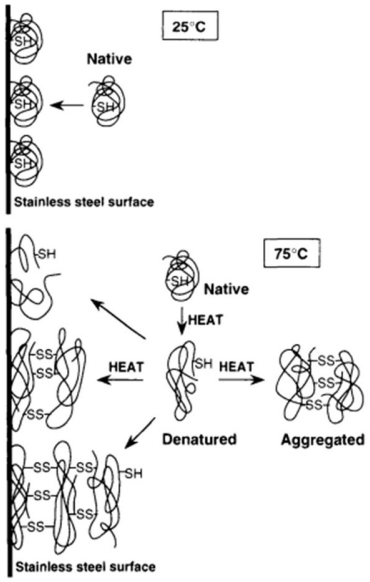

Figure 1.3. Schematic illustration of the effect of thermal denaturation of BLG on its adsorption process upon stainless steel surface. The image is re-used from (Itoh et al., 1995) by permission of Oxford University Press.

1.3.2 Thermal denaturation mechanisms of BLG

Historical development on BLG aggregation mechanism

Since thermal denaturation of BLG is crucial to its related adsorption or desorption behavior, tremendous efforts have been paid to investigate the effect of heat treatment on BLG using a range of different physical techniques including light scattering (Aymard et al., 1996; Elofsson et al., 1996; Gimel et al., 1994; Hoffmann et al., 1996; Roefs and De Kruif, 1994), circular dichroism spectroscopy (Griffin et al., 1993; Iametti et al., 1996; Prabakaran and Damodaran, 1997; Qi et al., 1997), calorimetry (Huang et al., 1994; Qi et al., 1995; Rüegg et al., 1977) and nuclear magnetic resonance spectroscopy (Iametti et al., 1998; Peres de sa Peixoto Junior et al., 2019). Despite this, the molecular mechanism of heat-induced denaturation and aggregation of BLG has not yet been fully determined. Historically, Mulvihill and Donovan (1987) firstly described thermal denaturation and aggregation of BLG using a two-stage reaction scheme. BLG naturally exists as native dimers (at ambient temperature and neutral pH) and reaches an equilibrium with its dissociated monomer form. Upon heating, this equilibrium shifts towards the direction into monomers, where almost all molecules are in their monomer form at temperature higher than 70 °C (Owusu Apenten and Galani, 2000). Simultaneously at high temperatures, BLG loses its native tertiary and secondary structures, and a previously hidden free thiol group becomes exposed (Figure 1.3). This activated molecule noted as unfolded BLG molecule, and can be involved in irreversible aggregation to form two types of aggregates: small aggregates were formed through either thiol group oxidation (-SH with –SH to form disulfide bonds) or sulfhydryl/disulfide interchange reactions (-SH with S-S) with other unfolded BLG molecules; while large aggregates were formed via “nonspecific” interactions without involvment of –SH group.

Later on, Steventon et al. (1991) proposed a three-stage reaction scheme to describe whey protein gelation based on percolation theory: *i.e.* denaturation composed of an unfolding step of BLG, an initiation step for two unfolded BLG molecules to form a dimer and finally a propagation step when the dimer can continue to interact with other denatured BLG to form larger aggregates. This model does not base on any molecular mechanisms regarding thermal denaturation of BLG, though the aggregation process was recognized to be the rate-limited stage with a reaction order of two. In analogy, Roefs and De Kruif (1994) described thermal denaturation and aggregation of

BLG as an ordinary radical polymerization reaction. The logic behind this model was adapted from Flory (1953) and Hiemenz (1984), where denatured BLG containing exposed sulphydryl groups act as radicals and would aggregate and polymerize in a similar way to ethylene monomers. Their model consists of three stages including an initiation, a propagation and a termination step. The initiation stage occurs when a native BLG molecule thermally unfolded and exposed its free thiol group to become activated. This free thiol group in unfolded molecule attacks disulfide bonds of other native BLG molecules through –SH/S-S interchange reactions to form an intermolecular S-S bond which simutaneously release a new reactive free –SH group (from the native molecule). This reactive dimer can continue interacting with other native BLG molecule to form linear aggregates. The propagation reaction terminates when this polymer interacts with another unfolded BLG via –SH oxidation so that no more reactive free –SH group can be created. Coincidentally, this model mathematically described the dynamic loss of native BLG during heating with a kinetic reaction order of 1.5 which was also found to be the best-fit reaction order when using a conventional one-step reaction scheme (described in the later section).

Another model proposed by Oldfield et al. (1998b) emphasized the role of hydrophobic interactions in the BLG denaturation process. It was proposed that the hydrophobic group of BLG is also exposed during the unfolding step which initiates the formation of hydrophobically associated aggregates of BLG at a lower temperature (≤75 °C). These hydrophobically linked aggregates can be rapidly converted into covalent-bound (through sulfhydryl/disulfide interchange reaction) aggregates when heated to higher temperatures. This idea was further supported by Verheul et al. (1998) by investigating the heat-induced denaturation and aggregation of BLG as a function of pH, heating temperature and NaCl concentration. The contribution of both physical (*i.e*. noncovalent interactions such as electrostatic, hydrophobic interactions) and chemical (*e.g*. –SH/S-S interchange) reactions on BLG aggregation greatly depends on these environmental parameters. For example, the involvement of chemical reactions is enhanced at high heating temperatures (above 85 °C), high pH values (> pH 6) and at low ionic strength (<0.1 M NaCl), whereas physical reactions are enhanced at low heating temperatures (65 to 85 °C), low pH values (< pH 6) with high ionic strength (> 0.1 M NaCl). Nevertheless, up to date, the exact extent of physical and chemical interactions involved in denaturation and aggregation of BLG still remains unclear, but it is evident that the aggregates of heated BLG are held together by a mixture of intermolecular non-covalent association and heat-induced non-native disulfide bonds.

Role of disulfide bonds in BLG aggregation

As discussed above, aggregation of BLG involves not only reactive free thiol group but also disulfide bridges within the molecular structure of BLG. Their interaction via –SH/-SH oxidation or –SH/S-S interchange reactions ultimately leads to aggregation and polymerization of BLG. Nevertheless, as BLG has one free –SH (Cys_{121}) and two disulfide bonds (Cys_{66}-Cys_{160} and Cys_{106}-Cys_{119}) as shown in Figure 1.2, the knowledge of which S-S bond is involved during the thermal aggregation process is not fully understood. Hypothetically, if all five cysteine residues of a BLG molecule can form two intramolecular disulfide bonds in a random way, there would be totally 30 different disulfide bond combinations and thus 30 conformationally different monomer proteins. And if we extend this to two BLG monomers, there will be large quantities of different dimer species. As a matter of fact, presumably due to its location on the external loop of the molecule, it was initially proposed that the Cys_{66}-Cys_{160} S-S bond is involved in –SH/S-S interchange reactions during aggregation. The other S-S group (*i.e.* Cys_{106}-Cys_{119}) located inside the protein structure was thus considered to be less available to interact with free –SH group. As expected, the involvement of Cys_{66}-Cys_{160} was firstly confirmed by Surroca et al. (2002) who revealed that heat-induced covalent aggregation of BLG at 68.5 °C, pH 6.7 is driven by thiol/disulfide exchanger reactions involving mainly three cysteine residues, which are Cys_{121}, Cys_{66} and Cys_{160}. More importantly, disulfide bond Cys_{160}-Cys_{160} was also identified implying that intramolecular –SH/S-S also occurs (*e.g.* Cys_{121} interacts with Cys_{66}-Cys_{160} to form a new Cys_{121}-Cys_{66} disulfide bond which releases a new free thiol group at Cys_{160}). This denaturation pathway was supported by other researchers (Livney et al., 2003; Morgan et al., 1997). Indeed, Creamer et al. (2004) have reported that approximately 35% of Cys_{160}, which is disulfide bound to Cys_{66} in the native protein, is present with a free thiol after heat treatment. These results imply Cys_{160} plays a more important role during intermolecular –SH/S-S interchange reaction over the native Cys_{121}, probably due to its location near the C terminus that makes it more accessible for intermolecular reactions. Besides that, instead of Cys_{160}, Croguennec et al. (2003) suggested that Cys_{119} also plays a dominant role in the thermal aggregation of BLG. They investigated BLG denaturation/aggregation at 85 °C and pH 6.6, and two denatured monomeric BLG species were recognized: one unfolded BLG with exposed Cys_{121} that could reversibly refold back to its native structure after cooling and the other stable non-native monomer with exposed Cys_{119} (cannot refold). They explained this preference of intramolecular –SH/S-S interchange reaction between Cys_{121} and Cys_{106}-Cys_{119} could be due to

the proximity of the sulfur atoms of Cys_{121} to Cys_{106}-Cys_{110} compared to the distance between Cys_{121} to Cys_{66}-Cys_{160}. Furthermore, based on these findings, Considine et al. (2007) proposed a new denaturation scheme where an intramolecular –SH/S-S occurs firstly to release a free thiol group Cys_{119} after which an intermolecular –SH/S-S occurs between this Cys_{119} with Cys_{66}-Cys_{160} of another BLG molecular and finally release a new thiol group at Cys_{160}. These different intra/inter-thiol/disulfide interchange interactions discussed above have been summarized into three main denaturation schemes as shown in Figure 1.4. Notice that, the distances of two different sulfur atoms between the one with –SH form at Cys_{121} and the others in disulfide bonds at (Cys_{66}-Cys_{160} and Cys_{106}-Cys_{119}) are 8.2/10.3/15.8/20.1 Å in native BLG molecular structure, respectively (between Cys_{121} and Cys_{119}/Cys_{106}/Cys_{160}/Cys_{66}) (Qin et al., 1998). The reason why Cys_{121} interacts preferably with Cys_{106} (not Cys_{119}) or Cys_{66} (not Cys_{106}) might be due to the conformational changes of native BLG molecular structure under heating.

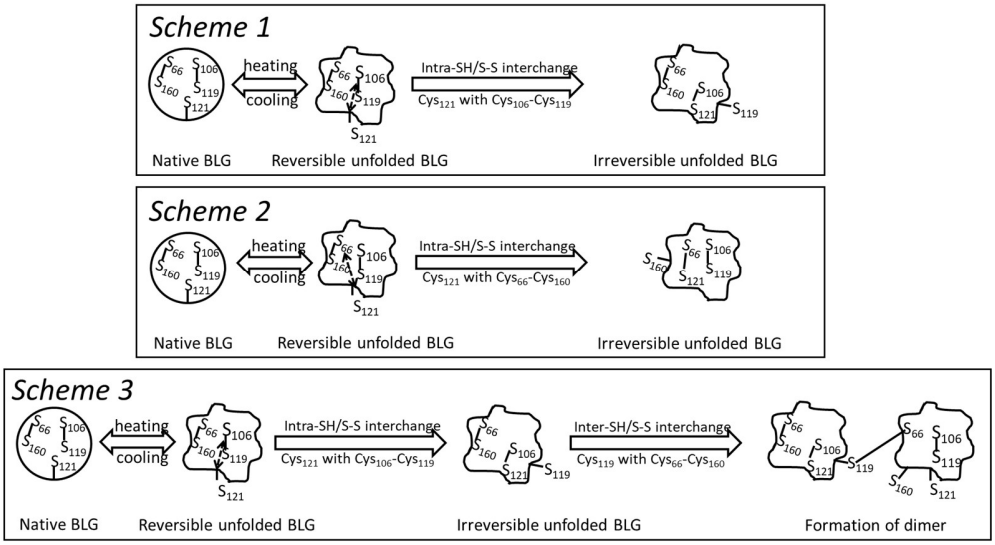

Figure 1.4. Three possible intra/inter-molecular sulfhydryl/disulfide interchange reaction schemes regarding heat-induced denaturation/aggregation of BLG. In scheme 1, the –SH/S-S interchange reaction occurs between Cys_{121} and Cys_{106}-Cys_{119} which releases a new free –SH group at Cys_{119}. This mechanism was supported by Croguennec et al. (2003). Whilst, in scheme 2, the intramolecular –SH/S-S interchange reactions occur between Cys_{121} and Cys_{66}-Cys_{160} which creates a new thiol group at Cys_{160}. This denaturation pathway was proved by Morgan et al. (1997), Surroca et al. (2002), Livney et al. (2003) and Creamer et al. (2004). The mechanism shown in

scheme 3 was proposed by Considine et al. (2007) where a free –SH group at Cys_{119} is released firstly through an intramolecular –SH/S-S interchange reaction between Cys_{121} and Cys_{106}-Cys_{119}. The free Cys_{119} then interacts with Cys_{66}-Cys_{160} of another BLG molecule which releases a new free thiol group at Cys_{160}.

One should notice that the thiol/disulfide interaction such as those proposed in (Roefs and De Kruif, 1994) where the free –SH group acts as a radical for polymerization is not in accordance with the well-known mechanism of –SH/S-S interaction in the realm of chemistry. In fact, instead of –SH, the thiolate ions (-RS^-) have been recognized to be the most activated reagents for the exchange of disulfide groups in proteins (Cecil, 1963). Therefore, the ionization of the thiol group is crucial (p*K*a 7.3-8.5): below its p*K*a, thiol group is protonated, oxidation of thiol group prevails with the presence of oxidizing agents (typically dissolved oxygen molecule in the solution) as shown in equation 1.1:

$$2RSH + oxidant \rightarrow RSSR + 2H^+ + 2e^- + reductant \qquad \text{(eq. 1.1)}$$

Whilst above its pKa, -SH/S-S interchange reaction is more dominant due to the deprotonation of the thiol group as shown in equation 1.2:

$$RS^- + R'SSR' \leftrightarrow RSSR' + R'S^- \qquad \text{(eq. 1.2)}$$

There are many pieces of evidence supporting these reaction schemes. For instance, Bauer et al. (1998) studied heat-induced denaturation of BLG at 67.5 °C (pH 6.8 at 15 min) by using combined static light scattering and size exclusion chromatography, and they found that over 90% of BLG was still present in the dimeric form. In addition, Watanabe and Klostermeyer (1976) observed a decrease of –SH groups and an increase of S-S groups when heating BLG at pH 6.9 under aerobic conditions with elevated temperatures and prolonged time, however, these behaviors were not significant under anaerobic conditions. Futhermore, the formation of thiol/disulphide induced oligomers was reported to increase from pH 7.0 to 8.7 as expected of an increased reactivity of the free thiol gourp (in thiolate ions form) (Bauer et al., 2000). However, even heating at pH >7 but at a low protein concentration (≤10 g/L) can also result in a minimal aggregation of BLG. For example, (De wit, 1981) centrifuged 10g/L BLG solutions after heating at 80 °C for 10 min, they found a dramatic decrease of precipitates at pH above 6.8 (less than 3% aggregates). This might

imply a preferred formation of intramolecular thiol/disulphide interchange reactions over the intermolecular one especially when the reactivity of the thiol group is sufficient high (Creighton, 1984).

Thermal denaturation pathway of BLG

After these extensive studies, the thermal denaturation pathway has nowadays well characterized as a multistage reaction (as summarized in Table 1.3). A comprehensive review of the thermal state of BLG which can be met during heating up to 150 °C has been reported by de Wit (2009). BLG exists in its dimer form under physiological conditions (neutral pH and concentration >50 μM) (Hambling et al., 1992). Upon heating up to 55 °C, BLG dimer starts to dissociate into two identical monomers. Simultaneously during heating (<60 °C), a minor conformational change of BLG which assembles the classical Tanford transition observed at room temperature by pH adjustment was detected (Qi et al., 1995). This state of BLG molecule exhibits greater accessibility of a single anomalous carboxyl group which appears to be buried inside the hydrophobic interior of the protein in its native conformation (Seo et al., 2010). The free thiol group at Cys_{121} was also reported to be slightly exposed, while this transition is mild and thus reversible and often noted as Reversible-state or simply R-state (R) (Qi et al., 1995). At 65 to 70 °C, almost all BLG dimers are dissociated into monomers at neutral pH (Owusu Apenten and Galani, 2000). Accompany this, irreversible modifications of dissociated BLG monomers start to appear with largely exposed hydrophobic surfaces as well as the free –SH group. BLG at this temperature range is generally noted as "molten globule state" (M) at which the protein molecules typically retain a largely native-like secondary structure content with no rigid tertiary structure and their large-scale intramolecular mobility is much larger than that in the native state (Ptitsyn, 1995). However, one should notice that irreversible damage of virtually all helical conformations and up to one-fifth of the β-sheets were lost during heating between 60 and 70 °C (Qi et al., 1997). Actually, 70 °C has been reported to represent a temperature threshold for irreversible occurrence of most of the detectable conformational changes observed upon heating of BLG at neutral pH (Bhattacharjee et al., 2005; Iametti et al., 1996). When temperature is above 70 °C, larger conformational changes are detected in the secondary structure and described as a progressively loss of β-sheets structures and a concomitant formation of disorder structures (Qi et al., 1997; Seo et al., 2010). BLG at this state is noted as unfolded state (U), which exhibits large reactivity for

subsequent polymerization or aggregation through –SH oxidation or –SH/S-S intra/inter-molecular exchange reactions as well as hydrophobic interactions as decribed above.

When temperature is higher than 85 °C, the secondary structures of BLG continue to break down while residual secondary structures can still be observed (*e.g.* 22% β-strand, 7% α-helix and 9% β-turn at heating at 95 °C) (de Jongh et al., 2001). Whilst at this stage, hydrophobic interactions were not considered to be important in the formation of BLG aggregates. At extreme temperature like 125 °C, a full denaturation of the BLG molecule occurs associated with the breakdown of the disulphide bonds (Watanabe and Klostermeyer, 1976).

Table 1.3. State and molecular reactions of BLG encountered as regard of temperature range during thermal denaturation progress.

Temperature range (°C)	BLG molecular state	Molecular reactions of BLG	Reversibility of reactions	Reference
20	Native dimer	Dimerization through 12 intermolecular hydrogen bonds and 2 ion pairs. The secondary and tertiary structures of the monomer are stabilized by hydrophobic, ionic and hydrogen-bond interactions as well as two disulphide bridges. These two disulphide bridges as well the free thiol group at Cys_{121} are all inaccessible to the solvent.	-	(Gottschalk et al., 2003; Kinsella et al., 1989)
20-45	Native monomer (N)	Dissociation of one dimer into two monomers that has identical structures.	Reversible	(Belloque and Smith, 1998; Townend et al., 1969)
45-60	R-state (R)	Dissociation of dimer keeps going toward the formation of monomer while minor conformational changes occur which assemble the classical Tanford transition. This transition exposes a single anomalous carboxyl group that appears to be buried inside the hydrophobic interior of the protein. At this stage, BLG also exhibits greater accessibility of Cys_{121}. This mild transition is reversible and therefore noted as R-state.	Reversible	(Qi et al., 1995; Seo et al., 2010)

65-70	Molten globule state (M)	Almost all dimers are dissociated into monomers. The dissociated monomer exposed large hydrophobic surfaces and a reactive –SH group. Meanwhile, irreversible damage on the secondary structure of BLG including helical conformation and β-sheets has also been found. Intramolecular –SH/SS interchange reaction may occur which leads to non-native-like monomer after cooling.	Irreversible	(Owusu Apenten and Galani, 2000; Qi et al., 1997)
70-85	Unfolded state (U)	Progress loss of β-sheets structures and a concomitant formation of disorder structures were found with elevated temperatures. Intra/Inter-molecular –SH/S-S interchange reactions, as well as hydrophobic interactions, occur which lead to the formation of aggregations.	Irreversible	(Manderson et al., 1999; Qi et al., 1997)
85-105	Unfolded state	Residual secondary structures of BLG can still be found while the participates of hydrophobic interactions in the formation of aggregations are negligible.	Irreversible	(de Wit, 2009)
>125	Completed denatured	BLG molecule is completely denatured associated with the breakdown of disulphide bonds.	Irreversible	(Watanabe and Klostermeyer, 1976)

Thermal denaturation of BLG with other whey proteins

Other major whey proteins such as αLa and BSA also contribute significantly to the BLG-based aggregation process mainly due to their possessions of either disulfide bonds (αLa, BSA) or free thiol group (BSA, Table 1.2) (Wijayanti et al., 2014). The denaturation and aggregation of whey proteins during heating has been studied extensively in solutions of whey protein mixtures such as whey protein concentrate, whey protein isolate and milk (Anema and Li, 2000; Havea et al., 1998; Oldfield et al., 2005). Due to the lack of a free –SH group, αLa is unable to form aggregates without the presence of BLG (Chaplin and Lyster, 1986). Heat-induced interactions within mixtures of αLa and BLG result in intermediate-sized aggregates that are stabilized by covalent (S-S) and noncovalent bonds, as well as large-size aggregates that are stabilized by S-S bonds (Havea et al., 1998). In the mixture of major whey proteins (*i.e.* in the presence of BLG, αLa and BSA), BSA is more effective than BLG in accelerating the formation of αLa aggregates (Havea et al., 2001). The

apparent response differences to heat treatment of αLa, BSA, BLG and mixtures of these proteins are mainly due to the ability of BSA and BLG, but not αLa, to undergo self-initiation of –SH/S-S interchange reactions, and the ability of αLa to form interprotein aggregates with BSA and BLG (Calvo et al., 1993; Gezimati et al., 1997). The presence of the free thiol group in BSA and BLG (Table1.2) is the major factor responsible for their self-initiation of SH/S-S interchange reactions.

1.3.3 Thermal denaturation kinetic models of BLG

Techniques used to assess BLG denaturation

A study of the kinetics of thermal denaturation of the whey proteins (mainly BLG) should lead to a better understanding of the relationship between heat treatment and its effect on the functional properties of milk products. The objective of experimental kinetic studies is the development of mathematical models to describe the rate of particular reactions as a function of various experimental variables and thus to gain an understanding of the key thermodynamic parameters associated to the reaction process. Another important objective of developing kinetic models is its capacity to numerically simulate the denaturation progress particularly during thermal processing (*e.g*. within a PHE) so as to correlate the thermal denaturation (the appearance/disappearance of BLG protein species, particularly fouling precursor species) and the fouling deposition. The prerequisite for developing a denaturation kinetic model lies in the dynamic measurement of the denaturation process. In the dairy science literature, denaturation of BLG has been measured in a variety of ways: loss of solubility (Gough and Jenness, 1962), shift in elution time in high-performance liquid chromatography (HPLC; Kehoe et al., 2011; Petit et al., 2011; Zúñiga et al., 2010) or size exclusion chromatography (SEC; Croguennec et al., 2004; Galani and Apenten, 1997; Law and Leaver, 2000), loss of band intensity in native polyacrylamide gel electrophoresis (PAGE; Anema et al., 2006a; Oldfield et al., 2005; Oldfield et al., 1998b), or the presence of a denaturation endotherm in differential scanning calorimetry (DSC; Park and Lund, 1984). Some selected literature studies concerning thermal denaturation of BLG either in milk or buffer systems as well as their measurement methods and reported kinetic orders are summarized in Table 1.4. As it is shown, most of the analytical methods performed in the literature, excepted DSC, provide 'off-line' analysis, which measures only denaturation that is not reversed during cooling and holding stages that the analyzed sample was subjected. For example, measuring solubility at specific pH

does not measure denaturation *per se*, it is more related to colloidal stability and thus correlates more to the aggregation process. In high-performance liquid chromatography (HPLC) systems such as RP-HPLC (reversed phase HPLC) which measures changes in surface chemistry (*e.g.* hydrophobicity of molecule) or SEC that measures gross changes in hydrodynamic radius (*e.g.* molecule size). For those performed in native PAGE, the proteins were differentiated through migration speed in the polyacrylamide gel, whilst it depends on molecular weight, covalent bonding, quaternary and tertiary structure of the molecule as well as non-covalent bonding and molecular charge. Although monitoring BLG denaturation in real-time is possible such as those using polarimetry (Sawyer et al., 1971) or circular dichroism spectroscopy (Bhattacharjee et al., 2005), they fail to provide quantitative information on the loss of native BLG content.

Table 1.4. Studies reported in literature dealing with BLG heat denaturation in various milk derivatives and their kinetic orders (eq. 1.5). Comments on αLa are given when heat denaturation of this whey protein has been studied.

Reference	Conditions	Temperature	Measurements	Kinetic orders† and main observations
		Denaturation in milk		
(Lyster, 1970)	Skim milk	68-135 °C	Immunodiffusion method	n=1 for αLa while n=2 for BLG
(Hillier and Lyster, 1979)	Skim milk	70-150 °C	PAGE*	n=2 for BLG
(Dannenberg and Kessler, 1988)	Skim milk	70-150 °C	Solubility at pH 4.6 with ultrathin-layer isoelectric focusing	n=1 for α-La while n=1.5 for BLG Arrhenius constants changed at 90 °C.
(Anema and McKenna, 1996)	Reconstituted whole milk	70-115 °C	Native PAGE	BLG followed a reaction order of 1.5. Arrhenius constants changed at 85 °C.
(Oldfield et al., 1998b)	Skim milk	70-130 °C	Native PAGE	Arrhenius constants showed two ranges: at 70-90 °C, n=1.2/1.6 for BLG A/B while at 95-130 °C, they followed 1.0/1.4.
(Law and Leaver, 2000)	Skim milk (pH 5.2-8.8)	80 °C	Solubility at pH 4.6 and FPLC*	n ranged from 1.5 at pH 5.2 to 2.3 at pH 8.8

(Oldfield et al., 2005)	Skim milk	80, 90 and 120 °C	Native PAGE	n ranged from 1.3-1.5 for BLG A and 1.4-1.7 for BLG B
(Anema et al., 2006a)	Reconstituted skim milk	75-100 °C	Solubility at pH 4.6 and Native PAGE	n=1 for α-La while n=1.5 for BLG Arrhenius constants changed at 90 °C.
Denaturation in buffer/water/milk derivatives				
(Gough and Jenness, 1962)	1% BLG in phosphate buffer pH 6.7, ionic strength 0.1 M	73 °C	Solubility at pH 5.0, Kjeldahl analysis	BLG A was more thermostable than B, first-order kinetics. 'Primary' and 'secondary'denaturation distinguished.
(Briggs and Hull, 1945)	0.5% BLG in phosphate buffer pH 6.9, ionic strength 0.1 M	60-99 °C	Moving boundary electrophoresis	Two-step process: reaction order of one for the first step and two for the second step
(Park and Lund, 1984)	10% BLG in various buffers from pH 4-9	30-120 °C	DSC*	n= 2 for BLG over the pH range of 4 to 9.
(Roefs and De Kruif, 1994)	2-95 g/L BLG in water (pH 6.75-6.95)	65 °C	Solubility at pH 4.7 and GPC*	BLG followed a reaction order of 1.46 which is in accordance with the model prediction.
(Verheul et al., 1998)	2-46 g/L BLG with 0-1 M NaCl	65-80 °C	Solubility at pH 4.7 and GPC	n=1.5 at pH 6.5 and 1.7 at pH 7. With 0.5 M NaCl, n=1/1.4 at pH 6.5/7
(Le Bon et al., 1999)	2.5-115 g/L BLG in 0.1 M CH_3COONH_4 buffer	52-76 °C	SEC*	n=1.5, independent of concentration and temperature
(Hoffmann and van Mil, 1999)	50 g/L BLG in water at pH 6-8	65 °C	Solubility at pH 4.7 and SEC	n=1.5 at pH 6.8, n<1.5 at lower pH and ≥2 at higher pH
(Galani and Owusu Apenten, 1999)	2 g/L of whey in 0.1 M tris-HCl buffer pH 6.8	75-150 °C	FPLC and SDS-PAGE	Consistent preference for the second-order kinetic model was found at 80-130 °C
(Croguennec et al., 2004)	5.8 g/L BLG in water, pH 6.6	85 °C	GPC	n=2 for both A nd B variants, the order changed when added NaCl or $CaCl_2$

(Tolkach and Kulozik, 2007)	50 g/L BLG in milk ultrafiltration permeate (pH 6.8)	63-120 °C	Solubility at pH 4.6 and HPLC	BLG followed a reaction order of 1.5. Arrhenius constants changed at 90 °C.
(Mounsey and O'Kennedy, 2007)	Up to 6% BLG in water at pH 7	78 °C	Solubility at pH 4.6	BLG followed a reaction order of 1.97
(Zúñiga et al., 2010)	5% BLG in water at pH6, 6.4 and 6.8	80 °C	Solubility at pH 4.6 and HPLC	n=1.5, increasing denaturation rate with decreasing pH
(Petit et al., 2011)	5.33% BLG in water at pH 6.8	68-96 °C	Solubility at pH 4.6 and HPLC	n=1.5 unaffected by the presence of Ca^{2+} up to 264 ppm
(Kehoe et al., 2011)	20-90 g/L BLG or WPI in water at pH 7	78 °C	Solubility at pH 4.6 and HPLC	n varies from 1 to 1.6 depending on the protein concentration. BLG denatured faster in whey than in pure BLG system
(Loveday et al., 2014)	5 g/L BLG in water at pH 7.4 or in phosphate buffer	78 °C	Native PAGE	n ranged from 1.68-4 depending on the temperature and buffer condition
(Croguennec et al., 2014)	10 g/L BLG at various pH (3-6.7) with elevated CMP*/BLG molar ratios up to 2	65-95 °C	Solubility at pH 4.6 and HPLC	n=1.5 at pH 6.7, irrespetive of CMP concentrations
(Wolz and Kulozik, 2015)	Up to 40% whey proteins at pH 6.7	70-95 °C	Solubility at pH 4.6 and HPLC	n=1.5, higher protein concentration induced faster denaturation
(Halabi et al., 2020)	3.3 or 5.1 g/L of BLG in model IMFs*	67.5-80 °C	Solubility at pH 4.6 and HPLC	n=1.5-1.6 with or without supplementation of lactoferrin in the model IMFs
(Leite et al., 2021)	3.3 or 5.1 g/L of BLG in model IMFs*	67.3-79.6 °C	Solubility at pH 4.6 and HPLC	n varies from 1.5-2 depending on the estimation methods

*Abbreviations are PAGE, polyacrylamide gel electrophoresis; FPLC, fast protein liquid chromatography; DSC, Differential scanning calorimetry; SEC, Size exclusive chromatography; GPC, high-performance gel permeation chromatography. CMP, caseinomacropeptide. IMFs, Infant Milk formulas.
†n represents reaction order.

BLG denaturation kinetic model

As discussed above, modern techniques used to access thermal denaturation of BLG failed to distinguish either between non-native BLG monomers with aggregates (such as in PAGE) or between native and reversibly refolded BLG monomer after cooling. For example, the BLG content detected in RP-HPLC was considered to consist of native BLG as well as those native-like BLG that return to their native states after cooling. Under this methodology, the pH adjustment of the heat-treated protein solutions to 4.6 followed with centrifugation process was generally required. These processes would precipitate all non-native BLG contents such as stable non-native BLG monomers (through intramolecular –SH/S-S interchange reactions) as well as those dimers, oligomers or large aggregates. This hypothesis has been recently proved by Delahaije et al. (2016) who observed that non-aggregated fractions for a heat-treated BLG solution consist of a native-like and two types of non-native-like conformations using circular dichroism and size exclusion chromatography. They confirmed the residual non-aggregated protein after pH adjustment to 4.6 had native-like molecular conformations.

Based on the knowledge from the literature studies as summarized so far, the thermal denaturation pathway of BLG has revealed to be a multistage process. Most of the time, it is expressed using the simple reaction scheme as shown in Equation 1.3(a-b):

$$D_2 \rightleftharpoons 2N \qquad \text{(eq. 1.3a)}$$

$$N \rightarrow U \rightarrow A \qquad \text{(eq. 1.3b)}$$

BLG naturally exists as native dimers (D_2 at ambient temperature and neutral pH) and reaches an equilibrium with its dissociated monomer form (N). Upon heating, this equilibrium shifts towards the direction into monomers, where almost all molecules are in their monomer form at temperatures higher than 70 °C. Simultaneously with heating, the BLG molecule starts to unfold, exposing the buried hydrophobic group as well as the free thiol group at Cys_{121}. This molecular state noted as the unfolded state (U) can initiate a series of intra/inter-molecular thiol/disulfide exchange reactions with other BLG or other whey proteins, casein proteins to from aggregates (A).

However, due to technical limitations as in the HPLC system to access the concentration of unfolded BLG species, the loss of native protein due to denaturation during isothermal heating is often described using a conventional one-step reaction scheme:

$$S \rightarrow A \quad \text{(eq. 1.4)}$$

where S refers to soluble BLG as detected using HPLC, which is the sum of native BLG contents as well as those native-like molecules refold back after cooling. This shortcoming leads to a one-step kinetic model with the general rate law for a single-specie reaction as applied:

$$-\frac{dC_s}{dt} = k_f C_s^n \quad \text{(eq. 1.5)}$$

where C_s ($g \cdot L^{-1}$) is the concentration of soluble BLG content as measured through HPLC, n is the reaction order, and k_f is the denaturation rate constant in a unit depending on n as $g^{1-n} \cdot L^{n-1} \cdot s^{-1}$.

The temperature dependence of k_f is typically deduced by the Arrhenius equation:

$$k_f = k_{f0}\left(\frac{-Ea}{RT}\right) \quad \text{(eq. 1.6)}$$

where k_{f0} is the denaturation pre-exponential factor ($g^{1-n} \cdot L^{n-1} \cdot s^{-1}$), Ea is the activation energy ($J \cdot mol^{-1}$), R is the universal gas constant (*i.e.* 8.314 $J \cdot mol^{-1} \cdot K^{-1}$) and T is the temperature in Kelvin.

Equation 1.6 is usually treated with logarithm as:

$$\ln(k_f) = -\frac{Ea}{R}\frac{1}{T} + \ln(k_{f0}) \quad \text{(eq. 1.7)}$$

$\ln(k_f)$ is then plotted against the reciprocal of the temperature (also known as Arrhenius plot) for calculation of Ea and k_{f0}. According to equation 1.7, a straight line is expected assuming Ea is constant within the temperature range. Nevertheless, a sharp bend has always been observed whatever thermal denaturation of BLG occurs in milk (Anema and McKenna, 1996; Dannenberg and Kessler, 1988), whey (Galani and Owusu Apenten, 1999; Khaldi et al., 2015b; Wolz and Kulozik, 2015) or in pure BLG systems (Petit et al., 2011; Tolkach and Kulozik, 2007). A representative Arrhenius plot showing this break-slope behavior is shown in Figure 1.5. This biphase phenomenon in the Arrhenius plot was first pointed out by (Lyster, 1970) who assumed the reason for this behavior was a difference in the relative importance of two reaction steps occurring either in parallel or in sequence (eq. 1.3(b)). This hypothesis has nowadays been frequently used to interpret such phenomenon: at lower temperatures as such lower than the critical temperature ($T<T_c$), the unfolding of BLG is slower than the aggregation, so the whole

denaturation reaction is limited by the unfolding subreactions (noted as unfolding limited region). When the temperature is higher than T_c (aggregation limited region), aggregation of BLG is slower and hence becomes the limited step. Based on this frame, the corresponding kinetic parameters can be calculated respectively from the unfolding and aggregation limited region using linear regression. The discrepancies found in the literature in critical temperature (T_c varies from 80 to 90 °C), reaction order (n varies from 1 to 2) or calculated kinetic parameters (*e.g.* 230~400 kJ/mol for unfolding step) as can be seen in Table 1.5 might due to their differences in the solution environments (pH, protein concentration, protein composition, presence of salts, etc).

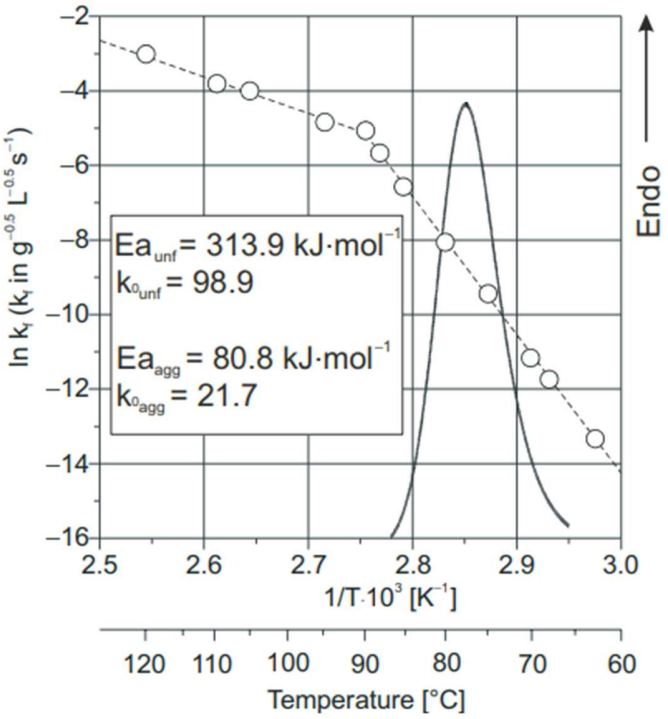

Figure 1.5. Representative Arrhenius plot of BLG denaturation combined with corresponding DSC thermogram. The figure is re-used from Tolkach and Kulozik (2007). Model solutions contain 50 g/L BLG and 45 g/L lactose at pH 6.8. Critical temperature T_c locates around 90 °C. The corresponding kinetic parameters for both unfolding and aggregation limited regions are shown. In this case, the best-fit reaction order n was found to be 1.5.

Table 1.5. BLG denaturation kinetic parameters reported in the literature using one-step reaction scheme (eq. 1.5).

Reference	Conditions	Temperature range (°C)	BLG variants	n	Ea (kJ·mol^{-1})	$\ln(k_{f0})$ (g^{1-n}·L^{n-1}·s^{-1})
(Lyster, 1970)	Skim milk	68-90	BLG	2	277.85	87.37
		90-135	A&B		54.79	13.77
(Dannenberg and Kessler, 1988)	Skim milk	70-90	BLG A	1.5	265.21	84.16
			BLG B		279.96	89.43
		95-150	BLG A		54.07	14.41
			BLG B		47.75	12.66
(Anema and McKenna, 1996)	Reconstituted whole milk	70-85	BLG A	1.5	263.49	NG*
			BLG B		296.46	
		100-115	BLG A		51.14	
			BLG B		33.87	
(Oldfield et al., 1998b)	Skim milk	70-90	BLG A	1	285.5	91
			BLG B	1.4	296.7	95.1
		95-130	BLG A	1.2	58.8	15.3
			BLG B	1.6	44.0	10.9
(Galani and Owusu Apenten, 1999)	2 g/L whey at pH 6.8	75-90		1	376.1	NG
		90-120			61.8	
		75-90	BLG A&B	1.5	413.2	
		90-120			66.1	
		75-90		2	450.2	
		90-120			69.6	
(Anema, 2000)	Reconstituted skim milk (9.6% total solid)	75-90	BLG A&B	1.5	259.8	82.3
		90-100			36.3	8.2
	Reconstituted skim milk (38.4% total solid)	75-90			319.1	100.8
		90-100			128.3	38
(Tolkach and Kulozik, 2007)	BLG in ultrafiltration permeate	63-90	BLG A&B	1.5	313.9	98.9
		90-120			80.8	21.7
(Petit et al., 2011)	5.33% with added 0 ppm Ca	68-80	BLG A&B	1.5	234.5	72.9
		80-96			95.0	25.4
		68-80			304.7	98.4

	5.33% with added 264 ppm Ca	80-96			111.0	32.1
(Croguennec et al., 2014)	10 g/L BLG at pH 6.7 with 30 mM NaCl	65-80	BLG A	1.5	318	NG
			BLG B		352	
		80-95	BLG A		194	
			BLG B		175	
(Khaldi et al., 2015b)	1% whey with 100 ppm Ca	65-80	BLG A&B	1.5	384.5	124.8
		80-92			360.7	86.3
	1% whey with 120 ppm Ca	65-80			271.2	117.2
		80-92			260.4	83.1
(Halabi et al., 2020)	5.1 g/L BLG in control IMFs (without lactoferrin)	67.5-80	BLG A&B	1.6	305	102
	3.3 g/L BLG in IMFs with 1.7 g/L lactoferrin			1.5	273	126
(Leite et al., 2021)†	5.1 g/L BLG in control IMFs (without lactoferrin)	67.3-79.6	BLG A&B	1.8	326	108
	3.3 g/L BLG in IMFs with 1.7 g/L lactoferrin			2.0	390	132

*NG refers to not given in the original publication. †Data was obtained using a nonlinear least-squares method.

Is the unfolding of BLG really a rate-limited step?

As described previously, even though the thermal denaturation pathway of BLG has been revealed with an intricate multi-stage mechanism (section 1.3.2), in practice, it is usually expressed using an overall one-step reaction (eq. 1.4). This one-step reaction provides valuable information about the key thermodynamic parameters (Table 1.5), however, it is plausible to extend these data in two-step consecutive reaction model (*i.e.* $N \rightarrow U \rightarrow A$, eq. 1.3(b)) in the application of fouling deposit modeling (Bouvier et al., 2014; Fryer and Slater (1985)). Indeed, in most simulation works, researchers tend to use two-step consecutive reaction model due to its ability to calculate the evolution of unfolded BLG species as they were generally considered as the fouling precursor

(Choi et al., 2013; Jun and Puri, 2005a; Pan et al., 2019) (More details about fouling model will be presented in the later section, section 1.6). Almost all of the kinetic parameters were used as published by De Jong (1996) where the BLG denaturation was considered as a two-step consecutive reaction with a reaction order equals to one for the unfolding step and two for the aggregation process. Nevertheless, if the break-slope behavior is solely due to the competition of these two subreactions at different temperatures, it is ambiguous why the break-slope phenomenon still exists in the aggregation process of two-step reaction model (De Jong, 1996).

And if such an abnormal break-slope behavior can not be interpreted in a mathematically way, the model is unlikely to formally describe the denaturation process. The BLG denaturation model providing mathematical interpretation on the break-slope phenomenon in the Arrhenius plot is scarce in the literature except in (Tolkach and Kulozik, 2007). In Tolkach's model, the formation of the molten globule state of BLG species during thermal treatment was characterized by an equilibrium between native and partially unfolded BLG species. The proportion of the unfolded BLG species among the total soluble BLG content (or the unfolding ratio) was set as a constant depending only on the temperatures such that when the temperature exceeds a critical value, the unfolding ratio reaches one implying that all the proteins are in their unfolded state. Based on this assumption, the break-slope behavior was properly explained mathematically, however, there was no supporting information on this assumption nor any explanation why this assumption was made. Nevertheless, the satisfaction of this model seems to imply that the unfolding of BLG can be treated as an instantaneous step (or very quick compared to the aggregation process). Is it really true?

Actually, in most denaturation models we have mentioned above, the unfolding of BLG was always treated as a straightforward reaction typically with a reaction order equal to one. This assumption is unlikely to be true, as in the realm of biology, the thermal damage of proteins happens in a time scale of milliseconds (Johnson et al., 1974). Other analytic technologies to assess the thermal denaturation of BLG such as Fourier transform infrared (FTIR; Casal et al., 1988) or circular dichroism (CD; Qi et al., 1997), which provide "on-line" analysis also support this hypothesis. For instance, Iametti et al. (1996) failed to follow the kinetics of BLG denaturation during heating or cooling using CD, and they considered these heat-induced modifications were complete within seconds. In addition, Cairoli et al. (1994) observed that the exposure of

tryptophan residues of BLG molecule was temperature-dependent and was essentially completed on the time scale of seconds. Furthermore, Fujiwara et al. (1999) monitored urea-induced denaturation of BLG using CD, and they found that a significant change in the CD intensity was observed within the dead time of measurements (25 ms). More recently, Euston (2013) used molecular dynamics simulation to follow the thermal unfolding of BLG, and the conformational changes of the molecule at 350 K were complete in ~0.7 μs. Indeed, if denaturation of BLG occurs within seconds, experiments would require the temperature "jumps" to the desired value while using "on-line" analytical measurements such as UV absorption. This has been done in Huttmann and Birngruber (1999) where a temperature-jump experiment was achieved by using infrared pulsed radiation. They monitored the real-time denaturation of chymotrypsin using UV absorption and the denaturation of protein at 380 K was observed within 300 μs. The rate constants for the unfolding of chymotrypsin followed the Arrhenius equation can reach up to 3000 s^{-1}. It is thus plausible to extend this to BLG although BLG is larger compared to small protein molecule as chymotrypsin.

Based on this, the thermal unfolding of BLG proteins is unlikely to be a rate-limited step at any temperature range. With this in mind, the deduced kinetic or thermodynamic data from the overall one-step reaction model are less accurate. Therefore, in the later chapter of this thesis, a novel BLG thermal denaturation model with a biological basis will be presented, which explains the break-slope phenomenon in the Arrhenius plot so as to provide more reliable kinetic and thermodynamic information. This model is also targeted to establish a link between thermal denaturation in the bulk and surface deposition reactions by quantifying the amount of different BLG species during thermal processing, particularly the unfolded BLG species.

1.3.4 Caseins and their chaperone-like functions

Caseins and their molecular structures

Casein is a group of unique acid-insoluble phosphoproteins, and it is also the major protein component of bovine milk, comprising approximately 80% of the total milk protein. There are four individual types of casein molecules, the α_{s1}-, α_{s2}-, β- and κ-caseins in approximately relative amounts of 4:1:3.5:1.5, respectively (Lucey and Horne, 2018). The properties of the proteins have been previously summarized (Farrell Jr et al., 2004; Swaisgood, 2003), some important features

for individual casein can be seen in Table 1.6. Caseins are natural unfolded proteins and viewed as intrinsically disordered proteins (Thorn et al., 2015). In milk, the caseins, together with the essential ingredient of calcium phosphate (De Kruif and Holt, 2003), form aggregates of several thousand individual protein molecules with average diameters of 150 to 200 nm (de Kruif, 1998) known as casein micelles (Fox and Brodkorb, 2008). For a casein content of 2.5 g/100 mL milk, there are some 10^{14}-10^{16} micelles/mL milk, which implies a relatively close packing with intersurface separations of less than one micelle diameter. Milk is white largely because the colloidal dimensions of the casein micelles are such that they scatter significant amounts of light, an effect that is compounded by their high number density. The micelles are highly hydrated, with approximately 3.5 kg of water per kg of protein (Jeurnink and Kruif, 1993). Thus, although the caseins make up approximately 2.5% of the total weight of milk, the micelles occupy approximately 10% of the volume.

Table 1.6. Casein proteins in bovine milk: compositions and some important properties. Data are summarized from the literature (Broyard and Gaucheron, 2015; Farrell Jr et al., 2004).

Casein proteins	Weight contribution (g/L in milk)	Molecular weight (kDa)	Disulphide bonds/molecule	Free thiol group/molecule	Proline	Glutamic acid	Phosphoserine
α_{s1}-casein	12-15	23.6	0	0	17	24	8
α_{s2}-casein	3-4	25.2	1	0	10	25	11
β-casein	9-11	24.0	0	0	35	18	5
κ-casein	2-4	19.0	1	0	20	13	1

"But why casein exists in a micellar structure?" Before introducing more details and recent advances about the micellar structure of the caseins (will be presented in the following section), one should be aware that in whatever situation the casein find themselves, their behavior is dictated by their primary structure and the interactions to which this can give rise. For the moment, let's confine ourselves to casein sequence properties first. Caseins were identified as members of the wider secretory calcium phosphate-binding family by their possession of functional and sequence features common to that family (Kawasaki and Weiss, 2006). Among the conserved motifs is the SXE peptide (Ser-X_{aa}-Glu) where X_{aa} may be any amino acid. In the caseins, this peptide provides a recognition template for posttranslational phosphorylation of the serine in the mammary gland by a casein kinase (Mercier, 1981). These phosphoserine residues are often found clusterd in

groups in the caseins (Table 1.6). Associated with these phosphoserine clusters are significant high densities of negative charge at the normal milk pH. The importance of these phosphoserine clusters relies in locking up micellar calcium phosphate to avoid supersaturation of milk in calcium and phosphate and thus protect mammary glad duct system from potential painful calcification.

Away from the phosphoserine clusters, the casein molecules are distinctly hydrophobic. This segregation of hydrophilic and hydrophobic residues, confers on the caseins a denifite amphipathic nature (Huppertz et al., 2018). To explore the distribution of hydrophobic residues along all the casein sequences, Horne (2017) carried out hydrophobic cluster analysis (HCA) as shown in Figure 1.6. According to the 2D-HCA plots, it is evident that the phosphoserine clusters (dotted squares) are located in different segments of the chains compared with the main hydrophobic clusters. For example, in α_{s1}-casein, a couple of distinct hydrophobic regions can be seen between residues 1-44, 90-113 and 132-199 while the phosphoserine clusters are located between residues 45-89. Obviously, the phosphorylation would increase the hydrophilicity of the regions where these serine groups are clustered, and thus would further decrease the likelihood of forming hydrophobic clusters close to these phosphorylated clusters. The phosphorylation of the caseins was considered as one of the main factors that are responsible for their flexible and non-globular molecular structures (Lucey and Horne, 2018). The high concentrations of proline (shown as stars) found in the caseins, is another main reason why caseins exhibit as intrinsically unstructured proteins since proline residues are universally viewed as disrupters of secondary structure (Callebaut et al., 1997).

According to the HCA plots, α_{s1}-casein has two main hydrophobic regions located at N and C-termini, separatey by a highly charged hydrophilic region, leading to a “train-loop-train” structure (Figure 1.7(a)). While for β-casein, which comprises a highly negatively charged hydrophilic N-terminal region and moderate hydrophobicity of the rest of the chains, results in a “loop-train” structure that makes it the most hydrophobic one among other caseins (Fig. 1.7(b)). All of this is in line with the results based on the self-consistent-field calculations of the conformations of these proteins adsorbed onto a hydrophobic interface (Dickinson et al., 1997; Leermakers et al., 1996). κ-casein is special as it contains only one phosphoserine residue (Table 1.6). The negative charges of κ-casein are mainly lcoated in the C-terminal region, while the N-termini is characterized by its hydrophobic properties. This feature of κ-casein is crucial to the micellar structure of casein as it

acts as a terminator the growth of the micelle. More details about the structure of casein micelle and its historial development will be presented in the following section.

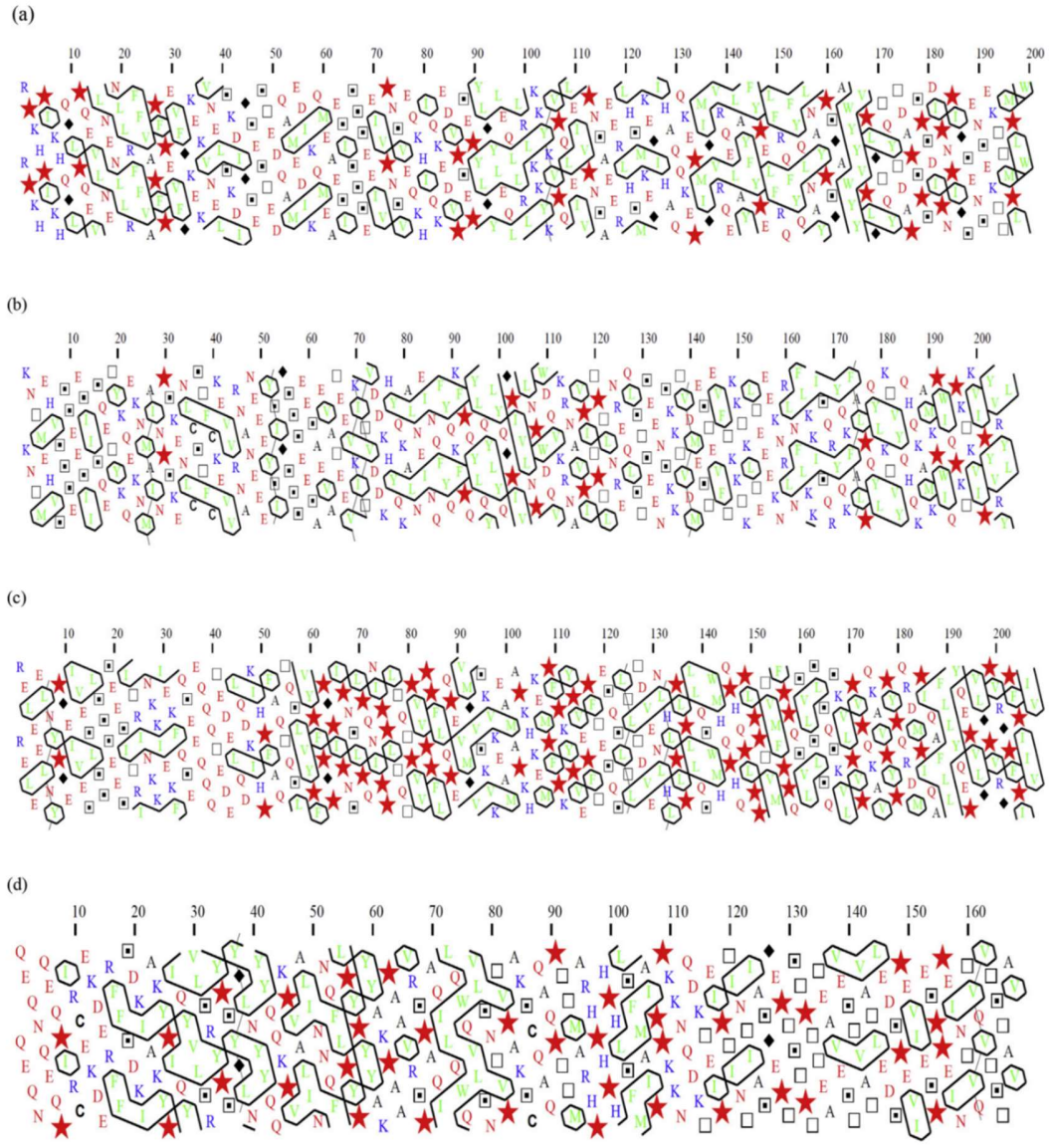

Figure 1.6. Hydrophobic cluster analysis (HCA) of (a) α_{s1}-casein (b) α_{s2}-casein (c) β-casein and (d) κ-casein, shown as 2D-HCA plots as reported in (Lucey and Horne, 2018). In the 2D-HCA plot, the sequence is written on an α-helical net that is unrolled and deplicated. The contours of hydrophobic amino acids are jointed together to indicate clusters. Special symbols are used fo proline (*star*), glycine (*diamond*), serine (*dotted square*), and theonine (*square*).

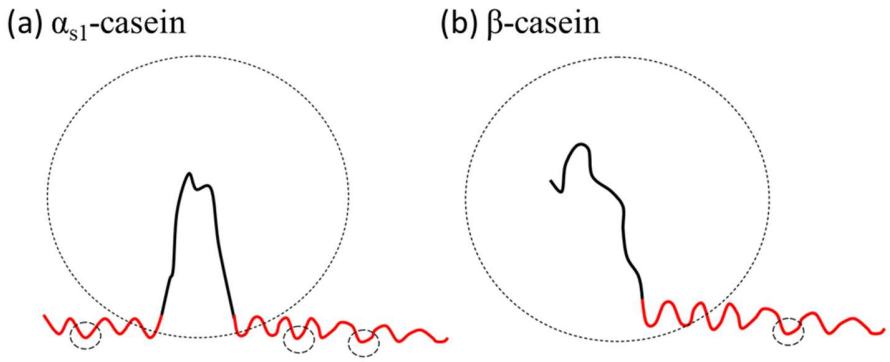

Figure 1.7. Schematic structures of α_{s1}-casein and β-casein, illustrating the train-loop-train structure of α_{s1}-casein and the loop-train structure of β-casein (Horne, 2020). The structures of the caseins are based on the results of the self-consistent-field calculations of the conformations of these proteins absorbed at a hydrophobic interface (Dickinson et al., 1997; Leermakers et al., 1996). The dashed circles give an idea of the range of the interaction potential components, the larger circle around the loops being the electrostatic repulsion arising from the negative charge centers thereon, and the smaller circle being the regions of hydrophobic attraction in the train.

Historical development of casein micelle structures

Understanding the structure of casein micelle and how it evolves during thermal processing is crucial to have a better view of the potential casein-whey interactions. The structure of the micelles has been debated for many years, and several reviews have appeared in the last decades, giving somewhat divergent points of view (Dalgleish, 2011; De Kruif and Holt, 2003; Farrell et al., 2006; Fox and Brodkorb, 2008; Horne, 2006). The development of casein micelle structure models has witnessed the progress of different proposers seeing through casein. For example, Waugh (1971) observed the role of κ-casein in rennet-induced coagulation, he suggested that κ-casein was resided on the casein micelle surface and elaborated his coat-core model. Later on, a so-called "submicelle model" has been addressed by Slattery and Evard (1973) where the micellar structure of casein requires the formation of two different submicelles, one κ-casein rich and the other κ-casein poor. In this submicelle model, the caseins first aggregate via hydrophobic interactions into subunits of 15-20 molecules each. The pattern of interaction is such that it brings about a variation in the κ-casein content of these submicelles. Those rich in κ-casein congregate on the micelle surface, and those poor or totally deficient in κ-casein are located in the interior of the micelle. Later on, this

model was elaborated by Schmidt (1980) where the colloidal calcium phosphate (CCP) was recognized as an essential linking agent between submicellar components as depicted in Figure 1.8(a). However, this submicelle model does not explain what drives the segregation of the κ-casein molecules, having preferred to associate with their own kind to form these segregated patches in the κ-casein rich submicelles. Further evidence has shown that CCP was uniformly distributed through the casein micelle, which precluded submicelles being linked by CCP to form the micelle. To reconcile this new evidence, the submicelle model of the casein micelle was refined to change the role of CCP from that of linking the submicelles to a charge-neutralizing agent to allow for a uniform distribution of CCP, and the submicelles were linked together via hydrophobic interactions (Fig. 1.8(b)) (Walstra, 1999). After that, Holt (1992) proposed a "nanocluster model" which used calcium phosphate (CaP) nanoclusters to cross-link between phosphoserine clusters on the caseins, crucially recognizing the existence of several such clusters on some of those molecules and allowing a three-dimensional network to be built up but omitting how κ-casein enters the picture (Fig. 1.8(c)).

The dual-binding model proposed by Horne (1998) and Horne (2002) seems to overcome these limitations. In the dual-binding model, the colloidal calcium phosphate does not just act as cross-linking agents but also as neutralizing agents which, being positively charged (Schmidt, 1982), bind to negatively charged phosphoserine clusters to reduce the protein charge to the level where attractive interactions between the hydrophobic regions of the caseins can be allowed to dominate. Hydrophobic interactions between the N-terminal region of κ-casein are also invoked to link κ-casein to these casein clusters which limit its growth. The only phosphoryl residue of κ-casein lies in the macropeptide forms the putative hairy layer at the external of the micellar structure (Fig. 1.8(d)). Later on, McMahon and Oommen (2008) proposed an interlocking lattice model based on the interpretation of high-resolution TEM (Transmission electron microscopy) of freeze-dried, immobilized, uranyl oxalate-stained casein micelles (Fig. 1.8(e)). In this model, CaP nanoclusters were considered to play an integral role in casein micelle synthesis and in maintaining supramolecule integrity and were presumed to be located at the interlocking sites as CCPs stabilized by phosphoserine-containing casein molecules. These calcium phosphate-casein aggregates serve as structure-forming sites to which other caseins can be bound, forming short chains between them. In analogy to the dual binding model, hydrophobic interactions, as well as hydrogen bonding, were thought to play predominant roles in maintaining supramolecule integrity.

To interpret the deformation of casein micelle structure due to osmotic stress observed through SAXS (small-angle X-ray spectroscopy), Bouchoux et al. (2010) proposed a sponge model showing a sponge-like micelle with a triple hierarchical structure (Fig. 1.8(f)). The lowest level of the structure consists of the CaP nanoclusters that serve as anchors for the casein molecules. The intermediate level consists of 10 to 40 nm hard regions that resist compression and contain the nanoclusters, where the soft regions are filled with solvent or serum phase (whey proteins, lactose, minerals, *etc*). The third level of structure is the casein micelle itself, with an average size of 100 nm. This sponge model has been recently improved by Nogueira et al. (2021) with more detailed information about the role of CaP nanoclusters in keeping the micellar structure. It was suggested that there are at least two types of CCPs in the interior of the casein micelle, indicating structural heterogeneity in the complex CCPs. Losing the less stable CCPs induces only a structural change at the smaller scale whilst structural changes at both small and medium scales were observed when losing more stable clusters.

Another model proposed by Dalgleish (2011) shows a relatively sparse hairy layer of κ-casein on the surface, dense enough to stabilize against approach by other casein micelles or other large colloidal particles but sufficiently diffuse to allow denatured whey proteins to interact with the para-κ-casein region or allow β-casein to dissociate from the micelles on cooling and to reassociate with the micelles on subsequent warming. This model attempts to reconcile the structural arrangement of the interior of the micelles with the high hydration of the micelle by giving a specific role of β-casein. It is proposed that β-casein acts as a surfactant in stabilizing the hydrated internal channels of the micelle (Fig. 1.8(g)). Another very recent model has been proposed by Huppertz et al. (2017) where casein micelle has a structure that is composed of nonspherical sub-particles, referred to as "primary casein particles" (PCPs) rather than submicelles (Fig. 1.8(h)). This model, though, in many aspects is similar to those submicelle models described by Schmidt (1982) and Walstra (1999), with the core of the micelle being composed of PCPs depleted in κ-casein (and enriched in α_{s2}-casein) and the surface of the micelle being composed of PCPs enriched in κ-casein (and depleted in α_{s2}-casein). The PCPs are cross-linked into a three-dimensional structure by the CCP through the phosphoserine centers on the α_{s1}/α_{s2}/β-caseins. The major difference from the submicelle model is that the PCPs are nonspherical whereas the submicelles in the earlier models were spherical.

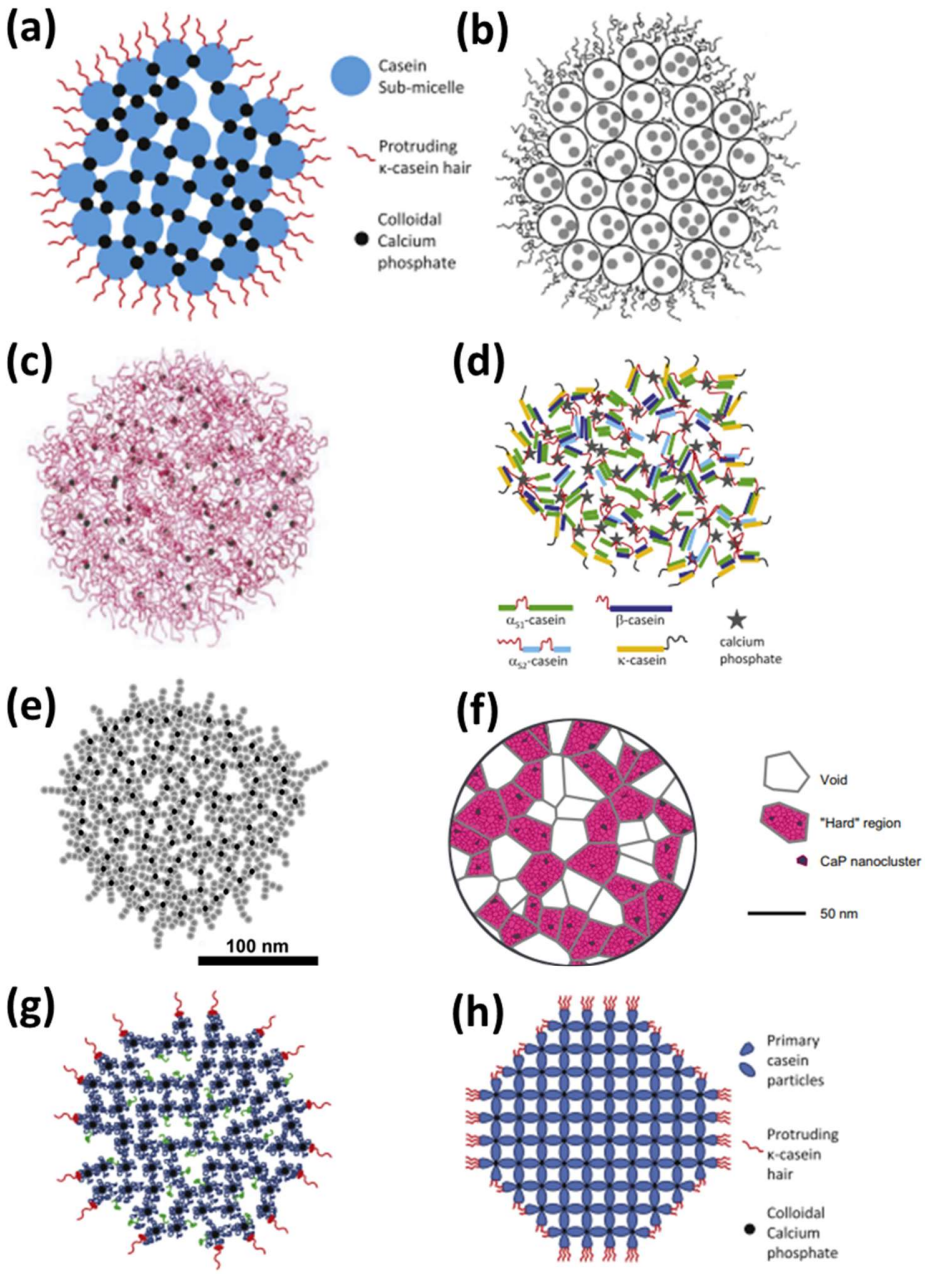

Figure 1.8. Recent models of the casein micelle. Figure is modified and adapted from (Anema, 2020). (a) Submicelle model as adopted from (Slattery and Evard, 1973) and (Schmidt, 1980) where the caseins first aggregate via hydrophobic interaction into subunits, after which, the κ-casein rich submicelle congregate on the micelle surface and those poor in κ-casein are located in the interior of structure with linking by colloidal calcium phosphate. (b) Modified hairy submicelle model from (Walstra, 1999) where colloidal calcium phosphate (CCP) acts as a charge-

neutralizing agent to allow for a uniform distribution and the submicelles are linked together via hydrophobic interactions. (c) Nanocluster model from (Holt, 1992) where calcium phosphate is in the form of nanoclusters (CCP) and the interaction sites on the caseins are the phosphoryl clusters of the calcium-sensitive caseins (*i.e.* α_s/β-casein, α_s-casein refers to combination of α_{s1}- and α_{s2}-casein). These caseins are able to cross-link the nanoclusters into extended 3-dimensional network structures. (d) Dual-binding model from (Horne, 1998) where caseins are clusted through their hydrophobic regions. These clusters are linked by their hydrophilic regions containing phosphoserine clusters to clloidal calcium phosphate clusters (CCP). The binding of κ-casein limits the growth and therefore constrains the size of casein micelle. (e) Interlocking lattice model from McMahon and Oommen (2008) where CaP nanoclusters were considered to play an integral role in casein micelle synthesis and in maintaining supramolecule integrity and were presumed to be located at the interlocking sites as CCPs stabilized by phosphoserine-containing casein molecules. (f) Sponge model from Bouchoux et al. (2010) showing a sponge-like micelle with a triple hierarchical structure. The casein micelle consists of hard regions that resist compression and contain the nanoclusters, where the soft regions are filled with solvent or serum phase. (g) Dalgleish model from (Dalgleish, 2011) where β-casein acts as a surfactant in stablizing the hydrated internal channels of the micelle. (h) Nonphserical subparticle model from Huppertz et al. (2017) where casein micelle has a structure that is composed of nonspherical sub-particles, referred to as "primary casein particles" rather than submicelles.

Dynamic equilibrium of casein micelle with serum phase

Yet no universal agreement on the casein micelle structure has been reached, the concept that a micellar structure with surface layers of κ-casein and internal structure maintained through hydrophobic interactions and CCP appears to enjoy universal acceptance (Horne, 2020). The knowledge on the casein micelle structure is undoubtedly helpful to understand and rationalize any changes to the properties and stability of milk, especially during thermal processing. Owing to their porous structures, casein micelles are under a dynamic mineral equilibrium with the serum phase (Figure 1.9) (Thomar, 2016). According to the physico-chemical conditions, they can also exchange casein molecules, calcium, inorganic phosphate and water with the aqueous phase. This equilibrium is brittle thus a small variation in the environmental conditions surrounding the casein micelle, such as pH, ionic strength, salt concentration, pressure, temperature can result in a change

of the equilibrium and therefore alters and modifies the structure and the stability of the casein micelle (Figure 1.10). The effects of these conditions on mineral equilibria have been explored and well discussed in several recent reviews (Abdallah et al., 2022; Dalgleish and Corredig, 2012; Dumpler et al., 2020).

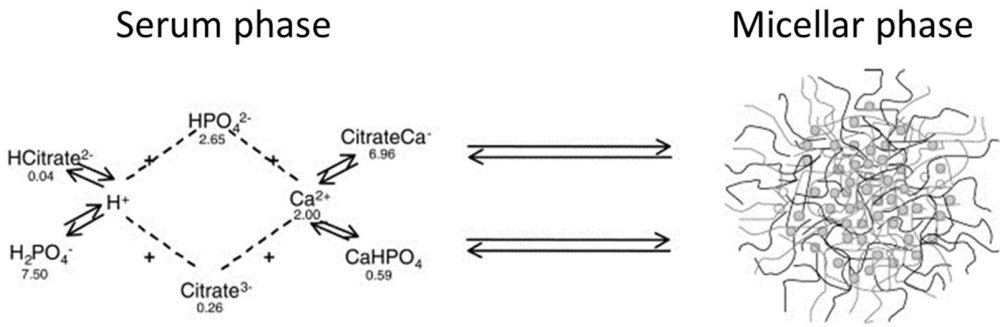

Figure 1.9. Mineral equilibrium between the serum and micellar phase from (Thomar, 2016). The concentrations of free salts are indicated in mM in the figure.

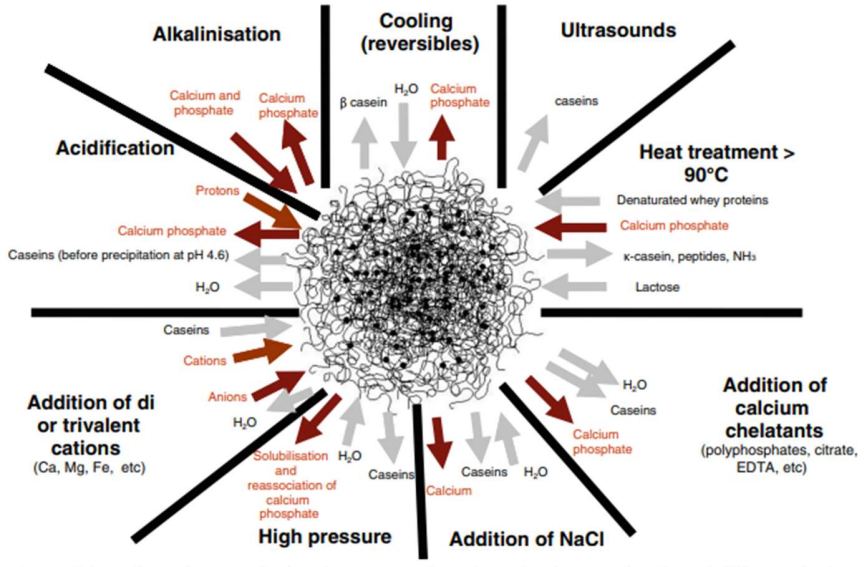

Figure 1.10. Schematic exchangers of minerals, water and casein molecules as a function of different physico-chemical condtions (Broyard and Gaucheron, 2015).

About 65 to 70% of total calcium and 50% of the total inorganic phospahte are present as CCP in the milk due to the low solubility of calcium phosphate at the natural pH of milk. Most of the

phosphate is present as HPO_4^{2-} and $H_2PO_4^-$ (in a ratio of 60:40), and most of the citrate is present as $citrate^{3-}$ at the natural pH of milk (Fox et al., 2015). The affinity of the phosphate ion to soluble calcium decreases with increasing protonation by a decrease in pH. A decrease in pH increases the amount of calcium and phosphate present in the milk serum, as CCP is dissolved when HPO_4^{2-} is protonated to $H_2PO_4^-$ (Frèche and Heughebaert, 1989). Heat treatment of milk results in a reduction of the serum calcium and phosphate level and an increase in CCP, due to the inverse solubility of calcium phosphate in milk with increasing temperature (Anema, 2009; On-Nom et al., 2010). The calcium and phosphate levels in the serum phase are readily restored upon cooling, except for heat treatments higher than 95 °C for several minutes (Van Dijk and Hersevoort, 1992). The precipitation of calcium phosphate during heat treatment of milk, and especially concentrated milk, leads to a decrease in pH, as protons are liberated from hydrogen and dihydrogen phosphate to form different forms of crystalline calcium phosphate, which might negatively affect the colloidal stability of the casein micelles in milk (Gaucheron, 2005). However, the precise location or the distribution of the newly formed calcium phosphate in milk upon heating and the effect of its phase transition to the insoluble crystalline or amorphous state reamins uncertain.

These effects of higher temperature (≤ 90 °C) as mentioned above do not appear to cause the disruption of the overall basic structure of the micelles or colloidal destabilization, although there is extensive heat-induced dissociation of κ-casein from micelles no matter in the presence or absence of whey proteins (Anema, 1998; Anema and Li, 2000). In fact, low levels of all individual caseins (*i.e.* α_s/β/κ-casein) were found to be dissociated from casein micelle at 20 °C at a wide pH range (6.3-7.1) (Anema and Klostermeyer, 1997). Increasing temperature generally leads to an increasing level of solubilized caseins, however, the dissociation behavior of α_s/β-casein shows highly pH-dependence than κ-casein (Anema 1997). Increasing temperature up to 90 °C hardly changes the level of dissociated α_s/β-casein at pH lower than 6.7, whilst at more alkaline conditions (*e.g.* 6.7-7.1), the quantity of solubilized α_s/β-casein increased with temperature to a maximum dissociation at about 70 °C. This abnormal dissociation pattern of α_s/β-casein against temperature was eliminated when most of the whey proteins were removed from the milk, therefore, it should be linked to the interactions between caseins and thermally denatured whey proteins (Anema and Li, 2000). However, at extreme temperatures such as those performed in UHT (≥ 120 °C), there is a readily increasing trend of dissociated caseins against temperature and heating time (Dumpler et al., 2017).

Interactions between denatured whey proteins and κ-casein

Since κ-casein is well-known to be located at the micelle surface, one of the major reactions of interest is the interaction between thermally denatured whey proteins and κ-casein. Early studies on model systems have confirmed interactions between heat-induced denatured BLG and κ-casein occur through intermolecular –SH/S-S exchange reactions (Sawyer, 1969; Zittle et al., 1962). Since both κ-casein and α_{s2}-casein have disulfide bonds (Table 1.6), one can expect both of them could participate in thiol-disulfide exchange reactions with denatured BLG or other denatured thiol-bearing whey proteins. However, it has been shown that α_{s2}-casein does not readily interact with denatured whey proteins when milk is heated, although some interactions in UHT milk have been reported (Snoeren et al., 1977). This low reactivity may be due to the interior location of α_{s2}-casein, which makes it less accessible for the interaction with denatured whey proteins compared to κ-casein. However, if the casein micelle structure is disrupted for example in pressure-treated milk, disulfide-bonded aggregates between α_{s2}-casein and denatured whey proteins were observed, suggesting that the disulfide bonds of α_{s2}-casein may become accessible to the thiol group of the denatured whey proteins (Patel et al., 2006).

It is, therefore, plausible that the interaction pattern between denatured whey proteins and casein micelles is significantly affected by the structural properties of the casein micelle which can depend on many variables including temperature, heating time, rate of heating, pH or concentration of milk salts (Anema and Li, 2003a; Oldfield et al., 1998a; Oldfield et al., 2005; Smits and Brouwershaven, 1980). For instance, when the temperature of milk is gradually increased above 70 °C, as in indirect heating systems, most of denatured BLG and αLa associate with the casein micelles, presumably as disulfide-bonded complexes with κ-casein at the micelle surface (Corredig and Dalgleish, 1996b; Smits and Brouwershaven, 1980). In the contrast, when milk is heated rapidly as in direct heating systems, only about half of the denatured BLG and αLa associate with the caseins with the rest remaining in the milk serum (Corredig and Dalgleish, 1996a; Singh and Creamer, 1991a). Corredig and Dalgleish (1999) suggested that, upon heating in milk, BLG and αLa would initially aggregate in the serum phase; these complexes subsequently interact with κ-casein at the casein micelle surface on prolonged heating. It is proposed that, under rapid heating conditions, BLG forms aggregates in the serum before interacting with the casein micelle and this limits the level of association with the casein micelles, wheras at slower heating rates, monomers

or smaller aggregates of BLG may interact with the micelles, and this may allow greater association with the casein micelles. However, other reports suggest that, on heating milk, the denatured whey proteins first interact with casein micelles and that the whey protein-κ-casein complexes subsequently dissociate from the casein micelles (Donato and Dalgleish, 2006; Donato and Guyomarc'h, 2009; Donato et al., 2007; Parker et al., 2005). This proposal was supported by the observation that the addition of sodium caseinate to milk did not increase the level of serum-phase complexes between the denatured whey proteins and κ-casein, which was interpreted as indicating that the complexes between the denatured whey proteins and κ-casein were formed on the casein micelle surface regardless of the pH at heating (Parker et al., 2005).

Temperature and pH have also been recognized to be the main factors affecting the level of interaction between the denatured whey proteins and the casein micelles as both of them can significantly affect the dissociation status of the casein micelle and/or the concentration of active proteins. When whey proteins are thermally denatured, their distribution between serum and colloidal phases is highly correlated to the BLG denaturation level and the level of κ-casein in the serum (Anema and Klostermeyer, 1997; Anema and Li, 2000). Higher levels of denatured whey proteins, particularly BLG, remained in the serum as the milk concentration increased along with the dissociated κ-casein (Anema, 1998; Nieuwenhuijse et al., 1991; Singh and Creamer, 1991b). Studies using very small pH steps showed that the association of the denatured whey proteins with the casein micelles was very dependent on pH when the milk was heated at temperatures above 70 °C. At a pH of about 6.5, 80% of the denatured whey proteins associated with the casein micelles when milk was heated at 90 °C. Increasing the pH in steps as small as 0.05 units progressively decreased the level associated with the micelles so that at about pH 6.7 (the natural pH of milk), only about 30% was associated with the casein micelles. At an even higher pH such as 7.1, almost all the denatured whey proteins were in the serum phase (Anema and Li, 2003a, b; Vasbinder and de Kruif, 2003). And the level of κ-casein and denatured whey protein in the serum were linearly correlated (Anema, 2007).

Gathering these pieces of evidence, Anema and Li (2000) proposed different pathways on casein-whey protein interactions depending on pH and temperature as illustrated in Figure 1.11. At pH below approximately 6.7, micellar integrity is maintained throughout the temperature range. At temperatures above ca. 70 °C, the whey proteins denature and associate with κ-casein at the

micelle surface. At pH 6.7 or above, heating at temperatures up to above 70 °C causes the casein proteins to dissociate from the micelles. Under these conditions, the calcium ion activity may be sufficiently low that the caseins disssociate as individual monomers or α_s/β-caseins and oligomers of κ-casein. The level of dissociated casein increases with increasing temperature. On cooling, the calcium ion activity increases and the dissociated caseins co-aggregate to form small complexes that are stablized by κ-casein. These aggregates are markedly smaller than the casein micelles and the majority of the these complexes remain in the serum on ultracentrifugation. Some of the dissociated casein may reassociate with the original casein micelle complex. At these temperatures, the whey proteins retain their native conformations and do not interact with the casein proteins. When heating above 70 °C at pH above 6.7, the casein proteins still dissociate from the micelles in a similar pattern as they do at lower temperatures. At these higher temperatures, the denatured whey proteins interact with both the micellar casein and the dissociated κ-casein to form disulphide-bonded aggregates. On cooling, the κ-casein/whey protein complexes remain soluble in the supernatant, however, due to its conjugation with BLG, κ-casein is less effective in stabilizing α_s/β-caseins in this scenario. Removal of the whey proteins reduces the association of denatured BLG and κ-casein, allowing κ-casein to stabilize the α_s/β-caseins and therefore higher levels of these proteins remain in the supernatant. And *vice versa*, the addition of high levels of BLG results in greater association between the denatured whey proteins and κ-casein which reduces the stabilizing action further.

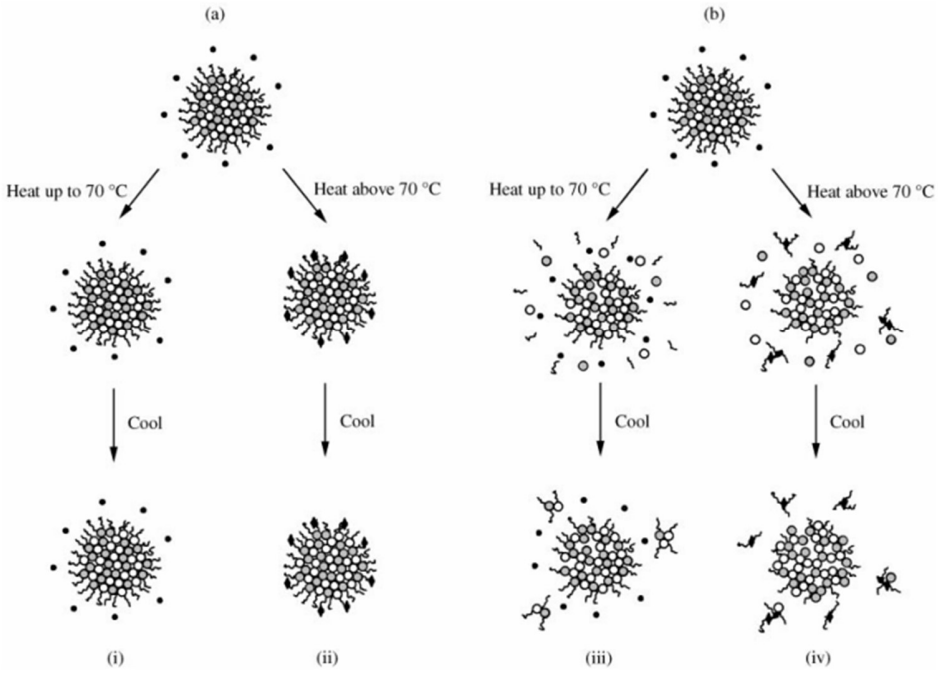

Figure 1.11. Diagrammatic representation of the effect of pH and temperature on the casein micelles and whey proteins in heated skim milk. (a) pH values below 6.7; (b) pH values above 6.7. (i) little change to the casein micelles on heating and cooling; (ii) whey proteins denature and associate with κ-casein at the casein micelle surface; (iii) all caseins dissociate from the micelles on heating. On subsequent cooling, the dissociated caseins from small aggregates are stabilized by κ-casein; (iv) all caseins dissociate from the micelles on heating. The whey proteins denature and associate with the dissociated κ-casein. On subsequent cooling, the dissociated α_s/β-caseins reassociate with the original micelles, but the κ-casein/whey protein complexes remain in the serum. Figure re-used with permission from (Anema and Li, 2000).

Chaperone-like functions of caseins

In the previous section, we have comprehensively described the structural changes of casein micelle as well as potential interactions between thermally denatured whey proteins and dissociated caseins under heat treatment. The most frequently mentioned are the interactions between heat-induced denatured BLG with κ-casein or α_{s2}-casein because of their possession of disulfide bridges so the thiol/disulfide exchange reaction can occur. But we also know that the micellar structure of casein can be significantly disrupted upon heating, and a great number of

α_s/β-caseins are dissociated into the serum phase. These two caseins (*i.e.* α_{s1}/β-casein) do not have any cysteine residues and therefore possess no free thiol group or disulfide bonds. This lack-of-cysteine feature of α_{s1}/β-casein as well as their intrinsically disorder structures have been noted to have the potential to act as molecular chaperones.

The term molecular chaperone was firstly used four decades ago by Laskey et al. (1978) to describe the ability of the thermostable nucleoplasmin to prevent the aggregation of folded histone proteins with DNA during the assembly of nucleosomes. However, it was only in 1987 that the initial concept of molecular chaperone was established by Ellis (1987), extending the possibility of many proteins to be identified as molecular chaperones. Molecular chaperones are defined as "*a large and diverse group of proteins that share the functional property of assisting the non-covalent folding/unfolding and the assembly/disassembly of other macromolecular structures but are not permanent components of these structures when they are performing their normal biological functions*" (Ellis, 2006).

In 1999, Bhattacharyya and Das (1999) first claimed that caseins have molecular chaperone properties. It was shown that α_s-caseins (a combination of α_{s1}-caseins and α_{s2}-caseins) have micellar structure that is similar to the oligomeric structures of many molecular chaperones. These proteins were able to decrease the heat-induced aggregation (turbidity) of other proteins (40-70 °C) or chemical modification (disulfide cleavage and photoaggregation). Since that, chaperone activity of caseins (individual caseins, casein micelle or sodium caseinate) has been found to suppress the amorphous or particulate type aggregation of various proteins under different stress (*e.g.* thermal, chemical and light) as summarized in Table 1.7.

Table 1.7. Chaperone activity of caseins from literature (adapted from Yong and Foegeding (2010)). Note that α_s-caseins refers a combination of α_{s1}-caseins and α_{s2}-caseins.

Reference	Caseins (g/L)	Substrate protein (g/L)	Temperature (°C)/Time (min) (unless stated otherwise)	Buffer conditions
Bhattacharyya and Das (1999)	α_s-casein (0.1)	Alcohol dehydrogenase (0.4)	40/35	10 mM Pi buffer, pH 7.0

	α_s-casein (0.03-0.06)	β-Crystallin (0.2)	60/33	
	α_s-casein (0.4)	Whey protein isolate (0.5)	70/58	
	α_s-casein (0.5)	Bovine serum albumin (0.5)	70/30	
	α_s-casein (4-6)	α-lactalbumin (2)+β-lactoglobulin (2)	70/5	
	α_s-casein (0.4)	γ-Crystallin (0.2)	UV-light	
Matsudomi et al. (2004)	α_s-casein (0.1-1) Dephosphorylated α_s-casein (0.1-1) β-casein (0.1-1) β-casein phosphopeptide (0.1-1)	Ovotransferrin (0.5)	80/20	10 mM Pi buffer, pH 7.0
	β-casein (0.5-1)	Alcohol dehydrogenase (1)	50/27	50 mM Pi buffer, pH 7.4
	β-casein (0.2-0.5)	Catalase (0.8)	60/27	
	β-casein (0.2-0.4)	Lysozyme (1)	37/20, DTT*	
	α_s-casein (0.5-5)	β-lactoglobulin (5)	70/480	50 mM Pi buffer, 0.1-0.2 M NaCl, 2.5 mM EDTA*, pH 7.1
Morgan et al. (2005)	α_s-casein (20)	apo α-lactalbumin (10)	25/120, DTT	50 mM imidazole buffer, 0.1 M NaCl, 5 mM $CaCl_2$, pH 7.1
	β-casein (0.0125-0.5)	apo α-lactalbumin (14.3)	37/25, DTT	
	κ-casein (0.0125-0.5)	apo α-lactalbumin (2)	37.360, DTT	
	α_s-casein (0.5-12)	holo α-lactalbumin (2)	37.360, DTT	
Thorn et al. (2005)	α_s-casein (1.88-11.25) β-casein (1.88-11.25)	κ-casein (3)	37.40, DTT	50 mM Pi buffer, 10 μM ThT* or 20 mM DTT, pH 7
O'Kennedy and Mounsey (2006)	α_s/β-casein (5) Micellar casein (1-5)	Whey protein isolate (5)	85/10	Simulated milk ultrafiltrate, pH 5.5-6.4
	α_{s1}-casein (1.4-8.5) β-casein (1.4-8.5)	α_{s2}-casein (1.4-8.5)	37-50/160, DTT	50 mM Pi buffer, pH 7.0
Khodarahmi et al. (2008)	Casein micelle (0.1-2)	Carbonic anhydrase (0.2)	25/5, GuHCl*	20 mM Tris-sulfate, pH 7.75

	β-casein (0.5-2)	Carbonic anhydrase (0.2)	25/6, GuHCl	
	Casein micelle (1) β-casein (1) α_s-casein (0.1-20)	Ovalbumin (1)	80/20	50 mM NaPi buffer, pH 7
Yong and Foegeding (2008)	β-casein (20) α_s-casein (20)+ β-casein (20)	β-lactoglobulin (60)	70-90/10-120	Deionized water, 1N HCl, pH 6.0
Barzegar et al. (2008)	β-casein (molar ratios of caseins/substrate are 0-3.3)	Alcohol dyhydrogenase (1.75 μM)	45-60/60	50 mM sodium phosphate buffer, pH 7.5
Guyomarc'h et al. (2009)	κ-casein (0-10) Sodium caseinate (0-50)	Whey protein isolate (0-25)	80/24 h	Distilled water, 0.1 M NaCl, 3 mM NaN_3, pH 7.0
	α_s-casein	α-lactalbumin (2)	37/360, DTT	2 mM EDTA and 0.1 M NaCl, pH 7.1
	β-casein	Ovotransferrin (0.5)	60/240	50 mM Pi buffer, pH 7.4
Koudelka et al. (2009)	Dephosphorylated α_s-casein	Alcohol dehydrogenase (1)	42/120	2 mM EDTA, pH 7.4
	Dephosphorylated β-casein (molar ratios of caseins/substrate are 0.5-3)	Reduced and carboxymetylated κ-casein (1)	37/20 h	50 mM Pi buffer, pH 7.4
Kehoe and Foegeding (2011)	β-casein (10)	β-lactoglobulin (50) α-lactalbumin (50) Bovine serum albumin (50)	80/20	In the absence or present of 10-20 mM NaCl or 5-10 mM $CaCl_2$, pH 6-6.5
He et al. (2011)	α_s-casein (0-6)	β-lactoglobulin (2)	400-800 MPa (5-60 min)	0.2 M Tris-HCl buffer, pH 7.0
(Hojati et al., 2018)	β-casein (molar ratio of casein/substrate are 0-1)	$A\beta_{1-42}$ protein (0.08)	37	Na_2HPO_4 bufferat pH 7.4
(Marciniak et al., 2018)	β-casein (0.219-1.75)	β-lactoglobulin (2.5)	600 MPa, 5 min	0.2 M Tris-HCl buffer at pH 6.6

(Chuang et al., 2019)	Sodium caseinate (0-2)	Hemp globulin (1)	90 (0-15 min)	50 mM sodium phosphate, pH 7
(Sanders et al., 2020)	β-casein (molar ratio of casein/substrate are 0.01-1)	α-lactalbumin (100 μM)	37/360, DTT	100 mM ammonium acetate, pH 7
(Gaspard et al., 2021)	Caseinomacropeptide (ratio of casein/substrate is 0.9	Whey proteins (25-100)	90/20	18 mM calcium chloride at pH 6.4 or 7.2

*Abbreviations are DTT: 1,4-dithiothreitol; EDTA: ethylenediamine tetraacetic acid; ThT: thioflavin T; GuHCl: guanidinium hydrochloride.

Nowadays, the chaperone activities of caseins are mainly attributed to their unique molecular structures. As with other well-characterized holdase chaperone proteins, such as sHsp (small heat-shock proteins) (Carver et al., 2003; Haslbeck et al., 2005), caseins contain regions that are dynamic, malleable, and flexible as a consequence of their unfolded conformation. When they are naturally self-aggregated as known as casein micelle, its porous structure with many water-field cavities and channels facilitates its interaction with, or binding to, a wide range of destabilized target proteins (Hanazono et al., 2012; Trejo et al., 2011). The chaperone actions of caseins are considered similar to that of sHsp and it is likely to involve the interaction of P,Q-rich sequences (Proline and Glutamine-rich, Table 1.6) in the caseins with exposed hydrophobic sequences in the partially unfolded target proteins (Holt et al., 2013).

However, this chaperone activity of caseins can be affected by the target protein, mode of aggregations (amorphous or fibrillar), buffer (*e.g*. pH) or stress conditions (*e.g*. temperature). For example, α_s-casein was found to be significantly better than β-casein at preventing the heat-induced aggregation of ovotransferrin (Matsudomi et al., 2004) or the reduction-induced aggregation of the insulin B-chain (Morgan et al., 2005). Whilst, β-casein is more effective than α_s-casein at inhibiting the heat-induced aggregation of catalase and the reduction-induced aggregation of lysozyme (Zhang et al., 2005). Moreover, both α_{s1}-casein and β-casein were found to be able to prevent the formation of fibrillar structures by α_{s2}-casein, κ-casein (Thorn et al., 2005), ovalbumin (Khodarahmi et al., 2008) and amyloid-β peptide (Carrotta et al., 2012). Besides, α_{s1}-casein seems to be more effective than α_{s2}-casein at inhibiting fibril formation by κ-casein (Thorn et al., 2008). pH has also been reported to be a major factor in the chaperone activity of caseins.

For instance, the chaperone activity of α_s-casein is higher at neutral than in more alkaline solutions (Morgan et al., 2005). O'Kennedy and Mounsey (2006) also observed higher chaperone activities of α_s/β-casein and casein micelle suppressing thermal aggregation of 0.5 wt% whey proteins (85 °C, 10 min) at pH ≥6 compared to that at lower pH values. Furthermore, investigated the effectiveness of β-casein as a chaperone in the heat-induced aggregation of whey proteins, and they found the maximum reduction in turbidity located at pH 6.0. Nevertheless, these findings do not actually mean that the caseins have their highest chaperone activity at pH 6.0 as these observations were based solely on the turbidity measurement, it could just because significantly turbidity of heated whey protein solution can only be found at pH ≤6.

Temperature is another well-known factor altering the chaperone activities of caseins. This factor being more interesting especially in the range of common thermal processing such as ≥72 °C for pasteurization or ~80 °C for HTST treatment. Previous research has shown that α_s-casein has a better chaperon activity than β-casein or κ-casein to prevent DTT-induced aggregation of insulin and its functionality increased as temperature increased from 25 to 37 °C, while its chaperone activity decreased at higher temperature to prevent DTT-induced aggregation of αLa (Morgan et al., 2005). Regarding thermal denaturation of whey proteins, α_s-casein was found to maintain its chaperone activity at 70 °C to inhibit aggregation of BLG (Morgan et al., 2005) or whey protein isolate (Bhattacharyya and Das, 1999). While when the temperature is higher than 75 °C, α_s-casein loses its chaperone-like activity, though β-casein is able to maintain its ability to inhibit thermal aggregation of BLG at temperature up to 90 °C (Yong and Foegeding, 2008). Based on this, if chaperone behavior of caseins also occurs during the thermal processing of milk, it is likely that β-casein plays a more dominant role as a molecular chaperone compared to α_s-casein despite its relative abundance in milk (Table 1.6). When casein is in its natural micellar structure, its chaperone-like behavior differs from that of individual caseins. For example, instead of inhibition, the presence of micellar casein during heating of whey proteins promotes the aggregation of whey proteins corresponding with an increase of total whey protein denaturation level (O'Kennedy and Mounsey, 2006). Despite this, the aggregation behavior of whey proteins was controlled by casein micelle as those obtained by use of α_s/β-casein resulting in smaller particle size of aggregates. Whilst, when using only α_s/β-casein, the denaturation of whey proteins was inhibited.

1.4 Mineral precipitations

Calcium phosphate precipitation

Mineral precipitation due to high temperature is another major contribution to fouling where more than 80% of the mineral fraction was found to be calcium phosphates (Lalande et al., 1984; Lyster, 1965; Skudder et al., 1981). Calcium phosphates in milk deposits were found to be a mixture of tricalcium phosphate ($Ca_3(PO4)_2$, TCP, Ca/P ratio = 1.5), dicalcium phosphate dihydrate ($CaHPO_4 \cdot 2H_2O$, DCPD, Ca/P ratio = 1.0) and octacalcium phosphate ($Ca_8H_2(PO4)_6 \cdot 5H_2O$, OCP, Ca/P ratio = 1.33), which at prolonger heating is eventually transferred to the least soluble calcium phosphate complex, hydroxyapatite ($Ca_5(PO4)_3OH$, HAP, Ca/P ratio = 1.67) (Visser and Jeurnink, 1997). This thermodynamically stable, microcrystalline HAP, initiated by a heterogeneous nucleation step, is typically formed when the heating temperature is sufficiently high. The formation of this spongy is preceded by a precursor phase, depending on the pH of the system. For example, at the pH of the milk (6.7), the precursor will be OCP, which is spherulitic in nature; whereas, at pH 5-6, it is either the structureless amorphous calcium phosphate (ACP) or brushite DCPD, which has a typical thin platelet crystalline structure (van Kemenade, 1988). This precipitation process of $\text{ACP} \rightleftharpoons \text{OCP} \rightarrow \text{HAP or DCPD}$ in moderate supersaturated calcium phosphate solutions is strongly dependent on the overall composition of the system and is affected by various additives. For instance, when low levels of magnesium or citrate ions are present, the crystal growth of OCP is retarded, and thus the conversion of ACP into HAP through OCP is inhibited (Brečević and Füredi-Milhofer, 1979). In the presence of caseins (*e.g.* α_{s1}/β-casein), the precursor phase (OCP) is stabilized through the mineral-protein bindings, and therefore, the formation of HAP is prohibited (Reynolds et al., 1982).

When a foreign material, *i.e.* the metal surface, is present as in the case of thermal processing of milk, calcium phosphate crystallization can occur upon the metal surface. Dey et al. (2010) demonstrated that the surface-induced crystallization of calcium phosphate starts with the aggregation of prenucleation ACP clusters. These clusters are formed in the bulk liquid which promote the subsequent growth of the ACP clusters on the surface. Dey et al. (2010) described this surface-directed mineralization of calcium phosphate in five different stages:

- Loose aggregation of prenucleation clusters in equilibrium with ions in solution

- Prenucleation clusters aggregate in the presence of the monolayer with loose aggregates still present in solution
- Aggregation leads to densification near the monolayer
- Nucleation of amorphous spherical particles only at the monolayer surface
- Development of crystallinity following the oriented nucleation directed by the monolayer

As a matter of fact, even in purely inorganic conditions, such as in the ternary system $Ca(OH)_2$-H_3PO_4-H_2O, eleven calcium phosphate compounds were identified with molar Ca/P varying from 0.5 to 2 (Tung, 1998). Consequently, considering a more complex system as in the milk (inorganic (*e.g.* presence of citrates) combined with organic (*e.g.* presence of whey or casein proteins)) as depicted in Figure 1.12, it is not surprising to imagine an intricate precipitation process of calcium phosphate. The deposition mechanism of calcium phosphate in milk not only depends on temperature gradients but is also affected by the presence of other inorganic compounds as well as the interactions between Ca^{2+}, PO_4^- ions with milk proteins. For example, it is suggested that calcium phosphate tends to associate with proteins during heating of milk rather than forming mineral particles in the bulk (Jeurnink et al., 1996b). Notice that around 70% of calcium is associated with casein micelle in the form as known as colloidal calcium phosphate, CCP. This native CCP bound in the casein micelle was considered to act as nucleation sites for the heat-precipitated calcium phosphate (Anema, 2009). In addition, the ion equilibrium in milk shifts with elevated temperatures by transferring the soluble calcium and inorganic phosphate to the casein micelle, with a concomitant decrease in pH within the first few minutes of heating.

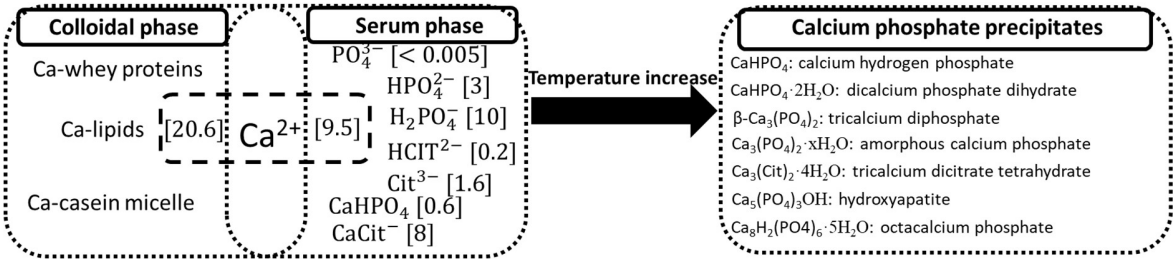

Figure 1.12. Calcium and inorganic phosphate equilibria in milk as well as various forms of precipitated calcium salts. The values in square brackets are concentrations of the specific ions in mM. The figure is modified from (Daufin and Labbé, 1998).

Effect of calcium on BLG denaturation and fouling

Apart from its precipitation behavior, calcium, or particularly ionic calcium, has recently been noted to play a predominant role in fouling. These results were obtained from casein-free whey protein solutions with additional ionic calcium (through Ca-rich tap water or $CaCl_2$), which means that the above-mentioned mineral balance by casein micelle is absent. Actually, before long, it has been recognized that the presence of calcium ions enhances the heat-induced aggregation of BLG (Haggett, 1976; Sherwin and Foegeding, 1997; Xiong et al., 1993). It was initially hypothesized that at least three effects, or a combination of them, are responsible for calcium-induced protein aggregation. The first effect is related to intermolecular cross-linking of adjacent negatively charged or carboxylic groups by forming protein-Ca^{2+}-protein complexes (Bryant and McClements, 1998; Hongsprabhas et al., 1999). The second effect is the intramolecular electrostatic shielding of negative charges on the protein (Hongsprabhas and Barbut, 1997). Both monovalent and divalent cations can act as counter-ions, while divalent ions are more effective at screening electrostatic interactions (Veerman et al., 2003). The third effect is ion-induced conformational changes, which lead to altered hydrophobic interactions and aggregation at elevated temperatures (Wang and Damodaran, 1991). However, observations from Simons et al. (2002) have ruled out the role of Ca^{2+} in the formation of intermolecular bridges, and they suggested that calcium was bound to carboxylates of BLG with a threshold affinity. Subsequent site-specific screening of surface charges resulted in protein aggregation, driven by the partial unfolding of BLG at elevated temeperatures, which was facilitated by the absence of electrostatic repulsion. Mounsey and O'Kennedy (2007) supported this idea by showing a reduction of zeta potential of BLG with increasing binding of calcium, and they suggested that Ca^{2+} can bind to BLG molecule at ambient temperature and thus producing a decrease in the surface charge: they found that increased binding of calcium reduced the apparent zeta potential of BLG to a minimum of -5 mV at neutral pH. This reduction of zeta potential of BLG during heating has also been observed in (Mounsey et al., 2008). The promoting effect of Ca^{2+} on BLG aggregation has been further proved by Petit et al. (2011) by investigating the effect of calcium on thermal denaturation kinetics of quasi pure BLG solutions (total protein $\geq$ 93.4 wt%) under various calcium concentrations. It was shown that the addition of calcium led to a significant increase in kinetic rate and more so in the aggregation-limited temperature range. Whilst, to a lesser extent, calcium has a slightly protective role on the unfolding step of BLG as shown by the increase in activation

energy. This idea was later confirmed for less pure whey protein solutions (total protein ≥ 80%) (Khaldi et al., 2018; Khaldi et al., 2015b). Recently, Peres de sa Peixoto Junior et al. (2019) investigated the molecular events leading to BLG unfolding and calcium-dependent aggregation by NMR. Their results also indicate a specific binding of calcium on the unfolded BLG species which might be a necessary feature to form protein aggregates.

Given these pieces of evidence of how calcium affects the thermal denaturation/aggregation of BLG, one could expect calcium can also play a role in the fouling behavior either by solely affecting the thermal denaturation of protein in the bulk or the build-up of the deposit on the metal surface or combined of both. Actually, the addition of Ca^{2+} has been found to facilitate the fouling growth of whey protein in a pilot plant PHE (Guérin et al., 2007). A spongy and soft texture of the deposit was observed at low calcium content (78 mg/L) whereas at higher calcium concentrations (86.5 mg/L), the deposits were denser and elastic. An explanation of the difference in structure is that, calcium ions lead to lower size aggregates with elevated calcium concentrations and favor the growth of fouled layer by formation of bridges between adsorbed proteins. This effect of calcium on deposit structure could be very similar to its role in the thermal aggregation of proteins. A similar effect of calcium on whey protein fouling was also observed by Khaldi et al. (2015a), and they suggested that Ca^{2+} form bridges between adsorbed proteins and those protein aggregates occurring in the bulk, consequently modifying the protein aggregation rate and leading to a greater cohesion between the protein aggregates which in turn, change the deposit structure (Phan-Xuan et al., 2013). Instead of absolute Ca content, Khaldi et al. (2018) demonstrated that the molar ratio of Ca/BLG was the key descriptor to controlling the whey protein fouling in PHE. Their experimental design was defined by varying the calcium/BLG molar ratio from 2.3 to 22.9 and fixing the total concentration of calcium at 100 ppm. They obtained a more extensive fouling at higher calcium/protein molar ratio (with less protein concentration) compared to low Ca/protein ratio even with high protein concentration. This finding is in accordance with Mounsey and O'Kennedy (2007) as they suggested that a significant reduction in surface charge was required to achieve maximal precipitation of the denatured protein which was correlated with the calcium/protein stoichiometry. Furthermore, Jimenez et al. (2013) used various techniques including Electron-Probe Micro Analysis (EPMA), Time-of-Flight Secondary Ion Mass Spectrometry (ToF-SIMS), Atomic Force Microscopy (AFM) and X-Ray Photoelectron Spectroscopy to monitor the whey protein fouling deposit with the prescence of Ca^{2+}. They

suggested that fouling mechanisms are initiated by the deposit of unfolded proteins on the substrate and start immediately till the first seconds of exposure with no lag time. When calcium was present (absence of phosphate), amorphous calcium carbonate nuclei was detected and act as achoring-point for unfolded proteins to depose.

However, if phosphate is present, the total fouling mass decreased dramatically regardless of the presence of calcium content (Christian et al., 2002). Another recent research from Blanpain-Avet et al. (2020) revealed more details on the role of phosphate on whey protein fouling when calcium is present. Their results confirmed a substantial role of phosphate/calcium molar ratio on whey protein fouling by dramatically suppressing the BLG aggregation behavior in the bulk as well as decreasing the amount of fouling deposit through a decreased reactivity of the unfolded proteins with elevated P/Ca ratio. Both Ca and calcium phosphate complexes were identified in the deposits, but the contribution of ionic calcium and calcium phosphate to the deposit build-up was considered probably through different mechanisms. A further study from Scudeller et al. (2021) suggested that phosphate acts as a calcium chelator, and two different fouling mechanisms were recognized depending on the amount of added phosphate. When P concentrations were lower than 20 ppm, the chelator effect of phosphate was not exhaustive enough to change the fouling behavior, and the deposited layer became progressively less compact and gave rise to a more voluminous protein/mineral deposit without any contribution of CaP clusters. It was assumed that the protein charge screening effect by Ca^{2+} was reduced, favoring the repulsion between proteins inside the deposit, and thus resulting in a more open structure. When phosphate content is higher than 20 ppm, there was sufficient P to chelate calcium ions and a reduction of total fouling mass was observed. It was hypothesized that fouling build-up starts from a CaP layer, which is concentrated close to the steel surface. In this case, there could be less CaP in the bulk, and by lack of binding agent as CaP, the overall fouling was mitigated. This effect of calcium chelators on whey protein fouling was also reported in a laboratory scale as in (Hebishy et al., 2019) where trisodium citrate, tripotassium citrate and disodium hydrogen phosphate were all shown to improve the thermal stability of whey proteins. These calcium chelators subsequently improved the heat transfer during thermal processing and resulted in lower viscosity and less fouling. Kindly remind that all these results mentioned above concerning the effect of ionic calcium content on fouling were obtained in the absence of caseins. With the presence of caseins, the fouling story could be wholly different due to their capacity on the mineral balance between the serum and colloidal phase.

1.5 Overall fouling mechanisms & Influencing factors

As described in the previous section, dairy fouling is undoubtfully an intricate, multi-dependent process involving thermal denaturation of proteins in the bulk fluid and subsequent aggregation depending on present protein species, mineral precipitations due to high temperature, salts population balance as well as complicated protein-mineral interactions. Under decades of studies, dairy fouling was considered to consist of several consecutive or concomitant sub-processes:

- **Bulk reaction** (thermal denaturation/aggregation of dairy proteins, mineral sub-nucleation);
- **Mass transfer** (transport of the activated materials to the fluid-metal interface);
- **Induction** (first deposition of the foulant on the substrate);
- **Build-up** (fouling growth based on the pre-fouled deposit layer);
- **Ageing** (internal reactions of deposit layer after fouling occurs).

In whatever conditions, before a protein or mineral molecule can adhere to a solid surface, it must arrive at the surface through transportation by mass convention in the bulk and then diffuse through the boundary layer. When these particles are within the immediate vicinity of the surface, long-range attractive forces such as van der Waals and electrostatic forces are responsible for "bringing" them upon the surface. Once this intimate contact between the particle and the surface has been attained, short-range forces such as chemical or hydrogen bonding might take place (Bott, 1995). The adhesion of macromolecules, such as proteins or polysaccharides upon a metal surface can be more complex compared to the case of small solids or colloidal particles (Lund and Sandu, 1981). The adsorption of a protein can be affected by the properties of the surface, such as surface free energy, roughness or electrochemical/electrostatic potential, as well as the solution conditions, including composition and ionic strength. Besides that, since proteins comprise different amino acids with various reactive groups, they can interact with the surface in different manners. For example, as introduced in section 1.3.1, the adsorption of BLG molecule upon the steel surface mainly through its peptide fragments containing acidic residues (*e.g*. Glutamic acid or Aspartic acid). These active groups of protein, once attached to the surface might induce local unfolding of the protein structure and rearrange its orientation on the surface (Chandrasekaran et al., 2013). If the adsorped proteins expose their reactive groups to the fluid, further protein-protein

intermolecular reactions can occur either via non-covalent (electrostatic interactions or hydrophobic interactions) or covalent bonds such as intermolecular –SH/S-S interchange reactions, leading to the formation of protein aggregates on the surface or forming a protein multilayer.

Since both proteins and minerals can absorb upon the steel surface, which deposits first during fouling has long been under debate. This question could be of vital importance especially for the cleaning concern as it determines the strength of the deposit-surface bond: once this first deposit layer was fouled, the deposit-deposit interaction rather than deposit-metal interaction will be the most significant factor (Brassart, 1990). It has been suggested that the first layer of the deposit is largely mineral (mostly calcium phosphate) (Foster et al., 1989; Tissier and Lalande, 1986). The analysis of thick deposits has suggested that minerals appear to form most of a thin (< 5 μm) layer of deposit immediately adjacent onto the wall (Tissier and Lalande, 1986), and there is some evidence that this deposit forms rapidly after less than 10 min (Daufin et al., 1987). Further analysis of deposit material *in situ* has been conducted using X-ray micro-analysis of deposits near the interface between the stainless steel and the fluid, showing that the mineral content increases with the depth of the deposit and the mineral content is greatest near the stainless steel surface (Belmar-Beiny et al., 1993). However, these analyses must be interpreted with caution, since the deposit was analyzed after fouling for an extended period, it is possible that the protein deposits first and some soluble minerals such as calcium phosphate diffuse through the deposited matrix during ageing and crystallize near the metal-fluid interface. This idea was confirmed by Belmar-Beiny and Fryer (1993) by performing X-ray photoelectron spectroscopy analysis on the whey protein deposits. Their results revealed that a first layer consisting mainly of proteins was formed within 4 seconds. In addition, only after 150 s of contact time, the signal of calcium was detected, however, it was only found on the top of the deposit; after 60 min contact time, both Ca and P were found at the interface between the deposit and the stainless steel surface. A more recent research from Jimenez et al. (2013) further supports this idea. By using 3D reconstructed ToF-SIMS (Time-of Flight Secondary Ion Mass Spectrometry), they found that calciums are mainly concentrated in the upper side of the grain bounday of the steel substrate while proteins were homogenously present both on the steel surface and grain boundaries after one minute fouling. They suggested that these calcium particles could be possibly trapped inside the protein layer before going further inside, and thus the protein layer would be the first one being deposited during fouling.

Although the existence of these five fouling sub-processes receives a universal agreement, their relative importance has been debated. The main discrepancy lies in whether bulk reaction, mass transfer or surface reaction (or all of them) is/are the limiting step(s) in the fouling process. Despite this, most experimental evidence seems to support that the bulk reaction is one of the essential steps. For example, Jeurnink et al. (1996a) measured whey protein denaturation and fouling behavior upon a chromium oxide surface using reflectometry and they found that deposition rather than absorption of a monolayer requires the presence of activated BLG molecules near the surface. And if the protein solutions were at ambient temperature, no deposition was observed (only monolayer, *i.e*. absorption) even though the surface was hot (*e.g*. 85 °C). Furthermore, if the proteins were pre-heated to induce a fully denaturation/aggregation, deposition was markedly reduced. In addition, also observed a strong correlation between the reaction kinetic constant ratio of unfolding and aggregation (*i.e*. k_U/k_A) with deposition mass. If this ratio is high, there would be more activated or unfolded BLG molecules to depose; whereas if this ratio is low, aggregation is more dominant, resulting in a lower amount of unfolded BLG species and thus less fouling. This correlation between the thermal denaturation behavior of whey proteins in the bulk and the total fouling was also shown in a pilot plant PHE (Blanpain-Avet et al., 2016; Bouvier et al., 2014; De Jong et al., 1992). Blanpain-Avet et al. (2012) also supported this by analyzing whey protein deposit using micro Raman spectroscopy (MRS) where loss of α-helix structures was detected as observed in unfolded BLG molecules without the detection of aggregates signatures.

Based on this complex frame of fouling behavior, it is no surprise why there are numerous influencing factors on fouling. These factors can be classified into three main categories, namely (i) the processed product composition and characteristics (*e.g*. protein composition, pH, etc), (ii) operating conditions (*e.g*. flow rate, temperature, etc), and (iii) surface properties (*e.g*. surface roughness, surface energy, etc). Some of the main influencing factors are summarized from the literature as shown in Table 1.8. Two recent reviews can be read for learning more on the way to mitigate fouling by acting on surface properties but it is not our concern here (Almeida et al., 2021; Saget et al., 2021). Again be aware that these results were not established with similar milk derivatives (most of them handled whey protein solutions which were casein-free).

Table 1.8. Summary of the influencing factors on dairy fouling from literature (Boxler, 2014).

Influencing factors	Effect on fouling	Remarkable observations	References
Whey protein concentration (↑)	+++	a maximum was found at solids concentration of 25 wt%	(Jeurnink, 1995a; Jeurnink et al., 1996b; Kessler and Beyer, 1991)
Protein composition (↑)	++	Whey proteins induce more fouling than milk or pure BLG solutions	(Daufin et al., 1987; Jeurnink et al., 1996a; Robbins et al., 1999)
Fluid type	-	Recombined or reconstituted milk generally has less fouling than fresh milk	(Jeurnink, 1995b; Srichantra et al., 2006; Srichantra et al., 2018)
pH (↑)	--	Reduction of pH generally induces more fouling while an increase of pH mitigates fouling	(Burton, 1968; Foster et al., 1989; Gordon et al., 1968; Hegg et al., 1985; Jeurnink et al., 1996b; Kastanas et al., 1995; Skudder et al., 1986)
pH (↓)	+++		
$[Ca^{2+}]$ (↑)	+++/-	Either increasing or decreasing the calcium concentration in the milk leads to lower heat stability and more fouling. While in the absence of casein, calcium consistently facilitates fouling	(Christian et al., 2002; Guérin et al., 2007; Jeurnink and Dekruif, 1995; Khaldi et al., 2015a; Khaldi et al., 2018)
Surface or processing temperature	+++	Enhance thermal denaturation of whey proteins as well as mineral precipitations	(Boxler et al., 2013; Burton, 1968; Daufin et al., 1987; Hegg et al., 1985; Petit et al., 2013)
Flow rate or Reynolds number (↑)	-	Increased shear stress hence favors the removal of fouling layer	(Belmar-Beiny et al., 1993; Gordon et al., 1968; Guérin et al., 2007)
Flow rate or Reynolds number (↓)	+	Increased mass transfer coefficient thus facilitates a more compact deposit	(Khaldi et al., 2015a; Santos et al., 2006)

Residence time (↑)	+	More time available for protein denaturation and deposition reactions	(Daufin et al., 1987; Gordon et al., 1968; Petit et al., 2013)
Entrained air (↑)	++	Air bubbles cause super-saturation conditions at the triple interface	(Gordon et al., 1968; Jeurnink et al., 1996b)
Pressure (↑)	-	Degassing of milk may cause an increase of pH	(Jeurnink, 1995a; Jeurnink et al., 1996b)
Surface roughness (↑)	+	Entrapment of soil in the crevices and greater surface area	(Gordon et al., 1968)

↑ = increasing parameter, ↓ = decreasing parameter, + = more fouling, - = less fouling.

1.6 Fouling models

Fouling characteristics

Tremendous researchers have devoted themselves to the development of computational models of heat exchangers to simulate dairy fouling (Changani et al., 1997; Jun and Puri, 2005b). The implementation of an adequate model will help to optimize the process to obtain both the best operating and efficient technical (direct or indirect heating) conditions that minimize undesirable side effects associated with heating such as fouling (Fillaudeau and Ghnimi, 2014; Fillaudeau et al., 2006; Ghnimi et al., 2014). An adequate understanding of the chemistry and fluid mechanics is the prerequisite to accurately predict and analyze fouling dynamics. Fouling is a transient process; the exchanger starts clean and becomes fouled. One of the critical issues of fouling is its negative effect on the heat transfer behavior with a concomitant increase of the thermal resistance. Figure 1.13 illustrates the various resistances to heat transfer encountered as heat flows from a heating medium (*e.g*. hot water) to the process fluid (*e.g*. milk) and the accompanying temperature drops due to the presence of fouling layers. Assuming a constant heat transfer rate and a formation of a uniform fouling layer, the heat flow for parallel plates in a steady state condition can be given by:

$$\dot{Q} = h_w A(T_w - T_{ws}) = \frac{\lambda_{ss}}{\delta_{ss}} A(T_{ws} - T_{sd}) = \frac{\lambda_d}{\delta_d} A(T_{sd} - T_d) = h_p A\left(T_d - T_p\right) \quad \text{(eq. 1.8)}$$

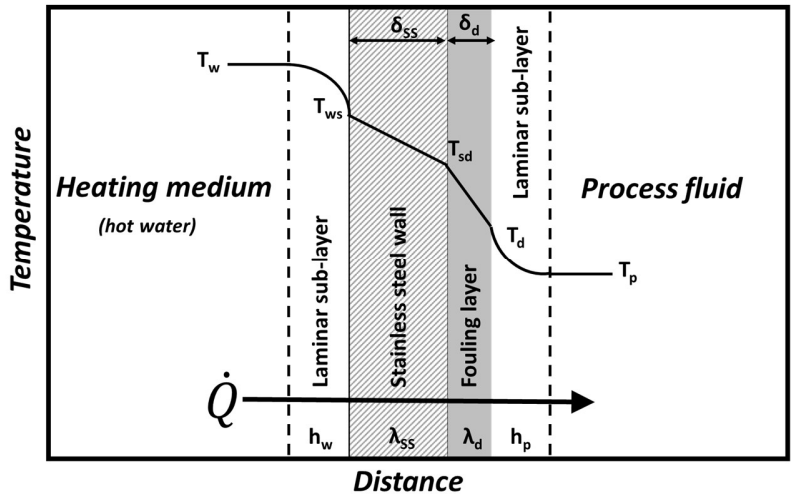

Figure 1.13. Temperature distribution across fouled heat exchanger surface. Note the scaling in the hot water side is ignored.

The overall temperature driving force, or $T_w - T_p$, is typically combined with an overall heat transfer coefficient U_f to describe the heat flux as:

$$\dot{q} = U_f(T_w - T_p) \quad \text{(eq. 1.9)}$$

where the reciprocal of U_f represents the overall heat transfer resistance R_T as a sum of the individual resistances:

$$R_T = \frac{1}{U_f} = \frac{1}{h_w} + \frac{\delta_{SS}}{\lambda_{SS}} + \frac{\delta_d}{\lambda_d} + \frac{1}{h_p} \quad \text{(eq. 1.10)}$$

Therefore, the thermal impact of the fouling layer R_f can be expressed in terms of the fouling resistance which is defined by the difference between the thermal resistance of the fouled and clean plates:

$$R_f = \frac{1}{U_f} - \frac{1}{U_{clean}} \quad \text{(eq. 1.11)}$$

If one assumes a uniform coverage of fouling layer upon the metal surface and a constant thermal conductivity and density of the deposit, the fouling mass coverage m_f is directly proportional to R_f:

$$R_f = \frac{\delta_d}{\lambda_d} \; and \; m_f = \delta_d * \rho_d = \lambda_d * R_f * \rho_d \quad \text{(eq. 1.12)}$$

However, given that the fouling layer distribution on the surface is seldom uniform, also the density ρ_d or thermal conductivity λ_d can also vary during ageing (Davies et al., 1997; Knudsen, 1981), equation 1.12 is rather an ideal assumption.

Instead of using thermal resistance R_f, a dimensionless local fouling factor Bi, also known as Biot number, is another important fouling characteristic:

$$Bi = \frac{h_f * \delta_d}{\lambda_d} \quad \text{(eq. 1.13)}$$

With definition of a proportion factor φ:

$$\varphi = h_p\left(\frac{1}{h_w} + \frac{\delta_{SS}}{\lambda_{SS}}\right) \quad \text{(eq. 1.14)}$$

The overall heat transfer coefficient U_f and Biot number Bi can be correlated as:

$$\frac{1}{U_f} = \frac{1+\varphi+Bi}{(1+\varphi)U_{clean}} \quad \text{(eq. 1.15)}$$

In a scenario with a constant metal surface temperature (*i.e.* constant T_{sd}) such that φ becomes negligible, equation 1.15 can be rewritten in a dimensionless pattern:

$$\frac{U_{clean}}{U_f} = 1 + Bi \quad \text{(eq. 1.16)}$$

And therefore,

$$Bi = R_f * U_{clean} \quad \text{(eq. 1.17)}$$

In most cases, the deposition is simultaneously accompanied by a removal process which is determined by the adhesion forces inside deposits and the shear stress from the fluid mechanics. Based on this, Kern and Seaton (1959) proposed that the net fouling rate of the fouling layer comprises two competing processes, *i.e.* the deposition growth $\dot{m}_d$ and removal $\dot{m}_r$:

$$\frac{dm_f}{dt} = \dot{m}_d - \dot{m}_r \quad \text{(eq. 1.18)}$$

The progress of a fouling process can be described by a plot of thermal fouling resistance against time. There are three typical fouling characteristic curves, namely linear, falling rate and asymptotic fouling as depicted in Figure 1.14. In a linear fouling scheme, the deposition proceeds at a constant rate with a negligible removal process or the deposition and removal rates have a

constant difference. For a falling rate fouling, the increasing rate of fouling thickness slows down as fouling evolves; this scenario is more typical when fouling is severe resulting in a higher flow rate and therefore stronger shear forces. In asymptotic fouling, there is a steadily decreasing difference between deposit formation and removal, in which the difference approaches zero and the fouling resistance or growth reaches a steady state. There may be an induction period during which conditions do not change significantly, followed by a fouling period during which heat transfer coefficient decreases and the pressure-drop increases. Despite this, most mathematical models failed to predict the extent of the induction phase, and therefore it is generally ignored (Fryer and Slater, 1985), *i.e.* fouling begins as soon as fluid flows through the heat exchange, and most attempts have been made to develop the generalized models for the fouling period (Bott, 1995).

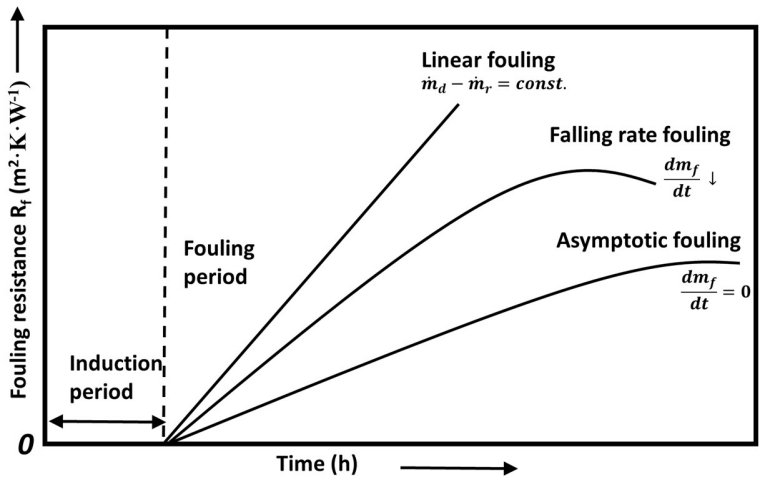

Figure 1.14. Possible ways in which the fouling resistance can evolve with time.

One-dimensional fouling models

Historically speaking, earlier works on fouling modeling consider only one or two protein species, *i.e*. only one-directional molecular breakdown of native protein exists as a function of temperature without (only adhesion mechanism is considered) or with considering the removal process (adhesion/removal mechanisms are simultaneously considered). For example, Delplace et al. (1994) performed a milk fouling simulation in the PHE with a complex flow arrangement consisting of 13 plates. They successfully simulated the quantity of denatured BLG in each channel of PHE with the numerical determination of temperature profiles. Their work was based on a

second-order BLG denaturation kinetic model proposed by Lyster (1970) (eq. 1.19), and was able to predict the native BLG concentration at the outlet of PHE with an error of less than 10% compared to the experimental measurement using an immunodiffusion method. Using the same denaturation kinetic model for BLG, Fryer et al. (1996) studied the effect of fouling on both pressure-drop and heat transfer coefficient (and also Biot number) as a function of several variables, including protein concentration, flow rate and the amount of reacted BLG within each section inside a plate heat exchanger under UHT processing. Changes in both heat transfer and pressure-drop could be correlated in terms of the local reaction rate of BLG, and change in Biot number was shown to be significantly affected by the amount of protein reacted and to a lesser extent by the flow rate.

$$C(t) = \frac{C_0}{1 + kC_0t}$$

$$log_{10}k = 37.95 - 14.51\left(\frac{10^3}{T}\right) \qquad T \leq 363.15\ K \qquad \text{(eq. 1.19)}$$

$$log_{10}k = 5.98 - 2.86\left(\frac{10^3}{T}\right) \qquad T \geq 363.15\ K$$

where $C(t)$ is the concentration of native BLG at time t (kg·m^{-3}), C_0 is the initial native BLG concentration (kg·m^{-3}), and k is the second-order rate constants depending on temperature T (K).

To further correlate BLG denaturation with total fouling deposit, Delplace and Leuliet (1995) studied milk fouling of several PHE flow arrangements by measuring both the heat transfer coefficient and dry mass of the deposit. They observed a linear evolution of deposit mass with time in the plate heat exchanger channels. It was found that only a small fraction of denatured BLG was involved in deposit formation (Delplace et al., 1997). The relation between deposit mass and the volume of fluid hot enough to produce denatured and aggregated proteins, proposed by Belmar-Beiny et al. (1993), was used to develop an empiric model. The dry mass of deposit md_i in a channel i was proportional to the native BLG concentration difference between inlet and outlet (ΔC_i, kg·m^{-3}) using the method of Lalande and Tissier (1985):

$$\frac{md_i}{s\bar{V}_i} = 0.127\Delta C_i^{0.5} \qquad \text{(eq. 1.20)}$$

where $\hat{V}_i$ accounts for the volume of fluid processed and S is the surface area of different plate geometries. This model was an attempt to correlate fouling mass with thermal denaturation behavior of BLG, although it was irrespective of Reynolds number or flow arrangement, it predicted dry mass of deposit in each channel within 20% accuracy.

In models where the deposit removal induced by shear forces is also included, Fryer and Slater (1985) developed a local fouling rate model based on the local temperature distribution (eq. 1.21). The concept is that, as introduced by Kern and Seaton (1959), deposited solids may be re-entrained from the fouled layer into the fluid by attrition to account for asymptotic, equilibrium fouling. The net rate of solid accumulation for chemical reaction fouling is the difference between the rate of solids deposition and that of re-entrainment attributed to fluid shear forces.

$$\frac{dBi}{dt} = k_d(\tau_w) \exp\left(-\frac{Ea}{R}\frac{1+\varphi+B}{T_w+(\varphi+Bi)T_p}\right) - k_r(\tau_w)Bi \qquad \text{(eq. 1.21)}$$

where k_d and k_r are the rate constants for solid deposition and re-entrainment, respectively. τ_w is the wall shear stress, and Ea is the activation energy. R is the universal gas constant (*i.e.* 8.314 $J \cdot K^{-1} \cdot mol^{-1}$). This model was successfully scaled up to solve a complex industrial fouling problem (Schreier and Fryer, 1995).

In more advanced fouling models, some of concomitant sub-processes are taking into account such that the multi-step thermal denaturation of BLG (bulk reaction) and deposition of BLG (surface reaction) are all considered. For example, De Jong et al. (1992) and De Jong (1996) described thermal denaturation of BLG as a two-step consecutive reaction, including unfolding and aggregation as equation 1.3b (section 1.3.3). Several ordinary differential equations were applied to describe a homogeneous bulk reaction:

$$-\frac{\partial C_N}{\partial t} = k_U C_N$$

$$\frac{\partial C_U}{\partial t} = k_U C_N - k_A C_U^2 \qquad \text{(eq. 1.22)}$$

$$\frac{\partial C_A}{\partial t} = k_A C_U^2$$

where C_N, C_U and C_A are the protein concentrations of native, unfolded and aggregated BLG, respectively. k_U and k_A are the reaction kinetic constants for the unfolding and aggregation step,

respectively. The deposition or the surface reaction was described as adsorption of the unfolded BLG specie:

$$J_f = k_D C_U^{1.2}$$

$$k_i = k_{0i} \exp\left(-\frac{Ea_i}{RT}\right), i = N, U, A, D \quad \text{(eq. 1.23)}$$

where D is the deposition of unfolded BLG, J_f is the fouling rate and Ea is the activation energy for corresponding reactions. This fouling model is available for both skim milk or whole milk to predict both the thermal denaturation of BLG and deposit distribution in the heat treatment equipment (De Jong et al., 1993). The kinetic parameters for denaturation of BLG and deposition can be found in (Dannenberg and Kessler, 1988; De Jong, 1996). This model was also applied and adopted by Petermeier et al. (2002), where the loss of unfolded BLG due to deposition was also considered in the bulk reaction.

It is clear that in de Jong's model, the fouling was only caused by BLG protein deposition, and particularly the unfolded BLG specie was taken as the fouling precursor. Toyoda and Fryer (1997) extended the work of de Jong, and they assumed that for each protein present, mass transfer takes place between the bulk and the thermal boundary layer. The major difference in their model is that only aggregated BLG can adhere to the wall in such a way that the amount of deposition is proportional to the concentration of aggregated proteins in the thermal boundary layer. The assumptions for the reaction/mass transfer scheme are as follows (shown in Figure 1.15):

- Proteins react in both the bulk and the thermal boundary layer in fluid milk. Native BLG (N) is transformed to the unfolded form (U) in a first-order reaction. The unfolded BLG then forms aggregates (A) in a second-order reaction.
- Mass transfer between the bulk and thermal boundary layer takes place for each protein.
- Only aggregated protein is deposited onto the wall. The rate of deposition is proportional to the concentration of aggregated protein in the thermal boundary layer.
- The fouling resistance to heat transfer is proportional to the thickness of the deposit.

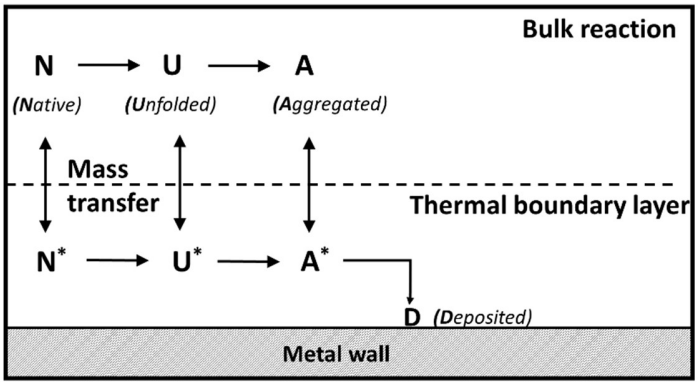

Figure 1.15. Fouling model from Toyoda and Fryer (1997).

Based on this fouling scheme, Georgiadis et al. (1998a) and Georgiadis and Macchietto (2000), presented mathematical modeling for complex PHE arrangements subjected to milk fouling by adapting a plug flow model with axial convention and radial dispersion effects. All the important factors affecting milk treatment were formally quantified. Note that the terms that represented the diffusion phenomena according to Fick's law were first introduced into the mass balance equations of Toyoda and Fryer (1997). The developed fouling model was coupled with a detailed dynamic model of a shell-and-tube heat exchanger where both radial and axial domains were taken into account (Georgiadis et al., 1998b). The two above-mentioned diverse fouling approaches, though ignore the role of minerals on fouling, were both successfully validated by the respective experimental data.

Two/Three-dimensional CFD fouling models

So far, the above fouling models were based on one-dimensional (1D) flow distribution for model simplification, which could hardly consider the effect of plate corrugations. Since the hydrodynamic performance of the fluid flow is mostly governed by the corrugation geometry in plate heat exchangers, the predictive errors of the fouling model can be minimized using computational fluid dynamics (CFD) in two-dimensional (2D) or even there-dimensional (3D), which has the potential to take into account the detailed geometry of the plates. Up to date, there have several 2D or 3D simulation models developed to target precise prediction of flow and temperature profiles in the channel of plate heat exchangers.

For instance, Grijspeerdt et al. (2003) carried out a detailed calculation of the flow pattern of milk between two corrugated plates using commercial 2D and 3D CFD models. The 2D calculation

showed the influence of the corrugation shapes, and the 3D calculation was necessary to assess the importance of the corrugation orientation. Besides, Jun et al. (2004) also compared the thermal performance of PHE using conventional 1D model and 2D dynamic model. The 1D model, which was based on unidirectional, constant velocity flow, showed limited predictive accuracy for the experimental data and was dependent on the flow characteristics. Whilst, the 2D model, which took into account the hydrodynamics of the flow system, was capable of predicting the temperature distribution of the fluid flow with an average 6.2% deviation, irrespective of the flow pattern. Later on, Jun and Puri (2006) extended their 2D model to couple with the material balance equations which was able to predict the localized distribution of milk deposits in multichannel PHEs. The Navier-Stokes equations for flow dynamics were solved and then coupled with the energy balance equation and three-phase fouling kinetics. Modification of Georgiadis and Macchietto (2000)'s work was implemented for the conservation of protein mass balances over the whole process. The predicted fouling distribution and amount of milk deposits in each channel were in good agreement with the past work of Georgiadis and Macchietto (2000), in addition to providing a realistic picture of fouled plates. Similarly, Mahdi et al. (2009) proposed a 2D dynamic milk fouling model in a 12-channel PHE for fouling prediction based on the hydrodynamic and thermodynamic performances of the PHE. It was found that an exponential increase in protein aggregation according to the increase of wall temperature results in a significant decrease in heat transfer coefficient. Bouvier et al. (2014) also performed a 2D CFD model to simulate the thermal unfolding and aggregation of BLG in a plate heat exchanger. Satisfactory agreements were reached between the denaturation level obtained by CFD and that obtained experimentally at the outlet of the PHE for both pure BLG and whey proteins solutions. The deposition mass distribution along the PHE channel correlated well with the unfolded BLG species, supporting the unfolded BLG species as the fouling precursor as De Jong et al. (1992) but his model did not mimic deposit installation onto surface. More recently, Pan et al. (2019) conducted a numerical simulation of milk fouling in a simplified heat exchanger in 2D environment. Of interest, the structural evolution of the fouling deposit was taken into account such that the dynamic contribution of the fouling layer to the momentum, heat transfer or bulk chemical reactions were considered.

Compared to 2D model, the 3D model can permit not only the consideration of the corrugation profiles of plates but also the design of plate geometry for the enhancement of PHE performance in terms of fouling. Jun and Puri (2005a) performed a fouling model for milk pasteurization in a

10-channel PHE system in a 3D environment using CFD. The chemical reaction equations employed for protein denaturation and absorption on the stainless steel surface were coupled to yield a satisfactory prediction of deposit mass with an error of 1%. This model was also used to simulate milk fouling behavior in a new PHE system which was designed for the uniformity of flow distribution. It was shown that the deposit mass could be reduced by 10% compared to the conventional PHE system under identical energy conditions. A 3D CFD model was also shown to have the capacity to estimate antifouling performance of a modified surface. For instance, Choi et al. (2013) simulated milk fouling and temperature distribution patterns on realistic corrugated surfaces of PHE unit with different surface treatments (*e.g.* coated with Lectrofluor 641 and Ni-P-polytetrafluoroethylene). Their simulation results were close to the experimental data within a maximum prediction error of 7%. Despite these advantages, due to the tremendous computing resources required for 3D model, the development of 3D fouling model would inevitably incur a cost penalty that must be balanced against the advantage of being able to predict the milk fouling close to reality.

Other fouling models

To reconcile these pitfalls of CFD-based fouling models, by integrating the basic model of Georgiadis et al. (1998b), Guan and Macchietto (2018) proposed a novel 2D moving boundary model where the fouling fluid flows in a channel delimited by two hot plates and the deposit may grow independently on each plate according to local conditions. In this model, the dynamic evolution of deposit thickness was simulated by fitting a proportionality constant β to data as:

$$\frac{d\delta}{dt} = \beta \frac{\lambda_d}{h_f} k_d C^n - k_\tau \delta \qquad \text{(eq. 1.24)}$$

where C is either the aggregated BLG concentration or the denatured BLG concentration, depending on the fouling precursor assumptions. And if the re-entrainment is not considered (ignores fouling removal), the $(-k_\tau \delta)$ is removed from the equation 1.24. Although this model adequately predicted the distribution of deposit along the plates, it was solely modeled for one single PHE channel. This model was thereafter extended by Sharma and Macchietto (2019) to enable the modeling of full PHEs with multiple plates arranged in two different configurations. Four fouling models were used to assess the deposit growth: two deposition mechanisms (assumed

either aggregated or denatured BLG as the fouling precursor) each with/without considering deposit re-entrainment effect. Their results were validated for all PHEs arrangements against experimental results, however, no single model was found capable of describing all arrangements. Worth mentioning in this model is that, the cleaning of fouled surfaces was also integrated, enabling the first time in the literature for the simulation of CIP (Cleaning-In-Place) procedures, establishing the duration of cleanings, and the seamless simulation of entire single and multiple heating-CIP cycles. This model was further elaborated to be more general, modular and versatile, and was applied to model a full heating-cleaning cycles for an overall unit with both HTST and UHT treatments (Zhu et al., 2020). By coupling fouling and cleaning, this model can be potentially used to optimize the overall operation, considering complex trade-offs between energy for heating, use of cleaning agents and rinsing water for CIP, downtime due to cleaning and cycle length (Sharma and Macchietto, 2021).

Other researchers tended to seek another way to model this intricate fouling phenomenon, for example, by using dimensional analysis (DA) to identify the key dimensionless numbers governing fouling during heat treatment. For instance, Khaldi et al. (2015a) used DA to correlate locally deposited mass collected in the last four channels of the plate in the PHE with various parameters, including geometry, physical properties (particularly calcium concentration) and processing parameters (*e.g.* velocity, fluid temperature). Their experiments were performed in a pilot plant PHE system with whey protein solutions under various Reynolds numbers (2000, 3200 and 5000), temperatures (77-97.1 °C), calcium content (70-87.5 $mg \cdot L^{-1}$) and showed a close agreement with the DA-predicted results with an accuracy of ± 20%. Furthermore, Petit et al. (2013) used DA approach to predict the BLG denaturation level, aggregation size and fouling mass using quasi-pure BLG solutions in a pilot-scale PHE under various processing parameters. Of great interest, the BLG denaturation and aggregation were taken into account by considering the thermodynamic parameters corresponding to these two subreactions (*i.e.* pre-exponential factors of reaction and activation energies for unfolding/aggregation). Again, their results showed a general satisfaction compared to experimental values with mean relative errors less than 25%. Recently, Gu et al. (2019) used DA to predict the total fouling mass in a pilot-scale PHE, covering a series of variables including whey protein solution concentration (2.5-25 g/L), calcium concentration (70-120 ppm), running time (90-330 min), flow rate (200-500 L/h), total fouling surface area, outlet temperature (82-97 °C) and differences in whey protein concentrate powders. Two dimensionless numbers

were identified as key parameters involved in the fouling growth: the Reynolds number (2000-5000) and calcium to BLG molar ratio (2.7-34.7). Other models based on data-intensive and mechanistic-model-poor techniques such as neural networks or machine learning are also starting to emerge (Escrig et al., 2020; Kwak et al., 2020; Rosa et al., 2019; Sundar et al., 2020; Tang et al., 2020).

From state of the art, it has been demonstrated that the structure of the models are greatly progressed to integrate the major molecular events responsible for fouling; meanwhile the increase of computational ability also allows to consider an increasing number of factors influencing fouling. However, it is worth mentioning that, the current drawback of the above-mentioned diverse fouling approaches is the fact that they generally ignore the role of minerals or caseins although they were all successfully validated by the respective experimental data. The use of Arrhenius law for deposition reaction is another point widely admitted but never discussed whereas no evidence is fully established. Another weakness of these models is that, most experimental validations are based on kinetic denaturation data extracted from the literature where the fouling solutions could vary significantly (*e.g.* fresh milk vs reconstituted milk from powder, with or without the presence of casein, different protein/salt/sugar concentrations, etc). Therefore, these data must be used with careful caution as the fouling has been confirmed to be extremely dependent on the type of milk derivative solutions (Jeurnink, 1995b; Srichantra et al., 2006; Srichantra et al., 2018).

1.7 Bench-top fouling devices

Most fouling experiments are performed in an industry-scale as those in pilot plant PHEs; those results obtained from PHE are valuable in an aspect of the industry, however, it can be somehow undesired as it is both time-consuming and energy-intensive. Moreover, fouling in PHEs is more in a “black box” pattern: the formation of fouling is unable to be visualized and the way to monitor fouling is typically indirect, either through pressure-drop between the inlet and outlet of the PHE (Lalande et al., 1984), fouling thermal resistance (Boxler, 2014) or electrical conductivity (Guérin et al., 2007). Readers are redirected to the publications from Wallhäußer et al. (2012), Collier et al. (2018) and Chen et al. (2019) to get an exhaustive view of the techniques that have been employed to detect and monitor fouling including ultrasonic and dynamic gauging methods.

Another universal way to detect the severity of the fouling is the measurement of deposit mass. However, unfortunately, it is extremely time-consuming and destructive as it requires to stop fouling run and dismantle the PHEs to weigh the deposit on each plate, therefore, making it hard to capture dynamic information on the fouling growth.

Fouling in PHEs is also very material-consuming. For example, hundred liters of fluid are typically required in one run of pilot-scale experiments, whilst generally less than one liter is needed in the laboratory scale. Besides, it is not always easy to fully control the hydrodynamic conditions in PHE which complicates the interpretation of fouling build-up: higher flow rate might facilitate fouling growth as it favors the mass transfer of activated protein from bulk toward the sol-metal interface, while it could also mitigate fouling due to its high shear stress favoring the removal of deposit. This is probably the reason which explains some contrary results observed in the literature: fouling decreased in a pipe heat exchanger from laminar to turbulent flow (Re 2000-7000) (Belmar-Beiny et al., 1993), yet fouling was found to be higher at Re 3200 than at 2000 or 5000 (Guérin et al., 2007; Khaldi et al., 2015a).

As early as 1960s, laboratory-scale apparatus was developed to investigate milk fouling. For example, Burton (1961) studied the effect of heating temperature and milk pH on the fouling behavior in a stainless steel U-tube. However, this device cannot be pressurized, and the fouling behavior can be disrupted by the dissolved air. After that, Burton (1965) updated his apparatus with an electrically heated Pt wire (as shown in Fig. 1.16(a)). This apparatus was used to investigate the effects of pH (Burton, 1965), ageing (Burton, 1966), seasonal variation (Burton, 1967), and preheating on milk fouling (Burton, 1965). Those findings agreed well with the results obtained from a small-scale UHT plant (Burton, 1966). While, that apparatus limits itself as the hot wire could be made only from Pt, so that other surfaces could not be studied. In order to investigate fouling behavior on different materials, Britten et al. (1988) installed a model laboratory plant to study the effect of various polymer-coated surfaces on the amount and the adhesion strength of milk deposits (Fig. 1.16(b)). This bench-scale device was also used to investigate the effect of pH, heating time, preheating of milk fouling (Foster et al., 1989).

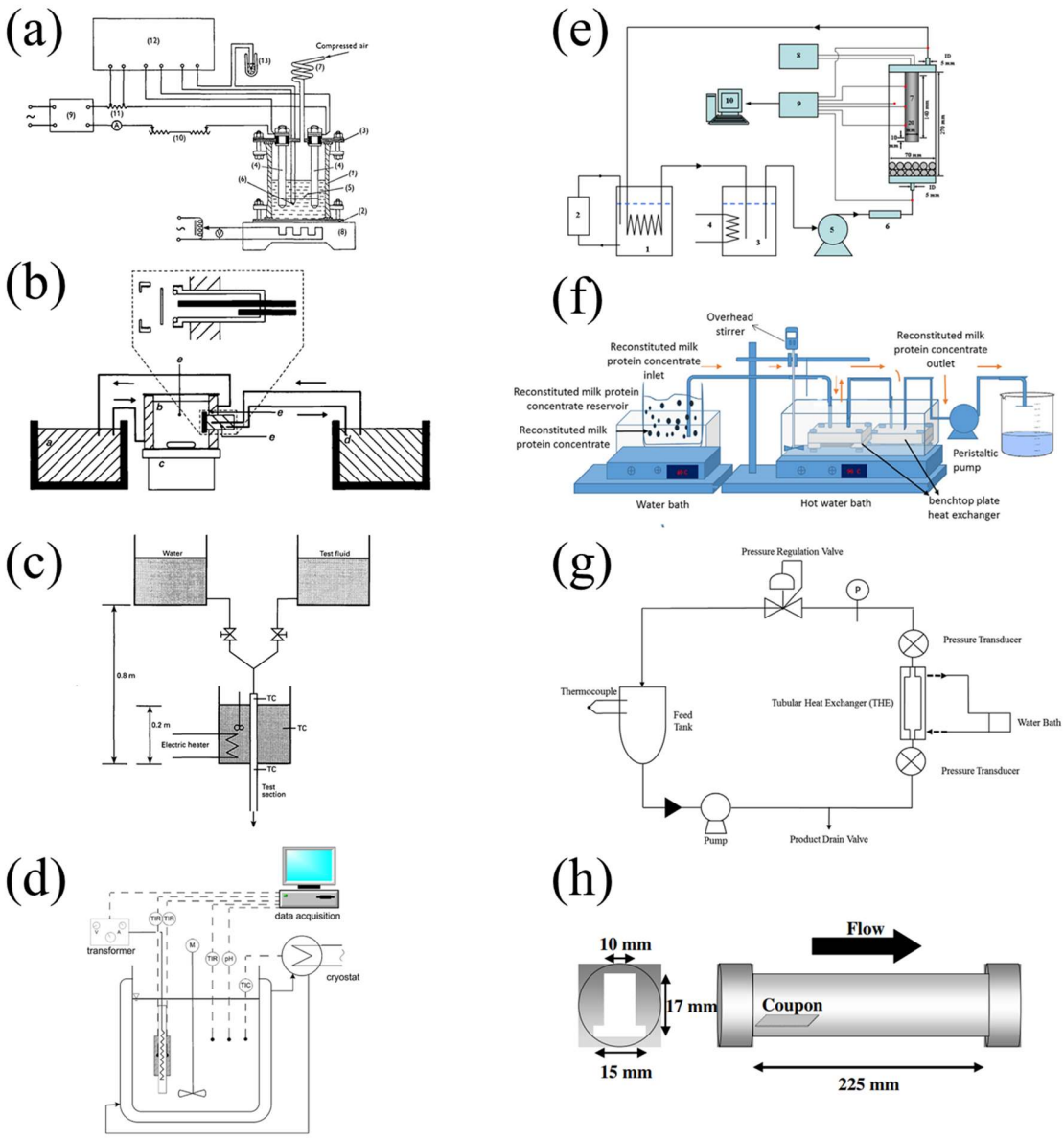

Figure 1.16. Experimental apparatuses developed for fouling studies in laboratory scale as outlined in the text. Figures are reprinted with permissions.

There have been various custom-built bench-scale devices dedicated to fouling depending on the investigation purpose. For instance, to figure out the sequence of protein and mineral deposition, Belmar-Beiny and Fryer (1993) constructed a simple rig where a stainless steel tube was used as a heat exchanger (Fig. 1.16(c)). The tube was immersed in a temperature-controlled water bath to maintain a constant surface temperature and the test fluid was flowed through the

tube in turbulent flow by gravity at a Re of ~ 15000. Boxler et al. (2013) investigated whey protein fouling on diamond-like carbon (DLC) coated stainless steel surfaces. The coated plates were put in direct contact with fouling solutions in a temperature-controlled stainless steel tank (Fig. 1.16(d)). Also, Li et al. (2013) installed a system to monitor fouling of both egg ovalbumin (OVA) and whey proteins. Fouling was performed in a heating rod fixed in a sealed transparent cylinder glass (Fig. 1.16(e)). The fouling fluid was pumped at low velocity via a peristaltic pump from the bottom inlet to the top outlet of the cylinder glass to minimize the effect of shear force on fouling removal. This system has also been utilized to study the effect of protein pre-absorption (Lv et al., 2015) or Fluorolink S10 coating (Huo et al., 2019) on whey protein fouling and cleaning behaviors. Additionally, Gandhi et al. (2017) designed a benchtop PHE system to study the effect of milk protein solubility on its susceptibility to initiate fouling on stainless steel surfaces. The benchtop PHE unit was fabricated from 6061 aluminum rectangular bar where a SS coupon was mounted for fouling to occur (Fig. 1.16(f)). The system consists of two benchtop PHE units which act as preheating and heating sections. This design makes it easier for subsequent characterization of fouling deposits by scanning electron microscopy (SEM), confocal laser scanning microscopy (CLSM) and energy dispersive spectroscopy (EDS). In a more recent study, Hebishy et al. (2019) developed a lab-scale tubular heat exchanger to investigate the effect of calcium-binding salts on the heat stability and fouling of whey proteins (Fig. 1.16(g)). This system was operated at a laminar flow rate in bath recirculation model and the heating temperature was conducted at 80 °C to simulate High-Temperature-Short-Time (HTST) thermal processing.

Another common way to perform fouling experiments, particularly in coating studies, is to insert a test pipe containing stainless steel coupons after PHE (holding zone, Fig. 1.16(h)) (Rosmaninho et al., 2007). This protocol, although not in the laboratory-scale, has advantages over conventional PHE experiments as it does not require dismantlement of the total PHE plates, and therefore is easier to manipulate. It was recently employed to characterize fouling mitigation using different surface-modified strategies (*e.g.* surface roughness, surface energy, coatings) (Zouaghi et al., 2018b; Zouaghi et al., 2018c; Zouaghi et al., 2017; Zouaghi et al., 2018d). However, one should be aware that the fouling obtained at this holding zone could differ slightly from that obtained in the heating zone of the PHE (Khaldi et al., 2018). A more important feature of this fouling set-up is its simplification on the characterization of the deposits. For instance, to monitor the microstructure of the deposited layer using Atomic Force Microscopy (AFM; Jimenez et al., 2013),

to determine the chemical composition using energy-dispersive X-ray spectroscopy (EDX; Hagsten et al., 2016), or specifically mapping of protein or calcium by confocal laser scanning microscopy (CLSM; Hagsten et al., 2019a; Hagsten et al., 2019b). Various sensors can also be mounted in this section, for example, to monitor the removal of milk fouling deposits along cleaning processes using an ultrasound sensor (Collier et al., 2015; Úbeda et al., 2016) to determine local fouling rate by a heat flux sensor (Truong et al., 2017) or to measure local fouling resistance using sensors that based on thermal excitation (Boukazia et al., 2020; Boukazia et al., 2021). Commercial devices such as Quartz Crystal Microbalance (QCM; Yang et al., 2018) or laboratory Pasteurizer/Plate Heat Exchanger (Armfield FT43; Barish and Goddard, 2013) were also applied for fouling experiments.

1.8 Cleaning of dairy fouling

Since fouling still remains an unresolved issue, the following clean-up becomes necessary in the quality control of thermal processing operations (Kulkarni et al., 1975). The problem of milk deposit's cleaning was firstly described in 1940s (Johnson and Roland, 1940a, b). It was until 1950s, the Cleaning-In-Place (CIP) was developed, initially as a manual process, for hygienic cleaning of plant surfaces (Davey et al., 2013). It nowadays evolves to be a standard automated technique with a circulation of cleaning solutions into the equipment (without dismantlement of the entire equipment) (Alvarez et al., 2010; Wilson, 2005). It is used not only for microbiological hygiene but also to restore heat transfer and pressure-drop characteristics of the plant. Fryer and Christian (2005) described a typical CIP procedure in five steps:

- **Pre-rinse**: circulation of water to remove loosely bound substances from the surface;
- **Detergent cycle**: action of the cleaning chemical components (acid or alkali) to release the deposit from the surface. The resulting components are held in solution and removed with the fluid flow. The majority of cleaning takes place during this cycle;
- **Post-rinse**: all trances of deposit and cleaning chemical are removed from the system by circulation of water;
- **Sanitization**: disinfection and surface conditioning;
- **Final rinse**: circulation of water prior to product processing.

In food industry, CIP process is frequently used while it is usually carried out semi-empirically (Fryer et al., 2006). Besiedes, CIP operation is generally harmful to the environment as it is both water/energy-consuming (Piepiórka-Stepuk et al., 2016). According to Piepiórka-Stepuk et al. (2012), as much as 13.5% of the total energy consumption is associated with the cleaning process, depending on the nature of the manufactured goods. As mentioned in (Collier et al., 2018), cleaning operations account for 50 to 90% of the wastewater sent to the wastewater treatment plant. This presents between 0.5 L and 5 L of water per liter of processed milk regardless of the type and size of the plant or equipment (Marty, 2001). Van Asselt et al. (2005) attributed 80% of production costs to the consequences of fouling and cleaning in the dairy industry.

Unlike petrochemical or marine fields, it is necessary to carry out CIP every 6-20 hours in the dairy industry, which further increases the cost of the product due to downtime. In CIP, two cleaning processes are commonly used to remove milk deposits, namely a single-stage process or a two-stage process (Timperley 1987) with or without re-use of detergent. In a single-stage cleaning, the deposit is removed by a highly acidic or alkaline solution or formulated detergents, which contain surface-active agents and chelating agents. In the two-stage process, the protein and fats are firstly removed with an alkaline solvent (*e.g*. NaOH), while the mineral deposits are removed by an acidic solution (*e.g*. HNO_3). The efficiency of CIP depends on various factors, for instance, the cleaning duration, temperature or hydrodynamic conditions (Piepiórka-Stepuk et al., 2012; Piepiórka-Stepuk et al., 2016). The optimization of cleaning or mechanism behind is beyond the scope of this thesis, the authors are redirected to the comprehensive reviews (Bird and Bartlett, 1995; Fryer and Christian, 2005; Fryer et al., 2006; Gillham et al., 1999; Graßhoff, 1997; Jennings, 1965; Kulkarni et al., 1975). Modeling of the cleaning processes based on different methodological approaches can also be found in the literature (Asteriadou et al., 2006; Deponte et al., 2020; Dürr and Graßhoff, 1999; Jensen and Friis, 2005). However, the transfer of the developed models to different cleaning processes is limited to a certain extent because of the differences between each cleaning situation (Schöler et al., 2012).

Conclusions

In this first chapter, a comprehensive literature review on dairy fouling has been presented. The underlined fouling mechanisms including thermal denaturation of whey proteins (BLG in particular) and mineral precipitations (mainly calcium phosphates) are all described in detail. So far, after decades of studies, most of the fouling phenomenon has been pointed out but not fully demystified. Moreover, some controversy persists.

Dairy fouling can be simplified into three sub-processes, namely bulk reaction, mass transfer and surface reaction. The thermal denaturation of the major whey protein BLG has been identified to dominate the bulk reaction. Upon heating, BLG follows a multi-stage denaturation pathway including dissociation of native dimer, unfolding of native monomer and aggregation. Despite its complicated nature, the complex system of milk itself brings more complexities due to the presence of other milk proteins (*e.g.* caseins, other whey proteins such as αLa or BSA) and minerals (*e.g.* Ca^{2+} or CaP, citrate ions). Because of this, most kinetic models are in a simplified pattern that considers only the denaturation of BLG molecule.

Caseins, being the major component of milk protein over whey proteins, are hardly considered to play a critical role in fouling simply due to their high thermal stability. However, recent researches have revealed several important features of caseins that might also affect the fouling behavior. For example, casein micelle was found to have the capability to balance the mineral contents, particularly shifting the ionic calcium toward the formation of micellar calcium phosphate. This induces a reduction of calcium content in the serum phase which should also affect the BLG-based denaturation pathway. Of great interest, casein micelle or particularly individual caseins such as α_s or β-casein were recognized to have chaperone-like activities that control the thermal denaturation of BLG, which might also play a role in the fouling process. Nevertheless, how exact caseins affect fouling has never been investigated in an exhaustive way. To partially fill this gap, in the next chapter (Chapter Two), the effect of casein on whey protein denaturation and subsequent fouling behavior in a pilot plant PHE is experimentally investigated.

Thermal denaturation kinetic experiments provide another view to evaluate and to understand the effect of other components such as minerals (*e.g.* Ca^{2+}) or other milk proteins (*i.e.* casein) on the heat-induced denaturation pathway of BLG. However, conventional one-step reaction model

neither being capable to explain the break-slope behavior in the Arrhenius plot nor to differentiate/quantify the amount of native and unfolded BLG species. A close inspection on the literature inspires that the unfolding step of BLG might be considered as an instantaneous reaction (or much faster compared to aggregation process). Based on this, a novel kinetic model describing thermal denaturation of BLG is developed as will be shown in Chapter Three. This model is subsequently applied to evaluate the corresponding thermodynamic parameters and to discuss how these parameters are affected in the presence of calcium ions and casein proteins. Finally, the ability of the model to quantify the amount of different BLG species under specific heat treatment is illustrated.

In the literature, most fouling experiments were performed in pilot-scale PHEs; this is valuable in the industrial aspect, however, its complexities in the configuration and thus complicated thermodynamics and fluid mechanics (turbulent scheme) make it hard to determine the deposition reaction. To overcome these obstacles, in Chapter Four, a laboratory-scale fouling device is installed such that whey protein fouling can be performed in a laminar regime. By coupling the kinetic denaturation model as previously developed in Chapter Three, a 3D CFD fouling model based on the real geometry of the device is achieved.

The casein-whey protein interactions have been partially demystified in the literature, whilst, it has seldom been linked to the fouling deposition and the subsequent deposition rate in such system is poorly known. In the last chapter (Chapter Five), with the built-up of the benchtop fouling device, the effect of casein micelle on the whey protein fouling behavior is studied in the laboratory scale. A renneting-based technique is used to reveal the molecular status of caseins (dissociated *vs* micellar casein) as well as potential casein-whey protein interactions (depending on the molecular status of casein proteins). Gathering all these pieces of experimental evidence, an overall fouling mechanism is finally proposed.

Chapter Two. Effect of casein/whey ratio on whey protein fouling in a plate heat exchanger

The present chapter, which is adapted from the paper entitled "Effect of casein/whey ratio on the thermal denaturation of whey proteins and subsequent fouling in a plate heat exchanger", published in *Journal of Food Engineering* in 2021 (Liu et al., 2021) (Annex I), will begin by a detailed presentation of the fouling set-up in a pilot-scale. Whey protein-based model fluids containing different casein concentrations and fixed content of added calcium were used, leading to various Casein/WPI mass ratios. Effect of casein on whey protein fouling performance in the PHE was monitored in an on-line manner by pressure-drop and overall heat transfer coefficient changes. Parallel laboratory experiments were performed to investigate the effect of casein on BLG denaturation kinetics in a molecular level. Fouling deposits formed at various Casein/WPI ratios were characterized using element mapping and Sodium Dodecyl Sulphate-Polyacrylamide Gel Electrophoresis (SDS-PAGE) to achieve a better comprehension of the impact of casein on the fouling behavior.

2.1 Presentation of pilot plant fouling set-up

2.1.1 Model fouling solution

Earlier fouling experiments used fresh milk as fouling fluid, however, the fouling performance deduced from those experiments appears bad reproducibility mainly due to the seasonal variation of the milk protein or fat content (Heck et al., 2009; Lu et al., 2018). Therefore, since the predominant role of whey protein on fouling has been recognized, modern researchers tend to use whey protein solutions as a standard solution instead of milk to ensure repeatable results (Delplace et al., 1997). In the present study, the fouling solutions were reconstituted from commercial protein powder with reverse osmosis water; whey protein isolate (WPI) powder PRODIET 90 S and whole casein powder PRODIET 87 B were provided from Ingredia (France). According to the manufacturer, WPI powder consists of 85.5% total protein, 5.5 wt% moisture, 0.2 wt% calcium and phosphorous. The casein powder contains 83 wt% total protein, 5 wt% moisture, 2.6 wt% calcium and 1.3 wt% phosphorous. For all experimental solutions, the whey protein concentration was fixed at 0.5 wt% to simulate the whey protein content in raw milk, typically varying from 2-4 g/L (Farrell Jr et al., 2004). In order to investigate the effect of casein on the fouling behavior, different amounts of casein powder were added to achieve elevated Casein/WPI mass ratios from 0 to 0.8. Preliminary experiments showed no visible fouling when using WPI alone or mixtures of WPI and casein without additional ionic calcium (Casein/WPI mass ratio up to one). $CaCl_2$ has

been widely used in the literature to introduce calcium ions into dairy systems and is authorized for ages to be added to milk during cheese making (Price, 1927). Therefore, it was decided to add 42 ppm of free calcium in the form of calcium chloride (anhydrous, 96%, Acros Organics, USA) in the fouling solutions. This value resembles an ionic calcium level in raw milk (On-Nom et al., 2010) and was found to be appropriate as it caused a significant amount of fouling without clogging the whole system (see later in the results section). This amount of $CaCl_2$ has also been determined to achieve a suitable total fouling mass in the PHE. The total amount of calcium is similar to those used for WPI fouling experiments (Guérin et al., 2007; Khaldi et al., 2015a; Khaldi et al., 2018).

2.1.2 Pilot-scale fouling run

Fouling experiments were performed in the pilot-scale set-up as shown in Figure 2.1. The system contained two PHEs (Model V7, Alfa-Laval Vicard, France); they were both configured using 21 plates thus providing 10 channels for both hot water and fouling fluid. The dimension of the plate is 150 mm × 495 mm × 0.8 mm with a corrugated surface (35° corrugation angle with a 3.9 mm flow gap), giving an effective contact area of 0.0743 m^2. The first PHE is named pre-heating PHE as it allows to increase the temperature of fouling solutions from 50 to 65 °C without inducing denaturation of BLG and fouling (Boye and Alli, 2000). The main fouling observations were focused on the second PHE, called heating PHE, which continues elevating the solutions up to 85 °C at its outlet; this temperature was kept constant by controlling the inlet temperature of hot water, thereby a constant temperature profile along the PHE was achieved. A quasi-linear temperature profile with PHE was obtained in a counter-current configuration of fouling fluid and hot water with the same flow rate at 300 $L{\cdot}h^{-1}$ (Figure 2.2(a)), the bulk temperature profile was simulated numerically using Sphere software (Fig. 2.2(b)) which was previously elaborated and validated by INRAE's group as mentioned in Blanpain-Avet et al. (2016) and Petit et al. (2013). This temperature profile resembles an HTST (Hight-Temperature-Short-Time) pasteurization process with a slightly higher temperature and duration. The temperature and flow rate measurements were performed using platinum resistance probes (Pt100, Fer Constantan) and electromagnetic flowmeters (Krohene IFM, Germany), respectively. All sensors were calibrated before the experiments were conducted; the accuracy of temperature measurements was expected to be better than ±0.2 °C and relative errors for the flow rate measurements were considered to be

less than ± 1%. All measurements were collected using a data acquisition system (Agilent Technologies 34970A, USA).

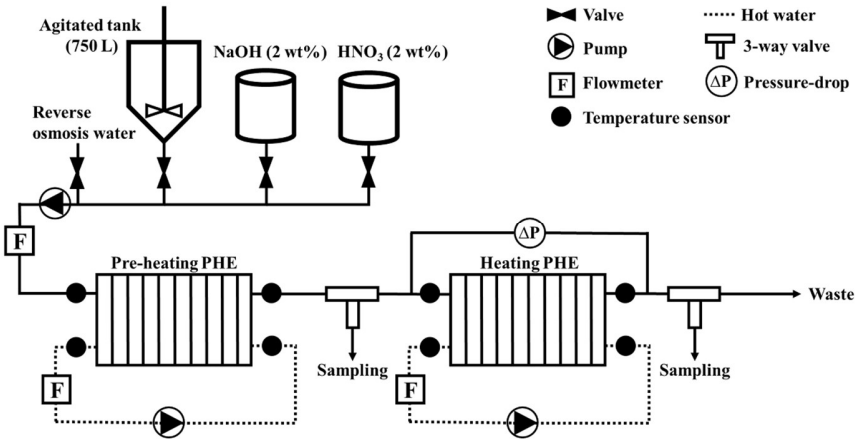

Figure 2.1. Schematic diagram of pilot-scale fouling experimental set-up. Two plate heat exchangers (PHEs) were coupled and named as pre-heating PHE and heating PHE, respectively.

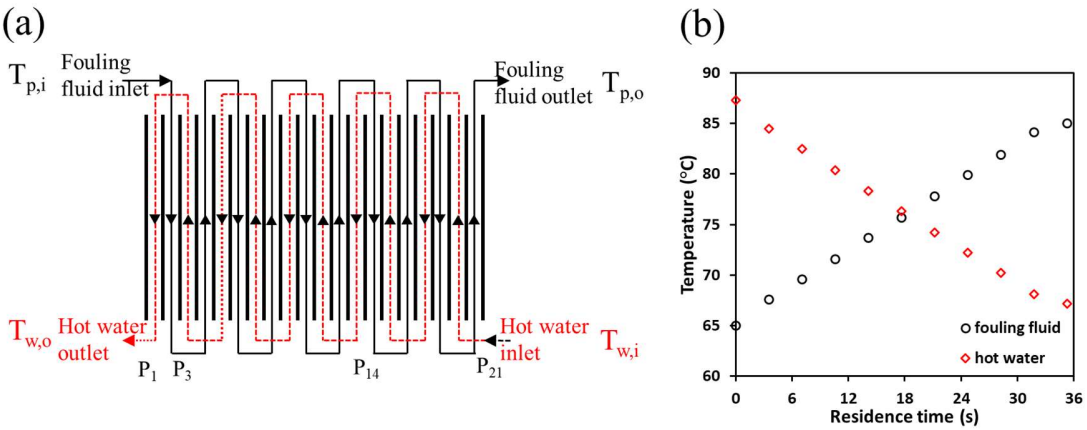

Figure 2.2. (a) Counter-current flow arrangement inside heating PHE, P_i represents plate number. (b) Temperature profiles of fouling fluid and hot water within heating PHE aginst residence time. Data were simulated using Sphere Software.

The average Reynolds number, *Re*, along the PHE was determined at a clean state from the following equation:

$$Re = \frac{\rho \upsilon D_h}{\mu} = \frac{2\rho Q}{\mu l} \qquad \text{(eq. 2.1)}$$

where ρ is the density of fouling fluid (kg·m^{-3}), υ is the average fluid velocity in m·s^{-1} (which is also equal to $Q/l \cdot e$, l is the plate width (m) and e is the flow gap (m)), D_h is the hydraulic

diameter (m) and is clasically defined as $D_h = 2 \cdot e$ in the literature (Scudeller et al., 2021), μ is the viscosity of fouling solution (Pa·s), and Q is the flow rate ($m^3 \cdot s^{-1}$). The calculated Re in the heating PHE was ~2900, corresponding to a turbulent regime. According to Leuliet (1988), for the corrugated V7 plates used in this work, the turbulence regime occurs over $Re = 260$.

Prior to fouling runs, the fouling solutions were stirred in a 750 L tank; the temperature of the solutions was increased to 50 °C and maintained for at least one hour to ensure full dissolution of protein powders. Before pumping fouling fluid, reverse osmosis water was firstly used to reach a thermal equilibrium of the system at the desired process temperature. After that, 600 L of fouling solution was processed in each pilot-scale experiment by switching from water to fouling fluid once-through, without recycling. This volume corresponds to a total running time of 2 hours, during which the fouling solutions were sampled at both inlet and outlet of the heating PHE three times; these solutions along with the solution in the launching tank (*i.e.* fouling solution at 50 °C before subjecting to PHE) were used for subsequent determination including pH, free calcium content, total calcium content, and BLG denaturation level. To quickly quench the denaturation of proteins in sample solutions, they were mixed immediately with cold water (<1 °C) in a centrifugation tube. The dilution effect was considered in the calculation of calcium and protein concentration. When the fouling experiments were finished, water was used again to replace fouling solutions in the channels; after that, the PHE was dismantled and placed under ambient conditions overnight before putting in an air-oven at 50 °C for at least 3 hours to dry the plates. The dry mass of the fouling deposit on each plate was calculated by the difference between bare and fouled plates. Fouling mass in each channel was the addition of two deposit mass values obtained for the plates constituting the pass walls. The total fouling mass for each run is the sum of the mass collected from all the channels.

Finally, these plates were installed again in the PHE system for the subsequent cleaning procedure by circulating 2 wt% sodium hydroxide (99%, Solvay, Belgium) and 2 wt% nitric acid (54%, Thermo Fisher Scientific) with a similar heating process to the fouling experiments. The duration for each step lasted at least 30 min, after that, the system was rinsed with osmosis water for the next heat treatment experiment. The cleanliness of the plates was checked visually to ensure efficient cleaning.

The amount of fouling was also monitored by the pressure-drop within PHE and the calculation of thermal resistance (R_f). Assuming uniform fouling layer, the average thermal resistance R_f can be described as:

$$R_f = \frac{1}{U_t} - \frac{1}{U_{clean}} \quad \text{(eq. 2.2)}$$

where U_{clean} and U_t are the overall heat transfer coefficients before the occurrence of fouling and at time t when fouling is formed, respectively.

The heat transfer coefficient was calculated from the energy balance between the heating fluid (hot water) and process fluid (model solution):

$$m_h C_{pw}(T_{w,i} - T_{w,o}) = US\Delta T_{LMTD} F_T \quad \text{(eq. 2.3)}$$

where m_h and C_{pw} represent the mass flow rate ($kg \cdot s^{-1}$) and the specific heat for the hot water ($J \cdot kg^{-1} \cdot K^{-1}$), respectively. The temperature dependence of C_{pw} was used as reported by Petit et al. (2013). $T_{w,i}$ and $T_{w,o}$ refers to the temperature of hot water at the inlet and outlet of PHE (K). S is the heat transfer area (m^2), and ΔT_{LMTD} is the logarithmic mean temperature difference (K) and can be calculated as:

$$\Delta T_{LMTD} = \frac{(T_{w,i} - T_{p,o}) - (T_{w,o} - T_{p,i})}{\ln\left(\frac{T_{w,i} - T_{p,o}}{T_{w,o} - T_{p,i}}\right)} \quad \text{(eq. 2.4)}$$

where $T_{p,i}$ and $T_{p,o}$ refers to the temperature of fouling fluid at the inlet and outlet of PHE (K). F_T is a correction factor taking into account an impure counter-current flow inside the PHE. In our case, F_T is a constant value since the arrangement of PHE is fixed. It was decided to fix the value of F_T at one since it is not far away from the value reported in a similar PHE arrangement (Rene et al., 1991).

2.2 Calcium content measurement

The ionic or free calcium $[Ca]_f$ of sample solutions was measured using a calcium ion-selective electrode (Ca-ISE, PS-3518, PASCO, USA). The calculation of the free calcium level was based on the potential difference between the sample solution and a constant reference through a gelled organophilic membrane. The potential values were recorded in the software from the manufacturer (PASCO capstone) through a Bluetooth module coupled with the electrode. A high and constant ionic strength environment was needed for reliable potential measurements, hence 3.85% (v/v) of the ionic strength adjuster (4M KCl) was added for all samples and standard solutions. The probe was calibrated with five Ca^{2+} standards ranging from 5 ppm to 100 ppm. The calibration curve was

derived from the logarithm of Ca^{2+} concentration and the potential values according to the Nernst equation. To avoid any temperature effect, all samples and standard solutions were allowed to equilibria in a 25 °C water bath for at least one hour before measurements. The total calcium content $[Ca]_t$ was determined by atomic absorption spectrometry (AAS) using a Spectro AA 55B apparatus (Varian, Palo Alto, USA) as performed in Khaldi et al. (2018).

2.3 High-performance liquid chromatography

The concentration of soluble BLG in the samples was evaluated using a high-performance liquid chromatography (HPLC) system (Alliance HPLC System, Waters, USA). The chromatographic system consists of a separation module integrated solvent and sample management functions (e2695 Separation Module), a column heater/cooler, a reverse-phase column (XBridge Protein BEH C4, 300 Å, 3.5 µm, Waters) associated with a guard column (Sentry Guard Cartridge, Waters), a UV-Vis spectrophotometer (2998 PDA Detector) and acquisition software (Empower Software).

The pH of the protein samples was adjusted to 4.6 following a centrifugation process (9056 × *g* for 30 min at 4 °C) to remove aggregated BLG and casein proteins if any. The supernatants were filtered through a 0.2 µm cellulose filter (Minisart RC, Sartorius, Germany) before injecting 20 µL in the HPLC system. Two mobile phases were used: solution A consists of 0.1% (v/v) trifluoroacetic acid (TFA, 99%, Acros Organics) in MilliQ water while solution B contains 0.1% (v/v) TFA, 80% acetonitrile (HPLC grade, Thermo Fisher Scientific) and 20% MilliQ. The separation was performed at a flow rate of 1 mL/min, 40 °C and a detection wavelength of 215 nm with gradient elution. Calibration curves were done by using pure BLG standards (0.25 to 3 g/L). To maintain the performance of the column, pure acetonitrile was eluted at 1 mL/min for 1 h after the experiment finished.

2.4 Characterization of fouling deposit

To provide a deeper insight into the fouling, the determination of element and protein composition was carried out using an Electron Probe Micro Analyzer (EPMA) and Sodium Dodecyl Sulfate Polyacrylamide Gel Electrophoresis (SDS-PAGE), respectively. The characterizations were performed for the fouling runs at four different Casein/WPI mass ratios at 0, 0.05, 0.2 and 0.8. For each experiment, the deposits formed at two different plates (*i.e.* P_{14} and

P_{21}, Fig. 2.2(a)), at two different bulk temperatures (78.9 and 84.6 °C for samples collected from P_{14} and P_{21}, respectively (Fig. 2.2(b)) were studied for comparison purposes.

For EPMA analysis, the samples were directly cut from the dried plate after the fouling experiments, the analyzed deposits were chosen on the flat surface of the plate. The cut coupons were firstly embedded in epoxy resin; after solidification, the surface was polished using an ESC 200 GT polishing machine (ESCIL, Chassieu, France) with different grades of SiC sheets (up to 0.25 μm) and carbon-coated with a Bal-Tec SCD005 sputter coater. These processes are necessary to ensure a very flat surface for EPMA measurement. The samples were placed in the vacuum and excited by an electron beam, the backscattered electron imaging and X-ray mapping were carried out using a Cameca SX-100 EPMA (CAMECA, Gennevilliers, France) at 15 kV, 15 nA, and 15 kV, 40 nA, respectively. For element determination, a PET crystal was used to detect Kα X-rays of sulfur, calcium, and phosphate, and a LiF crystal to detect iron Kα X-rays.

The SDS-PAGE was performed in a SE 600 Series vertical Slab Gel Unit (Hoefer Scientific instrument, San Francisco, US). The resolving gel contained 15% (w/v) acrylamide and 0.2% (w/v) SDS in 1.5 M Tris-HCl buffer at pH 8.8, and the stacking gel included 4% (w/v) acrylamide and 0.1% (w/v) SDS in 0.5 M Tris-HCl buffer at pH 6.8. The deposit samples were scraped from the dried plate after the fouling runs and dried again in a 105 °C oven for over 24 h. The dry powders were ground and dissolved in the sampling buffer (0.5 M Tris-HCl buffer, pH 6.8, containing 0.2% (w/v) SDS, 0.01% (v/v) bromophenol blue and 0.05% (v/v) β-mercaptoethanol) with a final concentration at 0.5 wt%. Pure proteins including α_s/β/κ-casein, αLa, BSA and BLG were also dispersed in the sampling buffer for a comparison purpose. These solutions were heated in a boiling water bath for 5 min; they were cooled to room temperature and injected into the gel along with a protein molecular weight ladder (Precision Plus Protein Unstained Standards, Bio-Rad Laboratories, UK). The gels were run under a constant current at 40 mA for immigration in the stacking gel and 60 mA for resolving gel. After electrophoresis, a fixation process was applied by immersing the gel in the solution with 10% (v/v) acetic acid (99.5%, Acros Organics) and 30% (v/v) ethanol. After that, the gel was stained for at least 2 h using 0.02% (m/v) Brilliant Blue R in 10% (v/v) acetic acid and 25% (v/v) isopropanol. After coloration, the gel was destained using a 10% (v/v) acetic acid solution until a clear background was achieved.

2.5 Thermal denaturation of BLG

2.5.1 Thermal denaturation experiments

The model solutions for denaturation experiments were selected according to the pilot-scale fouling results: 0.5 wt% WPI, 0.5 wt% WPI with 0.25 wt% casein, 0.5 wt% WPI with additional 42 ppm free calcium at different Casein/WPI mass ratio of 0, 0.05, 0.2 and 0.8, respectively. The compositions of these solutions were summarized in Table 2.1. The experimental protocol was similar as reported previously by Petit et al. (2011). Briefly, all model solutions were reconstituted using a similar protocol as applied in the fouling experiments (*i.e.* 50 °C for 3 hours), after that 2 ml aliquots were removed into plastic tubes (Eppendorf, Germany) prior to heat treatment. The heating process included three stages by using three water baths (Figure 2.3): the first water bath was set at 65 °C to pre-heat the solutions below the critical temperature for BLG denaturation (Paulsson and Dejmek, 1990), and the second bath was set at 10 °C higher than the desired holding temperature (T_d+10 °C) to quickly heat up the solution to reach T_d, at which it corresponded to time zero for kinetic calculation. After that, the samples were maintained at T_d by submitting into the third bath (temperature set at T_d+1 °C). The sample temperature was monitored by following the temperature evolution of a reference vial filled with the MilliQ, in which a thermocouple was inserted. A representative temperature profile with T_d set at 80 °C is shown in Fig 2.3. The holding temperature T_d varied from 70 to 90 °C was maintained for a proper period of time to induce significant BLG denaturation. At different times (including solution reach 65 °C in the first bath), the solutions were removed and cooled in melting ice to quench the BLG denaturation.

Table 2.1. Composition of model solutions for thermal denaturation experiments.

Solutions	[WPI] (wt%)	[Casein] (wt%)	[Casein]/[WPI]	Added Ca^{2+} (ppm)	$[Ca]_f$[a] (ppm)	$[Ca]_t$[b] (ppm)
Casein/WPI=0	0.5	0	0	0	14.7	22.3
Casein/WPI=0.5	0.5	0.25	0.5	0	58.1	91.0
Casein/WPI=0&Ca	0.5	0	0	42	53.1	64.7
Casein/WPI=0.05&Ca	0.5	0.025	0.05	42	61.2	74.3
Casein/WPI=0.2&Ca	0.5	0.1	0.2	42	67.9	90.9
Casein/WPI=0.8&Ca	0.5	0.4	0.8	42	96.2	169.4

[a]free calcium concentration determined using Ca-ISE

[b]total calcium concentration obtained from AAS

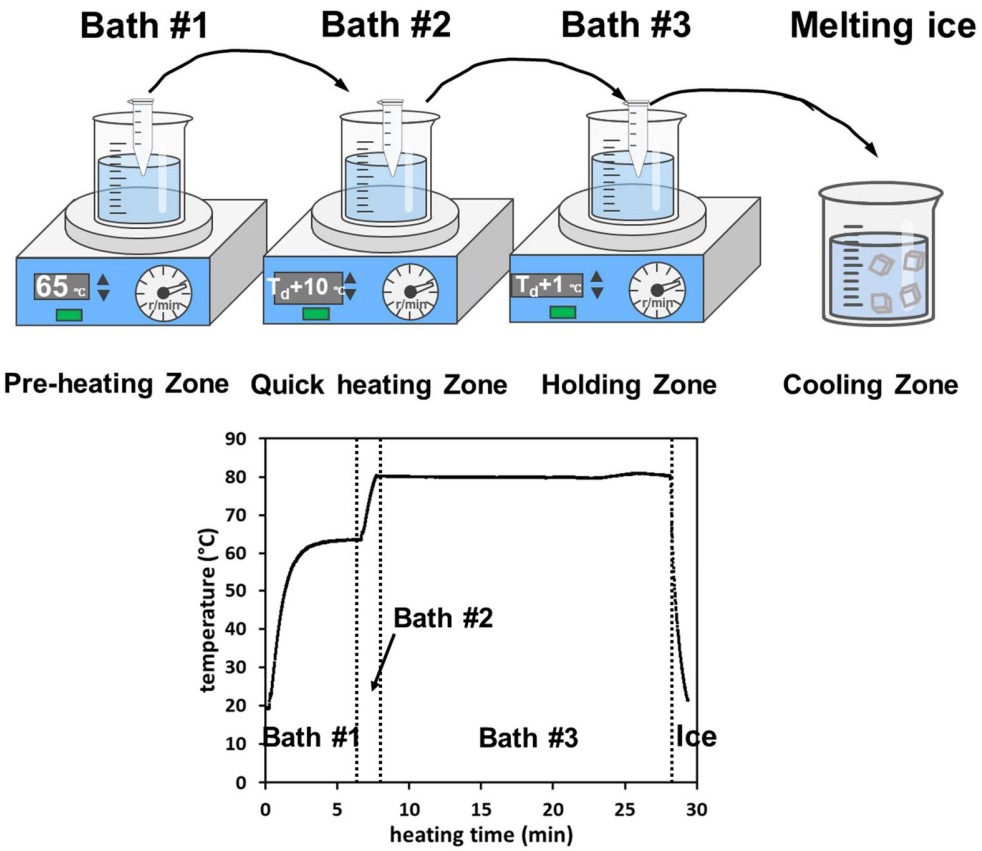

Figure 2.3. Expeimental design for measuring thermal denaturation kinetics of BLG. Figure shows a representative temperature profile set at a desired holding temperature at 80 °C.

2.5.2 Thermal denaturation kinetics of BLG

As aforementioned in the first chapter, the thermal denaturation of BLG is widely accepted in a multi-stage mechanism (Tolkach and Kulozik, 2007). Despite this intricate mechanism, the denaturation pathway of BLG is generally simplified due to the lack of ability to distinguish different BLG monomers (*e.g.* native and unfolded), for example when using polarimetric analysis (Ven Murthy and Carrier-Malhotra, 1989), gel permeation chromatography (Kehoe et al., 2011), immunodiffusion (Miyawaki et al., 2003), electrophoresis (Oldfield et al., 2005), or reverse-phase high-performance liquid chromatography (RP-HPLC) (Khaldi et al., 2015a; Petit et al., 2011). In the HPLC system, the determined BLG consists of both native and unfolded BLG molecules that refold back to their native state after cooling, which is also called soluble BLG. Hence, an overall one-step model was established by considering the transformation of soluble species (S) into

aggregated ones (A) (eq. 1.4, section 1.3.3). The reaction rate of this chemical reaction can be described as:

$$-\frac{dC_s}{dt} = k_f C_s^n \quad \text{(eq. 2.5)}$$

where Cs refers to the concentration of soluble BLG species as determined in the HPLC system, and k_f is the denaturation rate constant. The unit of k_f depends on the reaction order n (*i.e.* $g^{1-n} \cdot L^{n-1} \cdot s^{-1}$). The experimental data were fitted to equation 2.5 using nonlinear regression in Matlab to calculate the denaturation rate constant k_f with various reaction orders from 1 to 3 (Loveday, 2016). The reaction order was determined according to the RSS values (Residual sum of squares) obtained by fitting equation 2.5 to the experimental data, where the most suitable values were found to be 2 (in supplementary figure, Figure S2.1, page 116). This value is consistent with those found for BLG denaturation in skim milk (Hillier and Lyster, 1979; Lyster, 1970; Manji and Kakuda, 1986) or simulated milk ultrafiltrate (Park and Lund, 1984).

The relationship between k_f and the heating temperature is deduced by the Arrhenius equation:

$$\ln(k_f) = \ln(k_0) - \frac{Ea}{RT} \quad \text{(eq. 2.6)}$$

where k_0 is the denaturation pre-exponential factor ($g^{1-n} \cdot L^{n-1} \cdot s^{-1}$), Ea is the activation energy ($J \cdot mol^{-1}$), R is the universal gas constant ($J \cdot mol^{-1} \cdot K^{-1}$), and T is the bulk liquid temperature (K).

Figure 2.6 presents an example of an Arrhenius plot obtained from a solution containing 0.5 wt% WPI with the addition of 42 ppm Ca^{2+}, where the logarithm of k_f is plotted against the inverse temperature. A break of the slope appears around a critical temperature (T_c, *i.e.* 82 °C in this case) as previously observed and interpreted by Tolkach and Kulozik (2007). It is unexpected for a one-step reaction as described above, hence it is generally deduced with a two-step reaction mechanism ($N \rightarrow U \rightarrow A$) where the native BLG molecule (N) unfolds (U) prior to forming aggregates (A). At temperatures lower than the critical temperature T_c, the unfolding reaction rate is considered to be lower than the aggregation while when the temperature is higher than T_c, the unfolding rate is faster. Consequently, linear regressions of data at these two regions permit us to determine the kinetic parameters, including k_0 and Ea, for both unfolding and aggregation steps.

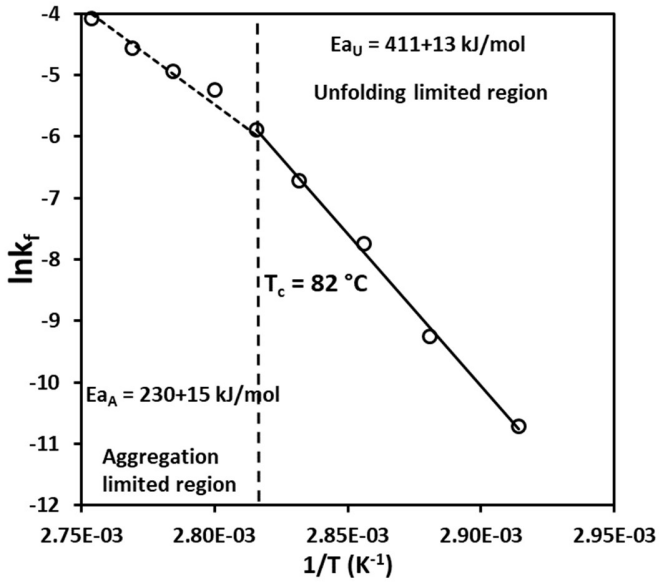

Figure 2.4. Arrhenius plot of 0.5 wt% WPI solutions with the addition of 42 ppm Ca^{2+}. The solution contains 53 ppm Ca^{2+} with 64.7 ppm total Ca. The denaturation reaction rate k_f was obtained by solving equation 2.5 with a reaction order of two.

2.6 Results and discussion

2.6.1 The essential role of Ca^{2+} on fouling

It is important to bear in mind that introducing casein powder can also bring additional minerals to the system, in particular, calcium in ionic and colloidal forms. It was decided to first investigate the effect of Ca^{2+} on the mass of whey protein fouling deposits formed inside PHE. Table 2.2 summarizes the calcium compositions of nine different fouling fluids and their corresponding fouling results, including soluble BLG concentrations at the inlet and outlet of PHE, BLG denaturation level within PHE, and total fouling mass.

Table 2.2. Calcium content of nine different fouling fluids and their corresponding fouling results. For each fouling experiment, the BLG concentrations at the inlet and outlet of PHE are also shown. Errors represent standard deviation (SD).

Fluid#	Casein/WPI	Added Ca^{2+} (ppm)	$[Ca]_f$[a] (ppm)	$[Ca]_t$[a] (ppm)	$[BLG]_{inlet}$[b] (g/L)	$[BLG]_{outlet}$[c] (g/L)	BLG denaturation level[d]	Total fouling mass (g)
#1	0	0	14.8±0.6	22.3±1.2	3.08±0.04	2.84±0.05	7.7%	N/A[e]
#2	0	25	38.7±0.7	48.4±1.9	3.30±0.02	2.40±0.09	27.2%	17.1
#3	0	35	37.5±1.6	59.4±1.8	3.55±0.15	2.1±0.4	40.8%	72.1
#4	0	42	53.0±1.9	64.7±2.6	3.28±0.06	1.87±0.03	43.1%	223.9
#5	0	56	55±3	79±4	3.3±0.2	1.8±0.3	44.5%	390.8
#6	0.5	0	58±3	91±10	3.25±0.09	3.08±0.03	5.5%	N/A
#7	0.5	0	56±4	90±4	3.23±0.03	3.07±0.01	5.0%	N/A
#8	1	0	78±6	213±6	3.09±0.06	2.70±0.04	12.7%	N/A
#9	0.5	42	86±4	141±9	3.28±0.12	2.09±0.03	36.3%	133.2

[a]Average values of fouling fluids obtained at both the inlet and outlet of PHE at three different running times and one from the launching tank
[b]Average values of fouling fluids obtained at the inlet of PHE at three different running times and one from the launching tank
[c]Average values of fouling fluids obtained at the outlet of PHE at three different running times
[d]BLG denaturation level = $1-[BLG]_{outlet}/[BLG]_{intlet}$
[e]N/A: the fouling mass is undetectable

The solution containing whey proteins alone was incapable to induce detectable fouling deposits under our operating conditions due to its minor content of calcium (22 ppm of total calcium with ~15 ppm ionic calcium). However, if Ca^{2+} was added to increase the level of free calcium (in the form of $CaCl_2$), fouling deposits were obtained. As shown in Figure 2.5, the total amount of dried

fouling deposits increases at elevated Ca/BLG ratios in a linear pattern (R^2=0.994). This effect of ionic calcium on fouling mass has also been observed previously by Guérin et al. (2007), Khaldi et al. (2015a) and Khaldi et al. (2018) for other aqueous solutions reconstituted from different WPI powders and heat-treated with a similar thermal schedule.

For example, Khaldi et al. (2018) have investigated the effect of Ca/BLG on whey protein fouling and pointed out that Ca/BLG ratio alters the structure of the fouling layer, and observed more surprisingly, that for the range of Ca/BLG ratios investigated (2.3-22.9), the fouling mass is dependent on this ratio and not driven by the protein concentration as commonly admitted. Their data are also presented in the figure 2.5 for comparison while a plateau is reached in their case at high Ca/BLG ratio, which might due to the lower protein concentration they used at higher Ca/BLG ratio. Another significant impact of Ca/BLG on whey fouling behavior can be found on the BLG denaturation level within PHE. For example, the BLG denaturation level is only 7.7% without additional Ca^{2+}, but the values increase up to 44.5% for the case where 390.8 g of fouling mass was obtained (close to the operating limitation (*i.e*. sytem clogging)). One might notice that the increased extent of BLG denaturation level is relatively lower than the increased fouling mass evolution at higher Ca/BLG ratio, suggesting that calcium could be a foulant intermediate facilitating the fouling growth and not only involved in the extent of protein denaturation.

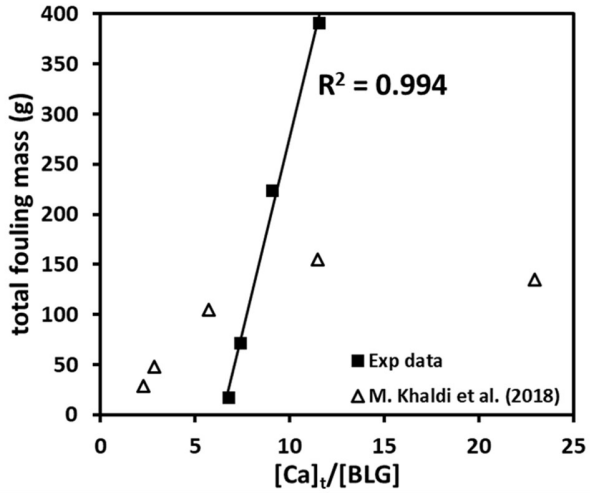

Figure 2.5. Effect of $[Ca]_t$/BLG ratio on the total dried fouling mass of 0.5 wt% WPI. The symbols in triangles refer to the data reported in (Khaldi et al., 2015a). Solid lines present linear regression with a value of R^2 at 0.994.

Knowing the effect of Ca^{2+} on fouling, an appropriate amount of casein was added instead of $CaCl_2$ attempting to achieve a similar Ca^{2+} level (Fluid#6, #7 compared to #4 and #5). Surprisingly, despite the high concentration of ionic calcium or even much more total calcium introduced by casein, no detectable fouling was obtained for fouling solutions without adding $CaCl_2$ (even up to Casein/WPI at 1). Besides that, a low BLG denaturation level was also observed in these cases, suggesting only few BLG molecules denatured during the thermal treatment within PHE. These results might due to the capacity of casein to transfer the ionic calcium into colloidal calcium phosphate inside casein micelle, especially at higher temperatures (Broyard and Gaucheron, 2015; Dalgleish and Corredig, 2012; On-Nom et al., 2010). Hence, even though the solutions contained a high level of Ca^{2+} (measured at 25 °C), the amount of Ca^{2+} could be reduced to a level that might not be sufficient enough to induce significant denaturation of BLG and subsequent fouling. The results of Fluid#9 confirm this idea by adding 42 ppm Ca^{2+} into fouling solution containing 0.5 wt% WPI and 0.25 wt% casein (*i.e.* Fluid#6 and #7). This solution induced 133.2 g of dried fouling deposit with 36.3% of denatured BLG inside PHE.

2.6.2 The effect of casein on fouling deposit mass

As shown in the last section, additional Ca^{2+} is required to observe significant fouling. Consequently, in order to investigate the effect of casein on the fouling mass, it was decided to add a constant amount of Ca^{2+} (*i.e.* 42 ppm) for all the fouling solutions containing casein. The calcium content of twelve different fouling fluids composed of elevated casein concentrations with supplemented 42 ppm Ca^{2+} and their fouling results are displayed in Table 2.3.

Table 2.3. Free calcium ($[Ca]_f$) and total calcium content ($[Ca]_t$) of twelve fouling fluids and their fouling results. For each fouling experiment, the BLG concentrations at the inlet and outlet of PHE are also shown. Errors represent standard deviation (SD). Note all solutions contain 42 ppm additional Ca^{2+}.

Fluid#[a]	Casein/WPI	$[Ca]_f$[b] (ppm)	$[Ca]_t$[b] (ppm)	$[BLG]_{inlet}$[c] (g/L)	$[BLG]_{outlet}$[d] (g/L)	BLG denaturation level[e]	Total fouling mass (g)
#1	0	53.0±1.9	64.7±2.6	3.28±0.06	1.87±0.03	43.1%	223.9
#2	0.05	53±5	74±2	3.37±0.08	1.90±0.12	43.4%	123.6

#3	0.05	56±5	71±1.1	3.36±0.07	1.83±0.06	45.6%	112.4
#4	0.1	61±3	84±5	3.33±0.08	1.88±0.17	43.6%	130.7
#5	0.15	66.5±1.7	89±6	3.26±0.05	1.95±0.06	40.2%	116.7
#6	0.15	72±4	92±7	3.17±0.05	1.98±0.18	37.7%	146.3
#7	0.2	71±3	91±3	3.24±0.04	2.23±0.01	31.1%	42.3
#8	0.2	68±4	113±3	3.15±0.03	1.82±0.01	42.3%	89.9
#9	0.3	77±3	107±2	3.29±0.04	2.1±0.11	36.0%	85.9
#10	0.5	86±4	141±9	3.28±0.12	2.09±0.03	36.3%	133.2
#11	0.6	93±4	165±5	3.15±0.11	2.04±0.07	35.1%	164.4
#12	0.8	96±9	203±6	3.31±0.07	2.21±0.06	33.3%	185.9

[a]All fouling fluids contain additional 42 ppm Ca^{2+} (in the form of $CaCl_2$)
[b]Average values of fouling fluids obtained at both the inlet and outlet of PHE at three different running times and one from the launching tank
[c]Average values of fouling fluids obtained at the inlet of PHE at three different running times and one from the launching tank
[d]Average values of fouling fluids obtained at the outlet of PHE at three different running times
[e]BLG denaturation level = 1-$[BLG]_{outlet}/[BLG]_{intlet}$

A clear view of how casein affects the fouling can be seen in Figure 2.6(a): at Casein/WPI lower than 0.2, fouling mass drops dramatically as Casein/WPI ratio increases, leading to a minimum mass of 42.3 g and that is almost 80% reduction compared to that without casein. Exceeding Casein/WPI of 0.2, the fouling mass increases gradually as Casein/WPI goes higher. More detailed information about fouling mass in each PHE pass is presented in Figure 2.6(b). In general, fouling mass increases along the PHE with maximum values at the last pass. Similar fouling starting points were found to be located between 4th and 5th pass, where the temperature ranges from 71.6 and 73.7 °C. These values are in accordance with the denaturation temperature of BLG at 72 °C (Boye and Alli, 2000). One exception can be observed at Casein/WPI of 0.2 (Fluid #7) where apparent fouling (>1 g) can only be found at the 7th pass with an average temperature at 79 °C. The surface coverage of fouling deposit inside PHE can be calculated using the area between the 4th and 10th pass of PHE as shown in supplemented Figure A2. Without adding casein, the fouling mass coverage is ~215 g/m^2, corresponding to a mean fouling rate at 1.8 g/(m^2·min). This fouling rate is comparable to the other large-scale fouling experiments with similar PHE configurations using 1 wt% whey protein concentrate fouling fluid at a calcium concentration of ~70 mg/L (Khaldi et al., 2015a). Surprisingly, the minimum fouling rate observed at Casein/WPI of 0.2 is close to that obtained for milk fouling in pasteurization studies, *e.g.* between 0.15 and 0.25 g/(m^2·min) (Barish and Goddard, 2013; Choi et al., 2013).

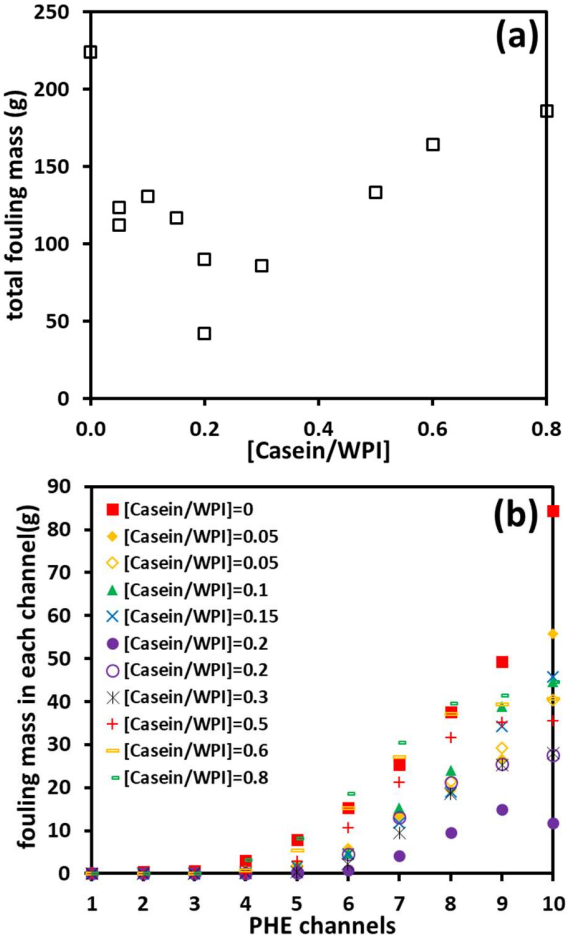

Figure 2.6. (a) Effect of Casein/WPI on the total fouling mass inside PHE. (b) Fouling mass distribution in each channel in the PHE at various Casein/WPI ratios. Note that replicated data at Casein/WPI of 0.05, 0.15 and 0.2 were obtained from individual experiments.

Pressure-drop and thermal resistance (R_f) are usually employed to monitor fouling within PHE systems in real-time. On one hand, fouling causes the hydraulic diameter to decrease during operating, arising the pressure-drop over time until the system collapses. On the other hand, due to the low heat conductivity of the deposits, the additional fouling layer hinders the heat transfer between the hot water and the process fluid. Figures 2.7(a) and (b) show the pressure-drop and thermal resistance (R_f) evolutions of fouling runs processed at various Casein/WPI ratios, respectively. The pressure-drop changes little at the first operating hour for all solutions and increases dramatically thereafter. While for R_f, the values keep increasing as fouling grows during the whole process. A similar trend can be observed for the maximum values of pressure-drop and R_f (*i.e.* values obtained at the end of fouling run), which both of them decrease as Casein/WPI

increases, reaching minimum values at Casein/WPI of 0.2. This is consistent with the fouling mass behavior. Worthy noticing is that, at Casein/WPI≥0.2, the extent of increased R_f resembles that of total fouling mass, while the increased pressure-drop is less significant. This is confirmed by plotting normalized values of fouling mass and maximum values of pressure-drop and R_f against Casein/WPI as shown in Figure 2.8. At Casein/WPI>0.2, high fouling mass can be obtained but induce much less pressure-drop (six times lower). This could be attributed to a different structure of fouling layers formed at Casein/WPI>0.2.

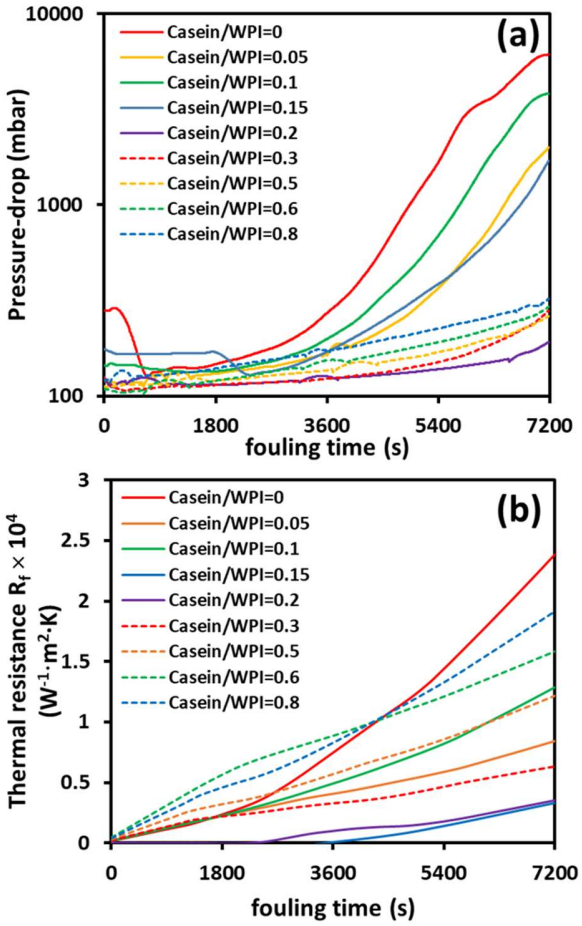

Figure 2.7. (a) Pressure-drop and (b) thermal resistance R_f evolution of fouling fluids containing different Casein/WPI ratios within 2 h fouling run. Data at Casein/WPI of 0.05, 0.15 and 0.2 are the average values obtained from two individual experiments. Solid lines represent the results at Casein/WPI ≤0.2 and dotted lines refer to that Casein/WPI >0.2. Note that log scale on y-axis in (a).

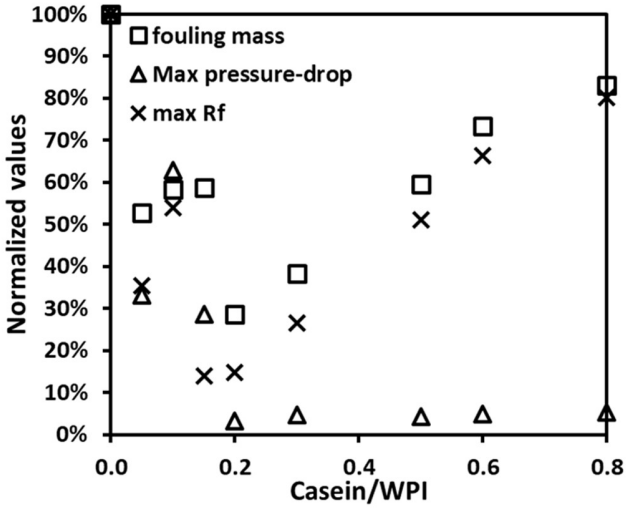

Figure 2.8. Effect of Casein/WPI on the normalized total fouling mass and maximum values of pressure-drop and thermal resistance R_f. Notice that the data at Casein/WPI of 0.05, 0.15 and 0.2 are the average values obtained from two individual experiments. Values are normalized by dividing values obtained at Casein/WPI of 0.

It has long been recognized that caseins have chaperone-like functions on the thermal denaturation or aggregation of whey proteins (Wijayanti et al., 2014; Yong and Foegeding, 2010). Consequently, we can expect that the fouling mass should be positively correlated to the BLG denaturation level. Nevertheless, our results do not really support the hypothesis and seem to indicate that BLG denaturation level alone is not a pertinent indicator to rank fouling behavior for casein-based protein solutions (Figure 2.9). Indeed, significant different fouling mass was obtained despite not significantly different values of BLG denaturation level (Fluid#1 compare with Fluid#2 to#12, Table 2.3). Besides, it was observed that the reduction of fouling mass is not accompanied by less denatured BLG proteins (Fluid#1 to#5, Table 2.3). On the other hand, the BLG denaturation level is significantly lower at higher Casein/WPI ratio (Fluid#9 to#12, Table 2.3, although in those conditions more fouling mass was observed.

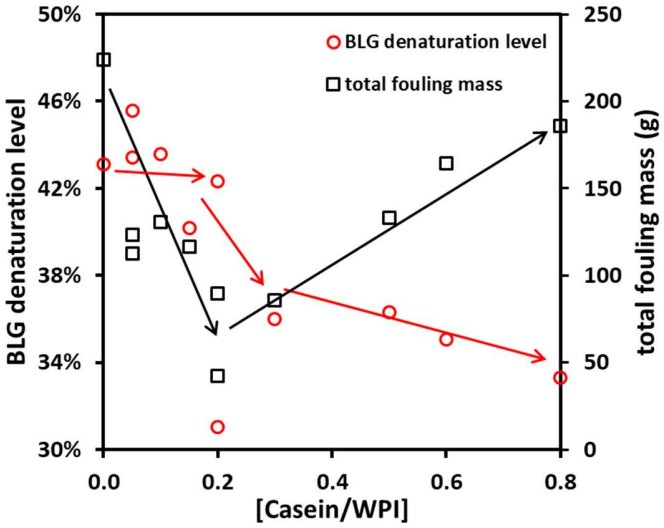

Figure 2.9. The effect of Casein/WPI ratio on the BLG denaturation level. The results on fouling mass were also presented for comparison. The conjugated arrows are used to guide the trend of BLG denaturation level.

These facts lead us to conclude that it is hard to correlate the BLG denaturation activity with fouling mass behavior in the presence of casein. It is important to note that the pHs of the solutions increased with the supplementary of caseins (from 6.5 at Casein/WPI = 0 to ~7.1 at Casein/WPI of 0.8). In more alkaline conditions, there are more dissociated caseins (*i.e.* individual α_s/β/κ-caseins released from casein micelle) in the serum phase (Anema, 1998), which might explain the progressive decrease of the BLG denaturation level due to potential chaperone-like activities. Nevertheless, why there is a significant drop in fouling mass even with the addition of a little amount of casein (*e.g.* Casein/WPI = 0.05, pH 6.6), or why fouling mass increased at high Casein/WPI ratios even with low BLG denaturation levels remain unclear. It is plausible that the casein micelle differentiates fouling layer composition and changes the dynamic of fouling growth without mobilizing more denatured BLG than in the case with the absence of casein. In fact, the BLG denaturation levels do not provide any detailed information on what exactly happens in the bulk fluid (*e.g.* casein-whey interactions) nor the deposition reaction in the PHE. Thereby, a more systematic study on how casein affects the thermal denaturation kinetics of BLG will be discussed in the following section.

2.6.3 The effect of casein on BLG denaturation kinetics

As mentioned previously, we have observed through heat treatment process within PHE that the denaturation level of BLG is almost unchanged when casein was added to WPI protein (Casein/WPI from 0 to 0.2). Nevertheless, simultaneously a decreasing fouling behavior is observed regarding fouling deposit mass. In order to provide a more exhaustive view on how casein affects the thermal denaturation process of BLG at different temperatures, the thermal denaturation kinetics of BLG were studied at a molecular level, using trials at laboratory scale and samples having the same compositions as the fouling fluids applied in the pilot-scale PHE (compositions are shown in Table 2.1).

Figure 2.10(a) is a typical example of the soluble BLG concentration (C_s) evolution with time for a 0.5 wt% WPI solution heat-treated at different holding temperatures (70°C to 90°C). For a given holding temperature, as expected, C_s decrease with time and for a fixed heating time, C_s decrease sharper with higher holding temperatures. The best-fit reaction order was determined according to the RSS values obtained by fitting equation 2.5 to the experimental data (supplementary figure, Figure S2.1, page 116), where the most suitable values were found to be 2. In the literature, the findings for the reaction order for the heat-induced denaturation of BLG commonly varied between 1.5 and 2. For example, several researchers have reported a reaction order of 1.5 (Anema and McKenna, 1996; Dannenberg and Kessler, 1988; Oldfield et al., 2005; Oldfield et al., 1998b), whereas (Hillier and Lyster (1979); Lyster (1970); Manji and Kakuda (1986); Park and Lund (1984)) found that BLG denaturation followed second-order reaction kinetics. This discrepancy among these studies may be explained by the variability of the medium of the protein solution (different buffers or simulated milk ultrafiltrate), the heating treatments (direct stream injection or sealed capillary tubes), protein compositions (isolated BLG or whey with or without casein), protein assays or even statistical approaches (Jaskulka et al., 2000; Leite et al., 2021; Loveday, 2016).

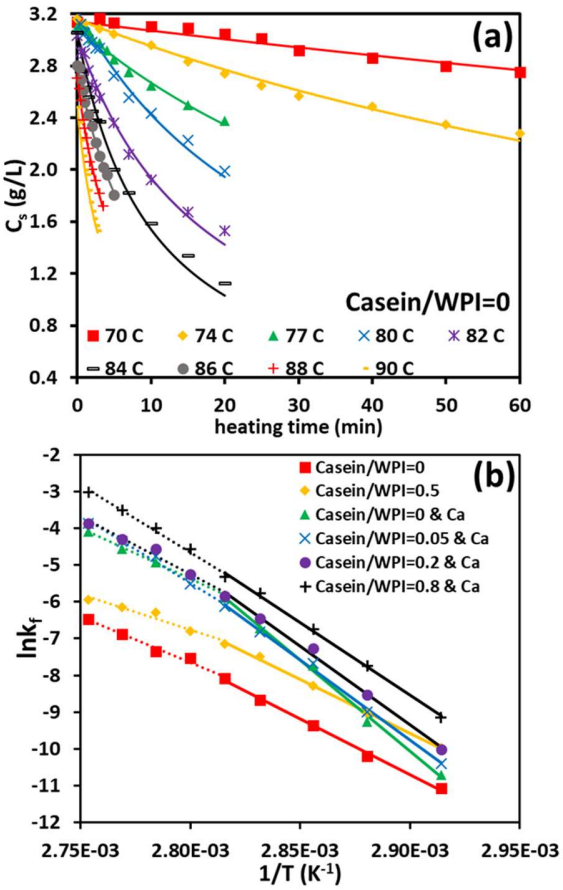

Figure 2.10. (a) Evolution of soluble BLG concentration against heating time at various heating temperatures (denoted in legend). The solution contains only 0.5 wt% WPI without adding Ca^{2+} (nor casein powder). Solid lines represent best-fit to equation 2.5 using a reaction order of 2. (b) Arrhenius plot for the BLG denaturation reaction at different protein compositions (shown in Table 2.3). Solid lines correspond to the linear regression in the unfolding region while dashed lines refer to the aggregation region.

Giving the best-fit values of k_f, the logarithm can be plotted against the inverse of the holding temperature in the Arrhenius plot as shown in Fig.2.10(b). Analysis of Fig.2.10(b) shows clearly that, the introduction of both ionic calcium and micellar casein modifies the denaturation rate constant of BLG while maintaining the same shape (broken slope). Inspection of model solutions containing different Casein/WPI ratios reveals a global increase of k_f when Casein/WPI goes up. The positive shift observed in the ordinate axis in the Arrhenius plot appears very moderate for Casein/WPI varying from 0 to 0.2, while at high Casein/WPI such as 0.8, the increase of k_f is more

remarkable. More precisely, for Casein/WPI ranges from 0 to 0.2 (corresponding to fouling mass decreasing region), increasing Casein/WPI enhances slightly the BLG denaturation constants for the unfolding step, while in the aggregation limited region, the values are overlapping, suggesting a limited effect of casein on the BLG aggregation process. It is difficult to compare our results with those of literature as in this field few kinetic data of dairy solutions exist. Nevertheless, the significant increase of k_f with higher casein content agrees with those reported in Kessler and Beyer (1991), who found increased denaturation constants at elevated casein/whey proportions from sweet whey to skim milk.

Table 2.4 is another view of the BLG denaturation behavior in the presence of micellar casein, as it summarizes the corresponding activation energies Ea in each denaturation step calculated from the linear regression in the Arrhenius plot. The calculated Ea for unfolding and aggregation for whey protein solutions when no ionic calcium or casein micelle is added are 252 and 210 $kJ \cdot mol^{-1}$, respectively. Note that there is no statistical difference between these two values, indicating there is only one dominant reaction at this temperature range, which is unfolding (70-90 °C). These present Ea are comparable to the range of Ea values in skim milk, 265-280 $kJ \cdot mol^{-1}$, reported by (Anema and McKenna (1996); Dannenberg and Kessler (1988); Oldfield et al. (1998b)) for temperature lower than 90 °C. The addition of Ca^{2+} resulted in similar values of aggregation Ea at 230 $kJ \cdot mol^{-1}$ to the whey protein but a much larger value of 411 $kJ \cdot mol^{-1}$ was found for the unfolding Ea. Similar Ea values have been reported for a 0.5 wt% whey protein with an additional 80 ppm Ca^{2+} (Khaldi et al., 2018). These results confirm the opposite binary effect of Ca^{2+} on the BLG unfolding step observed by Petit et al. (2011): on one hand, Ca^{2+} facilitates the BLG unfolding by increasing k_f, while on the other hand, Ca^{2+} limits the unfolding process by resulting in larger activation energy.

Table 2.4. Calculated kinetic parameters for BLG denaturation at various Casein/WPI using one-step reaction model. Errors denote standard errors from linear regression.

		Casein/WPI ratios							
		In this work						In literature	
	Denaturation parameters	0	0.5	0*	0.05*	0.2*	0.8*	4†	0§
Unfolding	$\ln(k_{0U})$	77±3	75.5±1.9	133±5	117±4	114±5	105±3	91.0±10.5	141.8
	Ea_U (kJ/mol)	252±9	243±6	411±13	363±11	354±14	327±9	285.5±30.8	431.6
Aggregati	$\ln(k_{0A})$	62±5	47±7	72±5	97±6	83±7	98±6	58.8±5.7	74.1
	Ea_A (kJ/mol)	210±15	160±20	230±15	305±18	260±20	303±16	15.3±1.8	233.5

*Solutions contain additional 42 ppm Ca^{2+}.
†Kinetic data for skim milk reported by Oldfield et al. (1998b), while the unfolding region was recognized between 70 to 90 °C.
§Kinetic data for whey proteins reported by Khaldi et al. (2018). Solution contained additional 80 ppm Ca^{2+}.

When analyzing more intimately Table 2.4 for Casein/WPI solutions (varying from 0 to 0.2), increasing Casein/WPI slightly decreases the activation energy for BLG unfolding. From the thermodynamical point of view, it can be assessed that in the presence of abundant ionic calcium, micellar casein does not represent an obstacle to limit the BLG unfolding. On the contrary, the presence of casein does not seem to strongly affect the activation energy for the aggregation process: a clear trend showing decrease or increase is not obtained for the range of Casein/WPI ratio investigated.

To sum up, from Figure 2.10 and Table 2.4, it appears again that the decreased fouling mass at Casein/WPI from 0 to 0.2 is hard to be explained by the minor changes in the BLG denaturation reaction due to the introduction of casein. It is more probably due to the change in mineral interactions introduced by casein that affects the origin of fouling build-up. For high Casein/WPI (*e.g.* 0.8), the increase of denaturation of BLG is more significant, implying more casein-BLG interactions. This is expected as BLG has a larger opportunity to interact with dissociated casein proteins or κ-casein located at the surface of casein micelle, facilitating the aggregation process (Anema and Li, 2003a). Nevertheless, the impact of casein on the denaturation level of BLG in

the PHE system shows contrary effects to the denaturation kinetic experiments with decreasing denaturation levels at elevated Casein/WPI ratios (Figure 2.9). This inconsistency might be due to the significantly different flow regimes between these two experiments (*i.e*. continuous mode with turbulent flow in PHE *vs* bath mode with static flow in the kinetic experiments). This result could also be attributed to the denaturation of proteins that already occurred in the quick heating zone in the kinetic experiments (Bath #2, Fig. 2.3). Depending on the conditions, the time required to reach the desired temperature could up to one or two minutes, which might strongly affect the kinetic results. Therefore, the results deduced from denaturation kinetic experiments must be analyzed with cautions to be extended to the pilot plant.

2.6.4 Element mapping of fouling deposit

In order to further investigate the effect of casein on the fouling, the morphology and chemical composition of the fouling layer was characterized using EPMA. For each fouling experiment, the deposits were collected from two different plates (*i.e*. P_{14} and P_{21}) so as to see the influence of temperature on the build-up of the fouling layer. In each EPMA analysis, Fe (iron), S (sulfur), P (phosphate) and Ca (calcium) were determined in the same area of fouling layer cross-section.

Figure 2.11 shows the element mapping results of fouling layers obtained from fouling solutions at four different Casein/WPI ratios collected from P_{14}. Repartition of Ca, P and the characteristic element of the protein (S) of the deposit formed at an average temperature of 78.9 °C without the addition of casein is shown in Fig. 2.11(a). A compact fouling structure was found in this case with homogenously distributed signals of both Ca and S. The P element inside the deposit, however, was negligible as the signal in the deposit is even weaker than the stainless steel substrate. The P signal is only significant in the fouling deposit formed at high casein concentration (Casein/WPI = 0.8) regardless the temperature it was formed (*e.g*. results obtained at a higher temperature (84.6 °C) is shown in Figure 2.12).

Moreover, the areas corresponding to Ca and S overlap each other, indicating a co-location of Ca and proteins inside the fouling layer. These results support the idea that in absence of casein and for the range of calcium/BLG ratio investigated (~9), Ca^{2+} acts as binding agents of denatured proteins to co-precipitate upon the hot stainless steel surface (Visser and Jeurnink, 1997). The effect of calcium on the morphology of the fouling layer for casein-free whey protein solutions

has been previously reported by Khaldi et al. (2018). These authors demonstrated that the fouling growth mechanism depends and evolve on the increase of Ca/BLG ratios: at a low Ca/BLG ratio (2.3), the fouling layer is compact, while in the case of higher Ca/BLG ratios such as 22.9, calcium-based particles act as anchor-points for an arborescent fouling growth.

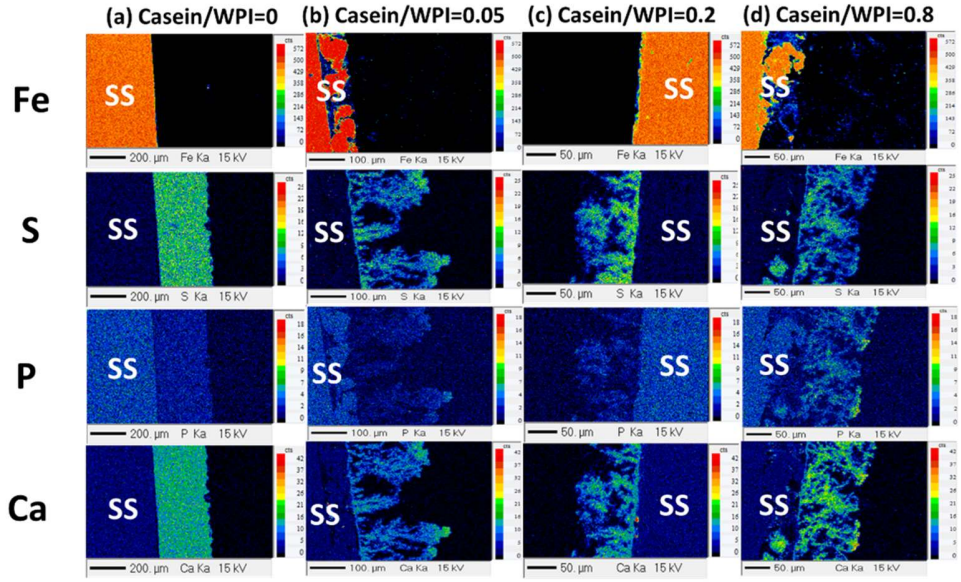

Figure 2.11. Fe, S, P and Ca mappings of the cross-section of the fouling layer for fouling fluids at various Casein/WPI ratios of (a) 0 (b) 0.05 (c) 0.2 and (d) 0.8. Deposits were collected from plate P_{14} with an average temperature of 78.9 °C. SS refers to stainless steel.

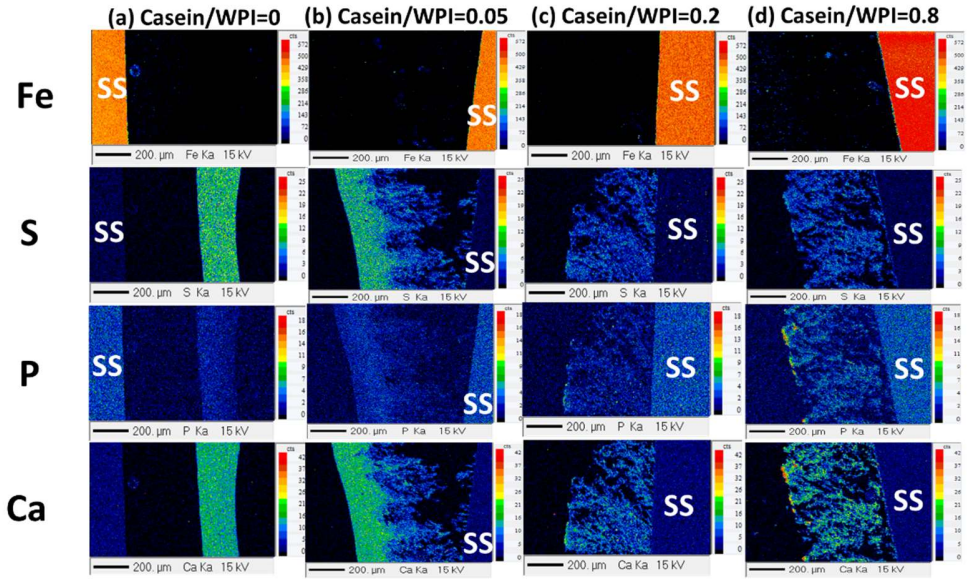

Figure 2.12. Fe, S, P and calcium mappings of the cross-section of the fouling layer for fouling fluids at various Casein/WPI ratios of (a) 0, (b) 0.05, (c) 0.2, and (d) 0.8. Deposits were collected from plate P_{21} with an average temperature of 84.6 °C. SS refers to stainless steel. Note that deposits in (a) and (b) were detached from SS surface during drying.

When casein was present as shown in Fig. 2.11-2.12(b)-(c), heterogeneous fouling structures were obtained. In these conditions, the fouling layer was less compact and airier. Besides, both Ca and S started to be unevenly distributed inside the fouling layer with less intensity of Ca, even though more Ca was present in the fouling fluids (scale bars for each element are identical). Despite this, co-location of Ca and S signals was still apparent in the deposit except at Casein/WPI of 0.8 where P element could no longer be ignored in the fouling layer. These findings could be another proof to support that i) the presence of casein micelle induces less ionic calcium so that there are less calcium ions participating in the fouling build-up ii) the presence of individual caseins alters the deposition pattern of denatured BLG molecules upon the surface, resulting in a less compact structure.

To obtain a deeper insight into the distribution of minerals (Ca, P) in the fouling layer and their interactions with protein (S), overlapped areas of Ca, P and S have been plotted in Figure 2.13. It is evident that protein favored two types of organization with mineral: either with Ca alone or with Ca-P as the overlapped area of Ca, P and S (Ca-P-S, green area) differs from that for Ca-S (pink area). Besides, Ca-P-S are more conjugated and act like “tree-trunk” while the Ca-S areas are more scattered around the Ca-P-S. This finding reveals the existence of CaP nanoclusters as Casein/WPI ratio progressively increases, acting as linking agents for fouling build-up. These CaP nanoparticles can be created in the bulk or more possibly introduced from amorphous CaP inside casein micelle (Holt et al., 2013). From this point of view, the increased amount of fouling mass at Casein/WPI from 0.2 to 0.8 could be due to the increased participation of casein micelle (containing CaP nanoclusters). When temperature was higher as shown in Fig. 2.13(b), the area representing Ca-P-S was relatively smaller but the general trend of CaP surrounding with proteins is consistent. This difference with observation at lower temperature might be caused by the lower level of Ca^{2+} in the bulk (transferred into casein-bound calcium) as Ca^{2+} might also contribute to the formation of CaP nanoclusters.

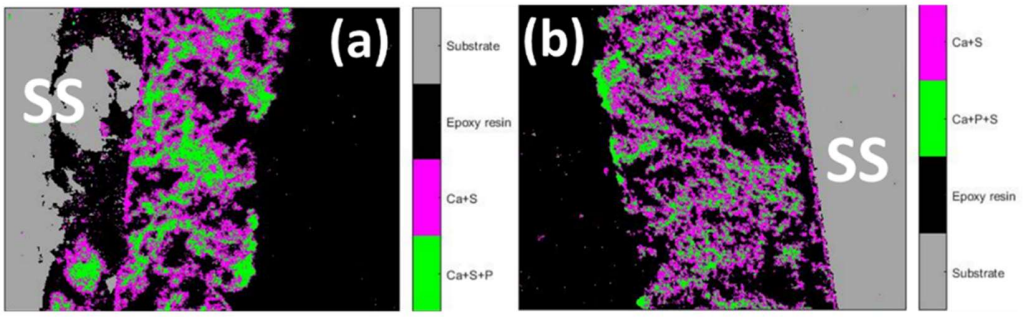

Figure 2.13. Overlapped areas of Fe, S, P and Ca elements of the cross-section of the fouling layer. The deposits were collected from the same fouling run using fouling fluid at Casein/WPI of 0.8 but in different plates: (a) P_{14} and (b) P_{21} resulting in different fouling temperatures at 78.9 and 84.6 °C, respectively. SS refers to stainless steel. The grey area denotes the SS substrate and the black area refers to the epoxy resin. The area in green corresponds to overlapped signals of Ca, S and P, while the pink area refers to the overlapped Ca and S.

2.6.5 SDS-PAGE

To further characterize the fouling deposits, they were analyzed using SDS-PAGE to study the protein composition. Figure 2.14 presents the electrophoresis results of eight different fouling deposits formed at four Casein/WPI ratios and collected from two different fouling locations. Pure protein standards were also performed to provide better identification of each protein in the fouling deposits. Results show all fouling deposits are mainly composed of α_s-casein, β-casein, BLG, and αLa, which is in agreement with those reported for milk fouling (Changani et al., 1997; Jeurnink, 1991). Note that even in the condition where casein was not supposed to be present (Casein/WPI of 0), few caseins were detected. This is probably due to powder elaboration and the difficulty to obtain WPI solutions free of casein during the membrane separation process of dairy fractions.

Inspection of casein content in fouling deposits shows a general trend of an increased amount of both α_s- and β-casein in the deposits with higher Casein/WPI ratios. On the other hand, BLG shows similar content inside the deposits for all conditions applied except a significantly larger band referring BLG was found for deposits collected from P_{14} at Casein/WPI of 0. Notice that all the fouling deposits were wholly dissolved prior to SDS-PAGE, hence, these results suggest a more proteinaceous deposit formed at a relatively lower temperature with the fouling solution without the addition of casein powder. On the contrary, a more mineral deposit was formed using

the same fouling fluid but at a higher temperature condition (*i.e.* P_{21}) as less BLG content was found despite a larger total fouling mass. Notice that the amount of total calcium content for these model fouling fluids is much lower compared to that of normal milk. At this low calcium level, the structure of casein micelle was proposed to swell and individual caseins such as α_s- or β-casein located at the interior of micelle become easier to dissociate into the bulk. Hence, the increased total fouling mass at Casein/WPI from 0.2 to 0.8 might be due to the larger participation of α_s/β-casein or submicelles in the formation of fouling. The absence of κ-casein in the deposit supports the idea that κ-casein is consistently dissociated from the casein micelle with higher temperatures and interact with denatured BLG molecules to form κ-casein/BLG complexes in the serum phase, which could explain its less involvement in fouling build-up (Jeurnink and Dekruif, 1995).

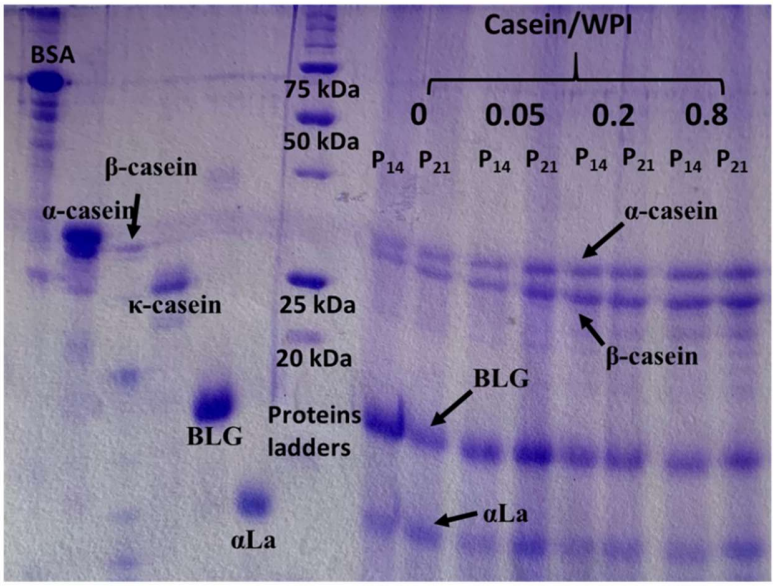

Figure 2.14. SDS-PAGE results including pure proteins standards, protein ladders, and fouling deposits. Pure proteins are (from left to right) BSA, α_s-casein, β-casein, κ-casein, BLG and αLa. Fouling deposits were obtained at different Casein/WPI ratios of 0, 0.05, 0.2 and 0.8; in each condition, deposits were collected from two different plates (P_{14} and P_{21}).

Conclusions

In this chapter, whey protein-based model solutions containing various Casein/WPI ratios were applied in order to study the influence of casein micelle on the fouling behaviors in a pilot-scale PHE applying a HTST pasteurization schedule. It was first established that for the WPI powder

used, the ionic calcium was a vital element promoting denaturation and fouling mass deposit. Secondly, for the casein-based protein solutions elaborated, the fouling mass dropped dramatically until a minimum value as Casein/WPI increased to 0.2. However, exceeding this critical Casein/WPI ratio, fouling mass increased with elevated Casein/WPI ratios. Casein/WPI ratio also alters the fouling structure: the fouling layer was compact and homogeneous with evenly distributed calcium and proteins when casein was absent, suggesting a binding role of Ca^{2+} between denatured proteins during the build-up of fouling. However, fouling deposits became heterogeneous and less dense: co-located Ca-S elements were scattered around the Ca-P conjugates. This inhomogeneity suggests that CaP nanoclusters, introduced by micellar casein, may act as new linking species between proteins as the fouling grows.

Results from gel electrophoresis revealed larger participation of α_s/β-casein in the fouling deposits at higher Casein/WPI conditions. These α_s/β-caseins are probably in a submicelles form (dissociated due to high temperature) containing CaP nanoclusters. This might explain why fouling mass increased at high Casein/WPI ratios as more caseins were involved in the formation of fouling. Concerning BLG denaturation, casein seems poorly affect the BLG denaturation process, and it was shown that the fouling behavior was not correlated to the BLG denaturation level at the conditions where fouling mass decreased (Casein/WPI≤0.2) or increased (Casein/WPI>0.2). It is finally proposed that micellar casein change deeply the calcium balance and the content of CaP nanocluster modifies sharply the interactions which occur between proteins species (BLG, caseins) and mineral elements (ionic calcium, Ca-P) thereby affecting the protein denaturation and mineral precipitation.

In this chapter, the effect of casein on the thermal denaturation behavior of BLG was evaluated using a conventional overall one-step reaction model. This model, despite a compromised description of the thermal denaturation pathway of BLG, provides a valuable overview of the denaturation behavior of BLG. However, this model neither failed to explain the break-slope phenomenon in the Arrhenius plot nor being a quantitative model which can assess the quantities of different BLG species during heating. In the next chapter, a novel kinetic model concerning BLG denaturation will be presented which provides a mathematical interpretation on the break-slope behavior in the Arrhenius plot by assuming the unfolding of BLG is instantaneous. This

developed model was used to evaluate bothe the effect of ionic calcium and casein micelle on the thermal denaturation pathway of BLG.

Supplementary figures for Chapter Two

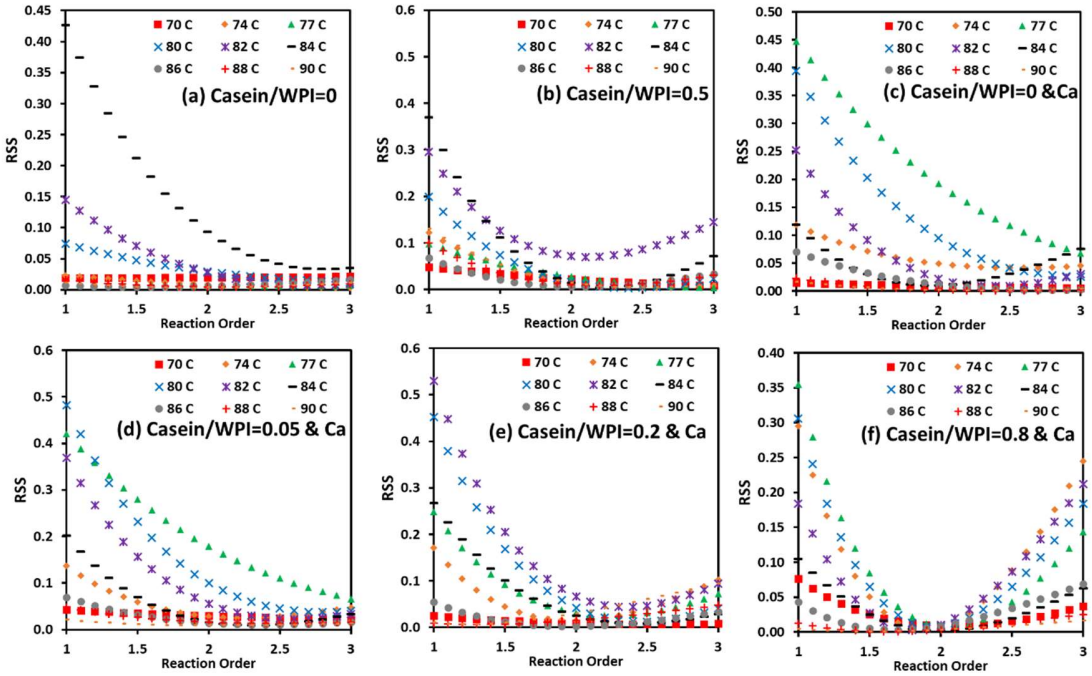

Figure S2.1. RSS (Residual sum of squares) obtained by fitting equation 2.5 to experimental data at various model fluids with different reaction orders.

Chapter Three. A novel kinetic model describing thermal denaturation pathway of BLG

In this chapter, a novel kinetic reaction model concerning thermal unfolding and aggregation of BLG will be developed. The developed model was then first applied to investigate the effect of ionic calcium on the thermal denaturation of BLG. Besides that, the kinetic results presented in Chapter One will be re-evaluated through this new frame to understand the role of casein on the thermal denaturation of BLG.

For sake of clarity, it was decided to present a short introduction on the state of the art about the thermal denaturation pathway of BLG including the limitations or obstacles on the derivated kinetic models. Therefore, some publications and equations might have been previously shown in Chapter One. Note that the main content of this chapter including the installation of the model as well as its application on evaluating the effect of calcium on BLG thermal denaturation has been drafted as an article submitted to the journal "Food Hydrocolloid" (under revision) entitled "Effect of calcium on the reversible and irreversible thermal denaturation pathway of β-lactoglobulin".

Introduction

The literature investigations in Chapter One has revealed the heat-induced denaturation pathway of BLG being a multistage reaction, which can be expressed using the simple scheme as shown below (de Wit, 2009):

$$D_2 \rightleftharpoons 2N \qquad \text{(eq. 3.1a)}$$

$$N \leftrightarrow R \rightarrow M \rightarrow U \rightarrow A \qquad \text{(eq. 3.1b)}$$

BLG naturally exists as native dimers D_2 under physiological conditions, (*e.g.* neutral pH and concentration >50 μM) (Hambling et al., 1992). Upon heating up to 55 °C, BLG dimer starts to dissociate and reaches an equilibrium with its dissociated monomer form (N). Simultaneously during heating (< 60 °C), minor conformational changes of BLG which assembles the classical Tanford transition observed at room temperature by pH adjustment was detected (Qi et al., 1995). This state of BLG molecule exhibits greater accessibility of a single abnormal carboxyl group which appears to be buried inside the hydrophobic interior of the protein in its native conformation (Seo et al., 2010). The free thiol group at Cys_{121} was also reported to be slightly exposed, while this transition is mild and thus reversible and often noted as Reversible-state or simply R-state (R). At 65 to 70 °C, almost all BLG dimers are dissociated into monomers at neutral pH (Owusu Apenten and Galani, 2000). Accompany this, irreversible modification of dissociated BLG

monomers start to appear which largely exposed hydrophobic surfaces as well as the free –SH group. BLG at this temperature range is generally noted as a "molten globule state" (M) at which the protein molecules typically retain largely native-like secondary structure contents with no rigid tertiary structure and their intramolecular mobility is much larger than that in the native state (Ptitsyn, 1995). However, one should notice that irreversible damage of virtually all helical conformation and up to one-fifth of the β-sheets were lost during heating between 60 and 70 °C (Qi et al., 1997). When temperature is above 70 °C, larger conformational changes are detected in the secondary structure and described as a progressive loss of β-sheets structures and a concomitant formation of disorder structures. This molecular state of BLG is typically noted as unfolded state (U), which exhibits large reactivity to initiate a series of thiol oxidation or –SH/S-S intra/inter-molecular exchanger reactions as well as hydrophobic interactions with other denatured whey proteins or with κ-casein on the casein micelle surface to form aggregates (A) (Creamer et al., 2004; Sawyer, 1969; Vasbinder and de Kruif, 2003; Verheul et al., 1998).

In the dairy science literature, denaturation of BLG has been monitored in a variety of ways: loss of solubility (Gough and Jenness, 1962), a shift in elution time in high-performance liquid chromatography (HPLC; Kehoe et al., 2011; Petit et al., 2011; Zúñiga et al., 2010) or loss of band intensity in native polyacrylamide gel electrophoresis (PAGE; Anema et al., 2006a; Oldfield et al., 2005; Oldfield et al., 1998b). These "off-line" analytical methods fail to distinguish between native and R-state BLG (or between M, U and A) as these techniques require cooling of the protein samples which triggers the refolding of R-state BLG. For example, in an HPLC system, the pH of the heat-treated protein solution was adjusted to 4.6 to precipitate those "denatured" contents followed by centrifugation prior to injecting the supernatant. This supernatant containing so-called "soluble BLG content" (S) was verified to consist of native and unfolded BLG which refolds back to its native state after cooling while the precipitates comprise the irreversibly denatured BLG (*i.e.* M or U or A) (Delahaije et al., 2016). If we only consider the temperature above 70 °C as in our case (*i.e.* 70-90 °C), equation 3.1(b) can be simplified as a two-step consecutive process as $N \rightarrow U \rightarrow A$. However, due to the technical limitation as in the HPLC system, a more simplified overall one-step reaction model is typically used to describe the denaturation process as $S \rightarrow A$. The apparent compromise of this one-step reaction model is that both native and unfolded BLG are all considered to be the reactants for aggregations which is unlikely to be true according to the denaturation mechanism. Whilst, the key limitation of this model is its incapacity to quantify the

amount of native and unfolded BLG species; the latter being more vital as it is often mentioned to be the foulant precursor, meaning that its concentration is required for predicting fouling deposits.

The reaction rate of the overall one-step reaction model can be described as:

$$\frac{dC_S}{dt} = -k_f C_s^{n_f} \quad \text{(eq. 3.2)}$$

where C_S (mol·m^{-3}) refers to the concentration of soluble BLG as measured in the HPLC system, n_f is the reaction order, and k_f is the denaturation rate constant in a unit depending on n_f as mol$^{1-n_f}$·m$^{3n_f-3}$·s^{-1}.

The temperature dependence of k_f is typically deduced by the Arrhenius equation:

$$k_f = k_{f0}\exp\left(\frac{-Ea}{RT}\right) \quad \text{(eq. 3.3)}$$

where k_{f0} is the denaturation pre-exponential factor (mol^{1-nf}·m^{3nf-3}·s^{-1}), Ea is the activation energy (J·mol^{-1}), R is the universal gas constant (*i.e.* 8.314 J·mol^{-1}·K^{-1}) and T is the temperature in Kelvin. Equation 3.3 is usually treated with logarithm as:

$$\ln(k_f) = -\frac{Ea}{R}\frac{1}{T} + \ln(k_{f0}) \quad \text{(eq. 3.4)}$$

$\ln(k_f)$ is then plotted against 1/T (also known as Arrhenius plot) for calculation of Ea and k_{f0}. According to equation 3.4, a straight line is expected assuming Ea is constant within the temperature range. Nevertheless, a sharp bend is always observed whatever thermal denaturation of BLG occurs in milk (Anema and McKenna, 1996; Dannenberg and Kessler, 1988), whey (Khaldi et al., 2015b), or in pure BLG systems (Petit et al., 2011). The general admitted interpretation of such behavior in milk community is that there are two different governing reactions depending on the temperature: at temperatures lower than the critical temperature ($T < T_c$), the unfolding of BLG is slower than the aggregation, so the whole denaturation reaction is limited by the unfolding subreactions (noted as unfolding limited region). When the temperature is higher than T_c (aggregation limited region), aggregation of BLG is slower and hence becomes the limited step of the whole reaction.

In this frame, the kinetic and thermodynamic parameters of unfolding and aggregation of BLG were generally calculated respectively from the unfolding and aggregation limited region. Although imperfect, the one-step reaction model is valuable to give an overview of the BLG

thermal denaturation behavior. The thermodynamic parameters deduced from one-step reaction model are also plausible to be extended to the two-step consecutive reaction model ($i.e.\ N \rightarrow U \rightarrow A$) in the attempts of building fouling deposit model (Bouvier et al., 2014). Indeed, in most simulation works, researchers tend to use two-step consecutive reaction model due to its ability to calculate the evolution of unfolded BLG species as they were generally considered as the fouling precursor (Choi et al., 2013; Jun and Puri, 2005a; Pan et al., 2019). Almost all of the kinetic parameters were used as published by De Jong (1996) where the BLG denaturation was considered as a two-step consecutive reaction with a reaction order equals to one for the unfolding step and two for the aggregation process. Nevertheless, it is ambiguous why the break-slope phenomenon still exists in the aggregation process of two-step reaction model (De Jong, 1996) if the break-slope behavior is solely due to the competition of these two subreactions at different temperatures. Moreover, nobody, when using two-step consecutive reaction model mentions or seems to be aware that the kinetic parameters are likely to be strongly influenced by protein type, protein concentration and mineral content of processed dairy derivatives as it was clearly shown numeous times by recent investigations (Khaldi et al., 2018; Petit et al., 2011; Petit et al., 2016; Scudeller et al., 2021).

Whatever denaturation models we have mentioned above, the unfolding of BLG was always considered as a straightforward reaction typically with a reaction order equal to one. However, this is unlikely to be true as in the realm of biology, the thermal damage of proteins happens in a time scale of milliseconds (Johnson et al., 1974). Other analytic technologies to assess the thermal denaturation of BLG such as Fourier transform infrared (FTIR; Casal et al., 1988) or circular dichroism (CD; Qi et al., 1997), which provide "on-line" analysis also support this hypothesis. For instance, Iametti et al. (1996) failed to follow the kinetics of BLG denaturation during heating or cooling using CD, and they considered these heat-induced modifications were complete within seconds. In addition, Cairoli et al. (1994) observed that the exposure of tryptophan residues of BLG molecule was temperature-dependent and was essentially completed on the time scale of seconds. Furthermore, Fujiwara et al. (1999) monitored urea-induced denaturation of BLG using CD, and they found that a significant change in the CD intensity was observed within the dead time of measurements (25 ms). More recently, Euston (2013) used molecular dynamics simulation to follow the thermal unfolding of BLG, and the conformational changes of the molecule at 350 K were complete in ~0.7 μs. Indeed, if denaturation of BLG occurs within seconds, experiments

would require the temperature "jumps" to the desired value while using "on-line" analytical measurements such as UV absorption. This has been done in Huttmann and Birngruber (1999) where a temperature-jump experiment was achieved by using infrared pulsed radiation. They monitored the real-time denaturation of chymotrypsin using UV absorption and the denaturation of protein at 380 K was observed within 300 μs. The rate constants for the unfolding of chymotrypsin followed the Arrhenius equation can reach up to 3000 s^{-1}. It is thus plausible to extend this to BLG although BLG is larger compared to small protein molecule as chymotrypsin. Based on this, the thermal unfolding of BLG proteins is unlikely to be a rate-limited step at any temperature range. With this in mind, the deduced kinetic or thermodynamic data from the overall one-step reaction model are less accurate. Therefore, the objective of this chapter is to develop a novel BLG thermal denaturation model consistent with biological basis and also able to explain the break-slope phenomenon in the Arrhenius plot so as to provide more reliable kinetic and thermodynamic information. The model solutions were reconstituted from whey protein isolate (WPI) powder at a fixed concentration of 0.5 wt% containing elevated calcium concentrations. The thermal denaturation of BLG was assessed by HPLC and the kinetic, thermodynamic information were evaluated using the developed denaturation model. The kinetic data from Chapter One was re-evaluated using the developed model to understand the role of casein micelle on the thermal denaturation of BLG in a new aspect.

3.1 Development of the mathematical model

As mentioned previously, with the biological basis, it is assumed that the thermal unfolding of BLG occurs instantaneously. However, the unfolding process of BLG is unlikely to be kinetically driven otherwise the break-slope phenomenon would not exist as aggregation would always be the limited step whatever the heating temperature. Instead, the unfolding of BLG was proposed to be thermodynamically driven followed by a kinetically controlled aggregation step as:

$$N \rightleftharpoons U \rightarrow A \qquad \text{(eq. 3.5)}$$

The major difference between equations 3.5 and 1.3b (section 1.3.3 in Chapter One) is that there is a chemical equilibrium that is instantaneously established between the native and unfolded state of BLG at one temperature while in equation 1.3b, the unfolding of BLG is a kinetically controlled straightforward reaction and the unfolded BLG can only refold to its native state after cooling. Note that Equation 3.5 does not consider the dissociation of BLG dimer as all of BLG molecules are in their monomeric state at the temperature investigated (≥70 °C) (Owusu Apenten and Galani, 2000). The equilibrium constant K_c for the unfolding reaction in equation 3.5 can then be expressed as:

$$K_c = \frac{C_U}{C_N} \qquad \text{(eq. 3.6)}$$

where C_N and C_U represent the concentration of native and unfolded BLG molecules, respectively.

The equilibrium constant K_c can be expressed by the enthalpy ΔH_u and entropy ΔS_u of the reaction according to van't Hoff equation:

$$\ln(K_c) = -\frac{\Delta H_u}{RT} + \frac{\Delta S_u}{R} \qquad \text{(eq. 3.7)}$$

And therefore

$$K_c = \exp\left(-\frac{\Delta H_u}{RT} + \frac{\Delta S_u}{R}\right) \qquad \text{(eq. 3.8)}$$

Considering that the soluble BLG concentration detected in HPLC is the sum of native and unfolded BLG, the concentration of unfolded BLG molecule can be accessed as:

$$C_U = \frac{K_c}{1+K_c} C_s \qquad \text{(eq. 3.9)}$$

The proportion of unfolded BLG in the total soluble BLG, or defined as unfolding ratio α is:

$$\alpha = \frac{K_c}{1+K_c} \quad \text{(eq. 3.10)}$$

And consequently,

$$C_U = \alpha \cdot C_s \quad \text{(eq. 3.11)}$$

Note that equation 3.11 has the same expression as reported in (Tolkach and Kulozik, 2007) where an unfolding constant was also defined as the proportion of unfolded BLG content in the total soluble BLG. In Tolkach's model, the unfolding of BLG seems to be instantaneous, for example, their values of α are equal to one when the temperature is higher than the critical temperature T_c, meaning that all BLG molecules are unfolded when a specific temperature was reached. While this is not the case as in our model, the defined α cannot reach the value of one according to equation 3.10 (*i.e.* $\alpha \in (0,1)$).

The subsequent reaction rate of aggregation or polymerization of unfolded BLG species can be expressed as:

$$-\frac{dC_{U,A}}{dt} = k_A \cdot C_U^n \quad \text{(eq. 3.12)}$$

where k_A and n are the reaction constant and reaction order for the aggregation step, respectively. As in the HPLC system, the loss of soluble BLG content is solely due to the aggregation of BLG:

$$\frac{dC_S}{dt} = \frac{dC_{U,A}}{dt} \quad \text{(eq. 3.13)}$$

Combining equation 3.2 and equation 3.12-3.13 results:

$$k_f = \alpha^n \cdot k_A \quad \text{(eq. 3.14)}$$

The logarithmic form of equation 3.14:

$$\ln(k_f) = n \cdot ln\alpha + \ln(k_A) \quad \text{(eq. 3.15)}$$

Equation 3.15 provides a mathematical interpretation of the break-slope phenomenon in the Arrhenius plot as shown in Figure 3.1. At low temperature, K_c is low, hence α is close to zero. While temperature increases, the thermoequilibrium shifts toward the unfolded state of the protein, resulting in higher K_c and α is getting close to one. As k_A is unknown, an initial guess of k_A is

deduced from linear regression using k_f values obtained at high temperature range ($T \geq T_c$). The corresponding activation energy Ea_A and pre-exponential factor $k_{0,A}$ for the aggregation step can be obtained using the Arrhenius equation. Thereafter, the unfolding ratio α can be calculated using equation 3.16 as:

$$\alpha = \exp\left(\frac{\ln(k_f) - \ln(k_A)}{n}\right) \quad \text{(eq. 3.16)}$$

The corresponding enthalpy ΔH_u and entropy ΔS_u for the unfolding equilibrium can be deduced using nonlinear regression combining equations 3.8 and 3.9 as:

$$\alpha = 1/\left[1 + \exp\left(\frac{\Delta H_u}{RT} - \frac{\Delta S_u}{R}\right)\right] \quad \text{(eq. 3.17)}$$

Note that the calculated α using the initial guess values of k_A (from equation 3.16) is unlikely to fit the nonlinear regression (equation 3.17) properly as there will be several values of α that are equal to one. Consequently, an iteration process is necessary to optimize the value of Ea_A and $k_{0,A}$ by minimizing the residual sum of square (RSS) between calculated values of α using equation 3.16 and fitted values that derivated from fitted ΔH_u and ΔS_u using equation 3.17. A detailed description of the above-mentioned optimization process is shown in the black frame in Figure 3.1 (Right side).

The corresponding Gibbs free energy ΔG_A for the aggregation step can be calculated using Eyring equation:

$$k = \frac{k_B T}{\hat{h}} \exp\left(-\frac{\Delta G_A}{RT}\right) \quad \text{(eq. 3.18)}$$

where k_B is the Boltzman constant ($\approx 1.38 \times 10^{-23}$ J·K^{-1}) and $\hat{h}$ is the Plank constant ($\approx 6.62 \times 10^{-34}$ J·s). k is the denaturation kinetic rate constant that is independent of the reaction order (s^{-1}) and can be calculated with initial protein concentration:

$$k = k_f \cdot C_{s,0}^{n-1} \quad \text{(eq. 3.19)}$$

Then, for a one-step reaction (aggregation step), the below relationship holds:

$$Ea_A = \Delta H_A + RT \quad \text{(eq. 3.20)}$$

And finally, the entropy ΔS_A of the aggregation can be obtained using:

$$\Delta G_{\mathrm{A}} = \Delta H_{\mathrm{A}} - T\Delta S_{\mathrm{A}} \qquad \text{(eq. 3.21)}$$

The optimized values of k_{A} and α allow to quantify the amount of soluble BLG content against the heating time by integration of equation 3.2 with substitution of equation 3.14 (for n≠1):

$$C_{s,t} = [C_{s0}^{1-n} - (1-n)\cdot\alpha^{n}\cdot k_{\mathrm{A}}\cdot t]^{1/(1-n)} \qquad \text{(eq. 3.22)}$$

And consequently for the amount of native and unfolded BLG content:

$$C_{N,t} = (1-\alpha)[C_{s0}^{1-n} - (1-n)\cdot\alpha^{n}\cdot k_{\mathrm{A}}\cdot t]^{1/(1-n)} \qquad \text{(eq. 3.23)}$$

$$C_{U,t} = \alpha[C_{s0}^{1-n} - (1-n)\cdot\alpha^{n}\cdot k_{\mathrm{A}}\cdot t]^{1/(1-n)} \qquad \text{(eq. 3.24)}$$

All the mathematical calculations were conducted using software Matlab®.

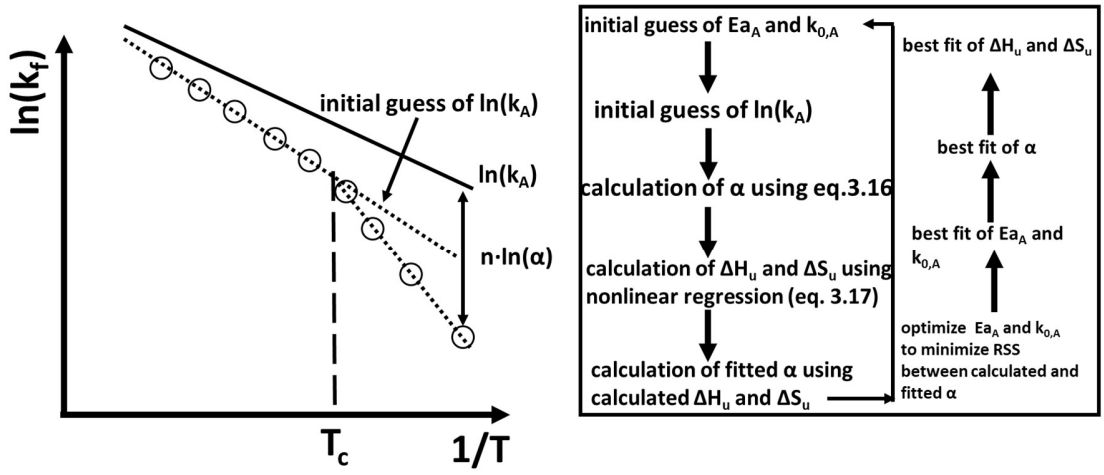

Figure 3.1. Left: mathematical interpretation of break-slope behavior in the Arrhenius plot regarding the thermal denaturation kinetics of BLG using equation 3.15. Right: optimization process for obtaining thermodynamic parameters ΔH_{u} and ΔS_{u} for the unfolding equilibrium and activation energy $E\mathrm{a}_{\mathrm{A}}$ and pre-exponential factor $\mathrm{k}_{0,\mathrm{A}}$ for the aggregation step.

3.2 Thermal denaturation kinetic experiments

Whey protein isolate (WPI) powder was purchased from Davisco Foods International Inc. (Le Sueur, MN, USA), with a protein content >90 wt% as given by the manufacturer, of which ~65% is β-lactoglobulin (BLG) and ~27% α-lactalbumin (α-La). WPI powder was reconstituted with MilliQ water to prepare model solutions at a protein concentration of 0.5 wt% to simulate the whey protein content in raw milk (Farrell Jr et al., 2004). The ionic and total calcium of the 0.5 wt% WPI solution was confirmed to be less than 0.1 and 1 ppm using calcium ion-selective electrode (9720BNWP, Thermofisher, USA) and atomic absorption spectrometry (Vista-MPX, Varian, USA), respectively. Various Ca^{2+} levels (40, 50, 60 and 70 ppm) were achieved by adding different amounts of $CaCl_2$ powder (anhydrous, Acros Organics, USA) in order to investigate the effect of Ca^{2+} on the thermal denaturation and aggregation of BLG. The pHs of the model solutions were fixed at 6.6 by adding concentrated HCl or NaOH to eliminate the effect of pH on the protein denaturation.

The experimental protocol for thermal denaturation of BLG was similar as reported by Petit et al. (2011) (as shown in Chapter Two). Briefly, all model solutions were prepared at room temperature and were stirred for at least one hour to ensure complete dissolution of protein powder and balancing with additional Ca^{2+}, if any. After that, 2 ml aliquots were removed into plastic tubes (Eppendorf, Germany) before heating. The heating processes included three stages by using three water baths: the first water bath was set at 65 °C to pre-heat the solutions without denaturing the proteins (Paulsson and Dejmek, 1990) and the second bath was set at 10 °C higher than the desired holding temperature (*i.e.* T_d +10 °C) to quickly heat up the solution to reach T_d, at which it corresponded to time zero for kinetic calculation. As soon as the solutions reach T_d, they were submitted into the third water bath (temperature set at T_d +1 °C) to maintain the solution temperature at T_d. The sample temperature was monitored by following the temperature evolution of a reference tube filled with MilliQ water, in which a T-type thermocouple was inserted. The holding temperature T_d varied from 70 to 90 °C was maintained for a proper period of time to induce signifcant BLG denaturation. At different holding time (includes at time zero when the solution just reach T_d), the denaturation of proteins were quenched by removing the solutions into melting ice.

The heat-treated solutions were allowed to return back to room temperature prior to adjusting the pH of the solutions to 4.6 to precipitate the aggregates. The precipitations were removed by centrifugation at 12000 *rpm* at 4 °C for 30 min. The BLG in the supernatant or the soluble BLG is considered to consist of native BLG as well as those unfolded BLG that refolds back to the native state. This has been confirmed by Delahaije et al. (2016) as they found the nonaggregated BLG at pH 4.6 has the identical secondary structure to that of native BLG using circular dichroism. The supernatant was filtered via a 0.22 μm PVDF filter before injecting 20 μL into the HPLC system (ThermoFisher UltiMate 3000). The soluble BLG concentration was detected using size exclusive chromatography (SEC) through an XBridge BEH 200 Å 3.5 μm column (Waters, USA). A 50 mM phosphate buffer at pH 7.0 and 0.7 ml/min with UV detection at 280 nm was used. Pure BLG powder (≥90%) was purchased from a domestic company (Shanghai yuanye Bio-Technology Co., Ltd, China) for calibration.

3.3 Results and discussions

3.3.1 Determination of best-fit reaction order

It is important to note that the prerequisite to obtain equation 3.14 is to equalize the reaction order n_f for overall one-step reaction model (eq. 3.2) and the reaction order n for the aggregation step (eq. 3.12). The best-fit reaction order n_f found in the literature generally varied from 1 to 2, typically 1.5 (Anema and McKenna, 1996; Dannenberg and Kessler, 1988; Petit et al., 2011; Tolkach and Kulozik, 2007). Figure 3.2(a) shows the evolution of soluble BLG concentration for a model solution containing 50 ppm Ca^{2+} heating at temperatures ranging from 70 to 90 °C. It is evident that the amount of soluble BLG keeps decreasing as heating time prolongs, and at higher temperatures, the loss of soluble BLG is more significant, indicating a more severe denaturation reaction. The best-fit reaction order n_f was then determined according to the RSS values (residual sum of squares) obtained by fitting equation 3.2 to the experimental data as shown in Figure 3.2(b). There is a general trend for RSS obtained at different heating temperatures with elevated reaction orders with minimum values located at around two. Increasing Ca^{2+} level slightly affects the best-fit reaction order, as at low Ca^{2+} concentration (≤ 40 ppm), the best-fit reaction order was found to be localized between 1.4-1.7 (see supplementary figure, Figure S3.1, page 140). However, for all calcium concentrations tested, the best-fit reaction order was found to be two (inset of Fig. 3.2(b)). Indeed, if n_f and n are the same, a reaction order of two is more likely to describe an aggregation

step assuming elementary reaction kinetics (Chen et al., 1998). Besides that, a reaction order of two can also be found for BLG denaturation in skim milk (Hillier and Lyster, 1979; Lyster, 1970; Manji and Kakuda, 1986), simulated milk ultrafiltrate (Park and Lund, 1984) or in whey protein solutions with or without the addition of casein micelles (Liu et al., 2021). Therefore, the best-fit reaction order in this study is considered to be two.

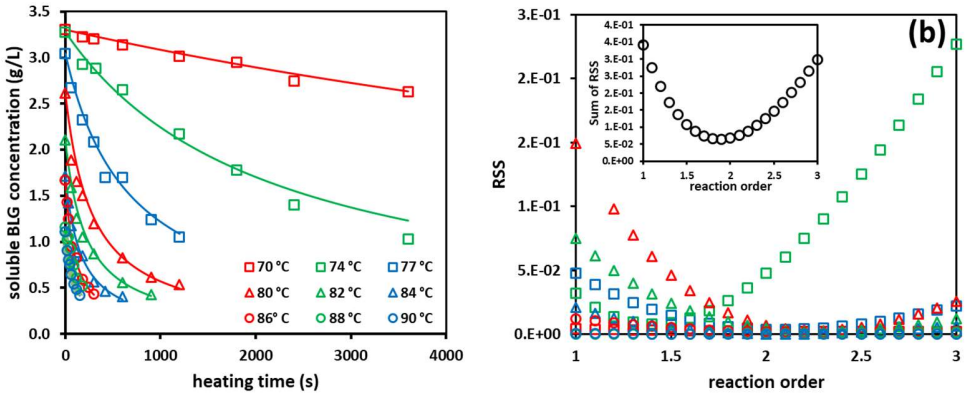

Figure 3.2. (a) Evolution of soluble BLG concentration against heating time at elevated heating temperatures (shown in legend) for a 0.5 wt% WPI solution containing 50 ppm Ca^{2+}. (b) Corresponding residual sum of squares (RSS) obtained at different heating temperatures fitted by equation 3.2. Inset shows the sum of RSS obtained using values from all heating temperatures at all calcium concentrations tested.

3.3.2 Reversible and irreversible denaturation pathway of BLG

The determination of best-fit values of reaction order allows the calculation of k_f values according to equation 3.2. Figure 3.3(a) presents the Arrhenius plot for a 0.5 wt% WPI solution containing 50 ppm Ca^{2+}. As described previously, an initial guess of k_A values was calculated using linear regression of k_f obtained at high temperatures ($\geq T_c$). The corresponding values of activation energy Ea_A and logarithmic pre-exponential factor $\ln(k_{0,A})$ are 221.1 kJ·mol^{-1} and 68.2 mol^{-1}·m^3·s^{-1}, respectively. However, as shown in Fig. 3.3(b), the calculated α is unlikely to fit the nonlinear regression using equation 3.17. These two values of Ea_A and logarithmic frequency factor $\ln(k_{0,A})$ are subsequently used as initial values to trigger the optimization process. As shown as the black line in Fig 3.3(a), the optimized values of Ea_A and logarithmic pre-exponential factor $\ln(k_{0,A})$ are 153.7 kJ·mol^{-1} and 49.3 mol^{-1}·m^3·s^{-1}, respectively. These two values permit us to

calculate α which fits better with equation 3.17 (black curve in Fig. 3.3(b)). Table 3.1 summarizes the thermodynamic parameters obtained at different Ca^{2+} levels, including enthalpy ΔH, entropy ΔS and the Gibbs free energy ΔG for both the unfolding equilibrium and aggregation process.

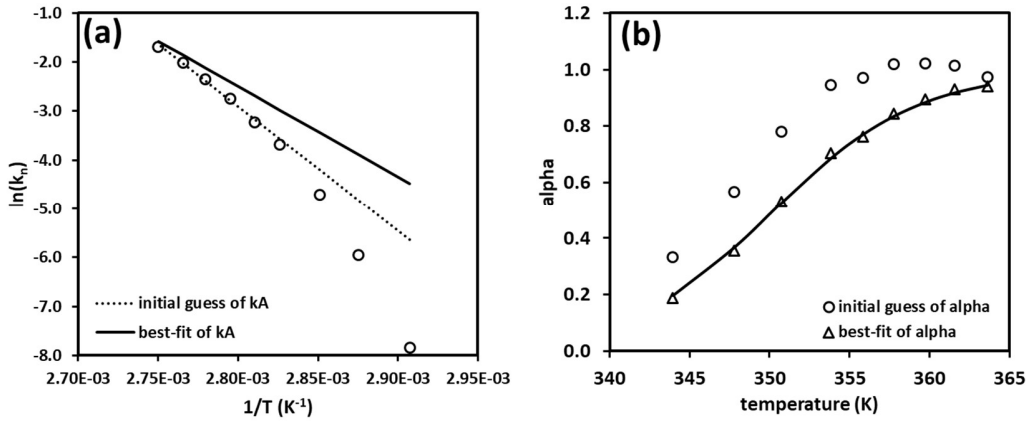

Figure 3.3. (a) Arrhenius plot obtained for a 0.5 wt% WPI solution containing 50 ppm Ca^{2+} with a reaction order of 2. The dotted line denotes the values of initial guess of k_A calculated using linear regression of k_f values obtained at high temperatures. The black line shows the optimized values of k_A as outlined in the text. (b) α values calculated using initial guess (in square symbols) and best-fit (in triangular symbol) values of k_A. The black curve denotes the best nonlinear regression fit of α using equation 3.17. The corresponding values of ΔH_u and ΔS_u are summarized in Table 3.1.

Table 3.1. Thermodynamic parameters calculated at various Ca^{2+} levels.

$[Ca^{2+}]$ (ppm)	Temperature* (°C)	Unfolding equilibrium			Aggregation				
		ΔH_u (kJ·mol^{-1})	ΔS_u (J·mol^{-1}·K^{-1})	ΔG_u (kJ·mol^{-1})	Ea_A (kJ·mol^{-1})	$\ln(k_{0,A})$ (mol^{-1}·m^3·s^{-1})	ΔH_a (kJ·mol^{-1})	ΔS_a (J·mol^{-1}·K^{-1})	ΔG_a (kJ·mol^{-1})
	70			-0.18			176.44	-275.01	270.76
0	80	125.39	366.12	-4.02	179.29	55.22	176.35	-269.10	271.46
	90			-7.66			176.27	-267.04	273.31
	70			3.23			157.92	-322.58	268.89
40	80	209.48	599.55	-2.71	160.78	50.98	157.84	-305.67	266.02
	90			-8.72			157.75	-302.04	267.67
	70			4.05			150.83	-342.32	268.57
50	80	224.62	641.28	-2.30	153.69	49.26	150.74	-320.46	264.14
	90			-8.56			150.66	-315.85	265.51
	70			5.01			104.27	-475.50	267.78
60	80	232.01	660.16	-1.53	107.13	33.99	104.19	-449.46	263.19
	90			-8.03			104.11	-443.13	265.23
	70			5.16			88.18	-518.75	266.58
70	80	255.59	728.18	-2.00	91.04	28.58	88.10	-493.61	262.71
	90			-9.14			88.02	-487.65	265.30

*Only data obtained at 70, 80 and 90 °C are shown for simplicity

The heat-induced denaturation or unfolding of the protein molecule, in which the tertiary structure is disrupted followed by break-down of weak intramolecular bonds is typically expressed as high values of ΔH and a positive ΔS as can be seen in our results. The addition of Ca^{2+} dramatically increases both the values of ΔH_u and ΔS_u, suggesting a reinforcement of intramolecular interactions and the state of order of the native BLG molecule with the presence of Ca^{2+}. This protective role of Ca^{2+} on the denaturation of BLG has been reported in Petit et al. (2011) where they found that higher activation energies were required for the unfolding step of BLG at a higher level of ionic calcium using an overall one-step reaction model. This phenomenon can be the result of the specific binding of calcium ions on the BLG molecules that strengthen the native BLG molecular structure (Simons et al., 2002).

A clearer view of the effect of Ca^{2+} on the thermal unfolding equilibrium of BLG is shown in Figure 3.4. For all ionic calcium levels tested, the unfolding equilibrium constant K_c increased with elevated temperatures, indicating a shift from native BLG into unfolded BLG molecule with higher heating temperatures (Fig. 3.4(a)). In the case without adding calcium, the calculated α is ~0.5 at 344 K (ca. 70 °C), meaning that around 50% of soluble BLG content is unfolded or reversibly denatured. At high temperature such as 91 °C, the proportion of unfolded BLG species increase up to 85%. The addition of ionic calcium shows two contrary effects on the unfolding equilibrium of BLG depending on the temperature. At low temperature range (≤ 82 °C), K_c decreases with an increased concentration of Ca^{2+} which corresponds to lower values of α and therefore lower proportion of unfolded BLG in the equilibrium. This behavior agrees with the above-mentioned protective effect of Ca^{2+} on the unfolding process. However, K_c shows higher values than those obtained with the absence of ionic calcium at higher temperatures, indicating Ca^{2+} favors the denaturation of BLG at such temperature range. This can be due to specific binding of Ca^{2+} with unfolded BLG molecules that facilitates the aggregation of unfolded BLG especially at higher temperatures (> 82 °C), and therefore the equilibrium towards unfolded BLG species is favored (Peres de sa Peixoto Junior et al., 2019).

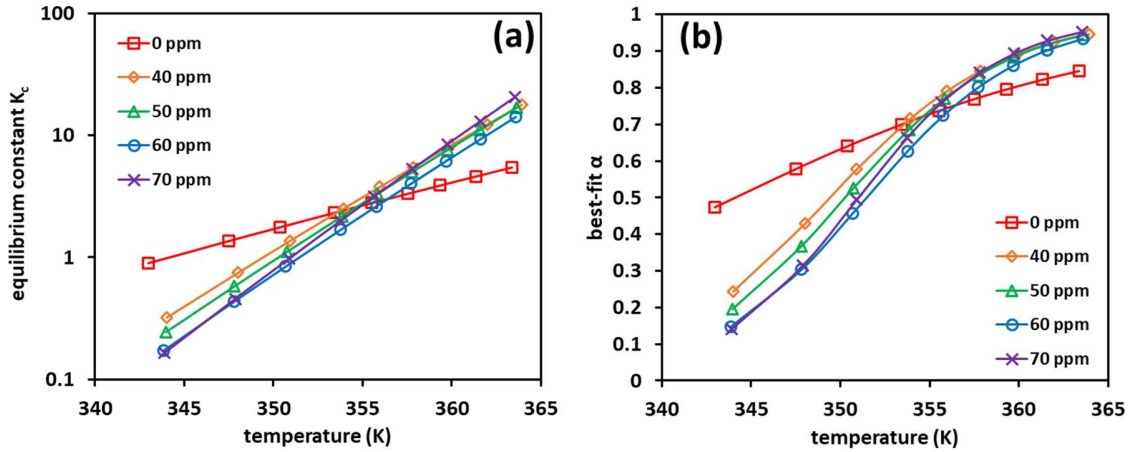

Figure 3.4. (a) Equilibrium constant K_c profiles against different heating temperatures at various ionic calcium concentrations (shown in legend). Note the logarithmic scale on y-axis. (b) Best-fit α values at different heating temperatures with elevated ionic calcium levels.

Our calculated value for the unfolding enthalpy ΔH_u at 70 ppm Ca^{2+} matches well to those obtained in milk (~80 ppm Ca^{2+}) at ~260 kJ·mol^{-1} evaluated using one-step reaction model (Anema and McKenna, 1996; Dannenberg and Kessler, 1988). It would be more interesting to compare our thermodynamic data with those measured using differential scanning calorimetry (DSC). The enthalpy measured from DSC is the sum of simultaneous unfolding and aggregational enthalpies and it was initially thought to be particularly suited to studying BLG thermal denaturation as aggregational enthalpies were considered to be small. This is the case when calcium is abundant such as in the milk where the aggregational enthalpy was reported to be relatively smaller at 47.9 kJ·mol^{-1} compared to the unfolding enthalpy at 260 kJ·mol^{-1}. Our results also support this idea, and more specifically show the evolution of both unfolding enthalpies ΔH_u and aggregational enthalpies ΔH_A with increased calcium concentrations. The overall denaturation enthalpies (*i.e.* $\Delta H_u+\Delta H_A$) increase slightly from 268 kJ·mol^{-1} with the absence of additional calcium to 344 kJ·mol^{-1} at 70 ppm Ca^{2+}. These values agree well with those denaturation enthalpies obtained in pH 6.6 phosphate buffer with pure BLG measured by DSC which typically ranges from 280~300 kJ·mol^{-1} (Gotham et al., 1992).

However, there is a major difference in the thermodynamic data reported in this work to those evaluated using the one-step reaction model, especially for the aggregation process. For instance, a significant decrease of the enthalpy ΔH_A for the aggregation process can be found from 176

kJ·mol^{-1} with the absence of Ca^{2+} to 88 kJ·mol^{-1} at 70 ppm Ca^{2+}. As well as reduced values of corresponding entropy ΔS_A from -275 J·mol^{-1} without additional Ca^{2+} to ca. -500 J·mol^{-1} with an additional 70 ppm Ca^{2+}. The decreasing trend of aggregational enthalpies ΔH_A clearly demonstrates a strong positive impact of Ca^{2+} on the aggregation of BLG. The phenomenon of calcium ions favoring the aggregation of BLG has long been experimentally supported either through measurements of aggregated sizes (Petit et al., 2012), zeta potential of the particle (Erabit et al., 2013) or solution turbidity (Ju and Kilara, 1998; Simons et al., 2002). However, the thermodynamic parameters deduced using one-step reaction model show contray effects of calcium on the aggregation process of BLG in the literature. For instance, increased Ca^{2+} concentration was reported to facilitate BLG aggregation by decreasing Ea_A from 360.7 kJ·mol^{-1} at 100 ppm to 260.4 kJ·mol^{-1} at 120 ppm (Khaldi et al., 2015b). Whilst, in a more systematic study, the calculated values of Ea_A do not differ with increased calcium concentrations (*e.g.* from 95 kJ·mol^{-1} at 0 ppm Ca^{2+} to 111 kJ·mol^{-1} at 264 ppm Ca^{2+} for enthalpy) (Petit et al., 2011). These contrary results suggest that one-step model needed to be improved to achieve better consistentcy.

Another important advantage of this model compared to the traditional overall one-step reaction model is its ability to quantify the amount of different BLG species under specific heat treatment. Figure 3.5 presents the evolution of different BLG species concentrations at two different ionic calcium levels and two heating temperatures using equations 3.22-3.24. The key assumption in this model is that the thermal unfolding of BLG protein occurs instantaneously as can be seen from the non-zero values of unfolded BLG concentrations at time zero. At low temperature such as 70 °C, the addition of 50 ppm Ca^{2+} significantly suppress the unfolding of BLG (α decreases from 0.47 to 0.2) as shown in Fig. 3.5(a) and (c). Nevertheless, as Ca^{2+} has a more predominant role favoring the aggregation process, the reduction of overall soluble BLG concentration is higher with the addition of calcium. At higher temperatures as shown in Fig. 3.5(b) and (d), the initial proportion of unfolded BLG is very close to one, and therefore the multi-step denaturation processes of BLG can be considered as a simple one-step reaction, *i.e.* aggregation.

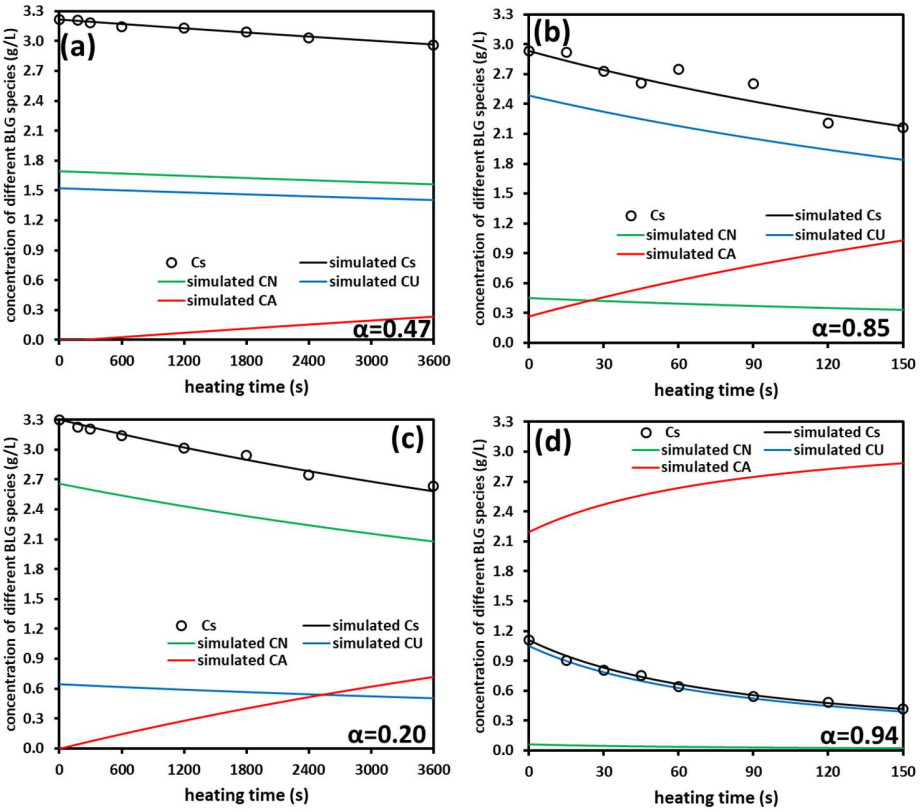

Figure 3.5. Evolution of different BLG species concentrations against heating time. Lines in black, green, blue and red denote simulated soluble, native, unfolded and aggregated BLG species, respectively. Symbols in circle refer to soluble BLG concentration as detected using HPLC. (a) and (b) were obtained at 70 and 90 °C without additional calcium, while (c) and (d) were obtained at 70 and 90 °C with the addition of 50 ppm Ca^{2+}. The non-zero values for aggregated BLG concentrations at time zero are due to the denaturation of BLG in the pre-heating process.

3.3.3 effect of casein on the denaturation pathway of BLG

The previous section has confirmed the ability of the developed model to evaluate the effect of Ca^{2+} on the thermal unfolding and aggregation process of BLG. Consequently, it was decided to re-evaluate the kinetic results obtained in Chapter Two to re-investigate the role of casein micelle on the thermal denaturation pathway of BLG. The calculated equilibrium constant K_c and best-fit α are shown in Figure 3.6. Despite using different whey protein solutions, the evolution of K_c and unfolding ratio α are almost identical for whey protein solutions alone (without the addition of calcium or casein), suggesting good reproducibility of the model. Adding 42 ppm Ca^{2+} (Casein/WPI=0&Ca, $[Ca]_f$ = 53 ppm, Table 2.1) shows consistent protective effects of Ca^{2+} on unfolding step of BLG by shifting native BLG⇌unfolded BLG equilibrium toward the formation of native BLG species (lower α). On the contrary to the effect of Ca^{2+}, increasing casein concentration progressively results in higher values of α regardless of the temperature, implying that casein favors the unfolding step of BLG. This is probably due to the chaperone-like activities of caseins that interact with unfolded BLG species through hydrophobic interactions. The formation of these unstable casein-BLG complexes could prohibit the unfolded BLG from refolding back to its native state.

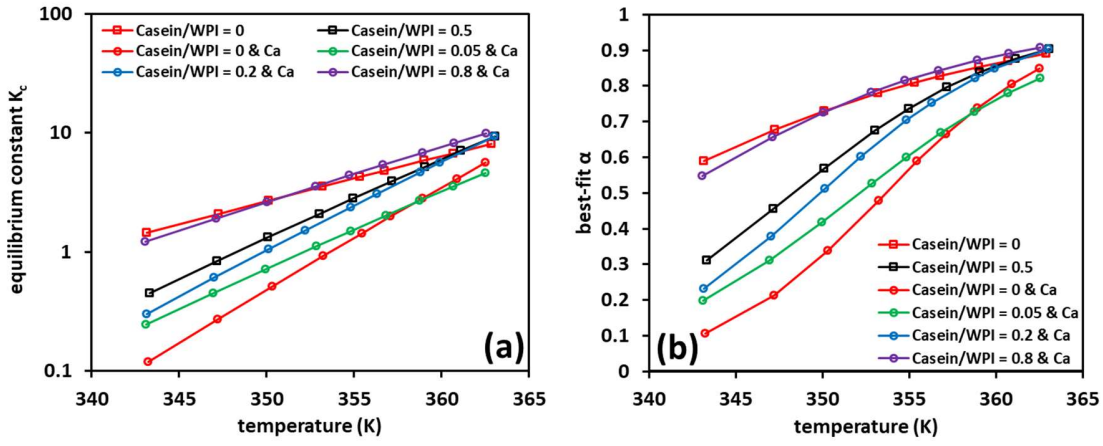

Figure 3.6. (a) Equilibrium constant K_c profiles against different heating temperatures at various casein/whey mass ratios (shown in legend). Note the logarithmic scale on y-axis. (b) Best-fit α values at different heating temperatures with elevated casein/whey ratios. Results were re-evaluated using the developed model from the kinetic results reported in Chapter One.

The corresponding thermodynamic parameters re-evaluated from Chapter One using the developed model are shown in Table 3.2. Again, the corresponding unfolding enthalpy ΔH_u and the activation energy Ea_A for the aggregation step show similar values for whey proteins solutions that were reconstituted from two different protein powders (without the addition of calcium or casein). Worth mentioning is that, for solutions with supplementary of 42 ppm Ca^{2+} (Casein/WPI=0&Ca, $[Ca]_f$ = 53 ppm), the thermodynamic parameters are comparable to those obtained with an ionic calcium level at 50 ppm (*e.g.* 210-220 kJ·mol^{-1} for ΔH_u and ~150 kJ·mol^{-1} for Ea_A). With the same amount of additional Ca^{2+}, increasing casein concentration up to Casein/WPI of 0.8 clearly shows a decreasing trend of ΔH_u with almost a half reduction from 206.8 to 111.4 kJ·mol^{-1}. These results support the idea that casein facilitates the unfolding step of BLG by decreasing the reaction enthalpy. On the other hand, caseins inhibit the aggregation process by increasing the activation energy for the aggregation process Ea_A almost two times from 148 to 271 kJ·mol^{-1}. This finding is in line with the chaperone-like functions of caseins that control the BLG-based aggregation process: either by forming α_s/β-casein-BLG complexes via hydrophobic interactions (Yong and Foegeding, 2010) or by the formation of disulfide-bonded κ-casein-BLG complexes that acts as a dead-end reaction for the propagation of BLG-based aggregation (Donato and Guyomarc'h, 2009).

Table 3.2. Thermodynamic parameters on BLG denaturation with the presence of calcium and caseins. Data were re-evaluated from the kinetic results reported in Chapter One.

Solutions	Temperature* (°C)	Unfolding equilibrium			Aggregation				
		ΔH_u (kJ·mol^{-1})	ΔS_u (J·mol^{-1}·K^{-1})	ΔG_u (kJ·mol^{-1})	Ea_A (kJ·mol^{-1})	$\ln(k_{0,A})$ (mol^{-1}·m^3·s^{-1})	ΔH_a (kJ·mol^{-1})	ΔS_a (J·mol^{-1}·K^{-1})	ΔG_a (kJ·mol^{-1})
Casein/WPI=0	70	90.46	266.64	-1.04	204.78	32.91	201.93	-195.01	268.85
	80			-3.72			201.84	-192.75	269.92
	90			-6.30			201.76	-189.60	270.06
Casein/WPI=0.5	70	159.41	457.68	2.28	108.01	32.91	105.15	-468.43	265.98
	80			-2.15			105.07	-456.77	266.31
	90			-6.75			104.99	-452.50	269.27
Casein/WPI=0&Ca	70	206.82	584.86	6.07	148.39	48.24	145.53	-356.66	267.96
	80			0.24			145.45	-336.86	264.43
	90			-5.19			145.37	-325.03	263.20
Casein/WPI=0.05&Ca	70	156.05	443.16	2.60	200.97	65.91	232.14	-101.81	267.06
	80			-1.18			232.05	-91.92	264.49
	90			-4.92			231.97	-84.34	262.55
Casein/WPI=0.2&Ca	70	178.84	511.22	1.92	184.53	60.35	227.66	-111.46	265.91
	80			-2.13			227.59	-100.10	262.84
	90			-7.02			227.50	-97.73	262.98
Casein/WPI=0.8&Ca	70	111.43	326.40	0.05	270.98	89.90	258.70	-13.4	201.93
	80			-3.28			258.61	-6.95	201.84
	90			-6.60			258.53	-4.20	201.76

*Only data obtained at 70, 80 and 90 °C are shown for simplicity.

Conclusions

In this chapter, a novel reaction model concerning thermal unfolding and aggregation of BLG with a biological basis has successfully been developed. The model assumes the thermal unfolding of the protein occurs instantaneously and more importantly, it is thermodynamically driven rather than kinetically controlled. Therefore, a chemical equilibrium between native and unfolded BLG species can be instantaneously established at one temperature followed by an irreversible aggregation step. This model interprets mathematically the break-slope behavior in the Arrhenius plot and provides detailed thermodynamic information for both unfolding and aggregation processes. Based on this model, the ionic calcium was confirmed to have a protective role on the thermal unfolding of BLG by decreasing the equilibrium constant K_c and increasing the corresponding enthalpy ΔH_u at low temperatures. Moreover, the addition of calcium clearly shows a reduction of the corresponding enthalpy and entropy for the aggregation reaction which cannot be seen as reported using the overall one-step reaction model. The positive impact of calcium on the aggregation helps to shift the unfolding equilibrium of BLG toward the formation of unfolded BLG species, especially at higher temperatures.

Re-visiting the kinetic data reported in Chapter Two using the model presented here permits us to investigate the role of casein micelle on the thermal denaturation pathway of BLG in a new aspect. On the contrary to the effect of Ca^{2+}, casein facilitates the unfolding process of BLG by decreasing the reaction enthalpies. Whilst, casein limits the aggregation of unfolded BLG by showing higher values of activation energy. These findings are in line with the chaperone-like functions of caseins that control the BLG-based aggregation process.

The presented model is likely to offer new perspectives to establish a link between protein denaturation and fouling growth onto the surface of heat exchangers by monitoring the evolution of unfolded BLG species during thermal processing for whey protein solutions. Therefore, in the next chapter, this model was applied to estimate the thermal denaturation behavior of BLG in the bulk fluid in the microchannel of a custom-built bench-scale fouling rig. A computational fluid dynamics (CFD) model in a 3D environment was used to simulate the thermodynamics of the fouling fluid. By coupling the thermal denaturation reactions, localized information of the unfolded BLG concentration can be obtained, permitting the calculation of the surface reaction kinetic constant, particularly at various ionic calcium concentrations.

Supplementary figures for Chapter Three

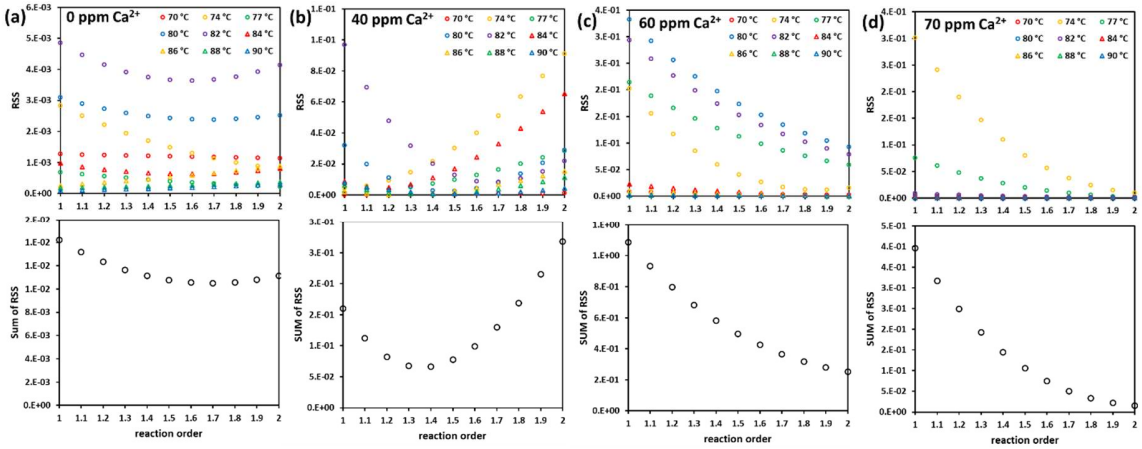

Figure S3.1. Residual sum of squares obtained at different heating temperatures (shown in legend) fitted by equation 3.2 for a model fluid containing (a) 0 ppm (b) 40 ppm (c) 60 ppm and (d) 70 ppm Ca^{2+}. The corresponding sum of RSS using values obtained from all heating temperatures are shown below.

Chapter Four. 3D modeling of whey protein fouling in a benchtop fouling device: effect of calcium

In this chapter, a custom-built laboratory device is designed in order to perform whey protein fouling with a similar bulk fluid temperature profile to that in the pilot-scale PHE system as presented in Chapter Two but in a laminar regime. The kinetic model developed in the previous chapter will be applied to monitor the thermal denaturation behavior in the microchannel of the device. Thanks to the simplicity of the configuration, whey protein fouling can be simulated using computational fluid dynamics (CFD) in a 3D environment. The model is validated by experimentally measuring the fluid temperature using fluorescence microscopy. By coupling the kinetic denaturation model as developed in Chapter Three (describing protein conversion through bulk reaction), the deposition reaction rate constant (surface reaction) can be calculated, particularly at various calcium levels. For sake of clarity, a short introduction section will be presented first, where some of the publications might have been mentioned in Chapter One. The work of this chapter has been summarized and drafted as an article entitled "Effect of calcium on the thermal denaturation of whey proteins and subsequent fouling in a bench-scale fouling rig: A 3D computational modeling" (Manuscript ready to be submitted when the article (Chapter Three) for evaluation on new denaturation kinetic model will be definitively accepted).

Introduction

Many studies dealing with the thermal processing of milk by-products have noted the key role of calcium in whey protein fouling behavior in the plate heat exchangers (PHEs). Calcium, particularly ionic calcium, is well known to have significant impacts both on the thermal denaturation of proteins in the bulk and deposition reactions on the surface. However, most of the attention has been paid on the calcium effect concerning thermal denaturation of BLG. For instance, ionic calcium was found to have a protective role on the unfolding step of BLG denaturation by showing increased activation energy with elevated calcium concentrations (Petit et al., 2011). Whilst, an ion-specific interaction between calcium and native BLG was found which induces local unfolding of the protein and exposition of its free thiol group (Jeyarajah and Allen, 1994). Moreover, calcium also takes part in the intramolecular electrostatic shielding of BLG negative charges that lowers the Columbian repulsion between proteins and favors the aggregation process (Simons et al., 2002). Despite what has been mentioned above, how calcium affects the fouling reaction kinetics has never been studied exhaustively.

Conceptually, dairy fouling can be considered to consist of mass transfer, thermal denaturation of proteins in the bulk as well as surface reactions (*i.e.* deposition) (Belmar-Beiny et al., 1993). The first two can be nowadays well calculated with a given geometry by using computational fluid dynamics (CFD) combined with thermal denaturation kinetic models. However, for the surface reaction, it was either empirically using the Biot number (Fryer, 1989) or using adsorption rates (De Jong, 1997), the latter being mathematically identical to a surface reaction. Most simulation models regarding dairy fouling considered unfolded BLG species as the fouling precursor. Since calcium both affects the denaturation pathway of BLG as well as the surface reaction, the bulk reaction has to be coupled to investigate the role of calcium on surface reactions. This has never been achieved, and one of the main obstacles is that most studies are performed in industry-like systems such as those in pilot plant PHEs. The complexities of the fluid mechanics and the configuration itself in the PHEs make it hard to investigate the surface reaction kinetics concerning the fouling growth. From an experimental point of view, it is still a great challenge to perform real-time measurements on the fouling deposition, particularly with similar temperatures and hydrodynamics to industry-like fouling experiments such as those in PHEs. It is rare to see dynamic measurement of fouling mass in PHEs in the literature as it is typically destructive (the plate has to be dismantled and dried), and therefore difficult to determine kinetics. There are only few studies that could provide dynamic measurements on the protein deposition, for example, Kroslak et al. (2007) studied the deposition kinetics of BLG at a solid-liquid interface with optical lightmode spectroscopy over a range of temperatures between 61 and 83 °C. Besides, Santos et al. (2006) studied the adsorption of whey proteins on modified and unmodified 316 2R stainless steel surfaces under well-defined flow conditions using *in situ* ellipsometry. These studies provide direct real-time information of the deposited protein mass, yet they have not been coupled with denaturation/aggregation reactions in the bulk to investigate the surface reactions.

The complex fluid mechanics in the system of PHEs brings more complexities to determine deposition kinetics in the simulation. For example, the flow regime shows a contrary effect on the fouling mass: the amount of fouling decreases with increased Reynolds number (Re) from 1800 to 7500 in a concentric tube heat exchanger (Belmar-Beiny et al., 1993), while a higher mass of deposit was found at Re of 3200 than that of 2000 or 5000 in PHE (Guérin et al., 2007; Khaldi et al., 2015a). Consequently, some bench-scale set-ups were designed to perform fouling experiments

in a laminar scheme in which the removal effect due to shear forces can be ignored (Hebishy et al., 2019; Huo et al., 2019).

Since a simpler flow regime such as laminar flow seems preferable in a preliminary approach to investigate the deposition kinetics, the first step of this chapter is to build a bench-scale fouling rig that could provide simple configuration and thus simple fluid mechanics (*i.e*. laminar regime). Model solutions that reconstituted from whey protein isolate (WPI) powders were used to perform fouling runs in the fouling rig at a fixed thermal profile. Various ionic calcium levels ranging from 40 to 70 ppm were applied in order to investigate the effect of Ca^{2+} on the surface reaction. The operating parameters for the fouling run were carefully selected to achieve a similar temperature profile as those operated in PHEs but in a laminar regime. Thanks to the simplicities of the geometry and flow regime, a realistic 3D simulation was developed to predict the thermal denaturation of β-lactoglobulin (BLG) in the bulk as well as deposition processes in the microchannel of the device using computational fluid dynamics (CFD) based on the geometry of the fouling rig. Of great interest, the denaturation kinetic model developed in Chapter Three was applied to evaluate the bulk reaction. The solution temperature in the microchannel was quantified using wide-field fluorescence microscopy to validate the numerical temperature profile (and consequently to perform a validation of hydrodynamic and heat transfer performance obtained by the numerical model), where the dye Pyrromethene 556 was utilized as a temperature indicator. And finally, the kinetic constants for the deposition reaction can be achieved with the combination of experimental deposition rates.

4.1 Build-up of benchtop fouling rig

A number of laboratory-scale devices have been developed in the literature to investigate milk fouling behavior (section 1.7, Chapter One). However, few of them were designed to target a similar temperature profile as those performed in pilot plant PHEs. In most cases, the fouling was performed in a batch mode in which the stainless steel was simply put in contact with the fouling fluids placed in a container with a controlled temperature (Boxler et al., 2013; Britten et al., 1988; Burton, 1965). Unfortunately, this way of heat processing does not correspond to reality as protein depletion occurs with time in batch mode, which will not happen in industrial practices. And when fouling was performed in a more traditional flow scheme (that is to say in continuous mode), the temperature evolution of the fluid was not well defined (Gandhi et al., 2017; Li et al., 2013). To

reconcile this issue, a benchtop fouling device was designed with a capacity for optical measurement so that, on one hand, the fouling growth can be visualized, on the other hand, the temperature profile of the fluid can be quantified using fluorescence-based techniques as described later. The 3D structure of the dismantled fouling rig is shown in Figure 4.1(a). This benchtop device consists of (from bottom to up) 6061 aluminum alloy substrate (68 × 44 × 6 mm^3), 304 stainless steel (SS) tube (i.d. 2 mm), SS plate (48 × 24 × 1 mm^3), silicone tunnel wall, silicone rubber, PMMA (polymethyl methacrylate) cover and a 3D-printed nylon bend tube. The SS plate was made from 316 L stainless steel and had been subjected to chemical pickling (treated in a mixture of 30 wt% nitric acid and 8 wt% hydrofluoric acid at room temperature for 45 min) (Hagsten et al., 2019b). In order to create a u-shape fluid tunnel, the SS plate was put inside the groove of the substrate before filling with silicone mixture (mixing ratio of 1:1, two-component silicone). PMMA was then placed upon the silicone to create a flat surface. The silicone was cast at 75 °C for at least one hour. After that, the PMMA cover was removed, a CO_2 laser was used to cut the silicone and a u-shape tunnel with a rectangular cross-section of 2 × 3.5 mm^2 (width × height) was created. The whole device is well-sealed via screws: it has been tested to be pressure-tolerant (at least 3 bar) and also allows to avoid any leakage and by-pass of the fluid. A picture-flow of the detailed preparation of u-shape tunnel is given in the supplementary figure, Figure S4.1, (page 168).

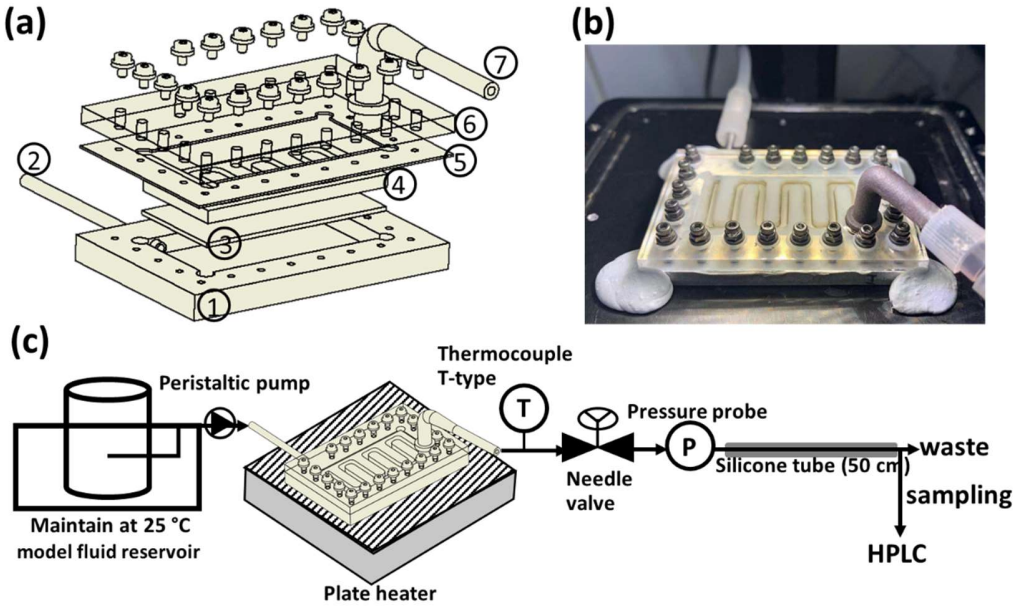

Figure 4.1. (a) 3D schematic of the dismantled benchtop fouling rig. The device is assembled with (from bottom to up) aluminum alloy substrate (1), 304 stainless steel tube (2), 316 stainless steel plate (3), silicone tunnel wall (4), silicone rubber (5), PMMA cover (6) and 3D-printed nylon bend tube (7). (b) The picture of the assembled state of the fouling rig mounted upon a plate heater. (c) experimental set-up for fouling runs.

4.2 Bench-scale fouling set-up

4.2.1 model fouling fluid

Whey protein isolate (WPI) was purchased from Davisco Foods International Inc. (Le Sueur, MN, USA), with a protein content >90 wt% as given by the manufacturer, of which ~65% is β-lactoglobulin (BLG) and ~27% α-lactalbumin (α-la). WPI powder was reconstituted with MilliQ water to prepare model solutions at a protein concentration of 0.5 wt% to simulate the whey protein content in raw milk (Farrell Jr et al., 2004). The ionic and total calcium of the rehydrated 0.5 wt% WPI solution was confirmed to be less than 0.1 and 1 ppm using calcium ion-selective electrode (9720BNWP, Thermofisher, USA) and atomic absorption spectrometry (Vista-MPX, Varian, USA), respectively. Various Ca^{2+} levels (40, 45, 50, 55, 60, 65 and 70 ppm) were achieved by adding different amounts of $CaCl_2$ stock solutions (Acros Organics, USA) in order to investigate

the effect of Ca^{2+} on the deposition of BLG in the fouling rig. The pHs of the fouling fluids were adjusted to be 6.6 by adding concentrated HCl or NaOH if needed.

4.2.2 bench-scale fouling runs

Fouling experiments were performed on the bench scale set-up as shown in Figure 4.1(c). Model fouling solutions that remained at 25 °C in a watch bath were pumped into the fouling rig through a peristaltic pump at a constant flow rate of 2 $ml \cdot min^{-1}$. The fouling rig was mounted upon a commercial plate heater (TP104SC, Instec, USA) in order to gradually heat up the solution (Figure 4.1(b)). The surface temperature of the plate heater was set at 90 °C resulting in a temperature profile of the solution ranging from 60 to 83 °C (in u-shape tunnel). This combination of the flow rate and the surface temperature was selected to have a thermal profile that mimics an HTST pasteurization process similar to that performed in the pilot plant PHE unit (Chapter Two) but in a laminar regime (supplementary figure, Figure S4.2, page 168). This was achieved by temperature quantification using fluorescence as described in the later section. A T-type thermocouple (accuracy ± 0.5 °C) was placed at the outlet of the fouling rig so as to monitor the experimental temperature of the fluid at the outlet. In order to avoid bubble formation during heating, the whole system was pressurized by providing a back pressure (~1 bar) using a stainless steel needle-type valve. A silicone tube (~ 50 cm) was connected to the outlet of the fouling rig which allows a natural cooling and sampling of the solution. Before pumping fouling fluid, Milli Q water was firstly used to reach a thermal equilibrium of the system at the desired process temperature. After that, fouling solutions were processed at different fouling durations, depending on the calcium level (*e.g*. 4 h for 40 ppm Ca^{2+} and 30 min for 65 ppm Ca^{2+}). During each fouling run, samples were taken at the end of the silicone tube typically three times (at beginning/middle/end). Brightview images were also captured during fouling experiments at different time intervals to dynamically monitor the morphology evolution of fouling deposits in the microchannel. More details of the microcopy system will be described in the later section. When the fouling experiments were finished, water was used again to replace fouling solutions in the channels; the fouling deposit at the end of each fouling run was also imaged. After imaging, the fouling rig was dismantled and the SS plate was dried at 50 °C overnight (with the removal of the silicone wall). The dried deposit mass was calculated by the difference between bare and fouled plates.

4.3 Temperature quantification using fluorescence

As mentioned in section 4.2, varying flow rate of the fluid in the tunnel and the bottom surface temperature of the plate heater can result in different temperature profiles of the fluid and therefore different thermal histories. It is of great importance to quantify the solution temperature in the channel in order to find suitable operating parameters. The fluorescence-based technique has been found to be a novel non-invasive method for quantitatively mapping solution temperature with high spatial resolution in microfluidic systems (Benninger et al., 2006). Rhodamine B (RhB) is one of the most commonly used dyes for thermometry (Paviolo et al., 2013), while it was not selected in this paper as RhB is well-known to interact/adsorb with many inorganic or organic materials, including silicone (Smart, 1977). Notice that, the initial aim applying fluorescence was to monitor whey protein fouling in a real-time manner by mapping the solution temperature during fouling. For this purpose, the RhB was ruled out due to the existence of dye-protein interactions that dramatically affects the fluorescence performance of the dye (Feng et al., 2021; Liu et al., 2018). Instead, the fluorescence dye Pyrromethene 556 (PM556) was selected due to its superior photostability without being disrupted by the presence of proteins. However, this first test failed due to the strong interference of the fouling deposit to the fluorescence measurement. Therefore, it was finally decided to apply PM556 solely as an indicator for temperature mapping of the fluid during heating in the microchannel (with the absence of proteins). A detailed description of this unsuccessful "initial test" is presented in Annex II.

PM556 was supplied from Exciton (USA) and was used as received. Fluorescent solutions of 10 μM PM556 were prepared by dilution of a concentrated stock solution (in acetone). The calibration curve was obtained by placing the solutions into a 1 mm thick glass cuvette with a T-type thermocouple to monitor the solution temperature. The cuvette was well-sealed to avoid evaporation of the solvent (*i.e.* water). The cuvette was put upon the plate heater at desired temperatures ranging from 25 to 90 °C; once the thermal steady state was reached, the fluorescence measurements were performed using a conventional wide-field microscope (WFM) as reported previously (Liu et al., 2017). In short, the WFM consists of a wide-field fluorescence microscope (MacroZoom Z16, Leica) and a ×1.0 planapochromatic objective (magnification 7.13×-115×). PM556 was excited at a wavelength of 470 nm (25 nm bandwidth, LED4D067, Thorlabs), and its fluorescence emission was recorded as 8-bit images with a monochrome CCD camera

(ICX285ALCCF, ToupTek, 1360 × 1024 pixels). The experiments were replicated at least three times.

To quantify the solution temperature in the fouling rig, the fluorescent solution of PM556 was used instead of fouling solutions. It was decided to fix the flow rate at 2 mL·min^{-1} (Re of 12, residence time of ~33 seconds in u-shape tunnel) while varying the surface temperature of the plate heater from 60 to 90 °C. As can be seen in Figure 4.2(a), due to the limited field of view (at lowest magnification 7.13 ×), typically six images were needed to obtain the whole view of the channel. Matlab® was used for image processing, including correction of the uneven illumination, alignment, image merging and thresholding as described in (Liu et al., 2018). The processed image containing only fluorescence information of the channel is shown in Figure 4.2(b). A 2D motorized stage (WN268TA50M, Winner Optics, Beijing, China) was coupled with the plate heater so as to move the fouling rig for imaging at different positions of the device.

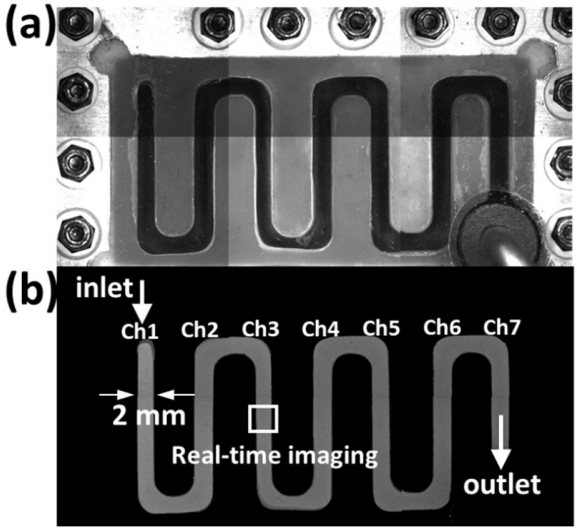

Figure 4.2. (a) Brightview and (b) fluorescence images of the microchannel in the bench-scale fouling rig. Each image was processed and merged from six different images. (b) was captured with 10 μM PM556 at a flow rate of 2 mL·min^{-1} and a constant bottom surface temperature at 90 °C. Images were obtained at the lowest magnification, *i.e.* 7.13 ×. Notice that a black-Ti 304 stainless steel was used in the case of fluorescence measurement instead of a normal 316 L SS plate in order to avoid the reflection effect. Channels are named from one to seven starting from the inlet as noted in the image.

The fluorescence captured in the WFM system is known to be the integration of the intensity along with the sample height (z-axis), therefore the fluorescence intensity I_f of PM556 in the microchannel can be described as (no photo-bleaching):

$$I_f = I_0 \hat{A} \Phi \varepsilon \delta_0 [Dye] \quad \text{(eq. 4.1)}$$

where I_0 is the excitation light intensity, $\hat{A}$ is the emitted light collection fraction, Φ is the quantum yield of the dye, ε ($m^2 \cdot mol^{-1}$) is the extinction coefficient of the dye at the excited wavelength, δ_0 (m) is the solution thickness, and [Dye] is the concentration of the dye ($mol \cdot m^{-3}$). If there is a temperature gradient in the z-axis (or quantum yield gradient) as in our case with a heating resource at the bottom surface in a laminar flow scheme, equation 4.1 should be modified as:

$$I_f = I_0 \hat{A} \Phi' \varepsilon \delta_0 [Dye] \quad \text{(eq. 4.2)}$$

The Φ' refers to the mean quantum yield of the dye in the whole solution thickness:

$$\Phi' = \frac{\int_0^{\delta_0} \Phi_\delta d\delta}{\delta_0} \quad \text{(eq. 4.3)}$$

where Φ_δ refers to the quantum yield of PM556 at the thickness position of δ. In this way, the mean value of solution temperature can be directly calculated using ratiometry by taking 25 °C as the reference. Because of this, the fluorescence of the solution channel in the fouling rig at 25 °C with no flow rate was firstly obtained for subsequent temperature calculation. One should notice that a black-Ti 304 SS plate was used instead of 316 L SS in fluorescence measurements to avoid the reflection effect of the stainless steel on the fluorescence that interrupts the experiments.

For real-time monitoring the fouling deposits, Brightview images were obtained using a full-color camera (MC170 HD, 5MP pixels, Leica) at the maximum magnification (*i.e.* 115 ×). To avoid the interruption of turbidity of the solution at high temperatures and high calcium concentrations, it was decided to fix the observation position at the middle of 3rd channel (Ch3).

4.4 3D simulation in bench-scale fouling rig

In this work, a realistic 3D simulation of the thermal denaturation and deposition of BLG inside the custom-built fouling rig was achieved by using COMSOL Multiphysics (COMSOL, version 5.3a). The geometry of the whole fouling set-up including laboratory fouling rig and outlet silicone tube were designed using the Autodesk Inventor and eventually imported to COMSOL. A physics-

controlled mesh was used to mesh the geometry as shown in Figure 4.3: a normal element size of meshing was applied for the solid phase, while a fine mesh was used in the solution domain (channel). Note that the effect of the formation of fouling layer on the flow regime or energy transfer was not taken into account in the simulation as the overall deposition layer was considered to be thin compared to the channel thickness (3.5 mm), so that the solution temperature, protein denaturation and hydrodynamics were not significantly affected due to the formation of fouling deposits (Pan et al., 2019). In other words, the fouling was assumed to follow a linear fouling pattern as presented earlier (Fig. 1.11, Chapter One). This was validated by performing a numerical simulation of milk fouling growth in the present benchtop fouling device (see Annex III).

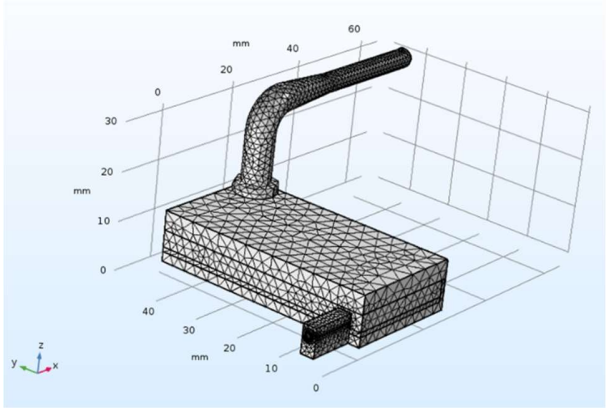

Figure 4.3. Mesh view of the benchtop fouling rig. The outlet silicone tube is hidden here to have a better focus on the device. Notice that some parts of the geometry were excluded to minimize the computing time.

4.4.1 The governing equations

A laminar incompressible flow model based on the Navier-Stokes equation is adopted to describe the fluid flow in the microchannel. The momentum and continuity equations in Cartesian coordinates are respectively:

$$\rho(\boldsymbol{u}\cdot\nabla)\boldsymbol{u} = \nabla\cdot[-p\boldsymbol{I} + \mu(\nabla\boldsymbol{u} + (\nabla\boldsymbol{u})^{\mathrm{T}}] + \boldsymbol{F} \qquad \text{(eq. 4.4)}$$

$$\nabla\cdot(\rho\boldsymbol{u}) = 0 \qquad \text{(eq. 4.5)}$$

where ρ is the density of the fluid (kg·m^{-3}); $\boldsymbol{u}$ is the velocity vector (m·s^{-1}); p is the pressure (Pa); μ denotes the viscosity of the fluid (Pa·s); $\boldsymbol{I}$ is a unit vector; $\boldsymbol{F}$ is the external force vector (N·m^{-3}).

The energy transfer takes place in the whole model geometry:

$$\rho C_{\mathrm{p}} \boldsymbol{u} \cdot \nabla T + \nabla \boldsymbol{q} = \boldsymbol{Q} \quad \text{(eq. 4.6)}$$

where **q** is the heat flux ($W \cdot m^{-2}$):

$$\boldsymbol{q} = -k \nabla T \quad \text{(eq. 4.7)}$$

And C_{p} is the specific heat capacity ($J \cdot kg^{-1} \cdot K^{-1}$); T represents the temperature in kelvin (K), $\boldsymbol{Q}$ denotes heat sources ($W \cdot m^{-3}$); k is the thermal conductivity ($W \cdot m^{-1} \cdot K^{-1}$). Note that in the solid domain, $\boldsymbol{u}$ is 0 $m \cdot s^{-1}$.

4.4.2 Thermal denaturation of BLG in the bulk

The thermal denaturation and aggregation of BLG in the bulk were simulated using the denaturation reaction model as developed in Chapter Three. In this model, it is assumed that the thermal unfolding of BLG occurs instantaneously. And the unfolding of BLG was proposed to be thermodynamically driven following by a kinetically controlled aggregation step:

$$N \rightleftharpoons U \rightarrow A \quad \text{(eq. 4.8)}$$

where a chemical equilibrium between native BLG (N) and unfolded BLG (U) is instantaneously established at a given temperature. As the soluble BLG (S) is the sum of native and unfolded BLG (*i.e.* $C_s = C_N + C_U$), the proportion of the unfolded BLG in the total soluble BLG in the equilibrium, or defined as unfolding ratio α is:

$$C_{\mathrm{U}} = \alpha \cdot C_{\mathrm{s}} \quad \text{(eq. 4.9)}$$

The value of α can be calculated by the corresponding enthalpy ΔH and entropy ΔS according to van't Hoff's equation:

$$\alpha = 1 / \left[1 + \exp\left(\frac{\Delta H}{RT} - \frac{\Delta S}{R}\right)\right] \quad \text{(eq. 4.10)}$$

The subsequent reaction of aggregation or polymerization of unfolded BLG species can be expressed as:

$$-\frac{dC_{\mathrm{U,A}}}{dt} = k_{\mathrm{A}} \cdot C_U^2 \quad \text{(eq. 4.11)}$$

where k_A is the reaction constant for the aggregation step. The temperature dependence of k_A can be deduced by the Arrhenius equation:

$$k_A = k_{0A}\exp\left(\frac{-Ea_A}{RT}\right) \quad \text{(eq. 4.12)}$$

where k_{0A} is the denaturation pre-exponential factor ($mol^{-1}\cdot m^3\cdot s^{-1}$), Ea_A is the activation energy ($J\cdot mol^{-1}$), R is the universal gas constant (*i.e.* 8.314 $J\cdot mol^{-1}\cdot K^{-1}$).

The loss of soluble BLG in the bulk is expressed:

$$\frac{\partial C_S}{\partial t} = -k_A \cdot \alpha^2 \cdot C_S^2 \quad \text{(eq. 4.13)}$$

The amount of unfolded BLG can be quantified using equation 4.9, and for the native BLG:

$$C_N = (1-\alpha)\cdot C_s \quad \text{(eq. 4.14)}$$

The details of the thermal denaturation model and the corresponding thermodynamic parameters including enthalpy ΔH and entropy ΔS for unfolding equilibrium, and activation energy Ea_A and logarithmic pre-exponential factor $\ln(k_{0,A})$ for the aggregation step can be found in Chapter Three. The values are summarized in Table 3.1.

The velocity in equation 4.4 is used in the mass conservation equations to characterize the convective mass transfer of all different BLG species in the solution domain:

$$\nabla\cdot(-D_i\nabla C_i) + \boldsymbol{u}\cdot\nabla C_i = R_i \quad \text{(eq. 4.15)}$$

$$\boldsymbol{N}_i = -D_i\nabla C_i + \boldsymbol{u}C_i \quad \text{(eq. 4.16)}$$

Where D_i and C_i represents diffusion coefficient ($m^2\cdot s^{-1}$) and concentration ($kg\cdot m^{-3}$) for different BLG species i; R_i is a reaction rate expression ($kg\cdot m^{-3}\cdot s^{-1}$); $\boldsymbol{N}_i$ is the mass flux ($kg\cdot m^{-2}\cdot s^{-1}$).

The diffusion coefficients of these different BLG species can be estimated by the Wilke-Chang equation (Wilke and Chang, 1955):

$$D_i = \frac{1.310\times10^{-17}\cdot T}{\mu\cdot V_i^{0.6}} \quad \text{(eq. 4.17)}$$

with V_i is the molar volume of the particles:

$$V_{\mathrm{i}} = N_{\mathrm{AV}} \frac{1}{6} \pi d_i^3 \qquad \text{(eq. 4.18)}$$

where N_{AV} is the Avogadro constant ($6.023 \cdot 10^{23}$ mol^{-1}) and d_{i} is the particle diameter of different BLG species (m). Note that since the unfolding of BLG is considered to be instantaneous, there is no need to treat native and unfolded molecules separately. Instead, they were considered as a unity (*i.e.* soluble BLG particle). The corresponding particle diameters were used as reported in the literature ($9.8 \cdot 10^{-11}$ m for soluble BLG and $9.91 \cdot 10^{-10}$ m for aggregated BLG molecule) (Georgiadis et al., 1998a).

4.4.3 Fouling reaction model

For deposition reaction, we assume a surface reaction that occurs only on the bottom surface of the channel (upon stainless steel) with a reaction order of one, the surface reaction rate of deposited BLG can be described as:

$$\frac{\partial C_{\mathrm{D}}}{\partial t} = k_{\mathrm{D}} C_{\mathrm{U}} \qquad \text{(eq. 4.19)}$$

The temperature dependence of the deposition reaction constant k_{D} can also be expressed by the Arrhenius equation:

$$k_{\mathrm{D}} = \mathrm{k_{D0}} \exp\left(\frac{-E\mathrm{a_D}}{\mathrm{RT}}\right) \qquad \text{(eq. 4.20)}$$

where $\mathrm{k_{D0}}$ is the pre-exponential factor of deposition reaction (m·s^{-1}) and $E\mathrm{a_D}$ is the activation energy (J·mol^{-1}) for the deposition.

The surface reaction directly determines the deposit flux across the liquid-solid interface. This can be implemented by specifying an outward flux of unfolded BLG on the interface. As described previously, the key objective of this work is to determine surface reaction kinetics, particularly at various Ca^{2+} levels. The deposition kinetic constant k_{D} can be calculated by combining the simulated unfolded BLG concentration on the surface C_{U} with the experimental deposition rates (average value for the whole deposition area). By fixing 45.1 kJ·mol^{-1} for the value of the activation energy $E\mathrm{a_D}$ for the deposition process as proposed by (De Jong, 1996), the deposition pre-exponential factor $\mathrm{k_{D0}}$ can be calculated at different ionic calcium concentrations.

4.4.4 Boundary and initial conditions

The parameters of boundary and initial conditions for the simulation were chosen from experimental conditions in order to provide a more realistic 3D simulation. In the solution domain, the solution with an initial soluble BLG concentration, Cs_0, flows from the inlet of the device (SS tube) to the outlet (silicone tube) at a fixed velocity of v_{in} and an initial temperature T_{in}. The outlet gauge pressure is set to be 0 Pa. Non-slip conditions are applied for all the walls contacted in the flow channel. Heat transfer takes place in all the simulation domains, and a constant temperature is specific on the bottom surface to simulate the heat resource from the plate heater. The bottom surface temperature was measured at 87.5 °C using an infrared thermal imager (Testo 869, Testo, Germany) when set at 90 °C (see supplementary figure, Figure S4.3, page 169). The heat loss of the fouling rig as well as the outlet silicone tube due to the air was achieved by applying an external natural heat convention with an air temperature of 25 °C. The corresponding parameters for boundary and initial conditions are listed in Table 4.1. The addition of this low concentration of whey proteins or calcium was not considered to significantly affect the physical properties of water, thus the corresponding properties of water were used for the fouling fluid (Petit et al., 2013). The physical properties of the solid phase are shown in Table 4.2.

Table 4.1. Simulation parameters for boundary and initial conditions

Variables	Values	Units
Initial solid temperature	25	°C
Inlet fluid temperature, T_{in}	25	°C
Inlet fluid velocity, v_{in}	0.0106	$m \cdot s^{-1}$
Inlet soluble BLG concentration, Cs_0	3	$kg \cdot m^{-3}$
Inlet aggregated BLG concentration	1×10^{-20}	$kg \cdot m^{-3}$
Bottom surface temperature	87.5*	°C
Air temperature	25	°C

*Value experimentally measured using an infrared thermal imager.

Table 4.2. Physical properties of the solid materials

Materials	Variables	Value	Units
Aluminum substrate	Specific heat, $C_{p,Al}$	896	$J \cdot kg^{-1} \cdot K^{-1}$

	Density, ρ_{Al}	2700	$kg \cdot m^{-3}$
	Thermal conductivity, k_{Al}	154	$W \cdot m^{-1} \cdot K^{-1}$
Stainless steel (SS)	Specific heat, $C_{p,SS}$	502.48	$J \cdot kg^{-1} \cdot K^{-1}$
	Density, ρ_{SS}	8030	$kg \cdot m^{-3}$
	Thermal conductivity, k_{SS}	16.27	$W \cdot m^{-1} \cdot K^{-1}$
PMMA	Specific heat, $C_{p,PMMA}$	1420	$J \cdot kg^{-1} \cdot K^{-1}$
	Density, ρ_{PMMA}	1190	$kg \cdot m^{-3}$
	Thermal conductivity, k_{PMMA}	0.19	$W \cdot m^{-1} \cdot K^{-1}$
Nylon	Specific heat, $C_{p,Nylon}$	1700	$J \cdot kg^{-1} \cdot K^{-1}$
	Density, ρ_{Nylon}	1150	$kg \cdot m^{-3}$
	Thermal conductivity, k_{Nylon}	0.26	$W \cdot m^{-1} \cdot K^{-1}$

In the present work, the hydrodynamics and the heat transfer of the simulation are firstly validated by temperature quantification of the fluid in the channel using fluorescence. Next, the soluble BLG concentration detected using SEC at the outlet of the system was used to confirm the reliability of the denaturation model of BLG in the bulk. Finally, with the calculated localized concentration of the unfolded BLG C_U, the reaction constant k_D can be calculated by coupling with experimental fouling rates. The simulation was performed in a steady-state regime. Matlab® scripts were developed to couple COMSOL for extracting calculated parameters, such as velocity, temperature, different BLG species concentrations as well as calculation of deposition reaction constant k_D.

4.5 Results and discussions

4.5.1 Hydrodynamics and temperature profiles of the fluid

The 3D CFD simulation allows providing comprehensive spatial distribution of the fluid mechanics and temperature of the microchannel inside the fouling rig. Figure 4.4(a) and (b) show the steady-state flow velocity and temperature gradients inside the microchannel, respectively. Simulation reveals a sudden drop of the fluid velocity at tunnel length of 10 mm due to tunnel geometry changed from a pipe to a rectangular tunnel (Fig. 4.4(c)). Meanwhile, as in this section, the SS tube is buried inside the aluminum substrate, the large heat transfer efficiency allows to quickly heat the solution from 25 °C to around 60 °C. The functionality of this section works as a "pre-heating" zone as those encountered in pilot process lines. The simulated temperature profile of the fluid inside the u-shape tunnel shows a gradual heating process ranging from 60 to 83 °C (Fig. 4.4(d)). This u-shape tunnel section was noted as heating section and is considered as the main domain where thermal denaturation and deposition occurs. The silicone tube is noted as a cooling section as the solution temperature gradually decreases to ~60 °C at the outlet. With this outlet temperature, thermal denaturation of BLG was considered to be stopped.

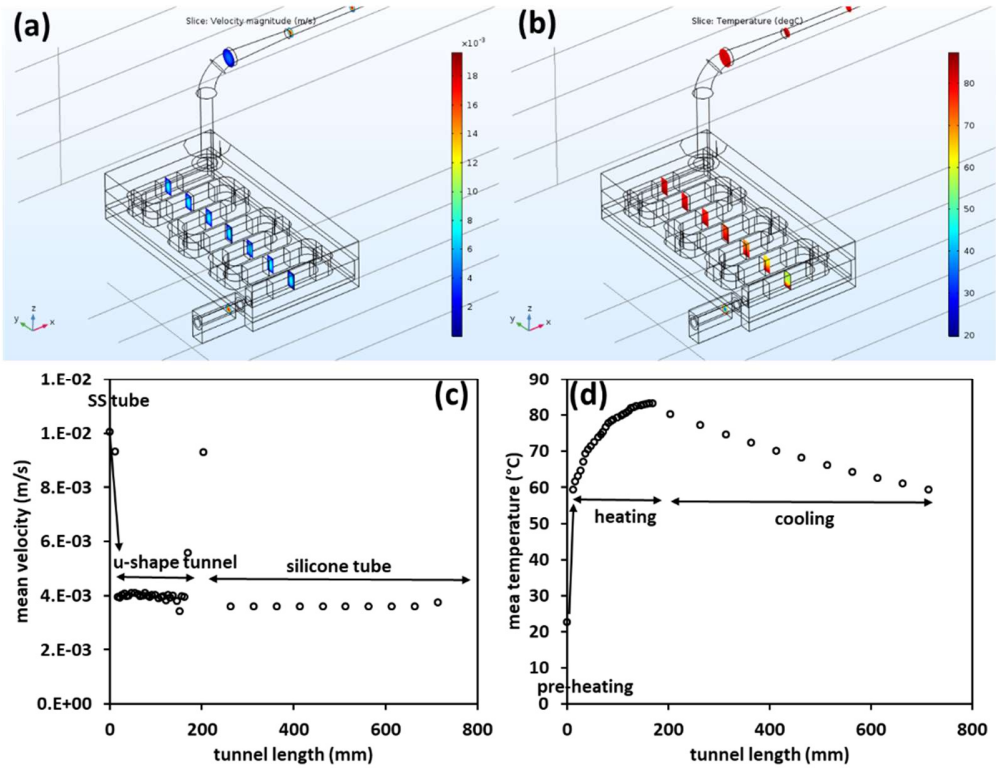

Figure 4.4. Simulated (a) velocity and (b) temperature of the fluid inside the microchannel of the fouling rig. (c) and (d) represent the mean values of velocity and temperature along the tunnel length, respectively.

4.5.2 Validation of numerical bulk temperature using fluorescence

As mentioned previously, in order to find proper operating parameters for the fouling run as well as to validate the simulated results, the solution temperature inside the microchannel was quantified using fluorescence ratiometry where PM556 was applied as the temperature indicator. The temperature dependence of 10 μM PM556 solution at various temperatures is shown in Figure 4.5. The reference temperature at 25 °C is used. It is clear that at higher temperatures, the fluorescence intensity or the quantum yield of the dye decreases, up to 50% loss at 90 °C compared to the reference. The decreased quantum yield of the dye at high temperature is generally due to an increase in the non-radiative deactivation process (López Arbeloa et al., 1999). For example, for the dye Rhodamine B, lower solvent viscosity at higher temperatures favors the intramolecular rotational motion of the two dialkylamino groups, leading to a non-emissive TICT-like (Twisted Intramolecular Charge-Transfer) state.

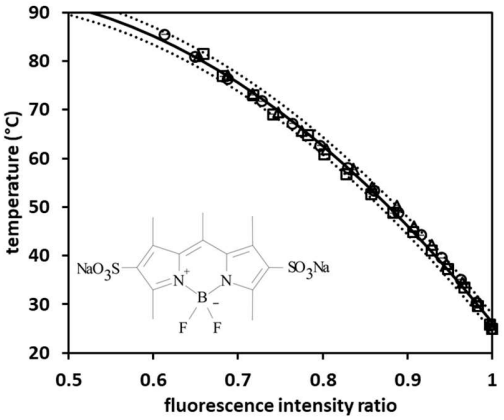

Figure 4.5. Relationship between solution temperature and fluorescence intensity ratio of 10 μM PM556. The fluorescence is normalized at those obtained at 25 °C. Triplicate experiments are displayed. Solid line represents polynomial fitting of the data, dashed lines denote 95% CI (Confident interval, ± 1.8 °C). Inset shows the molecular structure of PM556.

Figure 4.6(a) presents the evolution of fluorescence intensity ratio of 10 μM PM556 along the u-shape tunnel at different bottom surface temperatures. The fluorescence profiles generally show

decreasing trends along the tunnel with higher values at lower surface temperatures. With the calibration curve (Fig. 4.5), the corresponding mean temperatures of the fluid in the microchannel can be calculated as shown in Figure 4.6(b). Results show that the solution temperature drops suddenly right after exiting the SS tube (or entering the u-shape tunnel) and then increases to a plateau when it reaches the outlet (entering nylon tube). This temperature drop could be due to the significantly lower heat transfer coefficient of the u-shape tunnel compared to that in the pipe flow. This behavior is also recognized by the CFD simulation as shown in solid lines in Figure 4.6(b). In general, the temperature profiles calculated using fluorescence match well with simulated ones as well as those outlet temperatures measured using thermocouples (Fig. 4.6(b)). Notice that the fluctuation of temperature profiles is due to the elbows of the u-shape channel.

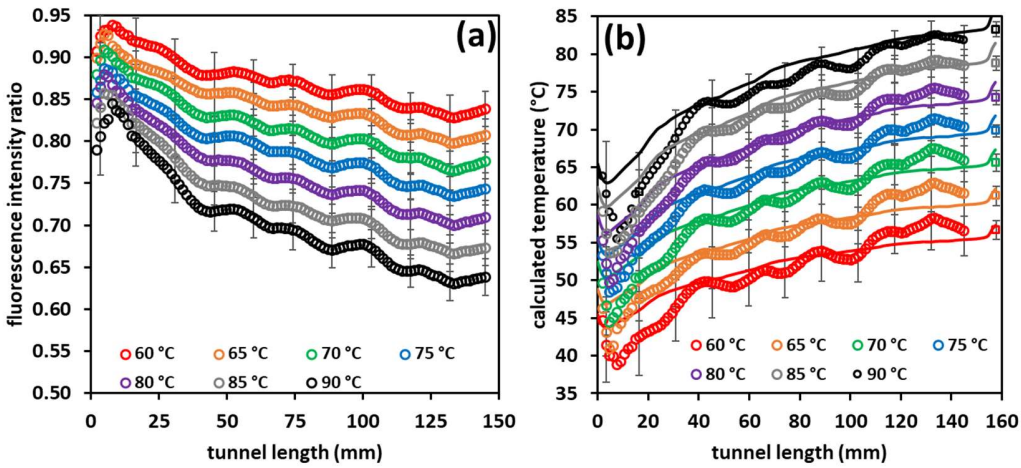

Figure 4.6. (a) Fluorescence intensity ratio profiles of 10 μM PM556 in the microchannel of the fouling rig (u-shape section) obtained at various bottom surface temperatures ranging from 60 to 90 °C as shown in the legend. The fluorescence is normalized at those obtained at 25 °C. The calculated mean solution temperatures inside the microchannel using fluorescence are shown in (b). Solid lines represent CFD simulation results. Note the symbols in square in (b) denote the outlet solution temperature measured using thermocouples. Error bars represent standard deviations (SD) from three individual experiments.

4.5.3 Thermal denaturation and deposition of BLG

The heat-induced denaturation and aggregation of BLG in the bulk were achieved using the denaturation model as described previously in Chapter Three. Figure 4.7(a) shows the simulated

native BLG profiles in the microchannel with a 0.5 wt% WPI model solution containing 40 ppm Ca^{2+}. More detailed information of bulk reaction can be seen in Fig. 4.7(b) by presenting mean concentration profiles of all three different BLG species, including native, unfolded and aggregated ones. The simulated BLG profiles obtained at other calcium concentrations are presented in the Supplementary Information (Figure S4.4, page 170). It can be concluded that the thermal denaturation of BLG mainly occurs in the u-shape tunnel section (*i.e.* heating section) and can be negligible in the cooling section as there is little formation of aggregated BLG. The native BLG keeps decreasing in the u-shape tunnel reaching a minimum value of ~0.5 $g \cdot L^{-1}$ at the outlet of the nylon tube (~200 mm), while it gradually recovers and reaches ~2 $g \cdot L^{-1}$ at the outlet of the silicone tube due to cooling. This value is almost equal to the soluble BLG concentration C_s at the same position, indicating that the native⇌unfolded equilibrium of BLG almost shifts back to the native state at such low temperature condition. Results also confirm a more significant impact of calcium on the aggregation compared to unfolding of BLG as the concentration of the aggregated BLG species are higher with elevated calcium concentrations whilst for the unfolded BLG, it differs little with increased calcium levels (Figure S4.4, p170).

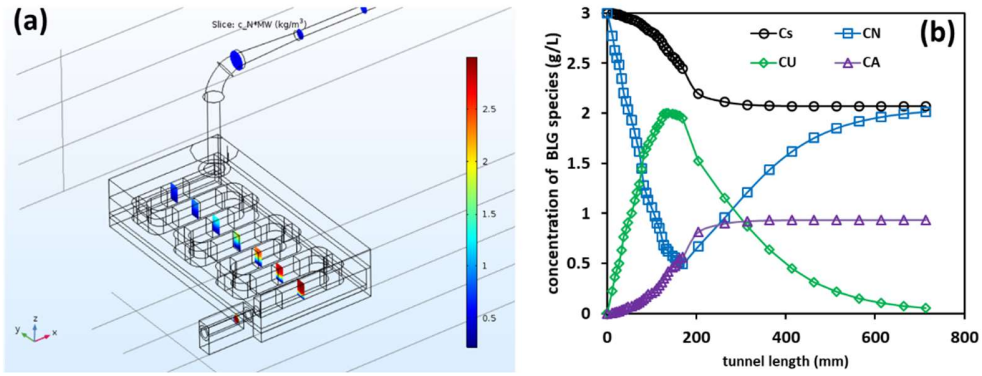

Figure 4.7. (a) 3D CFD simulated native BLG concentrations inside the microchannel. Model fluid contains 0.5 wt% WPI with the addition of 40 ppm Ca^{2+}. (b) Average values of simulated BLG species concentrations along the tunnel length. Three different BLG species are shown, including native, unfolded and aggregated ones. Solid lines are used to guide the eyes.

To further validate the reliability of the thermal denaturation model, the simulated soluble BLG concentrations at the outlet of silicone tube were compared with experimental results as shown in Fig. 4.8(a). It is evident that with higher calcium levels, the denaturation level of BLG increases in benchtop fouling system, with little differences at calcium concentrations between 60 and 70

ppm. Additionally, the simulated results agree well with the experimental data which again, consolidates the simulation methodology. Figure 4.8(b) shows a quasi-linear relationship of fouling rate at elevated ionic calcium concentrations. Our fouling rates (ranging from 1~6 $mg \cdot m^{-2} \cdot s^{-1}$, depending on the calcium levels) are almost two orders of magnitude higher than those reported in small scale studies with mostly pure BLG without adding calcium (*e.g.* ~0.026 $mg \cdot m^{-2} \cdot s^{-1}$ at 85 °C) (Santos et al., 2006), or with WPI and addition of calcium but at lower temperatures using QCM (Quartz Crystal Microbalance, ~0.042 $mg \cdot m^{-2} \cdot s^{-1}$ at 65 °C with 40 ppm Ca^{2+}) (Yang et al., 2018). Nevertheless, our results are more comparable to those performed in large scale fouling experiments in real heat exchangers in pilot plant. For example, the fouling results shown in Chapter One with 0.5 wt% WPI at an ionic calcium of 38.7 ppm report an overall dry deposits of 17.1 g in a 10-passes PHE (temperature ranges from 65 to 85 °C), resulting in mean fouling rates of ~1.6 $mg \cdot m^{-2} \cdot s^{-1}$) (Liu et al., 2021).

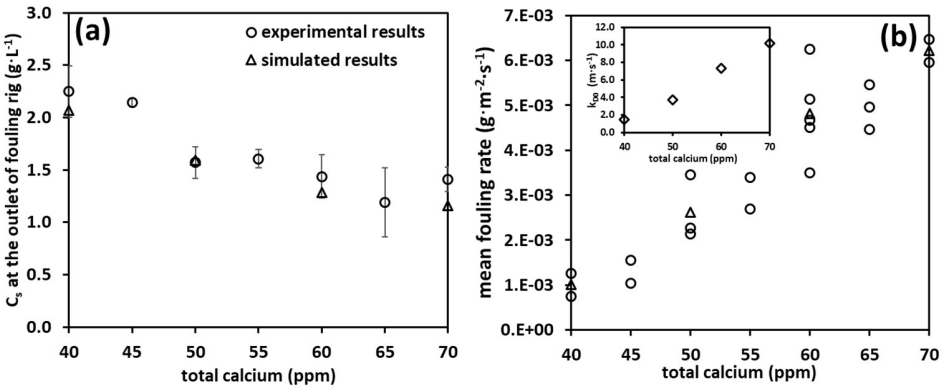

Figure 4.8. (a) Soluble BLG concentrations obtained at the outlet of fouling system (outlet of silicone tube). Symbols in circle represent experimental data while the ones in triangle denote simulated results. Error bars show SD of at least two replicates. (b) Mean fouling rate at various calcium levels. Note that symbols in triangle show average values at specific calcium level which was used for simulation. Inset figure shows the values of k_{D0} for deposition simulation which are reported in Table 4.3.

It is important to note that the calculation of surface reaction kinetics needs the localized information of unfolded BLG species (equation 4.9). However, the corresponding parameters are only available at four specific calcium concentrations (*i.e.* 40, 50, 60 and 70 ppm, Chapter Three). Therefore, only the fouling rates obtained at these four specific calcium concentrations were used to calculate the corresponding deposition pre-exponential factor k_{D0} in simulation as listed in

Table 4.3. The dependence of k_{D0} against various calcium concentrations is plotted in the inset of Figure 4.8(b). A quasi-linear dependence of k_{D0} on the calcium content can be found, implying that the deposition rate of unfolded BLG is proportional to the calcium concentrations (reaction order of one for deposition reaction). These results might suggest that only one calcium ion per BLG molecule is involved in the deposition reaction otherwise such evolution with an increase of calcium cannot be observed.

Table 4.3. Simulated values of k_{D0} at various calcium levels

$[Ca^{2+}]$ (ppm)	40	50	60	70
k_{D0} ($m \cdot s^{-1}$)	1.48	3.71	7.33	10.17

There is a great difference between our fouling rig system between a usual PHE. In PHEs, the temperature of the fouling fluid is increased by transferring the heat from the hot medium (usually hot water), thus both the bulk and surface temperature in the channel is gradually increased. However, in our laboratory-scale fouling rig system, the solution temperature in the bulk also increases along the tunnel but the surface temperature remains almost unchanged (supplementary figure, Fig. S4.5, page 171). In this scenario, the surface reaction rates were expected to be almost constant in the tunnel (as poorly affected by surfaced temperature increase along the tunnel) even slightly decreased along the tunnel due to lower content of unfolded BLG concentration as can be seen in the simulated deposition rate profiles (supplementary figure, Fig. S4.6, page 171). Therefore, if we consider the fouling mainly limited on the surface reaction, the fouling growth is unlikely to be dependent on the locations in the microchannel.

Our experimental results support this idea as the amount of deposits observed at downstream is slightly lower than observed at upstream of the microchannel as shown in Figure 4.9. At low calcium concentration, the fouling deposits are more spherical with up to ~50 μm in diameter (Fig. 4.9(a) and (b)). However, at high concentrations of calcium, deposits are denser and grow to a more rod-like structure perpendicular to the flow direction (Fig. 4.9(c) and (d)). These morphologies of the fouling deposit suggest a limited effect of the flow on the formation of deposition as expected for a laminar flow scheme. The dynamic imaging of the channel reveals a crystallization-like fouling behavior as shown in Figure 4.10. At low calcium concentrations such as 45 ppm, almost one hour is needed to visualize fouling deposits (Fig. 4.10(b)). After that, fouling

keeps growing based on the previously fouled layer. This finding suggests that the unfolded BLG species are preferred to interact with fouled layer for fouling growth instead of deposition upon the clean stainless steel surface. This behavior can also be seen at high calcium concentrations, however, the apparent fouling is denser and was found within 20 min at a calcium concentration of 60 ppm (supplementary figure, Fig. S4.7, page 172). All these results confirm an essential role of Ca^{2+} that it not only helps the anchoring of proteins upon the stainless steel surface but also facilitates the depositing by strengthening the protein-protein cross-linking.

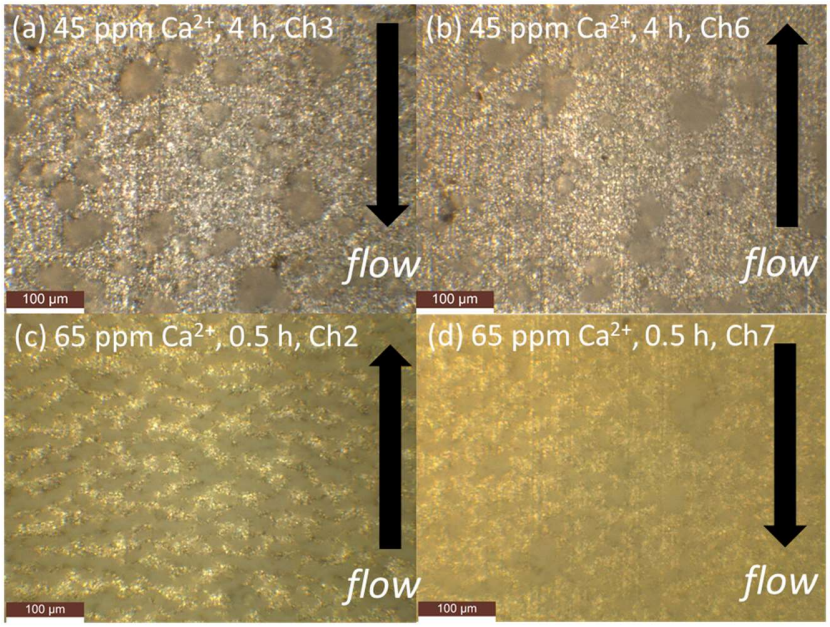

Figure 4.9. Fouling images in the microchannel of 0.5 wt% WPI with the addition of 45 ppm Ca^{2+} obtained at (a) 3rd channel Ch3 and (b) 6th channel Ch6 after 4 hour fouling runs, or with the addition of 65 ppm Ca^{2+} observed at (c) 2nd channel Ch2 and (d) 7th channel Ch7 after 30 min fouling runs. Arrows in the images represent the flow direction. The yellowish images in (c) and (d) are due to the formation of fouling deposits on the surface of PMMA cover. Images were all taken at the maximum magnification (*i.e.* 115 ×).

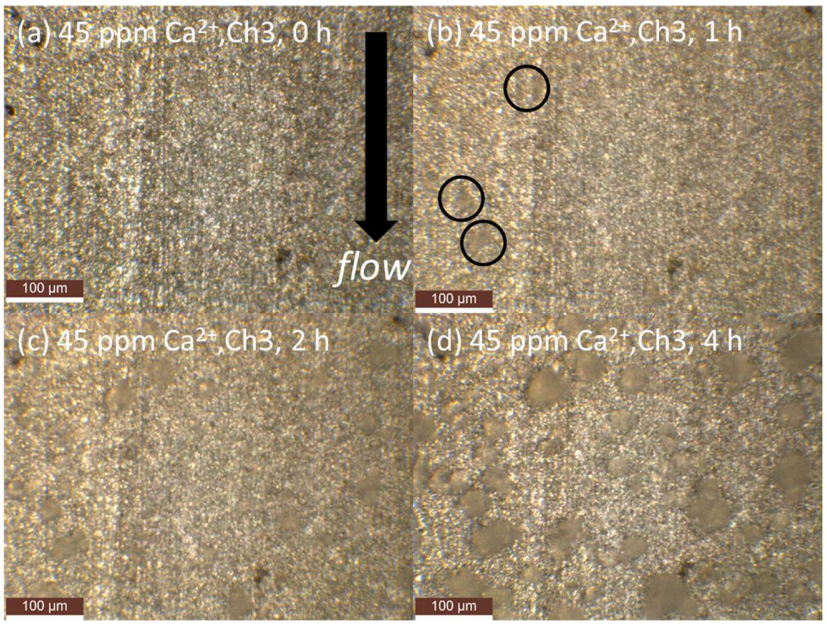

Figure 4.10. Fouling images in the 3rd microchannel (Ch3) of 0.5 wt% WPI with the addition of 45 ppm Ca^{2+} obtained at different fouling times: (a) 0 h, (b) 1 h, (c) 2 h and (d) 4 h. Arrow in (a) represents the flow direction. Apparent fouling deposits can be observed after 1 h fouling run as circled in (b). Images were all taken at the maximum magnification (*i.e.* 115 ×).

4.6 Proposed fouling mechanisms with Ca^{2+}

Based on the experimental fouling results shown in this chapter and the denaturation kinetic model developed in Chapter Three, we hereby propose a BLG-based fouling mechanism regarding the calcium effect as shown in Figure 4.11.

At low Ca^{2+} condition:

- Native BLG molecule encounters thermal unfolding and exposes its free thiol group at Cys_{121}. There is a higher proportion of unfolded BLG molecules (higher α) in the bulk fluid (away from the hot stainless steel surface). The lack of Ca^{2+} induces only mild aggregation forming small sizes of aggregates.
- When the native BLG molecule transfers to the vicinity of the hot surface (*e.g.* in the thermal boundary), it quickly denatures (unfolds) and attaches to the solid-liquid interface. Ca^{2+} facilitates the anchoring of the unfolded BLG molecules upon the surface, whilst, due to its low quantity, the deposition is limited.

At high Ca^{2+} condition:

- Native BLG molecules encounter thermal unfolding in a similar pattern as that observed at low Ca^{2+} conditions. Ca ions have a specific binding site on the BLG molecule, which strengthens its native molecule structure, resulting in higher proportion of native BLG molecules (lower α) in the bulk fluid (away from the hot stainless steel surface). With the abundance of Ca^{2+}, larger sizes of aggregates could be formed.
- The large amount of native BLG in the bulk does not limit the deposition reaction, as they can quickly unfold when transferring to the vicinity of the hot surface (*e.g.* in the thermal boundary), and attaches to the solid-liquid interface. Ca^{2+} facilitates the deposition reaction by acting as anchoring agents for unfolded BLG molecules and strengthening the interactions between two denatured BLG molecules.

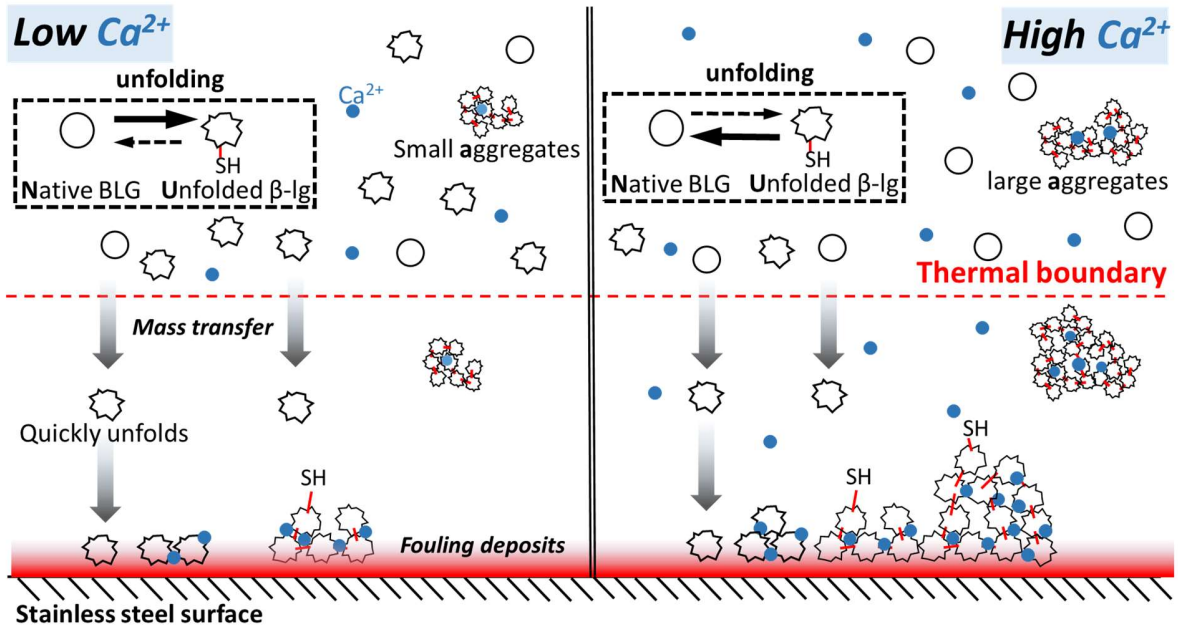

Figure 4.11. Schematic diagram representing BLG-based fouling mechanisms at different ionic calcium levels in the microchannel of custom-built laboratory-scale fouling device (laminar regime).

Conclusions

In this chapter, a bench-scale fouling rig has been successfully built to perform whey protein fouling at various ionic calcium concentrations in a laminar regime. Thanks to the simplicity of the configuration and previous efforts to have a consistent kinetic denaturation model, a realistic 3D CFD simulation is achieved to couple the thermal denaturation and aggregation of BLG in the channel (bulk reaction) as well as the deposition (surface reaction). To validate the simulation model, fluorescence was firstly used to spatially quantify the solution temperature in the channel where PM556 was applied as the temperature indicator. The soluble BLG concentrations detected using HPLC at the outlet of the system satisfactorily match the simulated values, which further consolidates the reliability of the numerical model. With the ability to provide reliable information of the localized unfolded BLG concentrations, the deposition kinetics can be calculated coupling with experimental fouling rates. The simulation reveals a linear relationship between the deposition pre-exponential factor k_{D0} and calcium, suggesting that only one calcium ion per each BLG molecule is involved in the deposition growth. The real-time imaging in the channel allows us to visualize the fouling growth showing a crystallization-like pattern. The formation of the fouling shows a preference for the previously fouled layer over the clean stainless steel surface. This custom-built bench-scale fouling device, although presents some limitations (laminar regime), shows valuable advantages compared to those PHEs as it is both energy and material saving, especially when a real-time optical measurement is desired. Gathering these pieces of experimental evidence, a mechanism presenting the role of Ca^{2+} on BLG-based whey protein fouling is finally proposed, where calcium ions are essential to fouling growth with significant effects both on thermal denaturation in the bulk and surface deposition processes.

Supplementary figures for Chapter Four

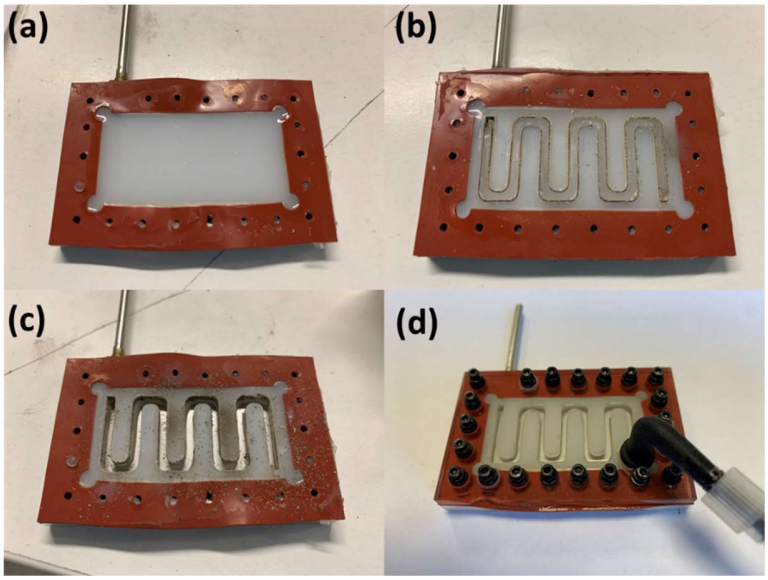

Figure S4.1. Creation of silicone u-shape microchannel inside the micro fouling rig by CO_2 laser. The silicone was firstly cast in the groove of the aluminum substrate (a). After that, the silicone was damaged by CO_2 laser (Speedy 400, Trotec, France) with 50% of maximum power (130 W) at a laser movement velocity of 2.45 mm/s (b). By carefully removing the cut part of the gel, a u-shape silicone tunnel can be created. The whole device was cleaned (remove ashes due to cutting) and mounted with PMMA cover and screwed (d).

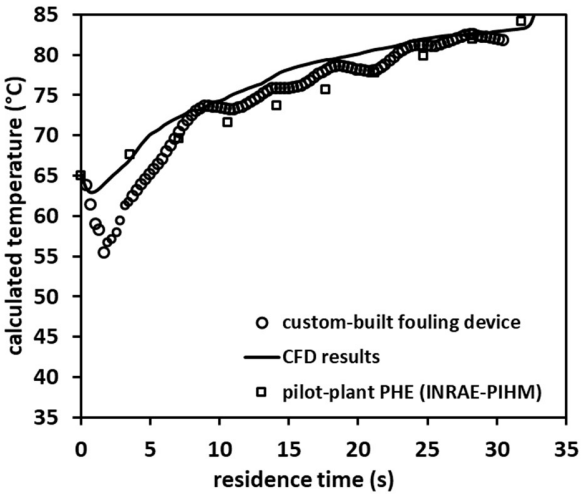

Figure S4.2. Comparison of thermal profile in the custom-built fouling device (u-shape tunnel) with that obtained in the pilot-scale PHE. Solid line presents the simulated results using CFD.

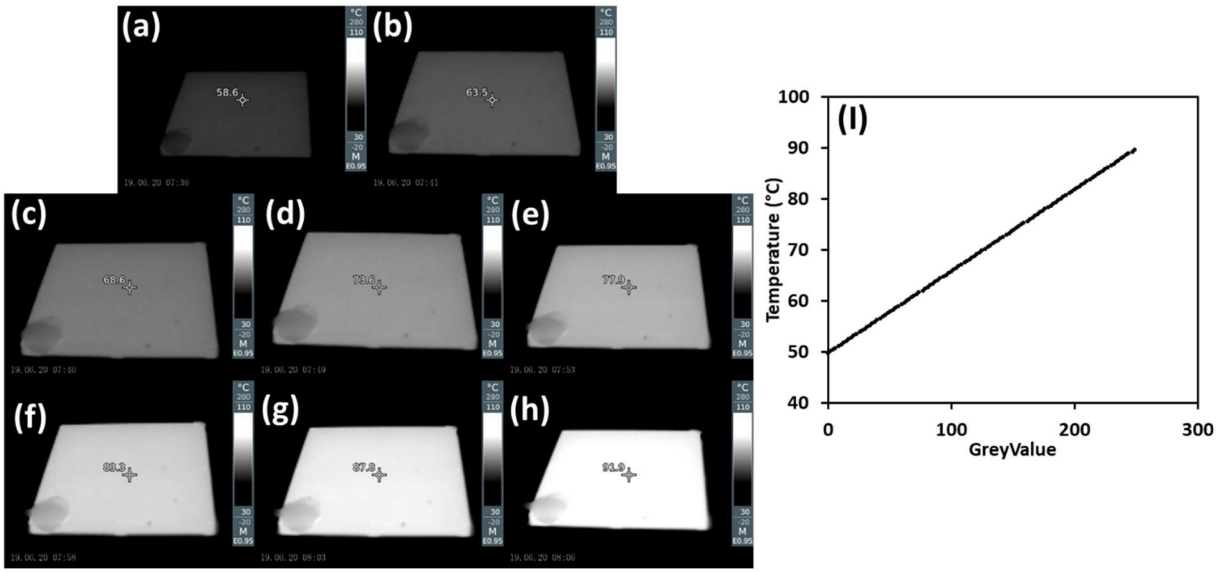

Figure S4.3. Thermo images of the plate heater surface using an infrared thermal imager (Testo 869, Testo, Germany) set at various temperatures: (a) 60 (b) 65 (c) 70 (d) 75 (e) 80 (f) 85 (g) 90 °C and (h) 95 °C. Images are shown in 8-bit type. The calibration curve of temperature against grey value is shown in (I).

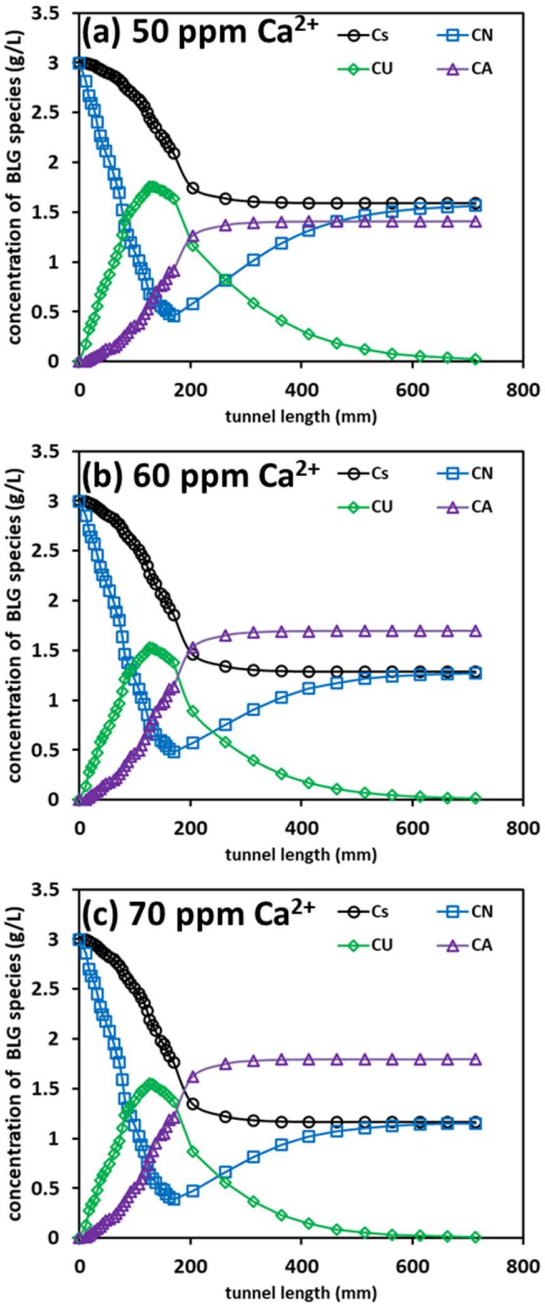

Figure S4.4. Simulated BLG species concentrations along the tunnel length in the bench-scale fouling system at ionic calcium concentrations of (a) 50 (b) 60 and (c) 70 ppm. Three different BLG species are shown, including native, unfolded and aggregated ones. Solid lines are used to guide the eyes.

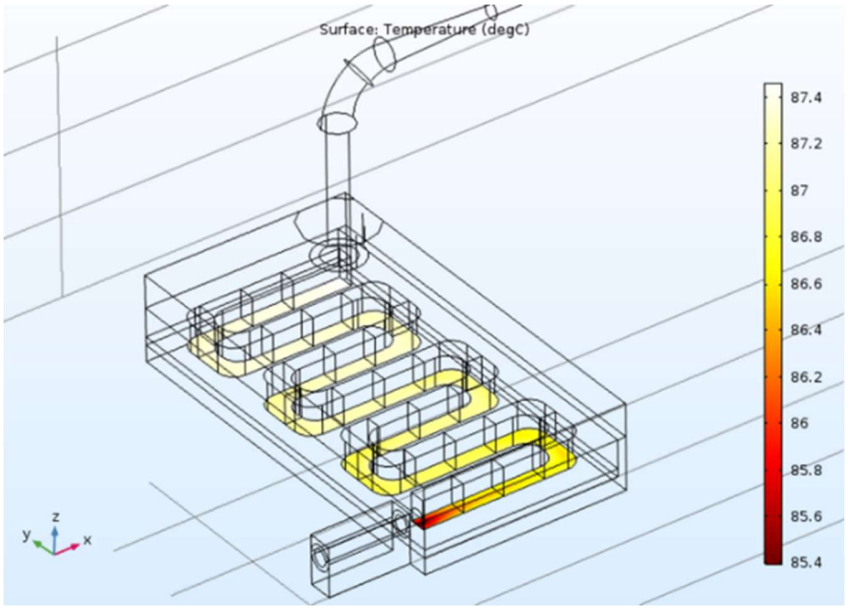

Figure S4.5. The simulated bottom surface temperature of the u-shape tunnel in the fouling rig.

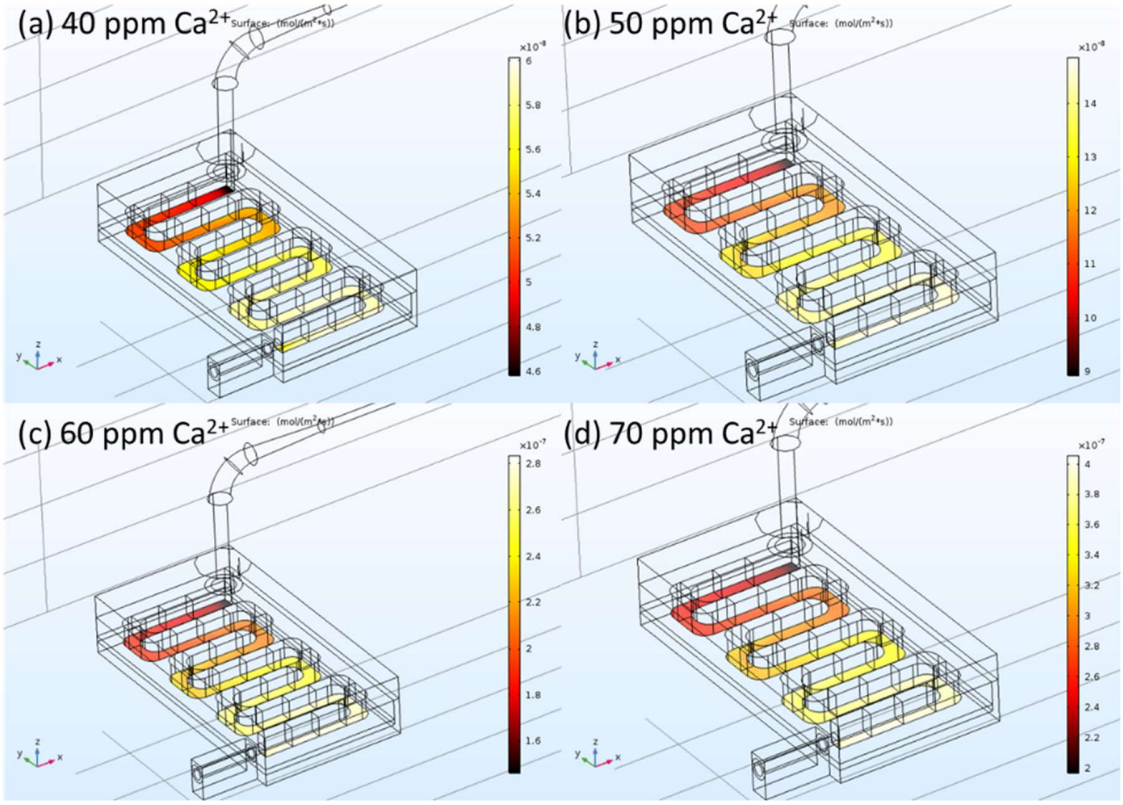

Figure S4.6. The simulated deposition rates on the bottom surface at a calcium concentration of (a) 40, (b) 50, (c) 60 and (d) 70 ppm.

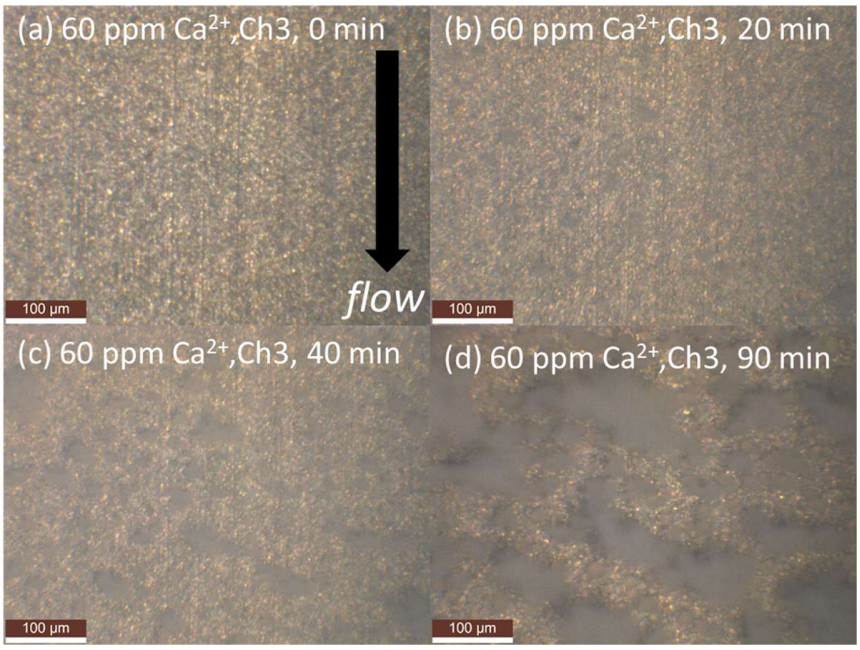

Figure S4.7. Fouling images in the 3rd microchannel (Ch3) of 0.5 wt% WPI with the addition of 60 ppm Ca^{2+} obtained at different fouling times: (a) 0 min, (b) 20 min, (c) 40 min and (d) 90 min. Arrow in (a) represents the flow direction. Apparent fouling deposits can be observed after 20 min fouling run as shown in (b). Images were all taken at the maximum magnification (*i.e.* 115 ×).

Chapter Five. Role of casein micelle on the whey protein fouling in a benchtop fouling device

In this last chapter, the role of casein micelle on the whey protein fouling is investigated again but in the developed laboratory-scale device (laminar regime). In this chapter, our aim is clearly to get a better view on how the changes of molecular status of caseins (dissociated form *vs* micellar casein) alter the interactions between BLG and casein proteins and their consequence on fouling deposition. This question was not tackled in the previous pilot-scale experiments, and therefore our goal in this chapter is to go further.

To obtain different proportions of dissociated and micellar caseins, in this laboratory-scale fouling experiment, the pH of the fouling fluids was either not controlled (unmodified), such that it increased as elevated casein/whey mass ratios (same in the pilot-scale experiments in Chapter Two), or fixed at pH 6.6. After that, the molecular status of caseins and their interactions with denatured BLG were studied through a renneting-based technique. SDS-PAGE (electrophoresis) was applied again to reveal protein composition for fouling deposits obtained at different casein/whey ratios under different pH adjustment strategies. Finally, a mechanism describing the thermal denaturation of BLG and its subsequent fouling behavior in the presence of casein micelle is proposed.

For sake of clarity, the results observed in the previous pilot-scale experiments will be discussed, obstacles encountered and emerging questioning will be pointed out first in the following introduction section. Note that the results presented here will be gathered in an article and will be submitted in an international journal in the continuity of this PhD thesis.

Introduction

In Chapter Two, the role of casein on the denaturation of whey protein and its fouling behavior has been investigated in a pilot-scale PHE. It was found that with even little amount of added casein, the total fouling mass drop dramatically at Casein/WPI ratio of 0.2 with ~80% suppression. However, fouling mass increased with elevated Casein/WPI ratios when exceeding that critical ratio. Unfortunately, this bi-phase phenomenon of casein effect on fouling performance is not well understood; for example, concerning BLG denaturation level, casein seems poorly affect the BLG denaturation process, and it was shown that fouling behavior was not correlated to the BLG denaturation level at the conditions where fouling mass decreased (*i.e.* Casein/WPI $\leq$ 0.2). It is evident that a dashboard containing only information about the evolution of the BLG denaturation

kinetics in the presence of casein is not exhaustive enough to obtain an overview of the underlying molecular mechanisms. The final native BLG content detected using HPLC cannot solely predict any detailed information of the BLG-casein interactions. How the thermal denaturation pathway of BLG changes in the presence of casein is still unclear. It is possible that denatured BLG tends to interact with casein micelles and/or individual caseins instead of other whey proteins or participation in fouling so that final fouling was mitigated. In this scenario, chaperone-like functions of individual caseins might play a role. To investigate this field, it is vital to get a better view of the proportion of individual and micellar caseins in the fouling solutions before heating and how this proportion evolves after heating. This is one aim of this chapter.

Another possibility to explain the fouling mitigation effect of casein is the increase of the solution pH induced by the addition of casein powder. It has long been recognized that increasing even slightly the milk pH can significantly suppress fouling (Foster et al., 1989; Hegg et al., 1985). And it seems to be like this case as the addition of casein to reach Casein/WPI of 0.2 increased the fouling solution pH from 6.5 to ~6.78, which should be sufficient to suppress almost all fouling. Adjustment of milk pH has also been found to alter the dissociation behavior of casein micelle during heating, where the level of dissociated casein increases with increasing temperature at pH 6.7 or above and at temperature higher than 70 °C (Anema and Li, 2000). Nevertheless, the pH effect cannot solely explain this fouling behavior as pH went even higher to neutral (pH reached around 6.9 at Casein/WPI of 0.8) at higher Casein/WPI ratios whilst fouling increased.

To further explore the mechanism behind fouling in the presence of casein, in this chapter, the effect of casein/whey mass ratio on the whey protein fouling behavior was investigated again but in the laboratory-scale fouling rig built before (in Chapter Four). Since the pH adjustment in the laboratory-scale device is easier to manipulate, the pHs of the fouling solutions were either unmodified such that pH kept increasing as higher Casein/WPI or adjusted to keep constant at pH 6.6 to evaluate whether the pH affects the fouling behavior with the presence of casein. To cast some light into the casein-whey interactions in the molecular level during thermal processing,

i) the proportion of individual and micellar caseins in these fouling solutions before and after heating will be calculated using a renneting-based technique.

ii) the protein composition of fouling deposits generated at various Casein/WPI ratios at two different pH conditions (*i.e.* unmodified and pH 6.7) was determined using SDS-PAGE.

5.1 Fouling runs in the benchtop fouling rig

Preparation of fouling fluids

In this study, several preliminary experiments have been conducted to perform fouling experiments using protein powders as similar as possible to those carried out in the pilot plant (Chapter Two). However, it was noticed that the initially used casein powder was somehow very hard to rehydrate in lab-scale conditions and induced blocking issues in the microchannel of the fouling device (More details about rehydration of the protein powder and its related blocking issues can be seen in Annex IV).

To overcome this obstacle and to achieve better rehydration of the casein powder, it was decided to:

i) change batch of powders, in order to make sure that ageing or caking problems are definitely discarded. A new casein powder (Promilk 852 B, Ingredia, France) and whey protein isolate powder (Promilk 852 FB1, Ingredia, France) were used in this laboratory-scale fouling experiments. The protein composition of WPI and casein were all characterized using RP-HPLC and was found to be similar to those performed in the pilot plant experiments (Chapter Two) as shown in the supplementary figure, Figure S5.1 (page 199). Similar to pilot-scale experiments, the fouling solutions contain a constant whey protein concentration at 0.5 wt% with varying casein concentrations to yield different Casein/WPI mass ratios up to 4.

ii) apply a longer rehydration step that could compensate for the effect of hydrodynamic conditions in the pilot plant on powder rehydration. Indeed, the casein powder might have better rehydration conditions in the pilot-scale experiments due to the bigger diameter of the impeller used for promoting turbulent flow scheme that might help the break-down of powder aggregates and thus towards better rehydration. To set the final rehydration operating conditions, further rehydration tests to monitor the particle size evolution during rehydration were carried out (see again in Annex IV).

Finally, the protein powders were rehydrated in a 500 mL glass bottle with magnetic stirring at a constant speed set at 350 rpm. Milli Q water was firstly heated to 50 °C prior to adding whey and casein protein powders to reach different Casein/WPI mass ratios up to 4. Concentrated sodium azide stock was added to reach a final concentration of 0.03% (w/v) to prohibit bacterial

growth. Instead of 1 h, the rehydration was prolonged to 24 h (at 50 °C) to ensure full rehydration of the casein powders. $CaCl_2$ was added only when the protein powder was fully rehydrated (after 24 h) as it showed a negative impact on the rehydration (for fouling experiments, a constant amount of ionic calcium is required to obtain fouling, see Chapter Two). The solutions were allowed to return to room temperature before the pH adjustment. The solution pH was either unmodified such that it increased with elevated Casein/WPI ratios or fixed at pH 6.6 by adding concentrated HCl, if needed.

Fouling experiments

Fouling experiments were performed on the bench scale set-up similar to that described in Chapter Four (Figure 4.1(c)). In this chapter, the fouling experiments were conducted in the UMET lab (INRAE, Hauts-de-France, Equipe PIHM) in France where the commercial plate heater is not available, thus a homemade plate heater was used to replace the commercial one as shown in Figure 5.1. This homemade plate heater was a re-use of the copper part of a sample plate from a rheometer (TA Instruments, USA). This copper part was embedded into a polystyrene substrate for thermal insulation; it was connected to a water bach (FC30-C, Julabo, USA) with a high flow rate (20 L/min) to ensure a constant surface temperature. The surface temperature was quantified using a high performance infrared thermometer (MX4, Raytek, Germany); results showed similar heating performance to that of commercial one with slightly worst homogeneity (± 2.3 °C compared to only ± 0.1 °C for the commercial one). More detailed comparison of these two plate heaters is shown in the supplementary figure, Figure S5.2, page 199. The operating parameters for fouling run were used the same as described in Chapter Four (*i.e.* 2 $mL \cdot min^{-1}$ flow rate, watch bath set at 90 °C) to obtain a similar thermal profile of the product in the microchannel (*i.e.* 60 to 83 °C in the u-shape tunnel). For each fouling experiment, before pumping fouling fluid, MilliQ water was firstly used to reach a thermal equilibrium of the system. A totally 350 mL solution prepared the day before as described previously was subjected to the fouling device by switching from water to fouling solutions. This amount of fouling solution was sufficient to support a total 2 hour fouling experiment without recycling, during which sample solutions were taken three times (beginning/middle/end of the experiment) at the end of the fouling set-up (silicone tube). The thermal denaturation in these solutions was stopped when they were collected due to their low temperatures (~60 °C, Fig. 4.4(b)). These thermal treated fouling solutions as well as the stock

solution before heat treatment were used for subsequent calcium measurements or protein fractionations. When the fouling experiments were finished, water was used again to replace fouling solutions in the channels; after that, the device was dismantled before putting in an air-oven at 70 °C overnight (> 8 hours) to dry the SS plates. The dry mass of the fouling deposit on each plate was calculated by the difference between bare and fouled plates.

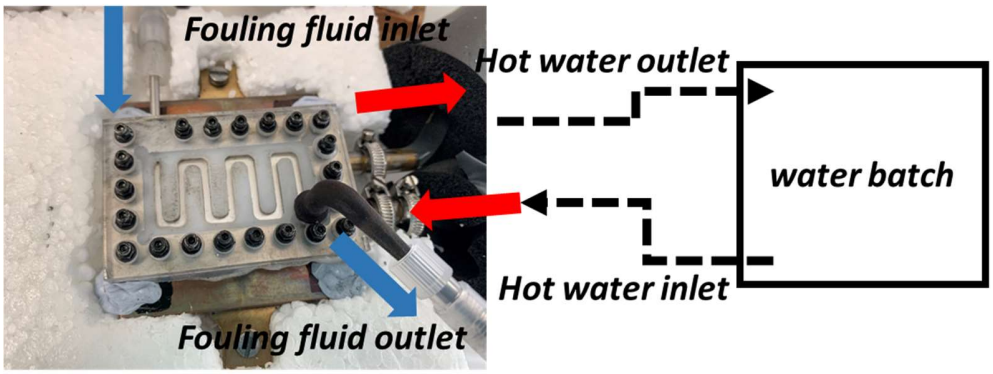

Figure 5.1. Picture of a micro fouling rig mounted upon a homemade plate heater. The heater was connected to a watch bath with a big flow rate so that a constant surface temperature can be achieved.

5.2 Calcium content measurement

The previous methodology to measure ionic calcium (or free calcium $[Ca]_f$) using a calcium ion-selective electrode (Ca-ISE, PS-3518, PASCO, USA) implied protein-membrane interactions that challenged the reproducibility and reliability of the results. In this work, another commercial calcium probe (LAQUAtwin-Ca-11, HORIBA, Japan) was used instead. Although being also ISE-based principle, it showed better performance. All protein samples as well as calcium standards ($CaCl_2$ ranged from 20 to 200 ppm) were thermoequilibrated in a water bath maintained at 25 °C prior to measurements. For each fouling run, the calcium standards were firstly measured; their potentials were recorded and the calibration curve was obtained according to the Nernst equation. The total calcium content $[Ca]_t$ was determined by atomic absorption spectrometry using a Spectro AA 55B apparatus (Varian, Palo Alto, USA) as performed in Chapter Two.

5.3 Fractionation of proteins in fouling solutions

To establish the distribution of proteins in the fouling solutions, the fractionation of proteins was done using the method adopted from (Pesic et al., 2012) (Figure 5.2). Briefly, the pHs of the samples were adjusted to pH 6.6 before renneting (Chymosin, MaxiRen 600, ≥ 600 IMCU (International milk clotting unit)/mL) at 30 °C for one hour and 15 min. After rennet coagulation, samples were centrifuged for 10 min at 5000 × g. The curd was considered to contain only micellar casein or micellar casein bound whey proteins. After that, the pH of the supernatant was adjusted to pH 4.6 followed by centrifugation for 30 min at 12000 rpm to precipitate soluble aggregates. These aggregates were considered to consist of whey protein aggregates as well as those formed with individual caseins which dissociated from the micellar structure (*e.g.* BLG-BLG, BLG-αLa, BLG-κ-casein aggregates). The final supernatant was considered to contain only native proteins, including native whey proteins and also native dissociated caseins that cannot return to casein micelle.

The supernatant as well as the precipitate and the rennet curd were either properly diluted or dissolved using a sampling buffer (8 M urea, 0.1 M bis-tris, 5.37 M sodium citrate and 20 mM DTT (Dithiothreitol) at pH 7) modified from Bonfatti et al. (2013). They were filtrated through a 0.2 μm cellulose filter (Minisart RC, Sartorius, Germany) before injecting 20 μL in the RP-HPLC system as described in Chapter Two. The two mobile phases were slightly modified to achieve a better separation for caseins: solution A consists of 0.1% (v/v) trifluoroacetic acid (TFA, 99%, Acros Organics) in MilliQ water while solution B contains 0.1% (v/v) TFA in pure acetonitrile (HPLC grade, Thermo Fisher Scientific). The separation was performed at a flow rate of 1 mL/min, 40 °C and a detection wavelength of 220 nm with gradient elution in a C4 column (C4-300, ACE, UK). Calibration curves were done by using pure protein standards, including BLG, αLa, α_s-casein, β-casein and κ-casein. Pure protein powders for calibration purposs were all purchased from Sigma (Sigma-Aldrich Chemie Gmbh, Steinheim, Germany).

Since the structure of casein can be altered by various environmental factors (mineral concentrations, ionic strength, pH, *etc*, see Chapter One, section 1.3.4), it is plausible that casein might not be able to maintain its micellar structure, particularly at such protein concentrations (and low ionic strength). If this is the case, careful attention must be paid as they (dissociated *vs* casein micelle) might have different interactions with serum proteins during thermal processing. Based on the protein fractionation technique as described above, the proportion of casein in its dissociated

form can be also quantified (*e.g.* individual caseins in the supernatant/total casein content found in fouling solutions before heating).

One should bear in mind that the casein micelle has never been investigated at such low concentrations, and the rennet coagulation performance for reconstituted milk/casein powder was typically studied at a concentration close to milk (2.5 wt%) or even higher (10 wt%) (Kethireddipalli et al., 2011; Osintsev et al., 2016). Besides that, heat treatment at temperatures allowing for whey protein denaturation is also known to impair the rennet coagulation properties of milk (Britten and Giroux, 2022). It was suggested that the rennet-induced hydrolysis of κ-casein is significantly inhibited or incomplete due to the less accessibility of the rennet sensitive bond of κ-casein (Phe_{105}-Met_{106}) by the formation of complexes with whey proteins resulting from heat treatment. Therefore, further studies should be performed to confirm the rennet coagulation performance at low casein concentrations, for example, by using ultracentrifugation combined with particle size measurements (Anema and Li, 2003a) (Dumpler et al., 2017).

To summarize, this procedure aimed at separating four different classes of protein particles:

i) *Fouling solutions before heating*: determines total amount of both whey and casein proteins

ii) *Curd*: consists of micellar caseins and whey protein-bound casein micelles

iii) *Precipitation*: includes protein aggregates in the serum phase (*e.g.* BLG-BLG, BLG-αLa, BLG-κ-casein aggregates).

iv) *Supernatant*: contains only native whey proteins and dissociated caseins that are released from micelle.

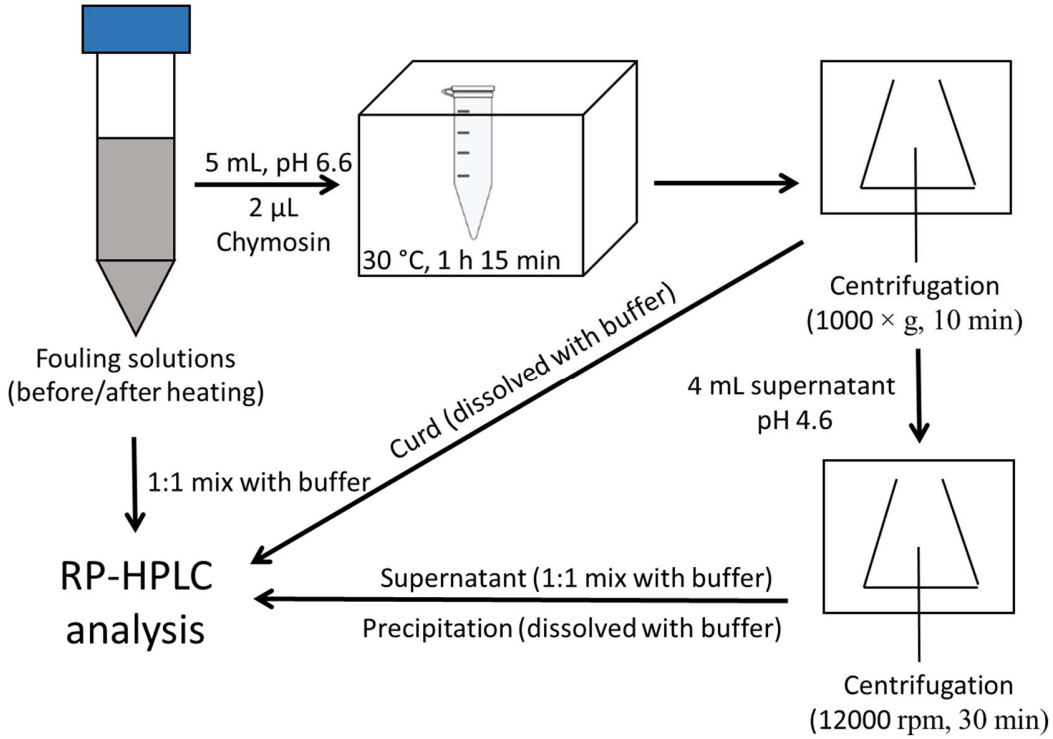

Figure 5.2. Schematic diagram of milk protein fractionation with renneting-based methodology.

5.4 Results and discussions

5.4.1 Effect of Casein/WPI ratio and pH adjustment on fouling rate

It is of great interest to see if the effect of casein on the whey protein fouling behavior can be reproduced on the laboratory scale. Previous experiments performed in pilot-scale PHE have limited Casein/WPI ranges, up to 0.8, mainly due to the large quantity of casein powder required. Therefore, particularly, the Casein/WPI ratio was extended to reach the value that is similar in milk (*i.e.* 4). Table 5.1 summarizes the calcium content and BLG denaturation level of fifteen fouling fluids as well as their total fouling mass. For all fouling solutions, a constant amount of Ca^{2+} (42 ppm, same amount as used in pilot-scale experiments, Chapter Two) was added to obtain significant fouling except for Fluid#1, where only casein powder was added to achieve a similar ionic calcium level (compare Fluid#1 with Fluid #2 and #3). Despite this, for Fluid #1, no deposit was visualized after 2 hours of fouling run, and the BLG denaturation level is very low. This behavior has been also observed in the pilot-scale experiments; if additional calcium is not supplemented, deposition is fully prohibited despite a high level of ionic calcium due to the addition of casein powder. This can be probably due to the capacity of casein micelle that shifts the ionic calcium in the serum phase towards the formation of micellar calcium phosphate during heating, resulting in low calcium content in the serum phase and therefore low BLG denaturation level (On-Nom et al., 2010).

Table 5.1. Free calcium ($[Ca]_f$) and total calcium content ($[Ca]_t$) of fifteen fouling fluids and their fouling results. For each fouling experiment, the BLG concentration at the inlet and outlet are also shown. Errors represent standard deviation (SD). Note the pH of the fouling solution was either unmodified or fixed at pH 6.6.

Fluid#	Casein/WPI	$[Ca]_f$[b] (ppm)	$[Ca]_t$[b] (ppm)	$[BLG]_{inlet}$ (g/L)	$[BLG]_{outlet}$[c] (g/L)	BLG denaturation level[d]	Total fouling mass (mg)
#1	0.8	52±3	94±1	3.37	3.12	7.4%	ND[e]
#2	0	50±2	61±4	3.47	1.66	52.1%	19.0
#3	0	53.0±0.2	60±2	3.34	1.67	50.1%	19.8
#4	0.05	59±2	71±5	3.37	1.71	49.2%	7.7

#5	0.1	62±2	79±2	3.32	2.09	37.0%	2.1
#6	0.2	69±4	85±1	3.48	2.11	39.4%	5.6
#7	1	100±4	195±9	3.50	2.41	31.2%	3.8
#8	2	110±5	310±10	3.60	2.46	31.8%	5.7
#9	3	139±6	520±11	3.52	2.24	36.3%	2.6
#10	4	140±10	620±30	3.46	2.42	30.1%	5.2
#11[a]	0.05	60±2	65.8±0.4	3.38	1.63	51.8%	8.3
#12[a]	0.1	64±4	80±1	3.11	1.84	40.7%	8
#13[a]	1	113±5	200±4	3.37	1.55	54.0%	6.8
#14[a]	2	137±5	333±8	3.50	1.82	48.0%	10.7
#15[a]	4	172±7	611±14	3.55	1.50	57.9%	27.7

[a]Solution pH was fixed at pH 6.6.
[b]Average values of fouling fluids obtained at the outlet at three different running times and one without thermal treatment
[c]Average values of fouling fluids obtained at the outlet at three different running times
[d]BLG denaturation level = 1-$[BLG]_{outlet}/[BLG]_{intlet}$
[e]ND refers to "Non-detected"

A clear view of how casein affects the fouling behavior can be seen in Figure 5.3(a). When the pH of the fouling solutions was unmodified such that it increased with elevated Casein/WPI ratios (from pH 6.6 without additional casein to pH 7.1 at Casein/WPI of 4), the total fouling was dramatically suppressed. The minimum value locates at Casein/WPI of 0.1, where ~90% of fouling was mitigated. This trend is in accordance with those results performed in the pilot plant, however, the enhanced effect of casein on total fouling deposit at high Casein/WPI ratios (>0.2) as found in the pilot plant is missing (Fig. 2.6(a)). In fact, comparing this fouling behavior with those using overall fouling mass in the entire PHE might not be suitable; since the surface temperature in the laboratory-scale device was kept almost constant (~87 °C, Fig. S4.5, page 171), considering deposit mass that formed in one channel that has similar surface temperature seems to make more sense.

Figure 5.3(b) confirms this idea by displaying the deposition rate at various Casein/WPI ratios calculated only using the deposit mass generated in the last channel of the PHE (*i.e.* P_{21}, Fig. 2.2(a)). This channel has an average bulk fluid temperature for fouling fluid at ca. 85 °C connected to the hot water channel that has an average bulk temperature at 87.3 °C (Fig. 2.2(b)). Therefore, the surface temperature of the plate in the last channel could be similar to that in the benchtop device. Using this calculation, the effect of casein on the fouling deposition rate shows similar trends in these two different devices with different scales (Fig. 5.5(b)). However, the deposition rate obtained in PHE is almost ten times higher than that in the laboratory scale. This could be due to

a better temperature homogeneity in the PHE channel or the turbulent flow which helps the transfer of denatured proteins from the bulk to the hot metal surface and thus facilitates the deposition.

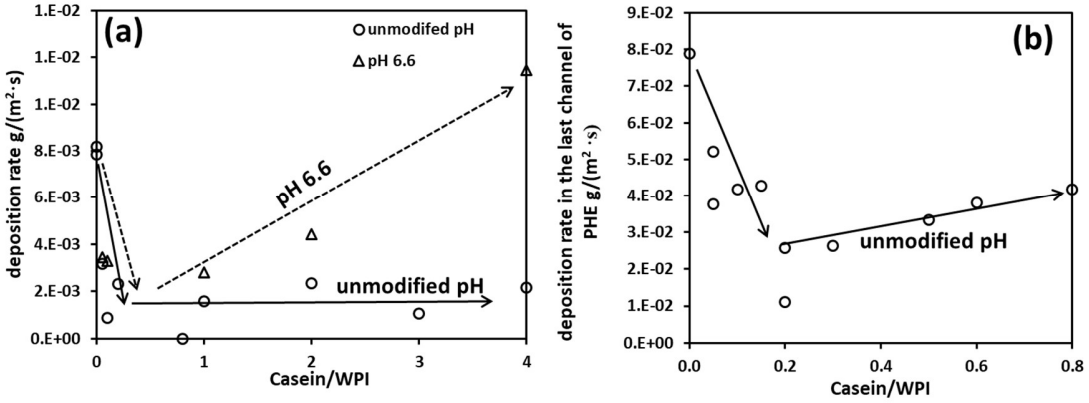

Figure 5.3. Effect of Casein/WPI mass ratio on the total fouling deposition rate in (a) custom-built laboratory-scale fouling device and (b) the last channel (*i.e.* P_{21}) of a 10 channel pilot-scale PHE. The pH of fouling fluids was either unmodified such that it increased with elevated Casein/WPI ratios or kept constant at pH 6.6 in the micro fouling rig; whilst it was always unmodified in the pilot-scale experiments. Note the value of zero at Casein/WPI of 0.8 in (a) was obtained without additional ionic calcium (Fluid #1 in Table 5.1). Results in (b) were calculated by using only the deposit mass generated in the last channel of the PHE (*i.e.* P_{21}, Fig. 2.2(a)). Arrows are used to guide the eyes.

The major difference regarding fouling behavior in these two systems (*i.e.* pilot/laboratory-scale) is their correlation with BLG denaturation level. The BLG denaturation level shows a higher correlation to the deposition rate particularly in the laboratory-scale experiments as shown in Figure 5.4: the denaturation level decreases with the addition of casein and keeps almost constant at a relatively low value (around 30%) for unmodified pH conditions. However, when pH was fixed at 6.6, the BLG denaturation level remained at a high level regardless of casein concentrations. This denaturation of BLG changes can be explained by a lower capacity of casein controlling the level of calcium content in the serum phase, especially at low pH conditions; the free calcium concentrations obtained when pH was fixed at pH 6.6 are significantly higher than those obtained with unmodified pH (*e.g.* 172 ppm at pH 6.6 compared to 140 ppm with unmodified pH at Casein/WPI of 4, Table 5.1). This higher calcium content should be responsible for the high BLG denaturation level as well as the fouling behavior.

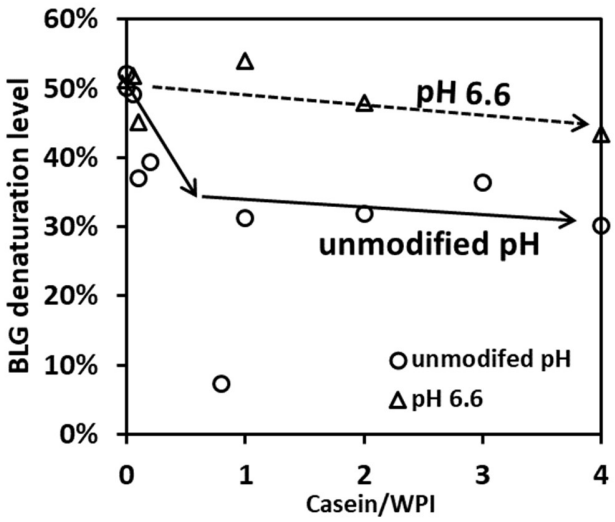

Figure 5.4. Denaturation level of BLG after thermal treatment in the benchtop fouling device at various Casein/WPI ratios. The pHs of the fouling solutions were either unmodified or kept at pH 6.6. Note the very low value located at Casein/WPI of 0.8 was obtained without additional calcium (*i.e*. Fluid #1 in Table 5.1). Arrows are used to guide the eyes.

5.4.2 Repartition of proteins and chaperone-like functions of casein

Repartition of caseins in dissociated and micellar forms

It is important to bear in mind that caseins, especially at such low concentrations, might not be in their micellar structure. This can be crucial as the functionality of micellar casein differs dramatically to that in the dissociated form. For instance, when caseins are in micellar structure, κ-casein is the most likely one to interact with denatured whey proteins under thermal stress due to their superior location in the micellar surface. However, for α_s/β-caseins that are naturally buried inside the interior of the micelle are less responsible for casein-whey interactions, unless they are dissociated. In almost all researches that used casein micelle powders, the casein solutions were reconstituted to reach the level that is similar to milk (*i.e*. 2.5%) (Le Ray et al., 1998) or even higher (*e.g*. 5%, 10%) (Chandrapala et al., 2014; Chandrapala et al., 2012a). It is also well-known that a critical micelle concentration has to be reached in order to induce self-association of caseins (*e.g*. 0.05 g/L for β-casein (de Kruif and Grinberg, 2002), and 0.2-0.5 g/L for κ-casein (Vreeman, 1979)). Therefore, for our fouling solutions, it is hypothesized that a large proportion of caseins are in their dissociated form, especially at low casein concentrations. One should notice that the

term "dissociated casein" does not refer to individual casein proteins (in monomer form). More likely, they tend to become κ-casein-depleted casein submicelles that have an increasingly loose structure and are much larger, and stronger hydrated compared to the native micellar structure probably due to the cleavage of the linkage between caseins and colloical calcium phosphate as described in (Aoki et al., 1990).

Our results suggest that more than 50% of the caseins at low Casein/WPI ratios (<1) are in the dissociated form (Figure 5.5). Whilst this proportion reduces significantly at Casein/WPI ratios ranging from 1 to 4. At the ratio that is close to milk (*i.e.* 4), more than 90% of caseins are in their micellar form. Fixing solution pH at 6.6 generally decreases the proportion of dissociated caseins (Fig. 5.5(b)). This pH-dependence of casein micelle dissociation behavior has also been reported (Anema, 1998). Unfortunately, the mechanism by which the casein is dissociated from the micelles remains unknown. Anema and Klostermeyer (1997) suggested that the dissociation of casein micelles may occur through changes in the nature of the CCP at elevated pH and temperatures to a form that is less capable of maintaining micellar structure.

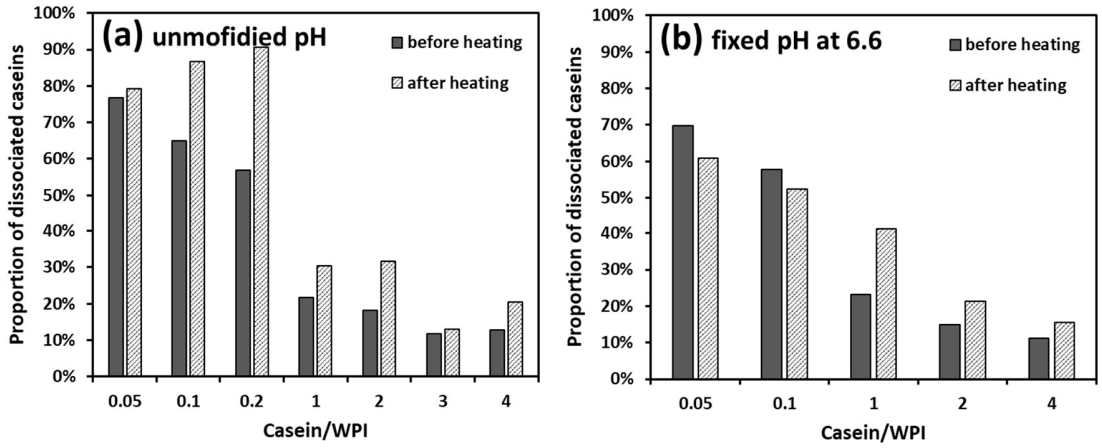

Figure 5.5. The proportion of caseins in their dissociated form in the fouling solutions at various Casein/WPI ratios under unmodified pH conditions (a) or fixed pH at 6.6 (b). The proportions were calculated using the sum of all casein concentrations (*i.e.* sum of α_s/β/κ-casein) detected in the supernatants divided by the values obtained from the solutions before fractionation.

Potential chaperone-like activities of caseins

After thermal processing in the laboratory-scale fouling device, the proportion of dissociated caseins shows a general increasing trend whatever the casein concentrations or pH conditions (Fig.

5.5). This phenomenon has been observed in (Anema and Li, 2000), and it was proposed that the denatured whey proteins interact with κ-casein both on the casein micelle surface or dissociated ones to form disulfide-bonded aggregates. On cooling, the κ-casein-BLG complex is less effective in stabilizing the entirety of the casein micelle, and therefore more α_s/β-caseins cannot reassociate back to its original micellar structure. This was confirmed as a larger quantity of κ-casein has been released/dissociated from casein micelle after heating (Figure 5.6(c)). More detailed information about the dissociation of α_s/β-caseins after thermal processing in the benchtop fouling device at various Casein/WPI ratios can be found in Figure 5.6(a)-(b). These two caseins have long been reported to express chaperone-like functions on the thermal denaturation of BLG, therefore, if they reach a significant amount in the serum phase, their interactions between denatured whey proteins, particularly unfolded BLG, should be considered.

A significant difference in the dissociation behavior of α_s/β-caseins under these two pH conditions can be seen in Fig. 5.6(a)-(b). The dissociated α_s/β-casein concentrations in the serum phase are always lower at pH 6.6 than those without pH adjustments. It is well-known that caseins show chaperone-like activities on the thermal denaturation of whey proteins such as inhibition of protein aggregation and stabilization of proteins (Treweek et al., 2011; Yong and Foegeding, 2010). However, a critical concentration of caseins has to be reached in order to express sufficient chaperone-like functions. For example, Morgan et al. (2005) found that the addition of α_s-casein to reach an α_s-casein/BLG molar ratio of 0.5 can dramatically prevent the thermally induced aggregation of BLG heated at 70 °C. β-casein generally shows a better efficiency of chaperone-like activities. For instance, the presence of 10 $g \cdot L^{-1}$ β-casein was found to be sufficient to suppress completely the thermal aggregation of 60 $g \cdot L^{-1}$ BLG even at 110 °C (Kehoe and Foegeding, 2011). Besides that, the chaperone-like function of α_s-casein is considered to be less significant compared to β-casein, as α_s-casein loses its chaperone-like activity when the temperature is higher than 75 °C, whilst β-casein is able to maintain its ability to inhibit thermal aggregation of BLG at temperature up to 90 °C (Yong and Foegeding, 2008). Nevertheless, in our experimental conditions, α_s-casein is not expected to be efficient to express chaperone-like functions as they do not reach a critical concentration (~2.3 g/L in this case). On the other hand, β-casein seems to have a sufficient quantity to express chaperone-like functions, especially at unmodified pH conditions (Fig. 5.6(b)). An increasing amount of dissociated κ-casein was also observed with slight higher level in unmodified pH conditions than those obtained in constant pH (Fig. 5.6(c)). These findings support

that the formation of κ-casein-BLG complexes prohibits the reassociation of individual caseins such that more casein micelles were disrupted after heating. However, there is no significant difference between the levels of dissociated κ-casein in these two pH conditions. Therefore, κ-casein is not responsible for the different fouling behaviors under these two pH conditions.

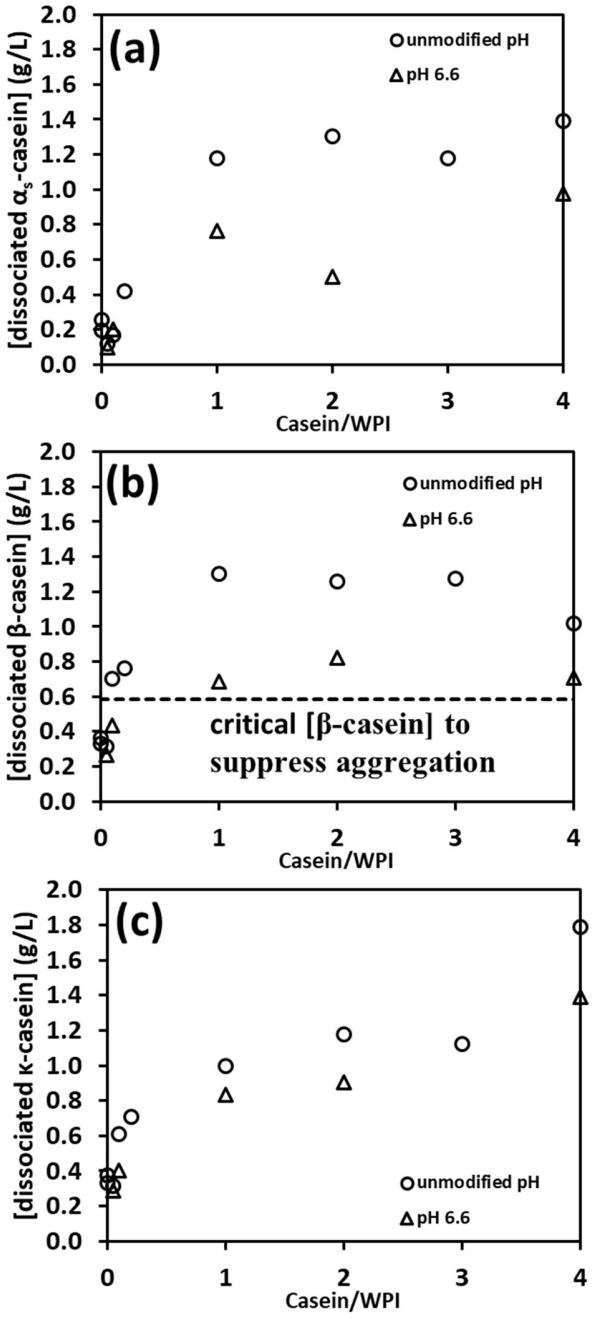

Figure 5.6. Concentrations of dissociated (a) α_s- (b) β- and (c) κ-casein in the fouling solutions after thermal treatment in a benchtop fouling rig at different pH conditions (denoted in the legend).

Dashed line in (b) presents critical concentration of β-casein (*i.e.* 5.83 g/L) to suppress thermal aggregation of BLG according to (Kehoe and Foegeding, 2011).

Repartition of BLG in casein micelle/aggregates/native forms

As addressed previously, since the dissociation of casein micelle is both concentration, temperature and pH dependent, the presence/absence of dissociated caseins in the serum phase and the entirety of the micellar structure of caseins will eventually alter the denaturation pathway of BLG. At pH close to the milk, casein micelle remains its entirety with low level of dissociated caseins in the serum. In this scenario, the denatured whey proteins or particularly BLG was reported to preferably interact with κ-casein on the casein micelle surface rather than forming κ-casein/whey protein complexes in the serum phase (Donato et al., 2007; Parker et al., 2005). For example, Smits and Brouwershaven (1980) showed that when model milk systems were heated at 90 °C, a maximum of ~83% of the BLG associated with the micelles at pH 5.8, and this decreased to ~76% at pH 6.3, ~44% at pH 6.8, and ~24% at pH 7.3. Similarly, Oldfield et al. (2000) examined the association behavior of whey proteins with the micelles for milk samples at pH 6.48, 6.60 and 6.83. On heating at 90 °C, ~90% of the whey protein associated with the micelles at pH 6.48, and this decreased to 80% at pH 6.60 and 60% at pH 6.83. They suggested that the decreased association of whey proteins with casein micelles at elevated pH was due to the partial dissociation of κ-casein from the micelles. This has been further supported by Anema (2007) who found that the level of κ-casein and denatured whey protein in the serum were linearly correlated.

Our experimental results agree with the above-mentioned findings by showing the same trend with higher BLG association level with casein micelles (casein-bound) at higher casein micelle entirety either by increasing casein concentrations or lower pH (Figure 5.7). For example, there is a clear increasing trend of the proportion of BLG associated with casein micelle with elevated casein concentrations under both pH conditions with a concomitant decrease of proportion involved in serum aggregation. When the pH of the fouling solutions was maintained at 6.6, a larger amount of casein remained in the micellar structure, therefore, a larger proportion of BLG was found to associate with casein micelles.

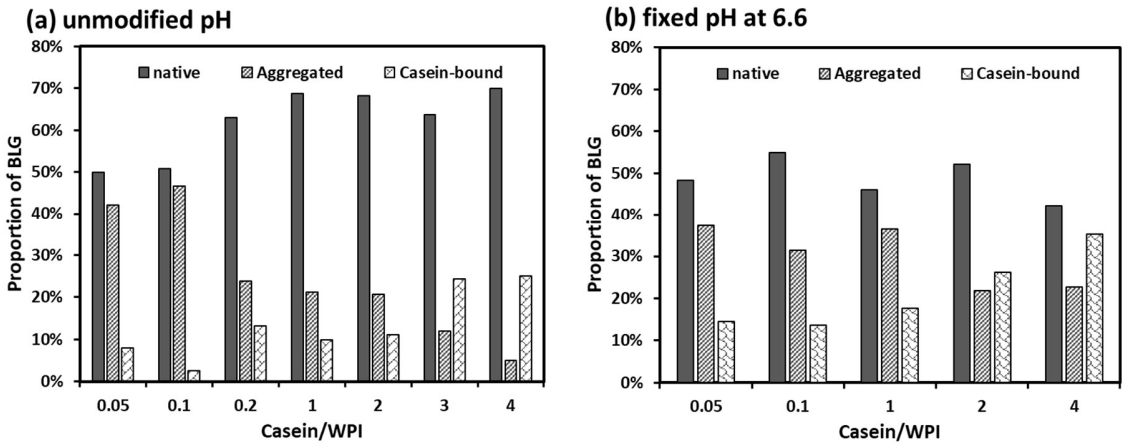

Figure 5.7. Proportion of BLG in heat-treated fouling solutions without pH modifications (a) or with fixed pH at 6.6 (b) in three different forms: native, aggregated and casein micelle-bound forms found in the supernatant, precipitates and rennet curd, respectively.

5.4.3 Protein composition in fouling deposits

To further compare the fouling behavior under these two different pH conditions (different casein-BLG interactions), the fouling deposits were analyzed using SDS-PAGE to study the protein composition. Figure 5.8(a) presents the electrophoresis results of deposits formed at various Casein/WPI mass ratios at unmodified pH conditions. It can be seen that BLG is the predominant component for deposits generated at all Casein/WPI ratios. Besides, other whey proteins such as αLa and BSA are also present but in a minor extent. In terms of caseins, they were absent at low Casein/WPI ratios (≤ 1), while α_s/β-casein appears to get involved in the formation of fouling deposits at higher Casein/WPI ratios (*e.g.* Casein/WPI = 3 and 4). Notice that, this transition of a larger proportion of casein in the deposits at elevated Casein/WPI ratios did not lead to a larger extent of fouling mass when the pH of the fouling solution was unmodified.

When fouling was performed in a constant pH at 6.6, the transition of a larger involvement of caseins in the deposit with increased Casein/WPI is more significant. Figure 5.8(b) compares the electrophoresis results of deposits formed at two different pH conditions at various Casein/WPI ratios. At low Casein/WPI ratios (Casein/WPI <1), the protein composition for deposits formed when the pH was fixed at 6.6 is not dramatically different from that formed when pH was unmodified. This could be due to the minor effect on the pH of the solution when adding such a

low concentration of casein. Therefore, it is not surprising to observe similarities in the fouling behavior (*e.g*. protein composition or deposit mass evolution) formed at low Casein/WPI ratios despite different pH strategies. At higher Casein/WPI ratios, an increased amount of casein proteins with contaminant decrease of BLG in the deposits can be seen especially when the solution pH was fixed at 6.6 (Casein/WPI = 1 and 4, Fig. 5.8(b)). This larger participation of caseins in the deposit was both observed at higher Casein/WPI ratios at two different pH strategies, hence it cannot be solely used to explain the contrary fouling behaviors. There is one thing worthy of noticing: there seems to have large aggregates in the fouling solutions that cannot be dissociated even under reducing conditions in SDS-PAGE so that some proteins were stuck before entering the gel channel. This phenomenon is more significant when deposits were formed at unmodified conditions and high Casein/WPI ratios (*e.g*. Casein/WPI = 1 and 4, Fig. 5.8(b)). This formation of large aggregates was harder to be dissociated compared to common –SH/SS based protein complexes, thus it might be related to the interactions between denatured whey proteins and dissociated caseins. The formation of these large stable aggregates might partially explain why fouling was significantly suppressed at unmodified pH conditions, as aggregated proteins are not considered to get involved in the formation of fouling.

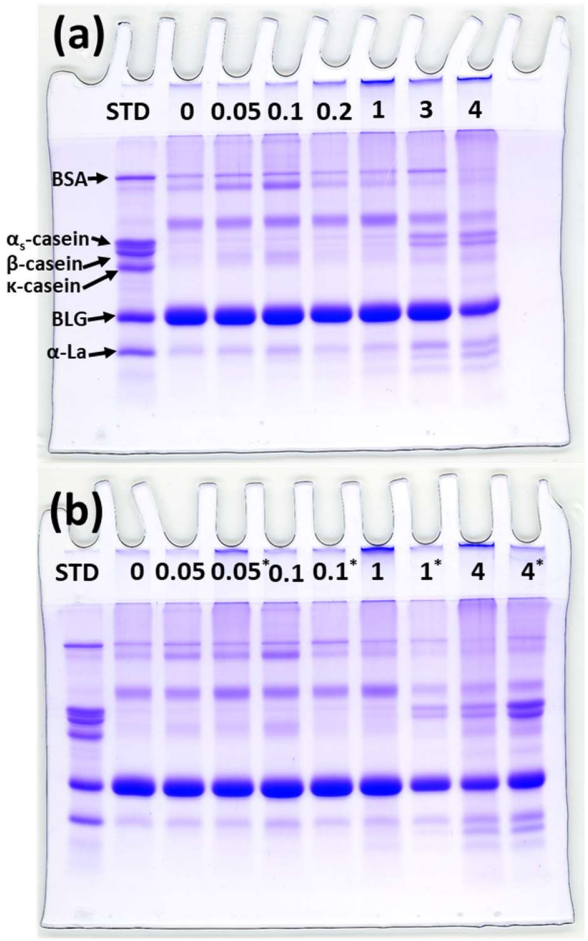

Figure 5.8. Electrophoretic patterns of fouling deposits formed at various Casein/WPI mass ratios (numbers in the upper part of each channel) under two different pH conditions (numbers with an asterisk refer to results obtained when solution pH was fixed at 6.6, otherwise it was unmodified) analyzed by SDS-PAGE under reducing conditions. Dried fouling deposits were completely dissolved using a sampling buffer as described in section 2.4 (Chapter Two) with a final concentration of 1 wt%. STD refers to protein standard solutions containing 0.25 $g \cdot L^{-1}$ α_s-casein, 0.2 $g \cdot L^{-1}$ β-casein, 0.3 $g \cdot L^{-1}$ κ-casein, 0.3 $g \cdot L^{-1}$ BLG, and 0.1 $g \cdot L^{-1}$ αLa and BSA.

5.5 Fouling drop at Casein/WPI ≤ 0.2

At this stage, it is not clear why there is a significant drop of fouling rate occurred even when a little amount of casein powder was added (*i.e.* Casein/WPI ≤ 0.2, corresponding to a casein concentration lower than 0.5 g/L). At these low casein protein concentrations, most caseins should be in the dissociated form, however, their effects on fouling were limited as they do not reach the critical quantity to express sufficient chaperone-like activities. Moreover, the effect of pH was also ruled out as the pHs of the solutions were not significantly affected/increased by such a small amount of casein powder. Following this logic, the fouling mitigation behavior should be attributed to the minerals that introduced by the addition of casein powder.

Indeed, the casein powder was confirmed to contain ~3 wt% calcium, most of which could exist in the form of colloidal calcium phosphate nanoclusters (CCP). These CaP complexes were not buried inside the micellar casein structure as most of the caseins are dissociated (the micellar structure was disrupted). Therefore, it is plausible that they remain in the serum phase and a new mineral balance has been established (*i.e.* $CaHPO_4 \rightleftharpoons Ca^{2+}+HPO_4^{2-}$). This would lead to an increase of free ($[Ca^{2+}]_f$) and total ($[Ca^{2+}]_t$) calcium levels which can be seen in Table 5.1. For instance, the fouling fluid without adding casein contains ~53 ppm Ca^{2+} and a total calcium level of 60 ppm. The amount of total calcium increases to 70 ppm at Casein/WPI of 0.05 and 80 ppm at Casein/WPI of 0.1. The ionic/free calcium level increases but do not fully cover the increase of total calcium (*e.g.* 59 ppm of $[Ca^{2+}]_f$ at Casein/WPI of 0.05 and 62 ppm at Casein/WPI of 0.1), indicating that parts of CCP dissolved into Ca^{2+} and HPO_4^{2-} while parts of them remain in the form of CCP. Nevertheless, these dissociated Ca^{2+} and HPO_4^{2-} should transform into $CaHPO_4$ under heating due to their inverse solubility against temperature.

In other words, adding these small amounts of casein powders is somehow equivalent to adding some CaP complexes. In fact, simultaneously adding calcium (in $CaCl_2$) and phosphorus (in NaH_2PO_4) have been reported to suppress whey protein fouling in both a pasteurizer and a UHT unit (Christian and Fryer, 2006). They tested four different fouling fluids: whey protein alone, and whey protein solutions with calcium and phosphorus content half that of milk/same as milk/twice that of milk. They found that increasing the content of both calcium and phosphorus progressively decreases the amount of protein and calcium in the deposit layer. In a recent article, the supplementary of a small amount of HPO_4^{2-} has been shown to dramatically suppress whey protein

fouling in a pilot-scale PHE (Blanpain-Avet et al., 2020). In that publication, the total calcium level was fixed at 2.43 mM, and the P/Ca molar ratio was increased with the addition of $NaHPO_4$. The HPO_4^{2-} was proposed to act as a calcium chelator, which reduces the level of Ca^{2+} by transforming into calcium phosphate complexes. What surprised us is that, even adding small amounts of $NaHPO_4$ can essentially suppress the total fouling mass. For example, increased P/Ca molar ratio to 0.068 and 0.134 essentially mitigated fouling with reductions of 39% and 70%, respectively. These amounts of HPO_4^{2-} were not sufficient to reduce dramatically the level of Ca^{2+}, therefore, the suppression effect on the fouling is likely linked to the presence of CaP complexes. In our case, if we assume an equimolar of P with Ca in the casein powder, the P/Ca molar ratios at Casein/WPI of 0.05 and 0.1 are approximately 0.071 and 0.136, respectively. The corresponding fouling reductions are comparable to those obtained by adding $NaHPO_4$ in the literature but in a larger extent at 60% (Casein/WPI of 0.05) and 89% (Casein/WPI of 0.1), respectively.

It was proposed that the calcium phosphate complexes that formed close to the hot surface, act also as a binding agent for fouling build-up. However, these newly formed CaP clusters could initiate fouling in a different pattern/mechanism of the one involving Ca^{2+} as they might exhibit less affinity to the denatured whey proteins compared to calcium ions (Scudeller et al., 2021). However, it might not be our case here as P can be hardly seen in the fouling deposits (see Fig. 2.21-2.22, EPMA results, Chapter Two). Instead, the pre-existed CCP nanoclusters (in casein powder) when introduced into the whey protein solutions, might act as nucleation points facilitating the precipitation of Ca^{2+} and HPO_4^{2-} around the CCP clusters (induced by higher temperature), and consequently decreases the Ca^{2+} level in the serum phase. The reduction of free calcium levels should be responsible for the lower BLG denaturation level in the bulk (Fig. 2.9 in Chapter Two for pilot-scale experiments, and Fig. 5.4 for laboratory-scale experiments) and fouling mitigation (Fig. 2.6 in Chapter Two for pilot-scale experiments, and Fig. 5.3(a) for laboratory-scale experiments).

To sum up, the suppression of fouling at very low Casein/WPI mass ratios is unlikely to be linked to the pH changes or casein-whey interactions (*e.g.* chaperone-like activities of caseins). It is more probably due to the introduction of CCP (pre-existed in the casein powder) that reduces the ionic calcium level, and therefore limits the thermal denaturation of BLG and also its subsequent deposition on the surface.

5.6 Proposed fouling mechanisms

Gathering all pieces of experimental evidence so far, we hereby propose several fouling mechanisms depending on the casein concentrations as well as pH conditions as presented in Figure 5.9.

At low Casein/WPI mass ratios (≤ 0.2, Fig. 5.9(a):

- At such low casein concentrations, most caseins are released from the micellar caseins, leading to the formation of more hydrated submicelles. The chaperone-like activities of dissociated caseins are not expected to occur due to their limited amount. The introduction of pre-existed CCP nanoclusters in the casein powder facilitates the precipitation of ionic calcium which reduces the Ca^{2+} level in the serum phase. κ-casein-BLG complexes could be created via thiol/disulfide interchange reactions.
- When the native BLG molecule transfers to the vicinity of the hot surface (*e.g.* in the thermal boundary), it quickly denatures (unfolds) and attaches to the solid-liquid interface. Ca^{2+} facilitates the anchoring of the unfolded BLG molecules upon the surface, whilst, due to its low quantity, the deposition is limited. Casein proteins can hardly participate in fouling due to their low quantity.

At high Casein/WPI mass ratios (different pH conditions, 5.9(b):

- At high casein concentrations, most caseins are in their native micellar structures. However, the micellar structure of caseins is disrupted more significantly at neutral pH compared to that at pH 6.6, resulting in a larger proportion of dissociated caseins. These dissociated caseins are sufficient to express chaperone-like functions, suppressing the thermal denaturation of BLG in the bulk. Regarding the minerals, casein micelles are capable to transfer ionic calcium into CCP during heating. However, this ability is weaker at lower pH, resulting in higher Ca^{2+} levels at pH 6.6.
- At neutral pH, due to the lower denaturation level of BLG (or lower amount of unfolded BLG species) and the lower Ca^{2+} levels, the fouling build-up is essentially prohibited, though some dissociated caseins submicelles could get involved in the fouling (mainly α_s/β-caseins). On the contrary, fouling was profound at pH 6.6 mainly due to the presence of a large quantity of calcium ions.

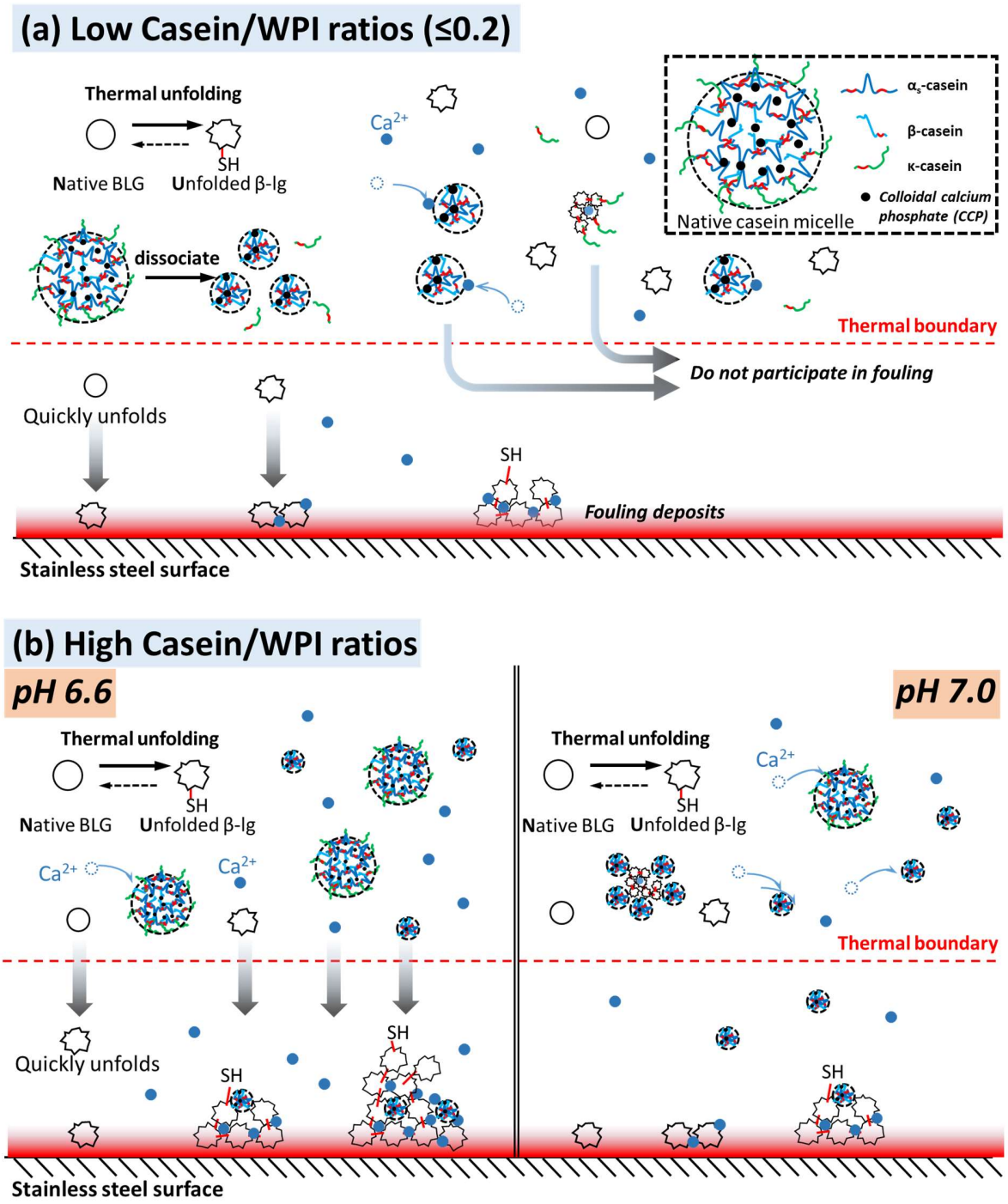

Figure 5.9. Schematic representation of the proposed fouling mechanism at (a) low Casein/WPI mass ratios and (b) high Casein/WPI ratios but at different pH conditions.

Conclusions

In this chapter, the effect of casein/whey mass ratio on whey protein fouling was investigated in the custom-built benchtop fouling device. It was designed to verify whether the effect of casein on whey protein fouling performed in the pilot plant can be reproduced in such a laboratory-scale device. There are several large differences in the benchtop device compared to the pilot plant: for example, the small fluid velocity as well as the laminar flow scheme allows to ignore the removal force of fouling so that the negative impact of fluid mechanic on fouling can be ruled out. Besides that, the surface temperature was kept almost constant not only against fouling time but also at all locations (along the path) so that the fouling deposition rate depends mostly on the amount of activated proteins near the surface. Of great interest in this chapter is to fractionate proteins using renneting-based technique. This method was expected to provide more detailed information about whey-casein interactions in the bulk and thus might cast some light into the surface reaction as well.

The fouling results conducted in the benchtop device confirm the ability of casein on fouling suppression as already observed in the pilot plant (Chapter Two). The total fouling mass drop immediately even though only a tiny amount of casein powder was added. Increasing Casein/WPI ratios do not lose this ability as fouling was always mitigated at a low extent even Casein/WPI reaches 4. This fouling behavior was achieved when the solution pH was unmodified as those in pilot plant, however, if the solution pH was fixed at 6.6, the suppression effect of casein starts to disappear at higher Casein/WPI ratios, resulting in even more deposit at Casein/WPI of 4 compared to that without adding casein. These two different fouling behaviors under different pH conditions show a strong correlation to the BLG denaturation level. At unmodified pH conditions, the BLG denaturation level decreases with elevated Casein/WPI with contaminant reduction of fouling mass; whilst, when solution pH was kept at 6.6, the BLG denaturation was less affected.

One of the most crucial questions could be “why does such a little amount of casein can reduce fouling mass to such a large extent?” Indeed, this significant suppression of fouling mass was found whatever the pH was modified or not. With such little amount of caseins, both the calcium content or the pH was not significantly changed, and their chaperone-like activities will not be significant since they are below the critical concentration. One plausible explanation is the introduction of colloidal calcium phosphates (CCP) complexes that accompanied with the addition

of casein powders. These CaP complexes favor the precipitation of Ca^{2+} during heating, decreasing the Ca^{2+} levels in the serum phase. The reduction of calcium ions decreases the thermal denaturation level of BLG in the bulk as well as prohibits fouling build-up on the surface.

At higher Casein/WPI ratios, caseins are more in their micellar structures whatever the pH conditions. In these scenarios, the capacity of balancing ionic calcium of casein micelle should play a more dominant role. When pH is lower, casein micelle gradually loses its ability on mineral balance, resulting in a higher calcium level in the serum phase. This larger content of calcium is responsible for the higher BLG denaturation level in the bulk fluid as well as the larger fouling deposition rate on the metal surface. Simultaneously, increasing pH favors the dissociation of individual caseins from the micellar structure. These dissociated caseins in the serum phase could present chaperone-like activities prohibiting the thermal denaturation of BLG, where β-casein is considered to have main contributions.

Supplementary figures for Chapter Five

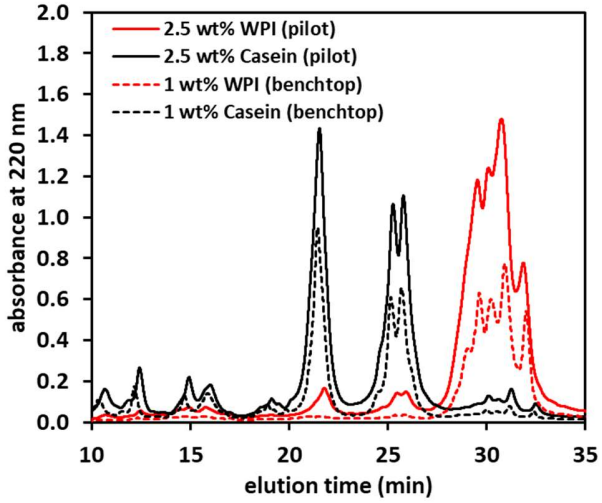

Figure S5.1. Chromatograms of reconstituted whey and casein solutions in two different scale experiments. In a pilot-scale as performed in Chapter Two, Prodiet 90 S and Promilk 87 B were used for WPI and Casein powder (denoted as pilot) while in a laboratory-scale experiment as conducted in Chapter Five, Promilk 852 FB1 and Promilk 852 B were used for WPI and Casein powder, respectively (denoted as benchtop).

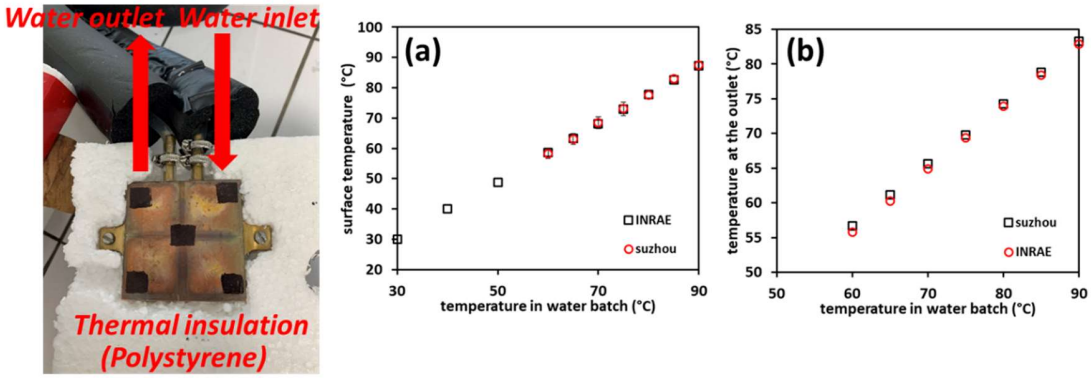

Figure S5.2. Picture shows the homemade plate heater embedded in the polystyrene substrate connected to a water bath. (a) presents the average surface temperatures of the homemade plate heater at various temperatures set in the water bath. (b) presents the solution temperature at the outlet of the benchtop fouling rig against the temperatures set in the water bath. Notice that the use of two different plate heaters is because the fouling experiments were performed in two different labs. A commercial plate heater (TP104SC, instec, USA) was used when the experiments were

performed in the lab of Soochow University (denoted as Suzhou, China); whilst when the fouling runs were conducted in the French lab (denoted as INRAE), a homemade plate heater was used. These results confirm the reliability of this homemade plate heater for replacing the commercial product.

Conclusions and outlooks

General conclusions

Most researches dealing with dairy fouling handle whey protein-based model fluids and consequently the role of casein micelle stay misunderstood. Therefore, one of the main and recurring objectives of this work is to investigate the effects of casein micelle in the whey protein fouling behavior in order to partially explain the possible underlying mechanisms.

To achieve this objective, a number of tools had been developed over time, allowing us to go further containing both experimental (Chapter Two and Five) and numerical approaches (Chapter Three and Four). One may mention the revisiting of the widely admitted kinetic models of BLG denaturation (Chapter Three) and its adaptation to be more in line with reality, but also a 3D CFD fouling simulation in a bench-scale fouling device. These advances have enabled us to achieve a certain number of results allowing us to compare the casein effect at the laboratory and pilot-scale and to propose some mechanisms at molecular scales and interesting descriptors to consider (individual casein proportions coupled with denaturation level, fouling rate) in order to better apprehend fouling behavior in various conditions (*e.g.* chemical composition of the fouling solutions, thermal profile or hydrodynamic conditions). The section below gives an overview of the results obtained chapter by chapter:

In the first chapter, the **effect of casein/whey mass ratio on the whey protein fouling performance was investigated in a pilot-scale plate heat exchanger**. Surprisingly, the total fouling deposit mass dropped significantly even though only a small amount of casein was added. The minimum value of the deposit was located at Casein/WPI of 0.2 where almost 80% amount of fouling was suppressed. Nevertheless, exceeding this critical ratio, fouling deposit increased with increased casein concentrations. At fouling decreasing region (Casein/WPI $\leq$ 0.2), thermal denaturation level of BLG in the bulk fluid was barely changed. Kinetic results also showed a moderate shift of values in the Arrhenius plot for Casein/WPI ranging from 0 to 0.2. These pieces of evidence led to the conclusion that this deposit mass drop is unlikely to be linked to the thermal denaturation of BLG. Instead, it is more probably due to the change in mineral interactions introduced by casein that affects the origin of fouling build-up. At fouling increasing region (Casein/WPI $\geq$ 0.2), a larger proportion of casein, particularly α_s/β-caseins, were found to be involved in the formation of fouling deposits in this region, which might suggest a co-precipitation of BLG-casein complex that enhances the fouling. Element mapping of the deposits revealed a

more heterogeneous and less dense fouling layer with co-located Ca-S elements scattering about Ca-P conjugates. This inhomogeneity suggests that CaP nanoclusters, introduced by micellar casein, may act as linking species between proteins as fouling grows. **It is finally proposed that micellar casein change deeply the calcium balance and the content of CaP nanocluster modifies sharply the interactions which occur between protein species (BLG, caseins) and mineral elements (ionic calcium, Ca-P) thereby affecting the protein denaturation and mineral precipitation.**

In the previous chapter, a compromised overall one-step reaction model was applied to investigate the effect of casein on the thermal denaturation of BLG. This model is rather simplified which can hardly present the well-known multi-stage reaction scheme of BLG denaturation so that the deduced thermodynamic parameters are less accurate. Therefore, in the second chapter, **a novel kinetic model concerning thermal unfolding and aggregation of BLG was established**. Of great importance, the model assumes that the thermal unfolding of protein occurs instantaneously; it is thermodynamically driven rather than kinetically controlled. Consequently, a chemical equilibrium between native and unfolded BLG species can be instantaneously established at one temperature followed by an irreversible aggregation step**. This model interprets mathematically the break-slope behavior in the Arrhenius plot and provides detailed thermodynamic information for both unfolding and aggregation processes**. Based on this model, the ionic calcium was confirmed to have a protective role on the thermal unfolding of BLG by decreasing the equilibrium constant and increasing the corresponding enthalpy at low temperatures. Moreover, the addition of calcium clearly shows a reduction of the corresponding enthalpy and entropy for the aggregation reaction which cannot be seen as reported using the overall one-step reaction model. The positive impact of calcium on the aggregation helps to shift the unfolding equilibrium of BLG toward the formation of unfolded BLG species, especially at higher temperatures. The developed model was also utilized to re-evaluate the kinetic results obtained previously (in Chapter Two) using one-step model. Based on this model, casein shows contrary effects on thermal denaturation behavior compared to that of Ca^{2+}. In short, casein favors the unfolding step of BLG while prohibiting the aggregation process. These results are in line with the chaperone-like functions of casein, inhibiting the thermal denaturation of BLG. Finally, this model was used to establish a link between protein denaturation in the bulk and deposition formation on the surface in the microchannel of a laboratory-scale fouling device as described in the next chapter.

Likewise, as described in Chapter One, most studies dealing with dairy fouling were performed in pilot-scale PHE. Despite it being industrial meaningful, the complexities of the fluid mechanics and the configuration of PHE itself make it hard to investigate the surface reaction regarding the fouling growth. Therefore, in Chapter Four, **a bench-scale fouling rig has been successfully built to perform whey protein fouling experiments with a similar bulk fluid temperature profile to that performed in pilot plant but in a laminar regime**. It was decided to first study the effect of ionic calcium on the deposition reaction so that the developed kinetic model in Chapter Three can be used to evaluate the bulk reaction. Thanks to the simplicity of the configuration, a realistic 3D CFD simulation was achieved. The simulated temperature profiles of the fluid matched well with those measured experimentally using fluorescence-based techniques. Further agreements were also found between the soluble BLG concentrations detected using HPLC at the outlet of the system and the simulated values, which verify the applied kinetic model. With the ability to provide reliable information of the localized unfolded BLG concentrations, the deposition kinetics can be calculated by coupling with experimental fouling rates. Results showed a linear relationship between the deposition pre-exponential factor and calcium concentration, **suggesting the fouling is built in such a pattern that only one calcium ion per BLG molecule is involved**. This custom-built device also allows real-time imaging of the fouling growth. The formation of the fouling shows a preference for the previously fouled layer over the clean stainless steel surface with a crystallization-like pattern. **Calcium was confirmed to be essential to fouling growth with significant effects both on the thermal denaturation and deposition processes.**

In the last chapter, the effect of casein/whey mass ratio on the whey protein fouling was investigated again but in the custom-built laboratory-scale fouling device as developed in Chapter Four. In the laboratory scale, the rehydration of casein powder could be harder which might cause blocking issues in the microchannel. The rehydration protocol of the protein powder was then optimized to ensure complete rehydration so that the protein functionality can be fully expressed. **Results revealed a similar effect of casein on fouling mitigation as those found in the pilot plant**. Fouling was suppressed dramatically with the addition of a small amount of casein and maintained at a low extent with elevated Casein/WPI ratios. At low casein concentrations, most caseins were confirmed to be in their dissociated form. The quantity of these dissociated caseins was too small to perform efficient chaperone-like activities. It was proposed that the pre-existed CCP nanoclusters (in casein powder) when introduced into the whey protein solutions,

might act as nucleation points facilitating the precipitation of Ca^{2+} and consequently decreases the Ca^{2+} level in the serum phase. The reduction of free calcium levels should be responsible for the fouling mitigation phenomenon at such low casein concentrations. At high casein concentrations and at pH 6.6, casein lost its mitigation effect on fouling. This behavior is related to its poor capacity of casein micelle controlling the ionic calcium in the serum phase at lower pH, resulting in a higher level of calcium facilitating both the denaturation of BLG and the deposition build-up. Lower amount of dissociated caseins in the serum phase at pH 6.6 might also be responsible for the increase of fouling mass as they were not sufficient to perform chaperon-like functions.

Outlooks

pH adjustment strategy

The present thesis is a pioneering work to explore the role of casein micelle on the whey protein fouling behavior. It is dedicated to revealing the underlying mechanism of dairy fouling. However, in this work, the mitigating effect of casein on whey protein fouling was not observed in the natural condition of raw milk. For example, caseins were considered to express their chaperone-like functions so as to prohibit BLG denaturation and its subsequent fouling. This was either achieved with low casein concentrations or high casein concentrations but at higher pH (higher than the natural pH of milk). At more alkaline conditions, casein micelle has a stronger capacity acting as a natural calcium chelator to reduce ionic calcium level in the serum phase and therefore, both BLG denaturation and fouling were inhibited with lack of calcium ions. Meanwhile, more individual caseins tend to release from the micellar structure into the serum phase; these individual caseins could express their chaperone-like activities with denatured BLG molecules to suppress fouling.

Slightly increasing the pH of milk leads to a dramatic suppression of dairy fouling has long been recognized since 1960s. Despite this, mitigating fouling by pH adjustment has never been employed in the industry. There could have some food safety concerns when adding a food-grade pH adjustor to increase the pH of milk, or quality concerns such as flavor changes after pH adjustment. Nevertheless, based on this work, the pH of the milk could be increased by adding caseins (*e.g*. powder). Future work could be extended to confirm if additional casein in milk could help mitigate dairy fouling.

Effect of individual casein on fouling

The custom-built laboratory device provides a platform to investigate fouling behavior in a less energy/material-expensive manner. The chaperone-like functions of α_s/β/κ-casein controlling the denaturation or aggregation of whey proteins (BLG) have been widely accepted, however, they have never been subjected to a fouling test to confirm their role on fouling. This is mainly due to the price of individual caseins and the large quantity needed in a pilot plant fouling run (*e.g*. in PHEs). Therefore, future work could be extended with the benchtop fouling device to investigate fouling behavior with the presence of different individual caseins.

Surface modifications or alternative materials

The custom-built laboratory device could also be extended to explore anti-fouling strategies by surface modification of the stainless steel surface (surface morphology, roughness, surface energy, *etc*) (Zouaghi et al., 2018d), surface coating (Zouaghi et al., 2018c), or alternative materials such as graphite-based composites (Zouaghi et al., 2018a). The configuration of the laboratory-scale device makes it easy for subsequent characterization on the fouled surface or deposits. More interesting, with the combined CFD fouling model, the effect of different surface properties or coatings on the deposition reaction can be addressed and quantified as described in Chapter Four.

Quantification of unfolded BLG species using fluorescence-lifetime-imaging-microscopy (FLIM)

The bottleneck of establishing a more advanced kinetic model concerning thermal denaturation of BLG lies in the failure to quantify the unfolded or denatured BLG species in "real-time". This could be achieved by monitoring the molecular environment of a fluorophore attached to the target protein molecule (*i.e*. BLG) during heating using fluorescence lifetime imaging microscopy (FLIM). Compared with the fluorescence intensity, fluorescence lifetime is another important parameter that determines the time available for the fluorophore to interact with or diffuse in its environment; it is a more robust feature revealing the microenvironmental conditions of the fluorophore and hence is independent of the molecule concentration (Lakowicz, 2006). One of the main advances of FLIM is its ability to differentiate fluorophores depending on their lifetimes. This important feature allows it to show the locations of different biomolecules within cells (Figure C1(a), (Lakowicz, 2006)), to map the pH of the skin stratum corneum (Figure C1(b), (Hanson et al., 2002)) or to map the temperature distribution in a microfluidic channel with 3D resolution (Benninger et al., 2006). A recent publication has revealed that the lifetime of whey protein conjugated Rhodamine B was affected due to the molecular disruption at alkaline conditions that interrupt the molecular environment of the dye (Feng et al., 2021). Therefore, for a native BLG molecule stained with a fluorophore, one could expect a lifetime variation of the fluorophore during heat-induced unfolding and aggregation of BLG (Figure C2). In this scenario, both native, unfolded, and aggregated BLG molecules can be quantified in a dynamic manner (against time). This would undoubtfully help to develop a more advanced kinetic model to describe thermal denaturation behavior of BLG.

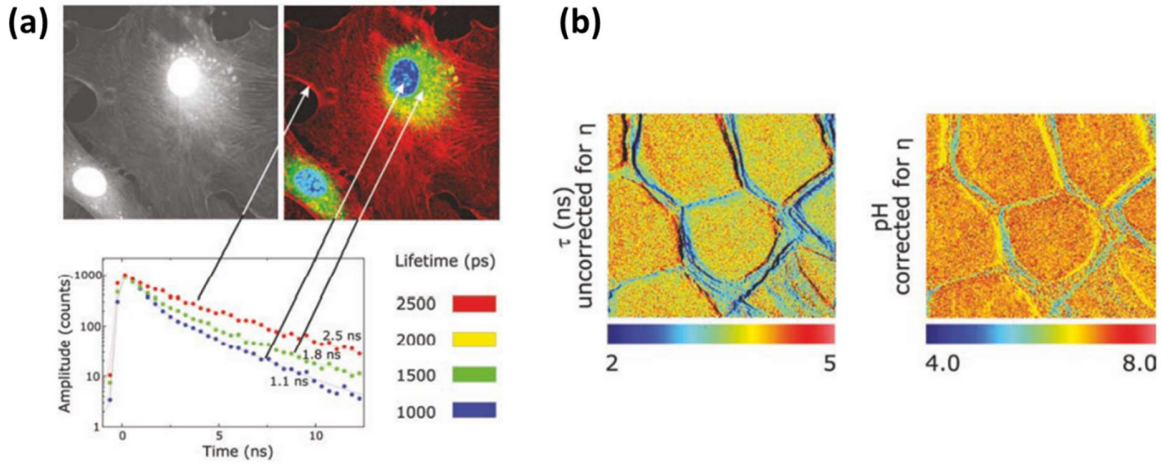

Figure C1. (a) Intensity (left) and lifetime image (right) of bovine artery endothelial cells. The nuclei were stained with diamidino-2-phenylindole for DNA (blue), F-actin was stained with Bodipy FL-phallacidin (red), and the mitochondria were stained with MitoTracker Red CMX Ros (green). Figure is re-used from (Lakowicz, 2006). (b) pH lifetime imaging of the skin stratum corneum at a depth of 6.8 μm. Figure is reprinted from (Hanson et al., 2002).

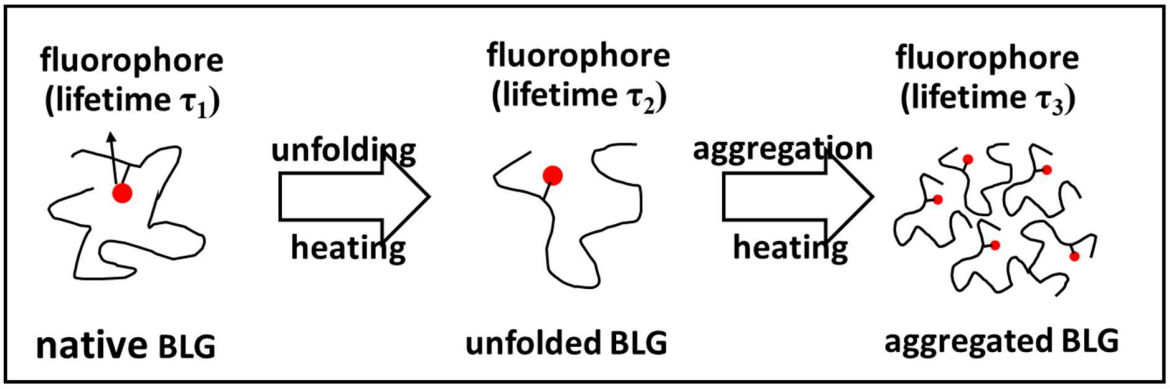

Figure C2. Schematic diagram of a fluorophore-labeled BLG molecule during thermal unfolding and aggregation. The lifetime of the fluorophore (τ) is expected to vary depending on the molecular state of BLG under thermal denaturation.

References

Abdallah, M., Azevedo-Scudeller, L., Hiolle, M., Lésure, C., Baniel, A., Delaplace, G., (2022). Heat stability of casein-based RTD beverages and fouling of heat exchangers: a review of underlying mechanisms (Submitted). Food & Bioproducts Processing.

Aigouy, L., Lalouat, L., Mortier, M., Löw, P., Bergaud, C., (2011). Note: A scanning thermal probe microscope that operates in liquids. Review of Scientific Instruments 82(3), 036106.

Almeida, C.F.d., Saget, M., Delaplace, G., Jimenez, M., Fierro, V., Celzard, A., (2021). Innovative fouling-resistant materials for industrial heat exchangers: a review. REVIEWS IN CHEMICAL ENGINEERING(000010151520200094).

Alvarez, N., Daufin, G., Gésan-Guiziou, G., (2010). Recommendations for rationalizing cleaning-in-place in the dairy industry: Case study of an ultra-high temperature heat exchanger. Journal of Dairy Science 93(2), 808-821.

Anema, S., G., (2009). Effect of milk solids concentration on the pH, soluble calcium and soluble phosphate levels of milk during heating. Dairy Sci. Technol. 89(5), 501-510.

Anema, S.G., (1998). Effect of Milk Concentration on Heat-Induced, pH-Dependent Dissociation of Casein from Micelles in Reconstituted Skim Milk at Temperatures between 20 and 120 °C. J Agric Food Chem 46(6), 2299-2305.

Anema, S.G., (2000). Effect of Milk Concentration on the Irreversible Thermal Denaturation and Disulfide Aggregation of β-Lactoglobulin. J Agric Food Chem 48(9), 4168-4175.

Anema, S.G., (2007). Role of κ-Casein in the Association of Denatured Whey Proteins with Casein Micelles in Heated Reconstituted Skim Milk. J Agric Food Chem 55(9), 3635-3642.

Anema, S.G., (2020). Chapter 9 - The whey proteins in milk: Thermal denaturation, physical interactions, and effects on the functional properties of milk, in: Boland, M., Singh, H. (Eds.), *Milk Proteins (Third Edition)*. Academic Press, pp. 325-384.

Anema, S.G., Klostermeyer, H., (1997). Heat-Induced, pH-Dependent Dissociation of Casein Micelles on Heating Reconstituted Skim Milk at Temperatures below 100 °C. J Agric Food Chem 45(4), 1108-1115.

Anema, S.G., Lee, S.K., Klostermeyer, H., (2006a). Effect of Protein, Nonprotein-Soluble Components, and Lactose Concentrations on the Irreversible Thermal Denaturation of β-Lactoglobulin and α-Lactalbumin in Skim Milk. J Agric Food Chem 54(19), 7339-7348.

Anema, S.G., Li, Y., (2000). Further Studies on the Heat-induced, pH-dependent Dissociation of Casein from the Micelles in Reconstituted Skim Milk. LWT - Food Science and Technology 33(5), 335-343.

Anema, S.G., Li, Y., (2003a). Association of denatured whey proteins with casein micelles in heated reconstituted skim milk and its effect on casein micelle size. The Journal of dairy research 70(1), 73-83.

Anema, S.G., Li, Y., (2003b). Effect of pH on the Association of Denatured Whey Proteins with Casein Micelles in Heated Reconstituted Skim Milk. J Agric Food Chem 51(6), 1640-1646.

Anema, S.G., McKenna, A.B., (1996). Reaction Kinetics of Thermal Denaturation of Whey Proteins in Heated Reconstituted Whole Milk. J Agric Food Chem 44(2), 422-428.

Anema, S.G., Pinder, D.N., Hunter, R.J., Hemar, Y., (2006b). Effects of storage temperature on the solubility of milk protein concentrate (MPC85). Food Hydrocolloids 20(2), 386-393.

Aoki, T., Umeda, T., Kako, Y., (1990). Cleavage of the linkage between colloidal calcium phosphate and casein on heating milk at high temperature. Journal of Dairy Research 57(3), 349-354.

Arvanitoyannis, I.S., Kassaveti, A., (2009). HACCP and ISO 22000 – A Comparison of the Two Systems, *HACCP and ISO 22000*, pp. 1-45.

Asteriadou, K., Hasting, A.P.M., Bird, M.R., Melrose, J., (2006). Computational Fluid Dynamics for the Prediction of Temperature Profiles and Hygienic Design in the Food Industry. Food and Bioproducts Processing 84(2), 157-163.

Aymard, P., Gimel, J.-C., Nicolai, T., Durand, D., (1996). Experimental evidence for a two-step process in the aggregation of β-lactoglobulin at pH 7. Journal de Chimie Physique et de Physico-Chimie Biologique 93, 987-997.

Bansal, B., Chen, X.D., (2006). A Critical Review of Milk Fouling in Heat Exchangers. Comprehensive Reviews in Food Science and Food Safety 5(2), 27-33.

Barilero, T., Le Saux, T., Gosse, C., Jullien, L., (2009). Fluorescent Thermometers for Dual-Emission-Wavelength Measurements: Molecular Engineering and Application to Thermal Imaging in a Microsystem. Analytical Chemistry 81(19), 7988-8000.

Barish, J.A., Goddard, J.M., (2013). Anti-fouling surface modified stainless steel for food processing. Food and Bioproducts Processing 91(4), 352-361.

Barzegar, A., Yousefi, R., Sharifzadeh, A., Dalgalarrondo, M., Chobert, J.-M., Ganjali, M.R., Norouzi, P., Ehsani, M.R., Niasari-Naslaji, A., Saboury, A.A., Haertlé, T., Moosavi-Movahedi, A.A., (2008). Chaperone activities of bovine and camel β-caseins: Importance of their surface hydrophobicity in protection against alcohol dehydrogenase aggregation. International Journal of Biological Macromolecules 42(4), 392-399.

Bauer, R., Carrotta, R., Rischel, C., Øgendal, L., (2000). Characterization and Isolation of Intermediates in β-Lactoglobulin Heat Aggregation at High pH. Biophys J 79(2), 1030-1038.

Bauer, R., Hansen, S., Øgendal, L., (1998). Detection of Intermediate Oligomers, Important for the Formation of Heat Aggregates of β-Lactoglobulin. International Dairy Journal 8(2), 105-112.

Belloque, J., Smith, G.M., (1998). Thermal Denaturation of β-Lactoglobulin. A 1H NMR Study. J Agric Food Chem 46(5), 1805-1813.

Belmar-Beiny, M.T., Fryer, P.J., (1993). Preliminary stages of fouling from whey protein solutions. Journal of Dairy Research 60(4), 467-483.

Belmar-Beiny, M.T., Gotham, S.M., Paterson, W.R., Fryer, P.J., Pritchard, A.M., (1993). The effect of Reynolds number and fluid temperature in whey protein fouling. Journal of Food Engineering 19(2), 119-139.

Benninger, R.K., Koç, Y., Hofmann, O., Requejoisidro, J., Neil, M.A., French, P.M., Demello, A.J., (2006). Quantitative 3D mapping of fluidic temperatures within microchannel networks using fluorescence lifetime imaging. Analytical Chemistry 78(7), 2272-2278.

Bernal, V., Jelen, P., (1985). Thermal stability of whey proteins – A calorimetric study. Journal of Dairy Science 68(11), 2847-2852.

Bhattacharjee, C., Saha, S., Biswas, A., Kundu, M., Ghosh, L., Das, K.P., (2005). Structural changes of beta-lactoglobulin during thermal unfolding and refolding - An FT-IR and circular dichroism study. PROTEIN JOURNAL 24(1), 27-35.

Bhattacharyya, J., Das, K.P., (1999). Molecular Chaperone-like Properties of an Unfolded Protein, s-Casein. Journal of Biological Chemistry 274(22), 15505-15509.

Bird, M., Bartlett, M., (1995). CIP optimisation for the food industry: relationships between detergent concentration, temperature and cleaning time. Food and bioproducts processing: transactions of the Institution of Chemical Engineers, Part C.

Blanpain-Avet, P., André, C., Azevedo-Scudeller, L., Croguennec, T., Jimenez, M., Bellayer, S., Six, T., Martins, G.A.S., Delaplace, G., (2020). Effect of the phosphate/calcium molar ratio on

fouling deposits generated by the processing of a whey protein isolate in a plate heat exchanger. Food and Bioproducts Processing 121, 154-165.

Blanpain-Avet, P., Andre, C., Khaldi, M., Bouvier, L., Petit, J., Six, T., Jeantet, R., Croguennec, T., Delaplace, G., (2016). Predicting the distribution of whey protein fouling in a plate heat exchanger using the kinetic parameters of the thermal denaturation reaction of beta-lactoglobulin and the bulk temperature profiles. Journal of Dairy Science 99(12), 9611-9630.

Blanpain-Avet, P., Hédoux, A., Guinet, Y., Paccou, L., Petit, J., Six, T., Delaplace, G., (2012). Analysis by Raman spectroscopy of the conformational structure of whey proteins constituting fouling deposits during the processing in a heat exchanger. Journal of Food Engineering 110(1), 86-94.

Bonfatti, V., Giantin, M., Rostellato, R., Dacasto, M., Carnier, P., (2013). Separation and quantification of water buffalo milk protein fractions and genetic variants by RP-HPLC. Food chemistry 136(2), 364-367.

Borad, S.G., Kumar, A., Singh, A.K., (2017). Effect of processing on nutritive values of milk protein. Critical Reviews In Food Science And Nutrition 57(17), 3690-3702.

Bott, T.R., (1995). *Fouling of heat exchangers*. Elsevier.

Bouchoux, A., Gésan-Guiziou, G., Pérez, J., Cabane, B., (2010). How to Squeeze a Sponge: Casein Micelles under Osmotic Stress, a SAXS Study. Biophys J 99(11), 3754-3762.

Boukazia, Y., Delaplace, G., Cadé, M., Bellouard, F., Bégué, M., Semmar, N., Fillaudeau, L., (2020). Metrological performances of fouling sensors based on steady thermal excitation applied to bioprocess. Food and Bioproducts Processing 119, 226-237.

Boukazia, Y., Delaplace, G., Cadé, M., Bellouard, F., Fillaudeau, L., (2021). On-line biofouling monitoring and qualification based on local thermal and periodic excitation with MEMS sensor. Food and Bioproducts Processing 126, 12-22.

Bouvier, L., Moreau, A., Ronse, G., Six, T., Petit, J., Delaplace, G., (2014). A CFD model as a tool to simulate β-lactoglobulin heat-induced denaturation and aggregation in a plate heat exchanger. Journal of Food Engineering 136, 56-63.

Boxler, C., (2014). Fouling by milk constituents and cleaning of modified surfaces. Von der Fakultät für Maschinenbau der Technischen Universität Carolo-Wilhelmina zu Braunschweig.

Boxler, C., Augustin, W., Scholl, S., (2013). Fouling of milk components on DLC coated surfaces at pasteurization and UHT temperatures. Food and Bioproducts Processing 91(4), 336-347.

Boye, J.I., Alli, I., (2000). Thermal denaturation of mixtures of α-lactalbumin and β-lactoglobulin: a differential scanning calorimetric study. Food Research International 33(8), 673-682.

Boye, J.I., Ismail, A.A., Alli, I., (2009). Effects of physicochemical factors on the secondary structure of β-lactoglobulin. Journal of Dairy Research 63(1), 97-109.

Brassart, E., (1990). Chemical interactions at the interface between milk compounds and austenitic stainless steel. University of Lille.

Brečević, L., Füredi-Milhofer, H., (1979). Precipitation of calcium phosphates from electrolyte solutions V. The influence of citrate ions. Calcified Tissue International 28(1), 131-136.

Briggs, D.R., Hull, R., (1945). Studies on Protein Denaturation. I. Electrophoretic Study Kinetics at Neutrality of Heat Denaturation of β-Lactoglobulin. Journal of the American Chemical Society 67(11), 2007-2014.

Britten, M., Giroux, H.J., (2022). Rennet coagulation of heated milk: A review. International Dairy Journal 124, 105179.

Britten, M., Green, M.L., Boulet, M., Paquin, P., (1988). Deposit formation on heated surfaces: effect of interface energetics. Journal of Dairy Research 55(4), 551-562.

Brownlow, S., Cabral, J.H.M., Cooper, R., Flower, D.R., Yewdall, S.J., Polikarpov, I., North, A.C.T., Sawyer, L., (1997). Bovine β-lactoglobulin at 1.8 Å resolution — still an enigmatic lipocalin. Structure 5(4), 481-495.

Broyard, C., Gaucheron, F., (2015). Modifications of structures and functions of caseins: a scientific and technological challenge. Dairy Science & Technology 95(6), 831-862.

Bryant, C.M., McClements, D.J., (1998). Molecular basis of protein functionality with special consideration of cold-set gels derived from heat-denatured whey. Trends in Food Science & Technology 9(4), 143-151.

Burton, H., (1961). A laboratory method for the investigation of milk deposits on heat exchange surfaces. Journal of Dairy Research 28(3), 255-263.

Burton, H., (1965). A method for studying the factors in milk which influence the deposition of milk solids on a heated surface. Journal of Dairy Research 32(1), 65-78.

Burton, H., (1966). A comparison between a hot-wire laboratory apparatus and a plate heat exchanger for determining the sensitivity of milk to deposit formation. Journal of Dairy Research 33(3), 317-324.

Burton, H., (1967). Seasonal variation in deposit formation from whole milk on a heated surface. Journal of Dairy Research 34(2), 137-143.

Burton, H., (1968). Reviews of progress of dairy science-Section G. Deposits from whole milk in heat treatment plant-a review and discussion. Journal of Dairy Research 35(2), 317-330.

Cairoli, S., Iametti, S., Bonomi, F., (1994). Reversible and irreversible modifications ofβ-lactoglobulin upon exposure to heat. Journal of Protein Chemistry 13(3), 347-354.

Callebaut, I., Labesse, G., Durand, P., Poupon, A., Canard, L., Chomilier, J., Henrissat, B., Mornon, J.P., (1997). Deciphering protein sequence information through hydrophobic cluster analysis (HCA): current status and perspectives. Cellular and Molecular Life Sciences CMLS 53(8), 621-645.

Calvo, M.M., Derafael, D., (1995). Deposit formation in a heat-exchanger during pasteurization of CO2 acidified milk. Journal of Dairy Research 62(4), 641-644.

Calvo, M.M., Leaver, J., Banks, J.M., (1993). Influence of other whey proteins on the heat-induced aggregation of α-lactalbumin. International Dairy Journal 3(8), 719-727.

Carrotta, R., Canale, C., Diaspro, A., Trapani, A., Biagio, P.L.S., Bulone, D., (2012). Inhibiting effect of αs1-casein on Aβ1–40 fibrillogenesis. Biochimica et Biophysica Acta (BBA) - General Subjects 1820(2), 124-132.

Carver, J.A., Rekas, A., Thorn, D.C., Wilson, M.R., (2003). Small Heat-shock Proteins and Clusterin: Intra- and Extracellular Molecular Chaperones with a Common Mechanism of Action and Function? IUBMB Life 55(12), 661-668.

Casal, H.L., Köhler, U., Mantsch, H.H., (1988). Structural and conformational changes of β-lactoglobulin B: an infrared spectroscopic study of the effect of pH and temperature. Biochimica et Biophysica Acta (BBA) - Protein Structure and Molecular Enzymology 957(1), 11-20.

Casey, K.G., Quitevis, E.L., (1988). Effect of solvent polarity on nonradiative processes in xanthene dyes: Rhodamine B in normal alcohols. The Journal of Physical Chemistry 92(23), 6590-6594.

Cecil, R., (1963). Intramolecular bonds in proteins. I. The role of sulfur in proteins. The proteins 1, 379-476.

Chandrapala, J., Martin, G.J.O., Kentish, S.E., Ashokkumar, M., (2014). Dissolution and reconstitution of casein micelle containing dairy powders by high shear using ultrasonic and physical methods. Ultrasonics Sonochemistry 21(5), 1658-1665.

Chandrapala, J., Martin, G.J.O., Zisu, B., Kentish, S.E., Ashokkumar, M., (2012a). The effect of ultrasound on casein micelle integrity. Journal of Dairy Science 95(12), 6882-6890.

Chandrapala, J., Oliver, C., Kentish, S., Ashokkumar, M., (2012b). Ultrasonics in food processing. Ultrasonics Sonochemistry 19(5), 975-983.

Chandrapala, J., Zisu, B., (2016). Novel trends in engineered milk products. Journal of Dairy Research 83(3), 268-280.

Chandrasekaran, N., Dimartino, S., Fee, C.J., (2013). Study of the adsorption of proteins on stainless steel surfaces using QCM-D. Chemical Engineering Research and Design 91(9), 1674-1683.

Changani, S.D., Belmar-Beiny, M.T., Fryer, P.J., (1997). Engineering and chemical factors associated with fouling and cleaning in milk processing. Experimental Thermal & Fluid Science 14(4), 392-406.

Chaplin, L.C., Lyster, R.L.J., (1986). Irreversible heat denaturation of bovine alpha-lactalbumin. Journal of Dairy Research 53(2), 249-258.

Chawla, R., Patil, G.R., Singh, A.K., (2011). High hydrostatic pressure technology in dairy processing: a review. Journal of Food Science and Technology 48(3), 260-268.

Chen, B., Callens, D., Campistron, P., Moulin, E., Debreyne, P., Delaplace, G., (2019). Monitoring cleaning cycles of fouled ducts using ultrasonic coda wave interferometry (CWI). Ultrasonics 96, 253-260.

Chen, X.D., Chen, Z.D., Nguang, S.K., Anema, S., (1998). Exploring the reaction kinetics of whey protein denaturation/aggregation by assuming the denaturation step is reversible. Biochemical Engineering Journal 2(1), 63-69.

Childs, P.R.N., Greenwood, J.R., Long, C.A., (2000). Review of temperature measurement. Review of Scientific Instruments 71(8), 2959-2978.

Choi, W., Jun, S., Nguyen, L.T., Rungraeng, N., Yi, H., Balasubramanian, S., Puri, V.M., Lee, J., (2013). 3-D Milk Fouling Modeling of Plate Heat Exchangers with Different Surface Finishes Using Computational Fluid Dynamics Codes. Journal of Food Process Engineering 36(4), 439-449.

Christian, G.K., Changani, S.D., Fryer, P.J., (2002). The Effect of Adding Minerals on Fouling from Whey Protein Concentrate: Development of a Model Fouling Fluid for a Plate Heat Exchanger. Food and Bioproducts Processing 80(4), 231-239.

Christian, G.K., Fryer, P.J., (2006). The Effect of Pulsing Cleaning Chemicals on the Cleaning of Whey Protein Deposits. Food and Bioproducts Processing 84(4), 320-328.

Chuang, C.-C., Wegrzyn, T.F., Anema, S.G., Loveday, S.M., (2019). Hemp globulin heat aggregation is inhibited by the chaperone-like action of caseins. Food Hydrocolloids 93, 46-55.

Collier, N., Callens, D., Campistron, P., Nongaillard, B., Jimenez, M., Alogaili, G., Debreyne, P., Delaplace, G., (2015). Ultrasonic Adhesion Measurement of Whey Protein Fouling. Heat Transfer Engineering 36(7-8), 771-779.

Collier, N., Debreyne, P., Delaplace, G., Chen, B., Callens, D., Campistron, P., Nongaillard, B., (2018). Contribution of the shear wave ultrasonic reflectometry to the stickiness measurements. Ultrasonics 89, 187-194.

Considine, T., Patel, H.A., Anema, S.G., Singh, H., Creamer, L.K., (2007). Interactions of milk proteins during heat and high hydrostatic pressure treatments — A Review. Innovative Food Science & Emerging Technologies 8(1), 1-23.

Corredig, M., Dalgleish, D., (1996a). The binding of alpha-lactalbumin and beta-lactoglobulin to casein micelles in milk treated by different heating systems. Milchwissenschaft (Germany).

Corredig, M., Dalgleish, D.G., (1996b). Effect of temperature and pH on the interactions of whey proteins with casein micelles in skim milk. Food Research International 29(1), 49-55.

Corredig, M., Dalgleish, D.G., (1999). The mechanisms of the heat-induced interaction of whey proteins with casein micelles in milk. International Dairy Journal 9(3), 233-236.

Creamer, L.K., Bienvenue, A., Nilsson, H., Paulsson, M., van Wanroij, M., Lowe, E.K., Anema, S.G., Boland, M.J., Jiménez-Flores, R., (2004). Heat-Induced Redistribution of Disulfide Bonds in Milk Proteins. 1. Bovine β-Lactoglobulin. J Agric Food Chem 52(25), 7660-7668.

Creamer, L.K., Parry, D.A.D., Malcolm, G.N., (1983). Secondary structure of bovine beta-lactoglobulin B. Archives of Biochemistry & Biophysics 227(1), 98-105.

Creighton, T.E., (1984). *Proteins: structures and molecular properties*. Macmillan.

Croguennec, T., Bouhallab, S.d., Mollé, D., O'Kennedy, B.T., Mehra, R., (2003). Stable monomeric intermediate with exposed Cys-119 is formed during heat denaturation of β-lactoglobulin. Biochemical and biophysical research communications 301(2), 465-471.

Croguennec, T., Leng, N., Hamon, P., Rousseau, F., Jeantet, R., Bouhallab, S., (2014). Caseinomacropeptide modifies the heat-induced denaturation–aggregation process of β-lactoglobulin. International Dairy Journal 36(1), 55-64.

Croguennec, T., O'Kennedy, B.T., Mehra, R., (2004). Heat-induced denaturation/aggregation of β-lactoglobulin A and B: kinetics of the first intermediates formed. International Dairy Journal 14(5), 399-409.

Dalgleish, D.G., (1990). Denaturation and aggregation of serum proteins and caseins in heated milk. J Agric Food Chem 38(11), 1995-1999.

Dalgleish, D.G., (2011). On the structural models of bovine casein micelles—review and possible improvements. Soft Matter 7(6), 2265-2272.

Dalgleish, D.G., Corredig, M., (2012). The Structure of the Casein Micelle of Milk and Its Changes During Processing. Annual Review of Food Science and Technology 3(1), 449-467.

Dannenberg, F., Kessler, H.G., (1988). Reaction Kinetics of the Denaturation of Whey Proteins in Milk. Journal of Food Science 53(1), 258-263.

Daufin, G., Labbé, J.-P., (1998). Equipment Fouling in the Dairy Application: Problem and Pretreatment, in: Amjad, Z. (Ed.), *Calcium Phosphates in Biological and Industrial Systems*. Springer US, Boston, MA, pp. 437-463.

Daufin, G., Labbe, J.P., Quemerais, A., Brule, G., Michel, F., Roignant, M., Priol, M., (1987). Fouling of a heat exchange surface by whey, milk and model fluids-an analytical study. Le Lait 67(3), 339-364.

Davey, K.R., Chandrakash, S., O'Neill, B.K., (2013). A new risk analysis of Clean-In-Place milk processing. Food Control 29(1), 248-253.

Davies, T.J., Henstridge, S.C., Gillham, C.R., Wilson, D.I., (1997). Investigation of Whey Protein Deposit Properties Using Heat Flux Sensors. Food and Bioproducts Processing 75(2), 106-110.

Day, D., Gu, M., (2010). Optical characterization of the heating performance of microchannel fluid flow. Optics and Lasers in Engineering 48(1), 32-36.

De Jong, P., (1996). Modelling and optimization of thermal processes in the dairy industry. Delft Univ. of Tech. Delft, The Netherlands.

De Jong, P., (1997). Impact and control of fouling in milk processing. Trends in Food Science & Technology 8(12), 401-405.

De Jong, P., Bouman, S., Van Der Linden, H.J.L.J., (1992). Fouling of heat treatment equipment in relation to the denaturation of β-lactoglobulin. International Journal of Dairy Technology 45(1), 3-8.

De Jong, P., Waalewijn, R., Van Der Linden, H.J.L.J., (1993). Validity of a kinetic fouling model for heat-treatment of whole milk. Lait 73(3), 293-302.

de Jongh, H.H.J., Gröneveld, T., de Groot, J., (2001). Mild Isolation Procedure Discloses New Protein Structural Properties of β-Lactoglobulin. Journal of Dairy Science 84(3), 562-571.

de Kruif, C.G., (1998). Supra-aggregates of Casein Micelles as a Prelude to Coagulation. Journal of Dairy Science 81(11), 3019-3028.

de Kruif, C.G., Grinberg, V.Y., (2002). Micellisation of β-casein. Colloids and Surfaces A: Physicochemical and Engineering Aspects 210(2), 183-190.

De Kruif, C.G., Holt, C., (2003). Casein Micelle Structure, Functions and Interactions, in: Fox, P.F., McSweeney, P.L.H. (Eds.), *Advanced Dairy Chemistry—1 Proteins: Part A / Part B*. Springer US, Boston, MA, pp. 233-276.

De wit, J.N., (1981). Structure and functional behavior of whey proteins. Netherlands Milk And Dairy Journal 35(1), 47-64.

de Wit, J.N., (1998). Nutritional and Functional Characteristics of Whey Proteins in Food Products. Journal of Dairy Science 81(3), 597-608.

de Wit, J.N., (2009). Thermal behaviour of bovine β-lactoglobulin at temperatures up to 150°C. a review. Trends in Food Science & Technology 20(1), 27-34.

Delahaije, R.J.B.M., Gruppen, H., van Eijk−van Boxtel, E.L., Cornacchia, L., Wierenga, P.A., (2016). Controlling the Ratio between Native-Like, Non-Native-Like, and Aggregated β-Lactoglobulin after Heat Treatment. J Agric Food Chem 64(21), 4362-4370.

Delplace, F., Leuliet, J., (1995). Modelling fouling of a plate heat exchanger with different flow arrangements by whey protein solutions. Food and Bioproducts Processing 73, 112-120.

Delplace, F., Leuliet, J.C., Leviex, D., (1997). A reaction engineering approach to the analysis of fouling by whey proteins of a six-channels-per-pass plate heat exchanger. Journal of Food Engineering 34(1), 91-108.

Delplace, F., Leuliet, J.C., Tissier, J.P., (1994). Fouling Experiments of a Plate Heat Exchanger by Whey Protein Solutions. Transactions of the Institution of Chemical Engineers Part C 72, 163-169.

Delsing, B.M.A., Hiddink, J., (1983). Fouling of heat-transfer surfaces by dairy liquids. Netherlands Milk And Dairy Journal 37(3), 139-148.

Deponte, H., Tonda, A., Gottschalk, N., Bouvier, L., Delaplace, G., Augustin, W., Scholl, S., (2020). Two complementary methods for the computational modeling of cleaning processes in food industry. Computers & Chemical Engineering 135, 106733.

deWit, J.N., Klarenbeek, G., (1984). Effects of Various Heat Treatments on Structure and Solubility of Whey Proteins. Journal of Dairy Science 67(11), 2701-2710.

Dey, A., Bomans, P.H.H., Müller, F.A., Will, J., Frederik, P.M., de With, G., Sommerdijk, N.A.J.M., (2010). The role of prenucleation clusters in surface-induced calcium phosphate crystallization. Nature Materials 9(12), 1010-1014.

Dickinson, E., Horne, D.S., Pinfield, V.J., Leermakers, F.A.M., (1997). Self-consistent-field modelling of casein adsorption - Comparison of results for alpha(s1)-casein and beta-casein. JOURNAL OF THE CHEMICAL SOCIETY-FARADAY TRANSACTIONS 93(3), 425-432.

Donato, L., Dalgleish, D.G., (2006). Effect of the pH of Heating on the Qualitative and Quantitative Compositions of the Sera of Reconstituted Skim Milks and on the Mechanisms of Formation of Soluble Aggregates. J Agric Food Chem 54(20), 7804-7811.

Donato, L., Guyomarc'h, F., (2009). Formation and properties of the whey protein/κ-casein complexes in heated skim milk — A review. Dairy Science & Technology 89(1), 3-29.

Donato, L., Guyomarc'h, F., Amiot, S., Dalgleish, D.G., (2007). Formation of whey protein/κ-casein complexes in heated milk: Preferential reaction of whey protein with κ-casein in the casein micelles. International Dairy Journal 17(10), 1161-1167.

Dumpler, J., Huppertz, T., Kulozik, U., (2020). Invited review: Heat stability of milk and concentrated milk: Past, present, and future research objectives. Journal of Dairy Science 103(12), 10986-11007.

Dumpler, J., Wohlschläger, H., Kulozik, U., (2017). Dissociation and coagulation of caseins and whey proteins in concentrated skim milk heated by direct steam injection. Dairy Science & Technology 96(6), 807-826.

Dürr, H., Graßhoff, A., (1999). Milk Heat Exchanger Cleaning: Modelling of Deposit Removal. Food and Bioproducts Processing 77(2), 114-118.

Ellis, J., (1987). Proteins as molecular chaperones. Nature 328(6129), 378-379.

Ellis, R.J., (2006). Molecular chaperones: assisting assembly in addition to folding. Trends in Biochemical Sciences 31(7), 395-401.

Elofsson, U.M., Dejmek, P., Paulsson, M.A., (1996). Heat-induced aggregation of β-lactoglobulin studied by dynamic light scattering. International Dairy Journal 6(4), 343-357.

Erabit, N., Flick, D., Alvarez, G., (2013). Effect of calcium chloride and moderate shear on β-lactoglobulin aggregation in processing-like conditions. Journal of Food Engineering 115(1), 63-72.

Escrig, J.E., Simeone, A., Woolley, E., Rangappa, S., Rady, A., Watson, N.J., (2020). Ultrasonic measurements and machine learning for monitoring the removal of surface fouling during clean-in-place processes. Food and Bioproducts Processing 123, 1-13.

Euston, S.R., (2013). Molecular dynamics simulation of the effect of heat on the conformation of bovine β-lactoglobulin A: A comparison of conventional and accelerated methods. Food Hydrocolloids 30(2), 519-530.

Farrell, H.M., Malin, E.L., Brown, E.M., Qi, P.X., (2006). Casein micelle structure: What can be learned from milk synthesis and structural biology? Current Opinion in Colloid & Interface Science 11(2), 135-147.

Farrell Jr, H.M., Jimenez-Flores, R., Bleck, G.T., Brown, E.M., Butler, J.E., Creamer, L.K., Hicks, C.L., Hollar, C.M., Ng-Kwai-Hang, K.F., Swaisgood, H.E., (2004). Nomenclature of the Proteins of Cows' Milk—Sixth Revision. Journal of Dairy Science 87(6), 1641-1674.

Feng, Y., (2019). Investigation of RhB-whey protein interactions on the photoproperties of RhB Soochow University, China.

Feng, Y., Liu, W., Mercadé-Prieto, R., Chen, X.D., (2021). Dye-protein interactions between Rhodamine B and whey proteins that affect the photoproperties of the dye. Journal of Photochemistry and Photobiology A: Chemistry 408, 113092.

Fernández García, L., Riera Rodríguez, F.A., (2014). Combination of microfiltration and heat treatment for ESL milk production: Impact on shelf life. Journal of Food Engineering 128, 1-9.

Fillaudeau, L., Ghnimi, S., (2014). Energy efficiency and control of the ohmic heating process. Ohmic heating in food processing, 179-196.

Fillaudeau, L., Winterton, P., Leuliet, J.C., Tissier, J.P., Maury, V., Semet, F., Debreyne, P., Berthou, M., Chopard, F., (2006). Heat Treatment of Whole Milk by the Direct Joule Effect—

Experimental and Numerical Approaches to Fouling Mechanisms. Journal of Dairy Science 89(12), 4475-4489.

Flory, P.J., (1953). *Principles of polymer chemistry*. Cornell University Press.

Fogolari, F., Ragona, L., Zetta, L., Romagnoli, S., De Kruif, K.G., Molinari, H., (1998). Monomeric bovine β-lactoglobulin adopts a β-barrel fold at pH 2. FEBS Letters 436(2), 149-154.

Foster, C.L., Britten, M., Green, M.L., (1989). A model heat-exchange apparatus for the investigation of fouling of stainless steel surfaces by milk I. Deposit formation at 100 °C. Journal of Dairy Research 56(2), 201-209.

Fox, P.F., Brodkorb, A., (2008). The casein micelle: Historical aspects, current concepts and significance. International Dairy Journal 18(7), 677-684.

Fox, P.F., Uniacke-Lowe, T., McSweeney, P.L.H., O'Mahony, J.A., (2015). Heat-Induced Changes in Milk, in: Fox, P.F., Uniacke-Lowe, T., McSweeney, P.L.H., O'Mahony, J.A. (Eds.), *Dairy Chemistry and Biochemistry*. Springer International Publishing, Cham, pp. 345-375.

Frèche, M., Heughebaert, J.C., (1989). Calcium phosphate precipitation in the 60–80°C range. Journal of Crystal Growth 94(4), 947-954.

Fryer, P.J., (1989). The uses of fouling models in the design of food process plant. International Journal of Dairy Technology 42(1), 23-29.

Fryer, P.J., Christian, G.K., (2005). Improving the cleaning of heat exchangers, in: Lelieveld, H.L.M., Mostert, M.A., Holah, J. (Eds.), *Handbook of Hygiene Control in the Food Industry*. Woodhead Publishing, pp. 468-496.

Fryer, P.J., Christian, G.K., Liu, W., (2006). How hygiene happens: Physics and chemistry of cleaning. International Journal of Dairy Technology 59(2), 76-84.

Fryer, P.J., Robbins, P.T., Green, C., Schreier, P.J.R., Pritchard, A.M., Hasting, A.P.M., Royston, D.G., Richardson, J.F., (1996). A Statistical Model for Fouling of a Plate Heat Exchanger by Whey Protein Solution at UHT Conditions. Food and Bioproducts Processing 74(4), 189-199.

Fryer, P.J., Slater, N.K.H., (1985). A direct simulation procedure for chemical reaction fouling in heat exchangers. The Chemical Engineering Journal 31(2), 97-107.

Fujiwara, K., Arai, M., Shimizu, A., Ikeguchi, M., Kuwajima, K., Sugai, S., (1999). Folding−Unfolding Equilibrium and Kinetics of Equine β-Lactoglobulin: Equivalence between the Equilibrium Molten Globule State and a Burst-Phase Folding Intermediate. Biochemistry 38(14), 4455-4463.

Galani, D., Apenten, R.K.O., (1997). The Comparative Heat Stability of Bovine β-Lactoglobulin in Buffer and Complex Media. Journal of the Science of Food & Agriculture 74(1), 89-98.

Galani, D., Owusu Apenten, R.K., (1999). Heat-induced denaturation and aggregation of β-Lactoglobulin: kinetics of formation of hydrophobic and disulphide-linked aggregates. International Journal of Food Science & Technology 34(5-6), 467-476.

Gandhi, G., Amamcharla, J.K., Boyle, D., (2017). Effect of milk protein concentrate (MPC80) quality on susceptibility to fouling during thermal processing. LWT - Food Science and Technology 81, 170-179.

Gaspard, S.J., Sharma, P., Fitzgerald, C., Tobin, J.T., O'Mahony, J.A., Kelly, A.L., Brodkorb, A., (2021). Influence of chaperone-like activity of caseinomacropeptide on the gelation behaviour of whey proteins at pH 6.4 and 7.2. Food Hydrocolloids 112, 106249.

Gaucheron, F., (2005). The minerals of milk. Reprod. Nutr. Dev. 45(4), 473-483.

Georgiadis, M.C., Macchietto, S., (2000). Dynamic modelling and simulation of plate heat exchangers under milk fouling. Chemical Engineering Science 55(9), 1605-1619.

Georgiadis, M.C., Rotstein, G.E., Macchietto, S., (1998a). Modelling and simulation of complex plate heat exchanger arrangements under milk fouling. Computers & Chemical Engineering 22, S331-S338.

Georgiadis, M.C., Rotstein, G.E., Macchietto, S., (1998b). Optimal design and operation of heat exchangers under milk fouling. AIChE Journal 44(9), 2099-2111.

Gezimati, J., Creamer, L.K., Singh, H., (1997). Heat-Induced Interactions and Gelation of Mixtures of β-Lactoglobulin and α-Lactalbumin. J Agric Food Chem 45(4), 1130-1136.

Ghnimi, S., Delaplace, G., Fillaudeau, L., (2014). Tubular and fluid jet units. Ohmic Heating in Food Processing, Electro-Technologies for Food Processing Series.

Gillham, C.R., Fryer, P.J., Hasting, A.P.M., Wilson, D.I., (1999). Cleaning-in-Place of Whey Protein Fouling Deposits: Mechanisms Controlling Cleaning. Food and Bioproducts Processing 77(2), 127-136.

Gimel, J.C., Durand, D., Nicolai, T., (1994). Structure and distribution of aggregates formed after heat-induced denaturation of globular proteins. Macromolecules 27(2), 583-589.

Goode, K.R., Asteriadou, K., Robbins, P.T., Fryer, P.J., (2013). Fouling and Cleaning Studies in the Food and Beverage Industry Classified by Cleaning Type. Comprehensive Reviews in Food Science and Food Safety 12(2), 121-143.

Gordon, K.P., Hankinson, D.J., Carver, C.E., (1968). Deposition of Milk Solids on Heated Surfaces. Journal of Dairy Science 51(4), 520-526.

Gosse, C., Bergaud, C., Löw, P., (2009). Molecular Probes for Thermometry in Microfluidic Devices, in: Volz, S. (Ed.), *Thermal Nanosystems and Nanomaterials*. Springer Berlin Heidelberg, Berlin, Heidelberg, pp. 301-341.

Gotham, S.M., Fryer, P.J., Pritchard, A.M., (1992). β-lactoglobulin denaturation and aggregation reactions and fouling deposit formation: a DSC study. International Journal of Food Science & Technology 27(3), 313-327.

Gottschalk, M., Nilsson, H., Roos, H., Halle, B., (2003). Protein self-association in solution: The bovine beta-lactoglobulin dimer and octamer. PROTEIN SCIENCE 12(11), 2404-2411.

Gough, P., Jenness, R., (1962). Heat Denaturation of β-Lactoglobulins A and B. Journal of Dairy Science 45(9), 1033-1039.

Grandison, A.S., (1988). UHT processing of milk: seasonal variation in deposit formation in heat exchangers. International Journal of Dairy Technology 41(2), 43-49.

Graßhoff, A., (1997). Cleaning of heat treatment equipment. Fouling and Cleaning in heat treatment equipment, IDF Monograph(328), 32-44.

Griffin, W.G., Griffin, M.C.A., Martin, S.R., Price, J., (1993). Molecular basis of thermal aggregation of bovine β-lactoglobulin A. Journal of the Chemical Society, Faraday Transactions 89(18), 3395-3405.

Griffiths, M.W., (2010). Pasteurization of milk with pulsed electric fields, in: Griffiths, M.W. (Ed.), *IMPROVING THE SAFETY AND QUALITY OF MILK, VOLUME 1: MILK PRODUCTION AND PROCESSING*, pp. 400-419.

Grijspeerdt, K., Hazarika, B., Vucinic, D., (2003). Application of computational fluid dynamics to model the hydrodynamics of plate heat exchangers for milk processing. Journal of Food Engineering 57(3), 237-242.

Grijspeerdt, K., Mortier, L., De Block, J., Van Renterghem, R., (2004). Applications of modelling to optimise ultra high temperature milk heat exchangers with respect to fouling. Food Control 15(2), 117-130.

Gu, Y., Bouvier, L., Tonda, A., Delaplace, G., (2019). A mathematical model for the prediction of the whey protein fouling mass in a pilot scale plate heat exchanger. Food Control 106, 106729.

Guan, S., Macchietto, S., (2018). A Novel Dynamic Model of Plate Heat Exchangers Subject to Fouling, in: Friedl, A., Klemeš, J.J., Radl, S., Varbanov, P.S., Wallek, T. (Eds.), *Computer Aided Chemical Engineering*. Elsevier, pp. 1679-1684.

Guérin, R., Ronse, G., Bouvier, L., Debreyne, P., Delaplace, G., (2007). Structure and rate of growth of whey protein deposit from in situ electrical conductivity during fouling in a plate heat exchanger. Chemical Engineering Science 62(7), 1948-1957.

Guyomarc'h, F., Nono, M., Nicolai, T., Durand, D., (2009). Heat-induced aggregation of whey proteins in the presence of κ-casein or sodium caseinate. Food Hydrocolloids 23(4), 1103-1110.

Haggett, T., (1976). The whipping, foaming and gelling properties of whey protein concentrates. New Zealand Journal of Dairy Science and Technology (New Zealand).

Hagsten, C., Altskär, A., Gustafsson, S., Lorén, N., Hamberg, L., Innings, F., Paulsson, M., Nylander, T., (2016). Composition and structure of high temperature dairy fouling. Food Structure 7, 13-20.

Hagsten, C., Altskär, A., Gustafsson, S., Lorén, N., Trägårdh, C., Innings, F., Hamberg, L., Paulsson, M., Nylander, T., (2019a). Structural and compositional changes during UHT fouling removal—Possible mechanisms of the cleaning process. Food Structure 21, 100118.

Hagsten, C., Innings, F., Trägårdh, C., Hamberg, L., Paulsson, M., Nylander, T., (2019b). Removal of UHT dairy fouling — An efficient cleaning process by optimizing the rate controlling alkaline cleaning step. Food and Bioproducts Processing 113, 101-107.

Halabi, A., Deglaire, A., Hamon, P., Bouhallab, S., Dupont, D., Croguennec, T., (2020). Kinetics of heat-induced denaturation of proteins in model infant milk formulas as a function of whey protein composition. Food chemistry 302, 125296.

Hambling, S.G., McAlpine, A.S., Sawyer, L., (1992). β-Lactoglobulin. Advanced dairy chemistry-1: Proteins.(Ed. 2), 141-190.

Hammer, P., idf (2004). Heat inactivation of classical mycobacteria in milk - A historical review In *Proceedings of the Conference Name*|, Conference Location|.

Hanazono, Y., Takeda, K., Yohda, M., Miki, K., (2012). Structural Studies on the Oligomeric Transition of a Small Heat Shock Protein, StHsp14.0. Journal of Molecular Biology 422(1), 100-108.

Hanson, K.M., Behne, M.J., Barry, N.P., Mauro, T.M., Gratton, E., Clegg, R.M., (2002). Two-Photon Fluorescence Lifetime Imaging of the Skin Stratum Corneum pH Gradient. Biophys J 83(3), 1682-1690.

Haslbeck, M., Franzmann, T., Weinfurtner, D., Buchner, J., (2005). Some like it hot: the structure and function of small heat-shock proteins. Nature Structural & Molecular Biology 12(10), 842-846.

Havea, P., Singh, H., Creamer, L.K., (2001). Characterization of heat-induced aggregates of β-lactoglobulin, α-lactalbumin and bovine serum albumin in a whey protein concentrate environment. Journal of Dairy Research 68(3), 483-497.

Havea, P., Singh, H., Creamer, L.K., Campanella, O.H., (1998). Electrophoretic characterization of the protein products formed during heat treatment of whey protein concentrate solutions. Journal of Dairy Research 65(1), 79-91.

He, J.-S., Zhu, S., Mu, T.-H., Yu, Y., Li, J., Azuma, N., (2011). αs-casein inhibits the pressure-induced aggregation of β-lactoglobulin through its molecular chaperone-like properties. Food Hydrocolloids 25(6), 1581-1586.

Hebishy, E., Joubran, Y., Murphy, E., O'Mahony, J.A., (2019). Influence of calcium-binding salts on heat stability and fouling of whey protein isolate dispersions. International Dairy Journal 91, 71-81.

Heck, J.M.L., van Valenberg, H.J.F., Dijkstra, J., van Hooijdonk, A.C.M., (2009). Seasonal variation in the Dutch bovine raw milk composition. Journal of Dairy Science 92(10), 4745-4755.

Hegg, P.-O., Castberg, H.B., Lundh, G., (1985). Fouling of whey proteins on stainless steel at different temperatures. Journal of Dairy Research 52(1), 213-218.

Hiemenz, P., (1984). Polymer chemistry—The basic concepts. Marcel Dekker, New York.

Hillier, R.M., Lyster, R.L.J., (1979). Whey-protein denaturation in heated milk and cheese whey. Journal of Dairy Research 46(1), 95-102.

Hoffmann, M.A.M., Roefs, S., Verheul, M., VanMil, P., DeKruif, K.G., (1996). Aggregation of beta-lactoglobulin studied by in situ light scattering. Journal of Dairy Research 63(3), 423-440.

Hoffmann, M.A.M., van Mil, P.J.J.M., (1999). Heat-Induced Aggregation of β-Lactoglobulin as a Function of pH. J Agric Food Chem 47(5), 1898-1905.

Hojati, S., Ghahghaei, A., Lagzian, M., (2018). The potential inhibitory effect of beta-casein on the aggregation and deposition of A(1-42) fibrils in Alzheimer's disease: insight from in-vitro and

in-silico studies. JOURNAL OF BIOMOLECULAR STRUCTURE & DYNAMICS 36(8), 2118-2130.

Holt, C., (1992). Structure and Stability of Bovine Casein Micelles, in: Anfinsen, C.B., Richards, F.M., Edsall, J.T., Eisenberg, D.S. (Eds.), *Advances in Protein Chemistry*. Academic Press, pp. 63-151.

Holt, C., Carver, J.A., Ecroyd, H., Thorn, D.C., (2013). Invited review: Caseins and the casein micelle: Their biological functions, structures, and behavior in foods. Journal of Dairy Science 96(10), 6127-6146.

Hongsprabhas, P., Barbut, S., (1997). Structure-forming processes in Ca2+-induced whey protein isolate cold gelation. International Dairy Journal 7(12), 827-834.

Hongsprabhas, P., Barbut, S., Marangoni, A.G., (1999). The Structure of Cold-Set Whey Protein Isolate Gels Prepared With Ca++. LWT - Food Science and Technology 32(4), 196-202.

Horne, D.S., (1998). Casein Interactions: Casting Light on the Black Boxes, the Structure in Dairy Products. International Dairy Journal 8(3), 171-177.

Horne, D.S., (2002). Milk Proteins | Caseins, Micellar Structure, in: Roginski, H. (Ed.), *Encyclopedia of Dairy Sciences*. Elsevier, Oxford, pp. 1902-1909.

Horne, D.S., (2006). Casein micelle structure: Models and muddles. Current Opinion in Colloid & Interface Science 11(2), 148-153.

Horne, D.S., (2017). A balanced view of casein interactions. Current Opinion in Colloid & Interface Science 28, 74-86.

Horne, D.S., (2020). Chapter 6 - Casein micelle structure and stability, in: Boland, M., Singh, H. (Eds.), *Milk Proteins (Third Edition)*. Academic Press, pp. 213-250.

Huang, X.L., Catignani, G.L., Swaisgood, H.E., (1994). Relative structural stabilites of beta-lactoglobulin-A and beta-lactoglobulin-B as determined by proteolytic susceptibility and differential scanning calorimetry. Journal of Agricultural & Food Chemistry 42(6), 1276-1280.

Huo, J., Xiao, J., Kirk, T.V., Chen, X.D., (2019). Effects of Fluorolink® S10 surface coating on WPC fouling of stainless steel surfaces and subsequent cleaning. Food and Bioproducts Processing 118, 130-138.

Huppertz, T., Fox, P.F., Kelly, A.L., (2018). 3 - The caseins: Structure, stability, and functionality, in: Yada, R.Y. (Ed.), *Proteins in Food Processing (Second Edition)*. Woodhead Publishing, pp. 49-92.

Huppertz, T., Gazi, I., Luyten, H., Nieuwenhuijse, H., Alting, A., Schokker, E., (2017). Hydration of casein micelles and caseinates: Implications for casein micelle structure. International Dairy Journal 74, 1-11.

Hussain, R., Gaiani, C., Aberkane, L., Scher, J., (2011). Characterization of high-milk-protein powders upon rehydration under various salt concentrations. Journal of Dairy Science 94(1), 14-23.

Huttmann, G., Birngruber, R., (1999). On the possibility of high-precision photothermal microeffects and the measurement of fast thermal denaturation of proteins. IEEE Journal of Selected Topics in Quantum Electronics 5(4), 954-962.

Iametti, S., De Gregori, B., Vecchio, G., Bonomi, F., (1996). Modifications Occur at Different Structural Levels During the Heat Denaturation of β-Lactoglobulin. European journal of biochemistry 237(1), 106-112.

Iametti, S., Scaglioni, L., Mazzini, S., Vecchio, G., Bonomi, F., (1998). Structural Features and Reversible Association of Different Quaternary Structures of β-Lactoglobulin. J Agric Food Chem 46(6), 2159-2166.

IDF, (2020). IDF World Dairy Situation Report 2020, Bulletin of the International Dairy Federation 506/2020.

Imamura, K., Kawasaki, Y., Awadzu, T., Sakiyama, T., Nakanishi, K., (2003). Contribution of acidic amino residues to the adsorption of peptides onto a stainless steel surface. J Colloid Interface Sci 267(2), 294-301.

Itoh, H., Nagata, A., Toyomasu, T., Sakiyama, T., Nagai, T., Saeki, T., Nakanishi, K., (1995). Adsorption of beta-lactoglobulin onto the surface of stainless-steel particels. BIOSCIENCE BIOTECHNOLOGY AND BIOCHEMISTRY 59(9), 1648-1651.

Jaskulka, F.J., Smith, D.E., Larntz, K., (2000). Determining the kinetic reaction rate order for the thermal denaturation of β-lactoglobulin using two statistical approaches. International Dairy Journal 10(9), 589-595.

Jeantet, R., Schuck, P., Six, T., Andre, C., Delaplace, G., (2010). The influence of stirring speed, temperature and solid concentration on the rehydration time of micellar casein powder. Dairy Science & Technology 90(2), 225-236.

Jennings, W.G., (1965). Theory and Practice of Hard-Surface Cleaning, in: Chichester, C.O., Mrak, E.M. (Eds.), *Advances in Food Research*. Academic Press, pp. 325-458.

Jensen, B.B.B., Friis, A., (2005). Predicting the cleanability of mix-proof valves by use of wall shear stress. Journal of Food Process Engineering 28(2), 89-106.

Jeurnink, T., Verheul, M., Stuart, M.C., de Kruif, C.G., (1996a). Deposition of heated whey proteins on a chromium oxide surface. Colloids and Surfaces B: Biointerfaces 6(4), 291-307.

Jeurnink, T.J.M., (1991). Effect of proteolysis in milk on fouling in heat-exchangers Netherlands Milk And Dairy Journal 45(1), 23-32.

Jeurnink, T.J.M., (1995a). Fouling of heat-exchangers in relation to the serum-protein concentration in milk. MILCHWISSENSCHAFT-MILK SCIENCE INTERNATIONAL 50(5), 257-260.

Jeurnink, T.J.M., (1995b). Fouling of heat exchangers by fresh and reconstituted milk and the influence or air bubbles. MILCHWISSENSCHAFT-MILK SCIENCE INTERNATIONAL 50(4), 189-193.

Jeurnink, T.J.M., Dekruif, K.G., (1995). Calcium-concentration in milk in relation to heat stability and fouling. Netherlands Milk And Dairy Journal 49(2-3), 151-165.

Jeurnink, T.J.M., Kruif, K.G.D., (1993). Changes in milk on heating: Viscosity measurements. Journal of Dairy Research 60(2), 139-150.

Jeurnink, T.J.M., Walstra, P., deKruif, C.G., (1996b). Mechanisms of fouling in dairy processing. Netherlands Milk And Dairy Journal 50(3), 407-426.

Jeyarajah, S., Allen, J.C., (1994). Calcium binding and salt-induced structural changes of native and preheated .beta.-lactoglobulin. J Agric Food Chem 42(1), 80-85.

Jimenez, M., Delaplace, G., Nuns, N., Bellayer, S., Deresmes, D., Ronse, G., Alogaili, G., Collinet-Fressancourt, M., Traisnel, M., (2013). Toward the understanding of the interfacial dairy fouling deposition and growth mechanisms at a stainless steel surface: a multiscale approach. J Colloid Interface Sci 404, 192-200.

Johnson, F.H., Eyring, H., Stover, B.J., (1974). *The theory of rate processes in biology and medicine*. Wiley-Interscience.

Johnson, J., Roland, C., (1940a). Study of dairy cleaning problems. I. Films and deposits on hot-milk equipment. Journal of Dairy Science 23, 457-461.

Johnson, J., Roland, C., (1940b). Study of dairy cleaning problems. II. Effectiveness of alkalies in removing heat-deposited milk solids and butterfat films. Journal of Dairy Science 23, 463-469.

Ju, Z.Y., Kilara, A., (1998). Aggregation Induced by Calcium Chloride and Subsequent Thermal Gelation of Whey Protein Isolate. Journal of Dairy Science 81(4), 925-931.

Jun, S., M. Puri, V., F. Roberts, R., (2004). A dynamic 2D model for thermal performance of plate heat exchangers. Transactions of the ASAE 47(1), 213-222.

Jun, S., Puri, V.M., (2005a). 3D milk-fouling model of plate heat exchangers using computational fluid dynamics. International Journal of Dairy Technology 58(4), 214-224.

Jun, S., Puri, V.M., (2005b). Fouling models for heat exchangers in dairy processing: A review. Journal of Food Process Engineering 28(1), 1-34.

Jun, S., Puri, V.M., (2006). A 2D dynamic model for fouling performance of plate heat exchangers. Journal of Food Engineering 75(3), 364-374.

Karlsson, C.A.C., Wahlgren, M.C., Trägårdh, A.C., (1996). β-Lactoglobulin fouling and its removal upon rinsing and by SDS as influenced by surface characteristics, temperature and adsorption time. Journal of Food Engineering 30(1), 43-60.

Kastanas, P., Lewis, M.J., Grandison, A.S., (1995). Design and development of a miniature UHT plant for fouling studies and its evaluation using milk adjusted to different pH values, goats milk and milk permeate. Food & Bioproducts Processing 73(C2), 83-91.

Kawasaki, K., Weiss, K.M., (2006). Evolutionary genetics of vertebrate tissue mineralization: the origin and evolution of the secretory calcium-binding phosphoprotein family. Journal of Experimental Zoology Part B: Molecular and Developmental Evolution 306B(3), 295-316.

Kehoe, J.J., Foegeding, E.A., (2011). Interaction between β-Casein and Whey Proteins As a Function of pH and Salt Concentration. J Agric Food Chem 59(1), 349-355.

Kehoe, J.J., Wang, L., Morris, E.R., Brodkorb, A., (2011). Formation of Non-Native β-Lactoglobulin during Heat-Induced Denaturation. Food Biophysics 6(4), 487.

Kern, D., Seaton, R., (1959). A theoretical analysis of thermal surface fouling. British Chemical Engineering 4(5), 258-262.

Kessler, H.-G., Beyer, H.-J., (1991). Thermal denaturation of whey proteins and its effect in dairy technology. International Journal of Biological Macromolecules 13(3), 165-173.

Kethireddipalli, P., Hill, A.R., Dalgleish, D.G., (2011). Interaction between Casein Micelles and Whey Protein/κ-Casein Complexes during Renneting of Heat-Treated Reconstituted Skim Milk Powder and Casein Micelle/Serum Mixtures. J Agric Food Chem 59(4), 1442-1448.

Khaldi, M., Blanpain-Avet, P., Guérin, R., Ronse, G., Bouvier, L., André, C., Bornaz, S., Croguennec, T., Jeantet, R., Delaplace, G., (2015a). Effect of calcium content and flow regime on whey protein fouling and cleaning in a plate heat exchanger. Journal of Food Engineering 147, 68-78.

Khaldi, M., Croguennec, T., André, C., Ronse, G., Jimenez, M., Bellayer, S., Blanpain-Avet, P., Bouvier, L., Six, T., Bornaz, S., Jeantet, R., Delaplace, G., (2018). Effect of the calcium/protein molar ratio on β-lactoglobulin denaturation kinetics and fouling phenomena. International Dairy Journal 78, 1-10.

Khaldi, M., Ronse, G., André, C., Blanpain-Avet, P., Bouvier, L., Six, T., Bornaz, S., Croguennec, T., Jeantet, R., Delaplace, G., (2015b). Denaturation Kinetics of Whey Protein Isolate Solutions and Fouling Mass Distribution in a Plate Heat Exchanger. International Journal of Chemical Engineering 2015, 139638.

Khodarahmi, R., Beyrami, M., Soori, H., (2008). Appraisal of casein's inhibitory effects on aggregation accompanying carbonic anhydrase refolding and heat-induced ovalbumin fibrillogenesis. Arch Biochem Biophys 477(1), 67-76.

Kim, S.H., Noh, J., Jeon, M.K., Kim, K.W., Lee, L.P., Woo, S.I., (2006). Micro-Raman thermometry for measuring the temperature distribution inside the microchannel of a polymerase chain reaction chip. Journal of Micromechanics and Microengineering 16(3), 526-530.

Kinsella, J., Whitehead, D., Brady, J., Bringe, N., (1989). Milk proteins: possible relationships of structure and function. Developments in dairy chemistry. 4. Functional milk proteins., 55-95.

Knudsen, J.G., (1981). Apparatus and techniques for measurement of fouling of heat transfer surfaces. Fouling of heat transfer equipment, 57-81.

Koudelka, T., Hoffmann, P., Carver, J.A., (2009). Dephosphorylation of αs- and β-Caseins and Its Effect on Chaperone Activity: A Structural and Functional Investigation. J Agric Food Chem 57(13), 5956-5964.

Kroslak, M., Sefcik, J., Morbidelli, M., (2007). Effects of Temperature, pH, and Salt Concentration on β-Lactoglobulin Deposition Kinetics Studied by Optical Waveguide Lightmode Spectroscopy. Biomacromolecules 8(3), 963-970.

Kulkarni, S.M., Maxcy, R.B., Arnold, R.G., (1975). Evaluation of Soil Deposition and Removal Processes: An Interpretive Review. Journal of Dairy Science 58(12), 1922-1936.

Kumosins.Tf, Timashef.Sn, (1966). Molecular interactions in beta-lactoglobulin. X. Stoichiometry of the beta-lactoglobulin mixed tetramerization. Journal of the American Chemical Society 88(23), 5635-&.

Kuwata, K., Hoshino, M., Forge, V., Era, S., Batt, C.A., Goto, Y., (1999). Solution structure and dynamics of bovine β-lactoglobulin A. PROTEIN SCIENCE 8(11), 2541-2545.

Kwak, S., Ma, Y., Huang, B., (2020). Extracting nonstationary features for process data analytics and application in fouling detection. Computers & Chemical Engineering 135, 106762.

Lakowicz, J.R., (2006). *Principles of Fluorescence Spectroscopy*. Springer US, Boston, MA.

Lalande, M., Tissier, J.-P., (1985). Fouling of Heat Transfer Surfaces Related to β-Lactoglobulin Denaturation During Heat Processing of Milk. Biotechnology Progress 1(2), 131-139.

Lalande, M., Tissier, J.P., Corrieu, G., (1984). Fouling of a plate heat exchanger used in ultra-high-temperature sterilization of milk. Journal of Dairy Research 51(4), 557-568.

Laskey, R.A., Honda, B.M., Mills, A.D., Finch, J.T., (1978). Nucleosomes are assembled by an acidic protein with binds histones and transfers them to DNA. Nature 275(5679), 416-420.

Law, A.J.R., Leaver, J., (2000). Effect of pH on the Thermal Denaturation of Whey Proteins in Milk. J Agric Food Chem 48(3), 672-679.

Le Bon, C., Nicolai, T., Durand, D., (1999). Kinetics of Aggregation and Gelation of Globular Proteins after Heat-Induced Denaturation. Macromolecules 32(19), 6120-6127.

Le Ray, C., Maubois, J.-L., Gaucheron, F., Brulé, G., Pronnier, P., Garnier, F., (1998). Heat stability of reconstituted casein micelle dispersions: changes induced by salt addition. Lait 78(4), 375-390.

Leermakers, F.A.M., Atkinson, P.J., Dickinson, E., Horne, D.S., (1996). Self-Consistent-Field Modeling of Adsorbed β-Casein: Effects of pH and Ionic Strength on Surface Coverage and Density Profile. J Colloid Interface Sci 178(2), 681-693.

Leite, B., Croguennec, T., Halabi, A., Costa Junior, E.F.d., (2021). Comparing different methods for estimating kinetic parameters of whey protein heat-induced denaturation in infant milk formulas. Journal of Food Engineering 292, 110272.

Leuliet, J.C., (1988). Comportements Hydaulique et Thermique des Echangeurs à Plaques Traitant des Produits Non-Newtoniens. Available online: http://www.thesis.fr/1988NAN10450.

Lewis, M.J., Deeth, H.C., (2008). Heat Treatment of Milk, *Milk Processing and Quality Management*, pp. 168-204.

Li, L., Lv, H.T., Deng, R.P., Liao, Z.K., Wu, X.E., Chen, X.D., (2013). Experimental investigation of egg ovalbumin scaling on heated stainless steel surface and scale-removal compared with that of whey protein. Colloids and Surfaces B: Biointerfaces 107, 198-204.

Liu, W., Chen, X.D., Jeantet, R., André, C., Bellayer, S., Delaplace, G., (2021). Effect of casein/whey ratio on the thermal denaturation of whey proteins and subsequent fouling in a plate heat exchanger. Journal of Food Engineering 289, 110175.

Liu, W., Wilson, D.I., Chen, X.D., Mercadé-Prieto, R., (2018). Quantification of the Local Protein Content in Hydrogels Undergoing Swelling and Dissolution at Alkaline pH Using Fluorescence Microscopy. Food and Bioprocess Technology 11(3), 572-584.

Liu, W.J., Chen, X.D., Mercadé-Prieto, R., (2017). Spatial quantification of hydrogels swelling using wide-field fluorescence microscopy. Chemical Engineering Science 158, 349-358.

Livney, Y.D., Verespej, E., Dalgleish, D.G., (2003). Steric Effects Governing Disulfide Bond Interchange during Thermal Aggregation in Solutions of β-Lactoglobulin B and α-Lactalbumin. J Agric Food Chem 51(27), 8098-8106.

López Arbeloa, T., López Arbeloa, F., López Arbeloa, I., (1999). Environmental effects on the photophysics of pyrromethene 556. Physical Chemistry Chemical Physics 1(5), 791-795.

Loveday, S.M., (2016). β-Lactoglobulin heat denaturation: A critical assessment of kinetic modelling. International Dairy Journal 52, 92-100.

Loveday, S.M., Peram, M.R., Singh, H., Ye, A., Jameson, G.B., (2014). Digestive diversity and kinetic intrigue among heated and unheated β-lactoglobulin species. Food & Function 5(11), 2783-2791.

Lu, J., Pickova, J., Vázquez-Gutiérrez, J.L., Langton, M., (2018). Influence of seasonal variation and ultra high temperature processing on lipid profile and fat globule structure of Swedish cow milk. Food chemistry 239, 848-857.

Lucey, J.A., Horne, D.S., (2018). Perspectives on casein interactions. International Dairy Journal 85, 56-65.

Lund, D., Sandu, C., (1981). Chemical reaction fouling due to foodstuffs. Editions Summerscales, Hemisphere Washington DC 437.

Lv, H., Huang, S., Mercadé-Prieto, R., Wu, X.E., Chen, X.D., (2015). The effect of pre-adsorption of OVA or WPC on subsequent OVA or WPC fouling on heated stainless steel surface. Colloids and Surfaces B: Biointerfaces 129, 154-160.

Lyster, R.L.J., (1965). Composition Of Milk Deposits In an Ultra-High-Temperature Plant. Journal of Dairy Research 32(2), 203-&.

Lyster, R.L.J., (1970). The denaturation of α-lactalbumin and β-lactoglobulin in heated milk. Journal of Dairy Research 37(2), 233-243.

Mahdi, Y., Mouheb, A., Oufer, L., (2009). A dynamic model for milk fouling in a plate heat exchanger. Applied Mathematical Modelling 33(2), 648-662.

Manderson, G.A., Creamer, L.K., Hardman, M.J., (1999). Effect of Heat Treatment on the Circular Dichroism Spectra of Bovine β-Lactoglobulin A, B, and C. J Agric Food Chem 47(11), 4557-4567.

Manji, B., Kakuda, Y., (1986). Thermal Denaturation of Whey Proteins in Skim Milk. Canadian Institute of Food Science and Technology Journal 19(4), xxxvii.

Marciniak, A., Suwal, S., Brisson, G., Britten, M., Pouliot, Y., Doyen, A., (2018). Studying a chaperone-like effect of beta-casein on pressure-induced aggregation of beta-lactoglobulin in the presence of alpha-lactalbumin. Food Hydrocolloids 84, 9-15.

Marty, P., (2001). Maîtrise de la consommation d'eau dans les industries agro-alimentaires: Dossier eau. Industries alimentaires et agricoles 118(5), 35-39.

Matsudomi, N., Kanda, Y., Yoshika, Y., Moriwaki, H., (2004). Ability of αs-Casein to Suppress the Heat Aggregation of Ovotransferrin. J Agric Food Chem 52(15), 4882-4886.

McMahon, D.J., Ganesan, B., Qian, M., Brothersen, C., (2011). Electrical Resistive Heating vs. Conventional UHT Technologies. Journal of Dairy Science 1(94), 231.

McMahon, D.J., Oommen, B.S., (2008). Supramolecular Structure of the Casein Micelle. Journal of Dairy Science 91(5), 1709-1721.

McSweeney, D.J., O'Mahony, J.A., McCarthy, N.A., (2021). Strategies to enhance the rehydration performance of micellar casein-dominant dairy powders. International Dairy Journal 122, 105116.

Mercier, J.C., (1981). Phosphorylation of caseins, present evidence for an amino acid triplet code posttranslationally recognized by specific kinases. Biochimie 63(1), 1-17.

Miyawaki, A., Sawano, A., Kogure, T., (2003). Lighting up cells: labelling proteins with fluorophores. Nature cell biology Suppl, S1-7.

Moore, S.A., Anderson, B.F., Groom, C.R., Haridas, M., Baker, E.N., (1997). Three-dimensional structure of diferric bovine lactoferrin at 2.8 angstrom resolution. Journal of Molecular Biology 274(2), 222-236.

Morgan, F., Léonil, J., Mollé, D., Bouhallab, S.d., (1997). Nonenzymatic Lactosylation of Bovine β-Lactoglobulin under Mild Heat Treatment Leads to Structural Heterogeneity of the Glycoforms. Biochemical and biophysical research communications 236(2), 413-417.

Morgan, P.E., Treweek, T.M., Lindner, R.A., Price, W.E., Carver, J.A., (2005). Casein Proteins as Molecular Chaperones. J Agric Food Chem 53(7), 2670-2683.

Mounsey, J.S., O'Kennedy, B.T., (2007). Conditions limiting the influence of thiol–disulphide interchange reactions on the heat-induced aggregation kinetics of β-lactoglobulin. International Dairy Journal 17(9), 1034-1042.

Mounsey, J.S., O'Kennedy, B.T., Fenelon, M.A., Brodkorb, A., (2008). The effect of heating on β-lactoglobulin–chitosan mixtures as influenced by pH and ionic strength. Food Hydrocolloids 22(1), 65-73.

Müller-Steinhagen, H., Malayeri, M.R., Watkinson, A.P., (2011). Heat Exchanger Fouling: Mitigation and Cleaning Strategies. Heat Transfer Engineering 32(3-4), 189-196.

Mulvihill, D.M., Donovan, M., (1987). Whey Proteins and Their Thermal Denaturation - A Review. Irish Journal of Food Science and Technology 11(1), 43-75.

Nieuwenhuijse, J.A., Vanboekel, M., Walstra, P., (1991). On the heat-induced association and dissociation of proteins in concentrated skim milk. Netherlands Milk And Dairy Journal 45(1), 3-22.

Nogueira, M.H., Humblot, L., Singh, R.P., Dieude-Fauvel, E., Doumert, B., Nasser, S., Lesur, C., Karoui, R., Delaplace, G., Peixoto, P.P.S., (2021). The heterogeneous substructure of casein micelles evidenced by SAXS and NMR in demineralized samples. Food Hydrocolloids 117, 106653.

O'Kennedy, B.T., Mounsey, J.S., (2006). Control of Heat-Induced Aggregation of Whey Proteins Using Casein. J Agric Food Chem 54(15), 5637-5642.

Oldfield, D.J., Singh, H., Taylor, M.W., (1998a). Association of β-Lactoglobulin and β-Lactalbumin with the Casein Micelles in Skim Milk Heated in an Ultra-high Temperature Plant. International Dairy Journal 8(9), 765-770.

Oldfield, D.J., Singh, H., Taylor, M.W., (2005). Kinetics of heat-induced whey protein denaturation and aggregation in skim milks with adjusted whey protein concentration. Journal of Dairy Research 72(3), 369-378.

Oldfield, D.J., Singh, H., Taylor, M.W., Pearce, K.N., (1998b). Kinetics of Denaturation and Aggregation of Whey Proteins in Skim Milk Heated in an Ultra-high Temperature (UHT) Pilot Plant. International Dairy Journal 8(4), 311-318.

Oldfield, D.J., Singh, H., Taylor, M.W., Pearce, K.N., (2000). Heat-induced interactions of β-lactoglobulin and α-lactalbumin with the casein micelle in pH-adjusted skim milk. International Dairy Journal 10(8), 509-518.

On-Nom, N., Grandison, A.S., Lewis, M.J., (2010). Measurement of ionic calcium, pH, and soluble divalent cations in milk at high temperature. Journal of Dairy Science 93(2), 515-523.

Onganer, Y., Quitevis, E.L., (1992). Effect of solvent on nonradiative processes in xanthene dyes: pyronin B in alcohols and alcohol-water mixtures. The Journal of Physical Chemistry 96(20), 7996-8001.

Osintsev, A.M., Syrtseva, A.P., Kolmykov, R.P., Braginsky, V.I., Lapshakova, O.Y., Osintseva, M.A., (2016). Study of calcium role in collodial stability of reconstituted skim milk under rennt coagulation conditions. FOODS AND RAW MATERIALS 4(1), 121-128.

Owusu Apenten, R.K., Galani, D., (2000). Thermodynamic parameters for beta-lactoglobulin dissociation over a broad temperature range at pH 2.6 and 7.0. Thermochimica Acta 359(2), 181-188.

ÖZer, B.H., Kirmaci, H.A., (2010). Functional milks and dairy beverages. International Journal of Dairy Technology 63(1), 1-15.

Pan, F., Chen, X.D., Mercadé-Prieto, R., Xiao, J., (2019). Numerical simulation of milk fouling: Taking fouling layer domain and localized surface reaction kinetics into account. Chemical Engineering Science 197, 306-316.

Park, K.H., Lund, D.B., (1984). Calorimetric Study of Thermal Denaturation of β-Lactoglobulin. Journal of Dairy Science 67(8), 1699-1706.

Parker, E.A., Donato, L., Dalgleish, D.G., (2005). Effects of Added Sodium Caseinate on the Formation of Particles in Heated Milk. J Agric Food Chem 53(21), 8265-8272.

Patel, H.A., Singh, H., Anema, S.G., Creamer, L.K., (2006). Effects of Heat and High Hydrostatic Pressure Treatments on Disulfide Bonding Interchanges among the Proteins in Skim Milk. J Agric Food Chem 54(9), 3409-3420.

Paulsson, M., Dejmek, P., (1990). Thermal Denaturation of Whey Proteins in Mixtures with Caseins Studied by Differential Scanning Calorimetry. Journal of Dairy Science 73(3), 590-600.

Paviolo, C., Clayton, A.H.A., McArthur, S.L., Stoddart, P.R., (2013). Temperature measurement in the microscopic regime: a comparison between fluorescence lifetime- and intensity-based methods. Journal of Microscopy 250(3), 179-188.

Peres de sa Peixoto Junior, P., Trivelli, X., Andre, C., Moreau, A., Delaplace, G., (2019). Formation of beta-lactoglobulin aggregates from quite, Unfolded conformations upon heat aαctivation. Langmuir 35(2), 446-452.

Pesic, M.B., Barac, M.B., Stanojevic, S.P., Ristic, N.M., Macej, O.D., Vrvic, M.M., (2012). Heat induced casein–whey protein interactions at natural pH of milk: A comparison between caprine and bovine milk. Small Ruminant Research 108(1), 77-86.

Petermeier, H., Benning, R., Delgado, A., Kulozik, U., Hinrichs, J., Becker, T., (2002). Hybrid model of the fouling process in tubular heat exchangers for the dairy industry. Journal of Food Engineering 55(1), 9-17.

Petit, J., Herbig, A.L., Moreau, A., Delaplace, G., (2011). Influence of calcium on β-lactoglobulin denaturation kinetics: Implications in unfolding and aggregation mechanisms. Journal of Dairy Science 94(12), 5794-5810.

Petit, J., Herbig, A.L., Moreau, A., Le Page, J.F., Six, T., Delaplace, G., (2012). Granulomorphometry: A suitable tool for identifying hydrophobic and disulfide bonds in β-lactoglobulin aggregates. Application to the study of β-lactoglobulin aggregation mechanism between 70 and 95°C. Journal of Dairy Science 95(8), 4188-4202.

Petit, J., Moreau, A., Ronse, G., Debreyne, P., Bouvier, L., Blanpain-Avet, P., Jeantet, R., Delaplace, G., (2016). Role of Whey Components in the Kinetics and Thermodynamics of β-Lactoglobulin Unfolding and Aggregation. Food and Bioprocess Technology 9(8), 1367-1379.

Petit, J., Six, T., Moreau, A., Ronse, G., Delaplace, G., (2013). β-lactoglobulin denaturation, aggregation, and fouling in a plate heat exchanger: Pilot-scale experiments and dimensional analysis. Chemical Engineering Science 101, 432-450.

Phan-Xuan, T., Durand, D., Nicolai, T., Donato, L., Schmitt, C., Bovetto, L., (2013). Tuning the structure of protein particles and gels with calcium or sodium ions. Biomacromolecules 14(6), 1980-1989.

Piepiórka-Stepuk, J., Diakun, J., Jakubowski, M., Mierzejewska, S., Masłowska, S., (2012). Influence of time and the cleaning liquid flow velocity on the effectiveness of cleaning the plate heat exchanger. Agric. Eng. 3(138), 171-176.

Piepiórka-Stepuk, J., Diakun, J., Mierzejewska, S., (2016). Poly-optimization of cleaning conditions for pipe systems and plate heat exchangers contaminated with hot milk using the Cleaning In Place method. Journal of Cleaner Production 112, 946-952.

Prabakaran, S., Damodaran, S., (1997). Thermal Unfolding of β-Lactoglobulin: Characterization of Initial Unfolding Events Responsible for Heat-Induced Aggregation. J Agric Food Chem 45(11), 4303-4308.

Price, W.V., (1927). Concerning the Addition of Calcium Chloride to Milk for Cheese Making. Journal of Dairy Science 10(5), 373-376.

Ptitsyn, O.B., (1995). Molten Globule and Protein Folding, in: Anfinsen, C.B., Richards, F.M., Edsall, J.T., Eisenberg, D.S. (Eds.), *Advances in Protein Chemistry*. Academic Press, pp. 83-229.

Qi, X.L., Brownlow, S., Holt, C., Sellers, P., (1995). Thermal denaturation of β-lactoglobulin: effect of protein concentration at pH 6.75 and 8.05. Biochimica et Biophysica Acta (BBA) - Protein Structure and Molecular Enzymology 1248(1), 43-49.

Qi, X.L., Holt, C., McNulty, D., Clarke, D.T., Brownlow, S., Jones, G.R., (1997). Effect of temperature on the secondary structure of β-lactoglobulin at pH 6.7, as determined by CD and IR spectroscopy: a test of the molten globule hypothesis. Biochemical Journal 324(1), 341-346.

Qin, B.Y., Bewley, M.C., Creamer, L.K., Baker, H.M., Baker, E.N., Jameson, G.B., (1998). Structural Basis of the Tanford Transition of Bovine β-Lactoglobulin. Biochemistry 37(40), 14014-14023.

Qin, B.Y., Jameson, G.B., Bewley, M.C., Baker, E.N., Creamer, L.K., (1999). Functional implications of structural differences between variants A and B of bovine β-lactoglobulin. PROTEIN SCIENCE 8(1), 75-83.

Rasane, P., Sharma, N., Fatma, S., Kaur, S., Jha, A., Kaur, D., Singh, J., (2020). Ultra-high Temperature (UHT) Processing: Technological Significance and Updates. CURRENT NUTRITION & FOOD SCIENCE 16(8), 1183-1195.

Rene, F., Leuliet, J., Lalande, M., (1991). Heat transfer to Newtonian and non-Newtonian food fluids in plate heat exchangers: experimental and numerical approaches. Food and Bioproducts Processing 69, 115-126.

Reynolds, E.C., Riley, P.F., Storey, E., (1982). Phosphoprotein inhibition of hydroxyapatite dissolution. Calcified Tissue International 34 Suppl 2, S52-56.

Richard, B., Le Page, J.F., Schuck, P., Andre, C., Jeantet, R., Delaplace, G., (2013). Towards a better control of dairy powder rehydration processes. International Dairy Journal 31(1), 18-28.

Robbins, P.T., Elliott, B.L., Fryer, P.J., Belmar, M.T., Hasting, A.P.M., (1999). A Comparison of Milk and Whey Fouling in a Pilot Scale Plate Heat Exchanger: Implications for Modelling and Mechanistic Studies. Food and Bioproducts Processing 77(2), 97-106.

Roefs, S.P.F.M., De Kruif, K.G., (1994). A Model for the Denaturation and Aggregation of β-Lactoglobulin. European journal of biochemistry 226(3), 883-889.

Roper, M.G., Easley, C.J., Legendre, L.A., Humphrey, J.A.C., Landers, J.P., (2007). Infrared Temperature Control System for a Completely Noncontact Polymerase Chain Reaction in Microfluidic Chips. Analytical Chemistry 79(4), 1294-1300.

Rosa, M.T.M.G., Guimarães, D.H.P., Arce, P.F., (2019). Experimental measurements and simulation of the fouling phenomena of natural proteins. International Journal of Heat and Mass Transfer 129, 1075-1085.

Rosmaninho, R., Santos, O., Nylander, T., Paulsson, M., Beuf, M., Benezech, T., Yiantsios, S., Andritsos, N., Karabelas, A., Rizzo, G., Müller-Steinhagen, H., Melo, L.F., (2007). Modified stainless steel surfaces targeted to reduce fouling – Evaluation of fouling by milk components. Journal of Food Engineering 80(4), 1176-1187.

Rüegg, M., Moor, U., Blanc, B., (1977). A calorimetric study of the thermal denaturation of whey proteins in simulated milk ultrafiltrate. Journal of Dairy Research 44(3), 509-520.

Sadeghinezhad, E., Kazi, S.N., Badarudin, A., Zubair, M.N.M., Dehkordi, B.L., Oon, C.S., (2013). A review of milk fouling on heat exchanger surfaces. REVIEWS IN CHEMICAL ENGINEERING 29(3), 169-188.

Saget, M., de Almeida, C.F., Fierro, V., Celzard, A., Delaplace, G., Thomy, V., Coffinier, Y., Jimenez, M., (2021). A critical review on surface modifications mitigating dairy fouling. Comprehensive Reviews in Food Science and Food Safety 20(5), 4324-4366.

Sakiyama, T., Tanino, K., Urakawa, M., Imamura, K., Takahashi, T., Nagai, T., Nakanishi, K., (1999). Adsorption characteristics of tryptic fragments of bovine β-lactoglobulin on a stainless steel surface. Journal of Bioscience and Bioengineering 88(5), 536-541.

Salter, A.M., (2016). Improving the sustainability of global meat and milk production. Proceedings of the Nutrition Society 76(1), 22-27.

Sanders, H.M., Jovcevski, B., Carver, J.A., Pukala, T.L., (2020). The molecular chaperone beta-casein prevents amorphous and fibrillar aggregation of alpha-lactalbumin by stabilisation of dynamic disorder. Biochemical Journal 477(3), 629-643.

Santos, O., Nylander, T., Schillén, K., Paulsson, M., Trägårdh, C., (2006). Effect of surface and bulk solution properties on the adsorption of whey protein onto steel surfaces at high temperature. Journal of Food Engineering 73(2), 174-189.

Sawyer, W.H., (1969). Complex between beta-lactoglobulin and kappa-casein. A review. Journal of Dairy Science 52(9), 1347-1355.

Sawyer, W.H., Norton, R.S., Nichol, L.W., McKenzie, G.H., (1971). Thermodenaturation of bovine β-lactoglobulin: Kinetics and the introduction of β-structure. Biochimica et Biophysica Acta (BBA) - Protein Structure 243(1), 19-30.

Schmidt, D., (1982). Association of caseins and casein micelle structure. Developments in dairy chemistry 1, 61-86.

Schmidt, D.G., (1980). Colloidal aspects of casein. Netherlands Milk And Dairy Journal 34(1), 42-64.

Schmidt, V.S.J., Kaufmann, V., Kulozik, U., Scherer, S., Wenning, M., (2012). Microbial biodiversity, quality and shelf life of microfiltered and pasteurized extended shelf life (ESL) milk from Germany, Austria and Switzerland. International Journal of Food Microbiology 154(1), 1-9.

Schöler, M., Föste, H., Helbig, M., Gottwald, A., Friedrichs, J., Werner, C., Augustin, W., Scholl, S., Majschak, J.-P., (2012). Local analysis of cleaning mechanisms in CIP processes. Food and Bioproducts Processing 90(4), 858-866.

Schreier, P.J.R., Fryer, P.J., (1995). Heat exchanger fouling: A model study of the scaleup of laboratory data. Chemical Engineering Science 50(8), 1311-1321.

Scudeller, L.A., Blanpain-Avet, P., Six, T., Bellayer, S., Jimenez, M., Croguennec, T., André, C., Delaplace, G., (2021). Calcium Chelation by Phosphate Ions and Its Influence on Fouling Mechanisms of Whey Protein Solutions in a Plate Heat Exchanger. Foods 10(2).

Seo, J.-A., Hédoux, A., Guinet, Y., Paccou, L., Affouard, F., Lerbret, A., Descamps, M., (2010). Thermal Denaturation of Beta-Lactoglobulin and Stabilization Mechanism by Trehalose Analyzed from Raman Spectroscopy Investigations. The Journal of Physical Chemistry B 114(19), 6675-6684.

Sharma, A., Macchietto, S., (2019). Fouling and Cleaning of Plate Heat Exchangers for Milk Pasteurisation: A Moving Boundary Model, in: Kiss, A.A., Zondervan, E., Lakerveld, R., Özkan, L. (Eds.), *Computer Aided Chemical Engineering*. Elsevier, pp. 1483-1488.

Sharma, A., Macchietto, S., (2021). Fouling and cleaning of plate heat exchangers: Dairy application. Food and Bioproducts Processing 126, 32-41.

Sherwin, C., Foegeding, E., (1997). The effects of CaCl2 on aggregation of whey proteins. Milchwissenschaft (Germany).

Simons, J.-W.F.A., Kosters, H.A., Visschers, R.W., de Jongh, H.H.J., (2002). Role of calcium as trigger in thermal β-lactoglobulin aggregation. Arch Biochem Biophys 406(2), 143-152.

Singh, H., Creamer, L.K., (1991a). Denaturation, aggregation and heat stability of milk protein during the manufacture of skim milk powder. Journal of Dairy Research 58(3), 269-283.

Singh, H., Creamer, L.K., (1991b). Influence of concentration of milk solids on the dissociation of micellar κ-casein on heating reconstituted milk at 120°C. Journal of Dairy Research 58(1), 99-105.

Skudder, P.J., Brooker, B.E., Bonsey, A.D., Alvarezguerrero, N.R., (1986). Effect of pH on the formation of deposit from milk on heated surfaces during ultra-high-temperature processing. Journal of Dairy Research 53(1), 75-87.

Skudder, P.J., Thomas, E.L., Pavey, J.A., Perkin, A.G., (1981). Effects of adding potassium iodate to milk before UHT treatment: I. Reduction in the amount of deposit on the heated surfaces. Journal of Dairy Research 48(1), 99-113.

Slattery, C.W., Evard, R., (1973). A model for the formation and structure of casein micelles from subunits of variable composition. Biochimica et Biophysica Acta (BBA) - Protein Structure 317(2), 529-538.

Smart, P.L.L., I. M. S, (1977). An evaluation of some fluorescent dyes for water tracing. Water Resources Research 13(1), 15-33.

Smits, P., Brouwershaven, J.H.V., (1980). Heat-induced association of β-lactoglobulin and casein micelles. Journal of Dairy Research 47(3), 313-325.

Snoeren, T., THM, S., VAN DER SPECK, C., (1977). The isolation of a heat-induced complex from UHTST milk.

Sreedhara, A., Flengsrud, R., Prakash, V., Krowarsch, D., Langsrud, T., Kaul, P., Devold, T.G., Vegarud, G.E., (2010). A comparison of effects of pH on the thermal stability and conformation of caprine and bovine lactoferrin. International Dairy Journal 20(7), 487-494.

Srichantra, A., Newstead, D.F., McCarthy, O.J., Paterson, A.H.J., (2006). Effect of Preheating on Fouling of a Pilot Scale UHT Sterilizing Plant by Recombined, Reconstituted and Fresh Whole Milks. Food and Bioproducts Processing 84(4), 279-285.

Srichantra, A., Newstead, D.F., Paterson, A.H.J., McCarthy, O.J., (2018). Effect of homogenisation and preheat treatment of fresh, recombined and reconstituted whole milk on subsequent fouling of UHT sterilisation plant. International Dairy Journal 87, 16-25.

Steventon, A.J., Gladden, L.F., Fryer, P.J., (1991). A precolation analysis of the concentration dependence of the gelation of whey protein concentrates. Journal of Texture Studies 22(2), 201-218.

Sundar, S., Rajagopal, M.C., Zhao, H., Kuntumalla, G., Meng, Y., Chang, H.C., Shao, C., Ferreira, P., Miljkovic, N., Sinha, S., Salapaka, S., (2020). Fouling modeling and prediction approach for heat exchangers using deep learning. International Journal of Heat and Mass Transfer 159, 120112.

Surroca, Y., Haverkamp, J., Heck, A.J.R., (2002). Towards the understanding of molecular mechanisms in the early stages of heat-induced aggregation of β-lactoglobulin AB. Journal of Chromatography A 970(1), 275-285.

Swaisgood, H.E., (2003). Chemistry of the Caseins, in: Fox, P.F., McSweeney, P.L.H. (Eds.), *Advanced Dairy Chemistry—1 Proteins: Part A / Part B*. Springer US, Boston, MA, pp. 139-201.

Tamime, A.Y., (2009). *Cleaning-in-place: dairy, food and beverage operations*. John Wiley & Sons.

Tang, S.-Z., Li, M.-J., Wang, F.-L., He, Y.-L., Tao, W.-Q., (2020). Fouling potential prediction and multi-objective optimization of a flue gas heat exchanger using neural networks and genetic algorithms. International Journal of Heat and Mass Transfer 152, 119488.

Thomar, P., (2016). Structuration of dense casein suspensions by phosphates in the presence of calcium : a study of their organization and rheological properties. Université du Maine.

Thorn, D.C., Ecroyd, H., Carver, J.A., Holt, C., (2015). Casein structures in the context of unfolded proteins. International Dairy Journal 46, 2-11.

Thorn, D.C., Ecroyd, H., Sunde, M., Poon, S., Carver, J.A., (2008). Amyloid Fibril Formation by Bovine Milk αs2-Casein Occurs under Physiological Conditions Yet Is Prevented by Its Natural Counterpart, αs1-Casein. Biochemistry 47(12), 3926-3936.

Thorn, D.C., Meehan, S., Sunde, M., Rekas, A., Gras, S.L., MacPhee, C.E., Dobson, C.M., Wilson, M.R., Carver, J.A., (2005). Amyloid Fibril Formation by Bovine Milk κ-Casein and Its Inhibition by the Molecular Chaperones αS- and β-Casein. Biochemistry 44(51), 17027-17036.

Tissier, J.P., (1984). A study of milk deposit on heat exchange surface during UHT treatment. Engineering and food, 49-58.

Tissier, J.P., Lalande, M., (1986). Experimental Device and Methods for Studying Milk Deposit Formation on Heat Exchange Surfaces. Biotechnology Progress 2(4), 218-229.

Tolkach, A., Kulozik, U., (2007). Reaction kinetic pathway of reversible and irreversible thermal denaturation of beta-lactoglobulin. Lait 87(4-5), 301-315.

Townend, R., Herskovits, T.T., Timasheff, S.N., Gorbunoff, M.J., (1969). The state of amino acid residues in β-lactoglobulin. Arch Biochem Biophys 129(2), 567-580.

Toyoda, I., Fryer, P., (1997). A computational model for reaction and mass transfer in fouling from whey protein solutions. In fouling mitigation of industrial heat-exchange equipment, Begell House, New York, 589-597.

Trejo, R., Dokland, T., Jurat-Fuentes, J., Harte, F., (2011). Cryo-transmission electron tomography of native casein micelles from bovine milk. Journal of Dairy Science 94(12), 5770-5775.

Treweek, T.M., Thorn, D.C., Price, W.E., Carver, J.A., (2011). The chaperone action of bovine milk αS1- and αS2-caseins and their associated form αS-casein. Arch Biochem Biophys 510(1), 42-52.

Truong, T., Anema, S., Kirkpatrick, K., Chen, H., (2002). The Use of a Heat Flux Sensor for In-Line Monitoring of Fouling of Non-Heated Surfaces. Food and Bioproducts Processing 80(4), 260-269.

Truong, T.H., Kirkpatrick, K., Anema, S.G., (2017). Role of β-lactoglobulin in the fouling of stainless steel surfaces by heated milk. International Dairy Journal 66, 18-26.

Tung, M.S., (1998). Calcium Phosphates: Structure, Composition, Solubility, and Stability, in: Amjad, Z. (Ed.), *Calcium Phosphates in Biological and Industrial Systems*. Springer US, Boston, MA, pp. 1-19.

Úbeda, M.A., Hussein, W.B., Hussein, M.A., Hinrichs, J., Becker, T.M., (2016). Acoustic sensing and signal processing techniques for monitoring milk fouling cleaning operations. Engineering in Life Sciences 16(1), 67-77.

Uhrínová, S., Uhrín, D., Denton, H., Smith, M., Sawyer, L., Barlow, P.N., (1998). Complete assignment of 1H, 13C and 15N chemical shifts for bovine β-lactoglobulin: Secondary structure and topology of the native state is retained in a partially unfolded form. Journal of Biomolecular NMR 12(1), 89-107.

Van Asselt, A., Vissers, M., Smit, F., De Jong, P., (2005). In-line control of fouling, *Heat Exchanger Fouling and Cleaning—Challenges and Opportunities, Engineering Conferences International Kloster Irsee.*

Van Dijk, H., Hersevoort, A., (1992). The properties of casein micelles. 5. The determination of heat-induced calcium phosphate precipitations in milk. Netherlands Milk and Dairy Journal (Netherlands).

van Kemenade, M.J.J.M., (1988). Influence of casein on precipitation of calcium phosphates. Rijksuniversiteit te Utrecht.

Vasbinder, A.J., de Kruif, C.G., (2003). Casein–whey protein interactions in heated milk: the influence of pH. International Dairy Journal 13(8), 669-677.

Veerman, C., Baptist, H., Sagis, L.M.C., van der Linden, E., (2003). A New Multistep Ca2+-Induced Cold Gelation Process for β-Lactoglobulin. J Agric Food Chem 51(13), 3880-3885.

Ven Murthy, M.R., Carrier-Malhotra, L., (1989). Progressive Unfolding of the Conformational States of Transfer RNA and Ribosomal 5S RNA by Methylene Blue Binding, in: Vijayalakshmi, M.A., Bertrand, O. (Eds.), *Protein-Dye Interactions: Developments and Applications*. Springer Netherlands, Dordrecht, pp. 316-330.

Verheul, M., Pedersen, J.S., Roefs, S., de Kruif, K.G., (1999). Association behavior of native beta-lactoglobulin. BIOPOLYMERS 49(1), 11-20.

Verheul, M., Roefs, S.P.F.M., de Kruif, K.G., (1998). Kinetics of Heat-Induced Aggregation of β-Lactoglobulin. J Agric Food Chem 46(3), 896-903.

Visser, J., Jeurnink, T.J.M., (1997). Fouling of heat exchangers in the dairy industry. Experimental Thermal & Fluid Science 14(4), 407-424.

Vreeman, H.J., (1979). The association of bovine SH-κ-casein at pH 7·0. Journal of Dairy Research 46(2), 271-276.

Walkling-Ribeiro, M., Rodríguez-González, O., Jayaram, S., Griffiths, M.W., (2011). Microbial inactivation and shelf life comparison of 'cold' hurdle processing with pulsed electric fields and microfiltration, and conventional thermal pasteurisation in skim milk. International Journal of Food Microbiology 144(3), 379-386.

Wallhäußer, E., Hussein, M.A., Becker, T., (2012). Detection methods of fouling in heat exchangers in the food industry. Food Control 27(1), 1-10.

Walstra, P., (1999). Casein sub-micelles: do they exist? International Dairy Journal 9(3), 189-192.

Wang, C.H., Damodaran, S., (1991). Thermal gelation of globular proteins: influence of protein conformation on gel strength. J Agric Food Chem 39(3), 433-438.

Watanabe, K., Klostermeyer, H., (1976). Heat-induced changes in sulphydryl and disulphide levels of β-lactoglobulin A and the formation of polymers. Journal of Dairy Research 43(3), 411-418.

Waugh, D.F., (1971). Formation and Structure of Casein Micelles, in: McKenzie, H.A. (Ed.), *Milk Proteins*. Academic Press, pp. 3-85.

Wijayanti, H.B., Bansal, N., Deeth, H.C., (2014). Stability of Whey Proteins during Thermal Processing: A Review. Comprehensive Reviews in Food Science and Food Safety 13(6), 1235-1251.

Wilke, C.R., Chang, P., (1955). Correlation of diffusion coefficients in diluted solutions. AIChE Journal 1(2), 264-270.

Williams, S.J., Chamarthy, P., Wereley, S.T., (2010). Comparison of Experiments and Simulation of Joule Heating in ac Electrokinetic Chips. Journal of Fluids Engineering 132(2).

Wilson, D.I., (2005). Challenges in Cleaning: Recent Developments and Future Prospects. Heat Transfer Engineering 26(1), 51-59.

Wolz, M., Kulozik, U., (2015). Thermal denaturation kinetics of whey proteins at high protein concentrations. International Dairy Journal 49, 95-101.

Xiong, Y.L., Dawson, K.A., Wan, L., (1993). Thermal Aggregation of β-Lactoglobulin: Effect of pH, Ionic Environment, and Thiol Reagent1. Journal of Dairy Science 76(1), 70-77.

Yang, W., Li, D., Chen, X.D., Mercadé-Prieto, R., (2018). Effect of calcium on the fouling of whey protein isolate on stainless steel using QCM-D. Chemical Engineering Science 177, 501-508.

Yong, Y.H., Foegeding, E.A., (2008). Effects of Caseins on Thermal Stability of Bovine β-Lactoglobulin. J Agric Food Chem 56(21), 10352-10358.

Yong, Y.H., Foegeding, E.A., (2010). Caseins: Utilizing Molecular Chaperone Properties to Control Protein Aggregation in Foods. J Agric Food Chem 58(2), 685-693.

Yoon, J., Lund, D., (1989). Effect of operating conditions, surface coatings and pretreatment on milk fouling in a plate heat exchanger, *Fouling and cleaning in food processing*. University of Munich Brussels, pp. 59-80.

Zhang, F., Xiao, J., Chen, X.D., (2015). Towards predictive modeling of crystallization fouling: A pseudo-dynamic approach. Food and Bioproducts Processing 93, 188-196.

Zhang, X., Fu, X., Zhang, H., Liu, C., Jiao, W., Chang, Z., (2005). Chaperone-like activity of β-casein. The International Journal of Biochemistry & Cell Biology 37(6), 1232-1240.

Zhu, M., Santamaria, F.L., Macchietto, S., (2020). A General Dynamic Model of a Complete Milk Pasteuriser Unit Subject to Fouling, in: Pierucci, S., Manenti, F., Bozzano, G.L., Manca, D. (Eds.), *Computer Aided Chemical Engineering*. Elsevier, pp. 247-252.

Zittle, C.A., Thompson, M.P., Custer, J.H., Cerbulis, J., (1962). κ-Casein—β-Lactoglobulin Interaction in Solution When Heated. Journal of Dairy Science 45(7), 807-810.

Zouaghi, S., Abdallah, M., André, C., Chihib, N.E., Bellayer, S., Delaplace, G., Celzard, A., Jimenez, M., (2018a). Graphite-based composites for whey protein fouling and bacterial adhesion management. International Dairy Journal 86, 69-75.

Zouaghi, S., Barry, M.E., Bellayer, S., Lyskawa, J., André, C., Delaplace, G., Grunlan, M.A., Jimenez, M., (2018b). Antifouling amphiphilic silicone coatings for dairy fouling mitigation on stainless steel. Biofouling 34(7), 769-783.

Zouaghi, S., Frémiot, J., André, C., Grunlan, M.A., Gruescu, C., Delaplace, G., Duquesne, S., Jimenez, M., (2019). Investigating the Effect of an Antifouling Surface Modification on the Environmental Impact of a Pasteurization Process: An LCA Study. ACS Sustainable Chemistry & Engineering 7(10), 9133-9142.

Zouaghi, S., Six, T., Bellayer, S., Coffinier, Y., Abdallah, M., Chihib, N.-E., André, C., Delaplace, G., Jimenez, M., (2018c). Atmospheric pressure plasma spraying of silane-based coatings targeting whey protein fouling and bacterial adhesion management. Applied Surface Science 455, 392-402.

Zouaghi, S., Six, T., Bellayer, S., Moradi, S., Hatzikiriakos, S.G., Dargent, T., Thomy, V., Coffinier, Y., André, C., Delaplace, G., Jimenez, M., (2017). Antifouling Biomimetic Liquid-Infused Stainless Steel: Application to Dairy Industrial Processing. ACS Applied Materials & Interfaces 9(31), 26565-26573.

Zouaghi, S., Six, T., Nuns, N., Simon, P., Bellayer, S., Moradi, S., Hatzikiriakos, S.G., André, C., Delaplace, G., Jimenez, M., (2018d). Influence of stainless steel surface properties on whey protein fouling under industrial processing conditions. Journal of Food Engineering 228, 38-49.

Zúñiga, R.N., Tolkach, A., Kulozik, U., Aguilera, J.M., (2010). Kinetics of Formation and Physicochemical Characterization of Thermally-Induced β-Lactoglobulin Aggregates. Journal of Food Science 75(5), E261-E268.

ANNEX

ANNEX I-published paper

Journal of Food Engineering 289 (2021) 110175

Contents lists available at ScienceDirect

Journal of Food Engineering

journal homepage: http://www.elsevier.com/locate/jfoodeng

Effect of casein/whey ratio on the thermal denaturation of whey proteins and subsequent fouling in a plate heat exchanger

Weiji Liu [a,b,e,*], Xiao Dong Chen [a,e], Romain Jeantet [c,e], Christophe André [d], Severine Bellayer [e], Guillaume Delaplace [b,e]

[a] School of Chemical and Environmental Engineering, Soochow University, Suzhou, Jiangsu, 215123, PR China
[b] Univ. Lille, CNRS, INRAE, Centrale Lille, UMR 8207 - UMET - Unité Matériaux et Transformations, F-59000, Lille, France
[c] STLO, INRAE, Institut Agro, 35042, Rennes, France
[d] HEI (Ecole des Hautes Etudes d'Ingénieur), Département Chimie, Textiles et Process Innovants, 13, rue de Toul, 59046, Lille, Cedex, France
[e] International Joint Laboratory (INRAE Villeneuve d'Ascq-Soochow University-Agrocampus Rennes), School of Chemical and Environmental Engineering, College of Chemistry, Chemical Engineering and Materials Science, Soochow University, Suzhou, Jiangsu, 215123, PR China

ARTICLE INFO

Keywords:
Casein/whey ratio
Whey protein fouling
Plate heat exchanger
Denaturation kinetic constant

ABSTRACT

Dairy fouling is a ubiquitous problem in food processing, however, the fouling mechanism is not fully understood and investigations arose mainly from experiments with model systems that contained only whey proteins, typically reconstituted from whey protein isolate powder (WPI). The effect of casein on fouling has been rarely considered despite it is the major component of milk proteins. To fill this gap, whey protein-based model fluids containing different casein concentrations and fixed content of added calcium were prepared, leading to various Casein/WPI mass ratios. The effect of Casein/WPI on β-lactoglobulin (BLG) denaturation at molecular level and subsequent fouling behavior in the pilot-scale plate heat exchanger during pasteurization treatment was investigated. It was shown that Casein/WPI significantly affects the fouling behavior: at low Casein/WPI, fouling mass dropped dramatically until a minimum value was reached located at Casein/WPI of 0.2. While at higher Casein/WPI, fouling mass increased with elevated Casein/WPI. Element mapping of the fouling layer also reveals that different structures and fouling mechanisms occur depending on Casein/WPI ratio. Finally, it was established that contrary to WPI solutions, BLG thermal denaturation is poorly correlated to decrease/extent of fouling for casein protein-based solutions showing that the presence of casein deeply modifies mineral and protein interactions and fouling build-up.

1. Introduction

Milk fouling upon plate heat exchanger (PHE) is a ubiquitous problem in the manufacturing processes of dairy factories as in the case of pasteurization, giving negative impacts on operating costs and product quality. It is responsible for several industrial issues, such as reduction of heat transfer efficiency (Mahdi et al., 2009), pressure-drop (Grijspeerdt et al., 2004), and also increasing risk of microbial contamination (Fryer et al., 2006). Another serious problem associated with fouling is the cleaning process for fouled surfaces, where environmentally offensive chemicals are usually employed.

Given these negative impacts of fouling in PHE, tremendous efforts have been paid to explore the mechanism lying behind. The overview of the fouling mechanism has been systematically addressed as reviewed by Sadeghinezhad et al. (2015) and Bansal and Chen (2006). Two dominant mechanisms are recognized for milk-based fouling named i) heat-induced denaturation of protein and ii) mineral precipitations. β-lactoglobulin (BLG) is the major protein responsible for the protein fouling due to its exposed thiol group after thermal denaturation and thus initializes the protein interaction through SH/S–S interchange reactions (Shimada and Cheftel, 2002).

Despite the comprehensive mechanism discovered in the literature, the role of casein proteins on fouling is not yet fully understood, the main reason being that the fouling phenomenon was most studied for whey protein solutions which are casein free. Unfortunately, the presence of individual caseins or micellar casein complicates seriously the mechanisms concerning both the protein denaturation and mineral precipitations. In the aspect of protein denaturation, the most frequently

* Corresponding author. School of Chemical and Environmental Engineering, Soochow University, Suzhou, Jiangsu, 215123, PR China.
E-mail address: liu.weiji@inrae.fr (W. Liu).

https://doi.org/10.1016/j.jfoodeng.2020.110175
Received 10 December 2019; Received in revised form 28 May 2020; Accepted 29 May 2020
Available online 2 June 2020

mentioned in the literature is the interaction between κ-casein and denatured BLG. It was proposed that denatured BLG can either interact with κ-casein on the surface of casein micelle or in the serum phase after being dissociated from the micellar structure (Wijayanti et al., 2014). Besides that, casein has been reported to have chaperone functions on the thermal denaturation of whey proteins. The BLG-initiated polymerization is disrupted due to the association between casein and denatured whey proteins probably through hydrophobic interactions (Bhattacharyya and Das, 1999; Morgan et al., 2005). Additionally, casein can affect the mineral balances in the milk, particularly, transfer the ionic calcium into micellar calcium phosphate upon heating (On-Nom et al., 2010; Udabage et al., 2000). Nevertheless, the exact role of micellar casein on fouling is still far away from clear.

A study of how casein affects the thermal denaturation kinetics of whey proteins could lead to a better understanding of the relationship between casein and whey protein under heat treatment. Indeed, there are numerous reports of kinetics studies on the thermal denaturation of major whey proteins (Anema and McKenna, 1996; Dannenberg and Kessler, 1988; Hillier and Lyster, 1979; Oldfield et al., 1998; Park and Lund, 1984; Sawyer et al., 1971), while few of them focused on the effect of casein. And if the effect of casein on fouling is desired, different proportions of casein/whey should be concerned (Kessler and Beyer, 1991; Patocka et al., 1993). In this paper, reconstituted whey protein isolate (WPI) solutions at 0.5 wt% with various casein protein concentrations to have different Casein/WPI proportions were used as model fluids. An appropriate amount of calcium chloride was also added in order to provide a suitable level of calcium for fouling to occur. The free Ca^{2+} concentrations used in this study are close to that observed in milk at ~80–170 mg/L (Lewis, 2011). The fouling experiments were carried out in a pilot-scale PHE for a given thermal profile. The mass of fouling deposits and the pressure-drop evolution in the PHE was recorded; the morphology and chemical compositions of the fouling layer were also investigated using Electron Probe Micro Analyzer (EPMA) and gel-electrophoresis, respectively. In addition, the effect of casein on molecular scale was also evaluated through the thermal denaturation kinetics of BLG using a one-step reaction model.

2. Materials and methods

2.1. Model fouling solutions

The fouling solutions used in this study were reconstituted from PRODIET 90 S WPI powder and PRODIET 87 B casein powder supplied by Ingredia (France). According to the manufacturer, WPI powder consists of 85.5 wt% total protein, 5.5 wt% moisture, 0.2 wt% calcium and phosphorous. The casein powder contains 83 wt% total protein, 5 wt % moisture, 2.6 wt% calcium and 1.3 wt% phosphorous. For all experimental solutions, the whey protein concentration was fixed at 0.5 wt% to simulate the whey protein content in raw milk (Farrell et al., 2004). In order to investigate the effect of casein on the fouling behavior, different amount of casein powder was added to achieved elevated Casein/WPI mass ratio from 0 to 0.8. Preliminary experiments showed no visible fouling when using WPI alone or mixtures of WPI and casein (Casein/-WPI mass ratio up to 1). Therefore, it was decided to add 42 ppm of free calcium in the form of calcium chloride (anhydrous, 96%, Acros Organics, USA) in the fouling solutions. $CaCl_2$ has been widely used in the literature to introduce calcium ios into dairy systems, and is authorized sicnce ages to be added to milk during cheece making (Price, 1927). The amount of $CaCl_2$ was determined to achieve a suitable total fouling mass in the PHE. The total amount of calcium is similar to those used for WPI fouling experiments (Guérin et al., 2007; Khaldi et al., 2015, 2018).

2.2. Pilot-scale fouling runs

Fouling experiments were performed on the pilot-scale set-up as shown in Fig. 1. The system contained two PHEs (Model V7, Alfa-Laval Vicard, France); they were both configured using 21 plates thus proving 10 channels for both hot water and fouling fluid. The dimension of the plate is 150 mm × 495 mm × 0.8 mm with a corrugated surface (35° corrugation angle with a 3.9 mm flow gap), giving an effective contact area of 0.0743 m^2. The first PHE is named pre-heating PHE as it allows to increase the temperature of fouling solutions from 50 to 65 °C without inducing denaturation of BLG and fouling (Boye and Alli, 2000). The main fouling observations were focused on the second PHE, called heating PHE, which continues elevating the solutions up to 85 °C at its outlet; this temperature was kept constant by controlling the inlet of hot water, thereby a constant temperature profile along the PHE was achieved. A quasi-linear temperature profile with PHE was obtained in a counter-current configuration of fouling fluid and hot water with the same flow rate at 300 $L{\cdot}h^{-1}$ (See Supplementary Information Fig. S1), the bulk temperature profile was simulated numerically using Sphere software (Fig. S2) which was previously elaborated and validated by INRA's group as mentioned in Blanpain-Avet et al. (2016) and Petit et al. (2013). This temperature profile resembles an HTST (High Temperature Short Time) pasteurization process with slightly higher temperature and duration. The temperature and flow rate measurements were performed using platinum resistance probes (Pt100, Fer Constantan) and electromagnetic flowmeters (Krohene IFM, Germany), respectively. All sensors were calibrated before the experiments were conducted; the accuracy of temperature measurements was expected to be better than ±0.2 °C and relative errors for the flow rate measurements were considered to be less than ±1%. All measurements were collected using a data acquisition system (Agilent Technologies 34970A, USA).

Prior to fouling runs, the fouling solutions were stirred in a 750 L tank; the temperature of the solutions was increased to 50 °C and maintained for at least 1 h to ensure full dissolution of protein powders. Before pumping fouling fluid, reverse osmosis water was firstly used to reach a thermal equilibrium of the system at the desired process temperature. After that, 600 L of fouling solution was processed in each pilot-scale experiment by switching from water to fouling fluid once-through, without recycling. This volume corresponds to a total running time of 2 h, during which the fouling solutions were sampled at both inlet and outlet of the heating PHE three times; these solutions along with the solution in the launching tank (*i.e.* fouling solution at 50 °C) were used for subsequent determination including pH, free calcium content, total calcium content, and BLG denaturation. To quickly quench the denaturation of proteins in sample solutions, they were mixed immediately with cold water (<1 °C) in a centrifugation tube. The dilution effect was considered in the calculation of calcium and protein concentration. When the fouling experiments were finished, water was used again to replace fouling solutions in the channels; after that, the PHE was dismantled and placed under ambient conditions overnight before putting in an air-oven at 50 °C for at least 3 h to dry the plates. The dry mass of the fouling deposit on each plate was calculated by the difference between bare and fouled plates. Fouling mass in each channel was the addition of two deposit mass values obtained for the plates constituting the pass walls. The total fouling mass for each run is the sum of the mass collected from all the channels.

Finally, these plates were installed again in the PHE system for the subsequent cleaning procedure by circulating 2 wt% sodium hydroxide (99%, Solvay, Belgium) and 2 wt% nitric acid (54%, Thermo Fisher Scientific) with a similar heating process to the fouling experiments. The duration for each step lasted at least 30 min, after that, the system was rinsed with osmosis water for the next heat treatment experiment. The cleanliness of the plates was check visually to ensure efficient cleaning.

The amount of fouling was also monitored by the pressure-drop within PHE and the calculation of thermal resistance (*Rf*). Assuming uniform fouling layer, the average thermal resistance *Rf* can be described as:

$$Rf = \frac{1}{Ut} - \frac{1}{U0} \quad (1)$$

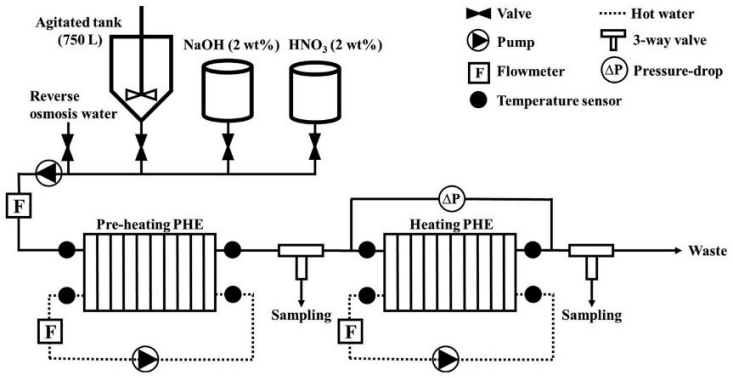

Fig. 1. Schematic diagram of pilot-scale fouling experimental set-up. Two plate heat exchangers (PHEs) were coupled and named pre-heating PHE and hearting PHE, respectively.

where *U*0 and *Ut* are the overall heat transfer coefficients before the occurrence of fouling and at time t when fouling is formed, respectively.

The heat transfer coefficient was calculated from the energy balance between the heating fluid (hot water) and processed fluid (model solution):

$$mhCph(Th,i - Th,o) = US\Delta TLMTD \quad (2)$$

where *mh* and *Cph* represents the mass flow rate ($kg{\cdot}s^{-1}$) and the specific heat for the hot water ($J{\cdot}kg^{-1}{\cdot}K^{-1}$), respectively. The temperature dependence of *Cph* was used as reported by Petit et al. (2013). *Th, i* and *Th, o* refers to the temperature of hot water at the inlet and outlet of PHE (K). *S* is the heat transfer area (m^2), and $\Delta TLMTD$ is the logarithmic mean temperature difference (K).

2.3. Calcium content measurement

The ionic or free calcium $[Ca]_f$ of sample solutions was measured using a calcium ion-selective electrode (Ca-ISE, PS-3518, PASCO, USA). The calculation of the free calcium level was based on the potential difference between the sample solution and a constant reference through a gelled organophilic membrane. The potential values were recorded in the software from the manufacturer (PASCO capstone) through a Bluetooth module coupled with the electrode. A high and constant ionic strength environment was needed for reliable potential measurements, hence 3.85% (v/v) of the ionic strength adjuster (4M KCl) was added for all samples and standard solutions. The probe was calibrated with five Ca^{2+} standards ranging from 5 ppm to 100 ppm. The calibration curve was derived from the logarithm of Ca^{2+} concentration and the potential values according to the Nernst equation. To avoid any temperature effect, all samples and standard solutions were allowed to equilibria in a 25 °C water bath for at least 1 h before measurements. The total calcium content $[Ca]_t$ was determined by atomic absorption spectrometry using a Spectro AA 55B apparatus (Varian, Palo Alto, USA) as performed in Khaldi et al. (2018).

2.4. High-performance liquid chromatography

The concentration of soluble BLG in the samples was evaluated using a high-performance liquid chromatography (HPLC) system (Alliance HPLC System, Waters, USA). The chromatographic system consists of a separation module integrated solvent and sample management functions (e2695 Separation Module), a column heater/cooler, a reverse-phase column (XBridge Protein BEH C4, 300 Å, 3.5 μm, Waters) associated with a guard column (Sentry Guard Cartridge, Waters), a UV–Vis spectrophotometer (2998 PDA Detector) and acquisition software (Empower Software).

The pH of the protein samples was adjusted to 4.6 following a centrifugation process (9056×*g* for 30 min at 4 °C) to remove aggregated BLG and casein proteins if any. The supernatants were filtered through a 0.2 μm cellulose filter (Minisart RC, Sartorius, Germany) before injecting 20 μL in the HPLC system. Two mobile phases were used: solution A consists of 0.1% (v/v) trifluoroacetic acid (TFA, 99%, Acros Organics) in MilliQ water while solution B contains 0.1% (v/v) TFA, 80% acetonitrile (HPLC grade, Thermo Fisher Scientific) and 20% MilliQ. The separation was performed at a flow rate of 1 mL/min, 40 °C and a detection wavelength of 215 nm with gradient elution. Calibration curves were done by using pure BLG standards (0.25–3 g/L). To maintain the performance of the column, pure acetonitrile was eluted at 1 mL/min for 1 h after the experiment finished.

2.5. Characterization of the fouling deposit

To provide a deeper insight into the fouling, the determination of element and protein composition was carried out using an Electron Probe Micro Analyzer (EPMA) and Sodium Dodecyl Sulfate Polyacrylamide Gel Electrophoresis (SDS-PAGE), respectively. The characterizations were performed for the fouling runs at four different Casein/WPI mass ratios at 0, 0.05, 0.2 and 0.8, and for each experiment, the deposits formed at two different plates were studied for comparison purposes (*i.e.* P_{14} and P_{21}, Fig. S1).

For EPMA analysis, the samples were directly cut from the dried plate after the fouling experiments, the analyzed deposits were chosen on the flat surface of the plate. The corresponding bulk temperatures are 78.9 and 84.6 °C for samples collected from P_{14} and P_{21}, respectively (Fig. S2). The cut coupons were firstly embedded in epoxy resin; after solidification, the surface was polished using an ESC 200 GT polishing machine (ESCIL, Chassieu, France) with different grades of SiC sheets (up to 0.25 μm) and carbon coated with a Bal-Tec SCD005 sputter coater. These processes are necessary to ensure a very flat surface for EPMA measurement. The samples were placed in the vacuum and excited by an electron beam, the backscattered electron imaging and X-ray mapping were carried out using a Cameca SX-100 EPMA (CAMECA, Gennevilliers, France) at 15 kV, 15 nA, and 15 kV, 40 nA, respectively. For element determination, a PET crystal was used to detect Kα X-rays of sulfur, calcium, and phosphate, and a LiF crystal to detect iron Kα X-rays.

The SDS-PAGE was performed in a SE 600 Series vertical Slab Gel Unit (Hoefer Scientific instrument, San Francisco, US). The resolving gel contained 15% (w/v) acrylamide and 0.2% (w/v) SDS in 1.5 M Tris-HCl

buffer at pH 8.8, and the stacking gel included 4% (w/v) acrylamide and 0.1% (w/v) SDS in 0.5 M Tris-HCl buffer at pH 6.8. The deposit samples were scraped from the dried plate after the fouling runs and dried again in a 105 °C oven for over 24 h. The dry powders were ground and dissolved in the sampling buffer (0.5 M Tris-HCl buffer, pH 6.8, containing 0.2% (w/v) SDS, 0.01% (v/v) bromophenol blue and 0.05% (v/v) β-mercaptoethanol) with a final concentration at 0.5 wt%. Pure proteins including α/β/κ-casein, αLa, BSA and BLG were also dispersed in the sampling buffer for a comparison purpose. These solutions were heated in a boiling water bath for 5 min; they were cooled to room temperature and injected into the gel along with a protein molecular weight ladder (Precision Plus Protein Unstained Standards, Bio-Rad Laboratories, UK). The gels were run under a constant current at 40 mA for immigration in the stacking gel and 60 mA for resolving gel. After electrophoresis, a fixation process was applied by immersing the gel in the solution with 10% (v/v) acetic acid (99.5%, Acros Organics) and 30% (v/v) ethanol. After that, the gel was stained for at least 2 h using 0.02% (m/v) Brilliant Blue R in 10% (v/v) acetic acid and 25% (v/v) isopropanol. After coloration, the gel was destained using a 10% (v/v) acetic acid solution until a clear background was achieved.

2.6. Thermal denaturation experiments

The model solutions for denaturation experiments were selected according to the pilot-scale fouling results: 0.5 wt% WPI, 0.5 wt% WPI with 0.25 wt% casein, 0.5 wt% WPI with additional 42 ppm free calcium at different Casein/WPI mass ratio of 0, 0.05, 0.2 and 0.8, respectively. The compositions of these solutions were summarized in Table 1. The experimental protocol was similar as reported previously by Petit et al. (2011). Briefly, all model solutions were reconstituted using a similar protocol as applied in the fouling experiments (*i.e.* 50 °C for 3 h), after that 2 mL aliquots were removed into plastic tubes (Eppendorf, Germany) prior to heat treatment. The heating process included three stages by using three water baths: the first water bath was set at 65 °C to pre-heat the solutions below the critical temperature for BLG denaturation (Paulsson and Dejmek, 1990), and the second bath was set at 10 °C higher than the desired holding temperature (T_d+10 °C) to quickly heat up the solution to reach T_d, at which it corresponded to time zero for kinetic calculation. After that, the samples were maintained at T_d by submitting into the third bath (temperature set at T_d+1 °C). The sample temperature was monitored by following the temperature evolution of a reference vial filled with the MilliQ, in which a thermocouple was inserted. The holding temperature T_d varied from 70 to 90 °C was maintained for a proper period of time to induce significant BLG denaturation. At different times (including solution reach 65 °C in the first bath), the solutions were removed and cooled in melting ice to quench the BLG denaturation.

2.7. BLG denaturation using one-step reaction model

The thermal denaturation of BLG is widely accepted in a multi-stages mechanism (Tolkach and Kulozik, 2007). Despite this intricate mechanism, the denaturation pathway of BLG is generally simplified due to the lack of ability to distinguish different BLG monomers (*e.g.* native and unfolded), for example when using polarimetric analysis (Ven Murthy and Carrier-Malhotra, 1989), gel permeation chromatography (Kehoe et al., 2011), immunodiffusion (Miyawaki et al., 2003), electrophoresis (Oldfield et al., 2005), or reverse-phase high performance liquid chromatography (RP-HPLC) (Khaldi et al., 2015; Petit et al., 2011). In the HPLC system, the determined BLG consists of both native and unfolded BLG molecules, which is also called soluble BLG. Hence, an overall one-step model was established by considering the transformation of soluble species (S) into aggregated ones (A). The reaction rate of this chemical reaction can be described as:

$$-\frac{dC_s}{dt} = k_f C_s^n \tag{3}$$

where *Cs* refers to the concentration of soluble BLG species as determined in the HPLC system, and k_f is the denaturation rate constant. The unit of k_f depends on the reaction order n (*i.e.* $g^{1-n}\cdot L^{n-1}\cdot s^{-1}$). The experimental data were fitted to equation (1) using Matlab to calculate the denaturation rate constant k_f with various reaction order from 1 to 3. The reaction order was determined according to the RSS values (Residual sum of squares) obtained by fitting equation (1) to the experimental data (Fig. S3), where the most suitable values were found to be 2. This value is consistent with those found for BLG denaturation in skim milk (Hillier and Lyster, 1979; Lyster, 1970; Manji and Kakuda, 1986) or simulated milk ultrafiltrate (Park and Lund, 1984).

2.8. Temperature dependence of k_f

The relationship between k_f and the heating temperature is deduced by the Arrhenius equation:

$$\ln(kn) = \ln(k0) - \frac{Ea}{RT} \tag{4}$$

where k0 is the denaturation frequency factor ($g^{1-n}\cdot L^{n-1}\cdot s^{-1}$), Ea is the activation energy ($J\cdot mol^{-1}$), R is the universal gas constant ($J\cdot mol^{-1}\cdot K^{-1}$), and T is the bulk liquid temperature (K).

Fig. 2 presents an example of Arrhenius plot obtained from a solution containing 0.5 wt% WPI with the addition of 42 ppm Ca^{2+}, where the logarithm of k_f is plotted against the inverse temperature. A break of the slope appears around a critical temperature (T_c, *i.e.* 82 °C in this case) as previously observed and interpreted by Tolkach and Kulozik (2007) is unexpected for a one-step reaction as described from equation (2), hence it is generally deduced with a two-step reaction mechanism:

$$N \rightarrow U \rightarrow A \tag{5}$$

where the native BLG molecule (N) unfolds (U) prior to forming aggregates (A). At temperatures lower than the critical temperature T_c, the unfolding reaction rate is considered to be lower than the aggregation while when the temperature is higher than T_c, the unfolding rate is faster. Consequently, linear regressions of data at these two regions permit us to determine the kinetic parameters, including k_0 and Ea, for both unfolding and aggregation steps.

Table 1
Composition of model solutions for thermal denaturation experiments.

Solutions	[WPI] (wt%)	[Casein] (wt%)	[Casein]/[WPI]	Added Ca^{2+} (ppm)	$[Ca]_f$[a] (ppm)	$[Ca]_t$[b] (ppm)
Casein/WPI = 0	0.5	0	0	0	14.7	22.3
Casein/WPI = 0.5	0.5	0.25	0.5	0	58.1	91.0
Casein/WPI = 0&Ca	0.5	0	0	42	53.1	64.7
Casein/WPI = 0.05&Ca	0.5	0.025	0.05	42	61.2	74.3
Casein/WPI = 0.2&Ca	0.5	0.1	0.2	42	67.9	90.9
Casein/WPI = 0.8&Ca	0.5	0.4	0.8	42	96.2	169.4

[a] Free calcium concentration determined using Ca-ISE.
[b] total calcium concentration obtained from AAS.

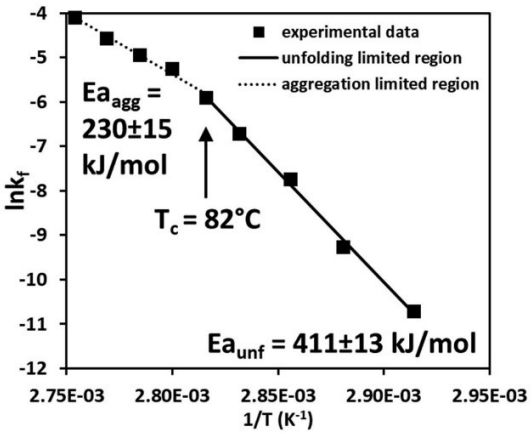

Fig. 2. Arrhenius plot of 0.5 wt% WPI solutions with the addition of 42 ppm Ca^{2+}. The solution contains 53 ppm Ca^{2+} with 64.7 ppm total Ca. The denaturation reaction rate k_f was obtained by solving equation (1) with a reaction order of 2.

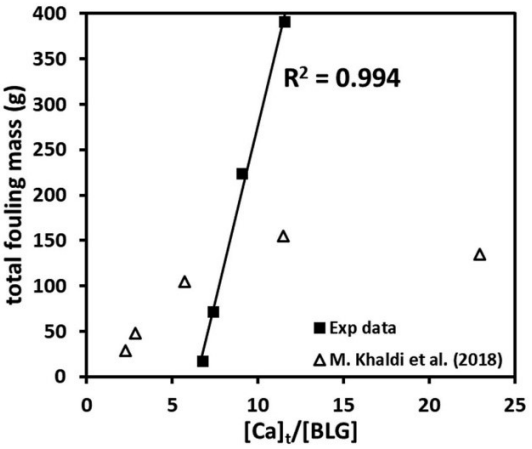

Fig. 3. Effect of $[Ca]_t$/BLG ratio on the total dried fouling mass of 0.5 wt% WPI. The symbols in triangles refer to the data reported in Khaldi, Croguennec, André, Ronse, Jimenez, Bellayer, Blanpain-Avet, Bouvier, Six, Bornaz, Jeantet and Dclaplacc *(18)*. Solid line presents linear regression with a value of R^2 at 0.994.

3. Results and discussion

3.1. The essential role of Ca^{2+} on fouling

It is important to bear in mind that introducing casein powder can also bring additional minerals to the system, in particular, calcium on ionic and colloidal forms. It was decided to first investigate the effect of Ca^{2+} on the mass of whey protein fouling deposits formed inside PHE. Table 2 summarizes the calcium compositions of nine different fouling fluids and their corresponding fouling results, including BLG concentrations at the inlet and outlet of PHE, BLG denaturation level within PHE, and total fouling mass.

The solution containing whey proteins alone was incapable to induce detectable fouling deposits under our operating conditions due to its minor content of calcium (22 ppm of total calcium with ~15 ppm ionic calcium). However, if Ca^{2+} was added to increase the level of free calcium (in the form of $CaCl_2$), fouling deposits were obtained. As shown in Fig. 3, the total amount of dried fouling deposits increase at elevated Ca/BLG ratio in a linear pattern ($R^2 = 0.994$). This effect of ionic calcium on fouling mass has been proved previously by Guérin et al. (2007), Khaldi et al. (2015) and Khaldi et al. (2018) for other aqueous solutions reconstituted from different WPI powders and heat-treated with similar thermal schedule. For example, Khaldi et al. (2018) have investigated the effect of Ca/BLG on whey protein fouling and pointed out that Ca/BLG ratio alters the structure of the fouling layer, and observed more surprisingly, that for the range of Ca/BLG ratios investigated (2.3–22.9), the fouling mass is dependent on this ratio and not driven by the protein concentration as commonly admitted. Their data are also presented in the figure for comparison while a plateau is reached in their case, which might due to the lower protein concentration they used at higher Ca/BLG ratio. Another significant impact of Ca/BLG on fouling behavior can be found on the BLG denaturation level within PHE. For example, the BLG denaturation level is only 7.7% without additional Ca^{2+}, but the values increase up to 44.5% for the case where 390.8 g of fouling mass was obtained (close to the operating limitation). One might notice that the increased extent of BLG denaturation level is relatively lower than the increased fouling mass evolution at higher Ca/BLG ratio, suggesting that calcium could be a foulant intermediate facilitating the fouling growth and not only involved in the extent of protein denaturation.

Knowing the effect of Ca^{2+} on fouling, an appropriate amount of casein was added instead of $CaCl_2$ attempting to achieve a similar Ca^{2+} level (Fluid#6, #7 compared to #4 and #5). Surprisingly, despite the high concentration of ionic calcium or even much more total calcium

Table 2
Calcium content of nine different fouling fluids and their corresponding fouling results. For each fouling experiment, the BLG concentration at the inlet and outlet of PHE are also shown. Errors represent standard deviation (SD).

Fluid#	Casein/WPI	Added Ca^{2+} (ppm)	$[Ca]_f$[a] (ppm)	$[Ca]_t$[a] (ppm)	$[BLG]_{inlet}$[b] (g/L)	$[BLG]_{outlet}$[c] (g/L)	BLG denaturation level[d]	Total fouling mass (g)
#1	0	0	14.8 ± 0.6	22.3 ± 1.2	3.08 ± 0.04	2.84 ± 0.05	7.7%	N/A[e]
#2	0	25	38.7 ± 0.7	48.4 ± 1.9	3.30 ± 0.02	2.40 ± 0.09	27.2%	17.1
#3	0	35	37.5 ± 1.6	59.4 ± 1.8	3.55 ± 0.15	2.1 ± 0.4	40.8%	72.1
#4	0	42	53.0 ± 1.9	64.7 ± 2.6	3.28 ± 0.06	1.87 ± 0.03	43.1%	223.9
#5	0	56	55 ± 3	79 ± 4	3.3 ± 0.2	1.8 ± 0.3	44.5%	390.8
#6	0.5	0	58 ± 3	91 ± 10	3.25 ± 0.09	3.08 ± 0.03	5.5%	N/A
#7	0.5	0	56 ± 4	90 ± 4	3.23 ± 0.03	3.07 ± 0.01	5.0%	N/A
#8	1	0	78 ± 6	213 ± 6	3.09 ± 0.06	2.70 ± 0.04	12.7%	N/A
#9	0.5	42	86 ± 4	141 ± 9	3.28 ± 0.12	2.09 ± 0.03	36.3%	133.2

[a] Average values of fouling fluids obtained at both the inlet and outlet of PHE at three different running time and one from the launching tank.
[b] Average values of fouling fluids obtained at the inlet of PHE at three different running time and one from the launching tank.
[c] Average values of fouling fluids obtained at the outlet of PHE at three different running time.
[d] BLG denaturation level = 1-$[BLG]_{outlet}/[BLG]_{intlet}$.
[e] N/A: the fouling mass is undetectable.

introduced by casein, no detectable fouling was obtained for fouling solutions without adding $CaCl_2$ (even up to Casein/WPI at 1). Besides that, a low BLG denaturation level was also observed in these cases, suggesting only few BLG molecules denatured during the thermal treatment within PHE. These results might due to the capacity of casein to reduce the ionic calcium at higher temperatures (Broyard and Gaucheron, 2015; Dalgleish and Corredig, 2012; On-Nom et al., 2010). Hence, even though the solutions contained high level of Ca^{2+} (measured at 25 °C), the amount of Ca^{2+} could be reduced to the level that might not be sufficient enough to induce significant denaturation of BLG and subsequent fouling. The results of Fluid#9 confirm this idea by adding 42 ppm Ca^{2+} into fouling solution containing 0.5 wt% WPI and 0.25 wt% casein (*i.e.* Fluid#6 and #7). This solution induced 133.2 g of dried fouling deposit with 36.3% of denatured BLG inside PHE.

3.2. The effect of casein on fouling deposit mass

As shown in the last section, additional Ca^{2+} is required to observe significant fouling. Consequently, in order to investigate the effect of casein on the fouling mass, it was decided to add a constant amount of Ca^{2+} (*i.e.* 42 ppm) for all the fouling solutions containing casein. The calcium content of twelve fouling fluids composed of elevated casein concentration with supplemented 42 ppm Ca^{2+} and their fouling results are displayed in Table 3.

A clear view of how casein affects the fouling can be seen in Fig. 4(a): at Casein/WPI lower than 0.2, fouling mass drop dramatically as Casein/WPI increases, leading to a minimum mass of 42.3 g and that is almost 80% reduction compared to that without casein. Exceeding Casein/WPI of 0.2, the fouling mass increases gradually as Casein/WPI goes higher. More detailed information about fouling mass in each PHE pass is presented in Fig. 4(b). In general, fouling mass increases along the PHE with maximum values at the last pass. Similar fouling starting points were found to be located between 4th and 5th pass, where the temperature ranges from 71.6 to 73.7 °C. These values are in accordance with the denaturation temperature of BLG at 72 °C (Boye and Alli, 2000). One exception can be observed at Casein/WPI of 0.2 (Fluid #7) where apparent fouling (>1 g) can only be found at the 7th pass with an average temperature at 79 °C. The surface coverage of fouling deposit inside PHE can be calculated using the area between the 4th and 10th pass of PHE as shown in Fig. S4. Without adding casein, the fouling mass coverage is ~215 g/m^2, corresponding to a mean fouling rate at 1.8 g/(m^2·min). This fouling rate is comparable to the other large scale fouling experiments with similar PHE configurations using 1 wt% WPC (whey protein concentrate) fouling fluid at a calcium concentration of ~70 mg/L (Khaldi et al., 2015). Surprisingly, the minimum fouling rate observed at Casein/WPI of 0.2 is close to that obtained for milk fouling in pasteurization studies, *e.g.* between 150 and 250 mg/(m^2·min) (Barish and Goddard, 2013; Choi et al., 2013).

Pressure-drop and thermal resistance (*Rf*) are usually employed to monitor fouling within PHE systems. On one hand, fouling causes the hydraulic diameter to decrease during operating, arising the pressure-drop over time until the system collapses. On the other hand, due to the low heat conductivity of the deposits, the additional fouling layer hinders the heat transfer between the hot water and the processing fluid. Fig. 5(a) and (b) show the pressure-drop and thermal resistance (*Rf*) evolutions of fouling runs processed at various Casein/WPI ratios, respectively. The pressure-drop changes little at the first operating hour for all solutions and increase dramatically thereafter. While for *Rf*, the values keep increasing as fouling growing during the whole process. Similar trend can be observed for the maximum values of pressure-drop and *Rf* (*i.e.* values obtained at the end of fouling run), which both of them decrease as Casein/WPI increases, reaching minimum values at Casein/WPI of 0.2. This is consistent with the fouling mass behavior. Worthy noticing is that, at Casein/WPI≥0.2, the extent of increased *Rf* resembles that of total fouling mass, while the increased pressure-drop is less significant. This is confirmed by plotting normalized values of fouling mass and maximum values of pressure-drop and *Rf* against Casein/WPI as shown in Fig. 6. At Casein/WPI>0.2, high fouling mass can be obtained but induce much less pressure-drop (six times lower). This could be attributed to a different fouling structure formed at Casein/WPI>0.2.

It has long been recognized that caseins have chaperone-like functions on the thermal denaturation or aggregation of whey proteins (Wijayanti et al., 2014; Yong and Foegeding, 2010). For instance, κ-casein is the most frequently mentioned one in the literature that can interact with denatured BLG molecule through SH/SS interchange reaction and also hydrophobic interactions (Haque and Kinsella, 2009; Jang and Swaisgood, 1990). These interactions were proposed to terminate the SH/SS exchanges between denatured BLG and thus act as a dead-end reaction for the propagation of BLG aggregation (Donato and Guyomarc'h, 2009). On the other hand, the chaperone behavior of α and β-casein has also been revealed to suppress the thermal denaturation of whey proteins or other unrelated proteins, such as insulin, alcohol dehydrogenase probably through hydrophobic interactions (Bhattacharyya and Das, 1999; Morgan et al., 2005). Consequently, we can expect that the fouling mass should be positively correlated to the BLG denaturation level. Nevertheless, our results do not really support the hypothesis and seem to indicate that BLG denaturation level is not a pertinent indicator to rank fouling behavior for casein-based protein solutions (Fig. S5). Indeed, significant different fouling mass was

Table 3
Calcium content of twelve fouling fluids and their fouling results. For each fouling experiment, the BLG concentration at the inlet and outlet of PHE are also shown. Errors represent standard deviation (SD). Note all solutions contain 42 ppm additional Ca^{2+}.

Fluid#[a]	Casein/WPI	$[Ca]_f$[b] (ppm)	$[Ca]_i$[b] (ppm)	$[BLG]_{inlet}$[c] (g/L)	$[BLG]_{outlet}$[d] (g/L)	BLG denaturation level[e]	Total fouling mass (g)
#1	0	53.0 ± 1.9	64.7 ± 2.6	3.28 ± 0.06	1.87 ± 0.03	43.1%	223.9
#2	0.05	53 ± 5	74 ± 2	3.37 ± 0.08	1.90 ± 0.12	43.4%	123.6
#3	0.05	56 ± 5	71 ± 1.1	3.36 ± 0.07	1.83 ± 0.06	45.6%	112.4
#4	0.1	61 ± 3	84 ± 5	3.33 ± 0.08	1.88 ± 0.17	43.6%	130.7
#5	0.15	66.5 ± 1.7	89 ± 6	3.26 ± 0.05	1.95 ± 0.06	40.2%	116.7
#6	0.15	72 ± 4	92 ± 7	3.17 ± 0.05	1.98 ± 0.18	37.7%	146.3
#7	0.2	71 ± 3	91 ± 3	3.24 ± 0.04	2.23 ± 0.01	31.1%	42.3
#8	0.2	68 ± 4	113 ± 3	3.15 ± 0.03	1.82 ± 0.01	42.3%	89.9
#9	0.3	77 ± 3	107 ± 2	3.29 ± 0.04	2.1 ± 0.11	36.0%	85.9
#10	0.5	86 ± 4	141 ± 9	3.28 ± 0.12	2.09 ± 0.03	36.3%	133.2
#11	0.6	93 ± 4	165 ± 5	3.15 ± 0.11	2.04 ± 0.07	35.1%	164.4
#12	0.8	96 ± 9	203 ± 6	3.31 ± 0.07	2.21 ± 0.06	33.3%	185.9

[a] All fouling fluids contain additional 42 ppm Ca^{2+} (in the form of $CaCl_2$).
[b] Average values of fouling fluids obtained at both the inlet and outlet of PHE at three different running time and one from the launching tank.
[c] Average values of fouling fluids obtained at the inlet of PHE at three different running time and one from the launching tank.
[d] Average values of fouling fluids obtained at the outlet of PHE at three different running time.
[e] BLG denaturation level = $1-[BLG]_{outlet}/[BLG]_{inlet}$.

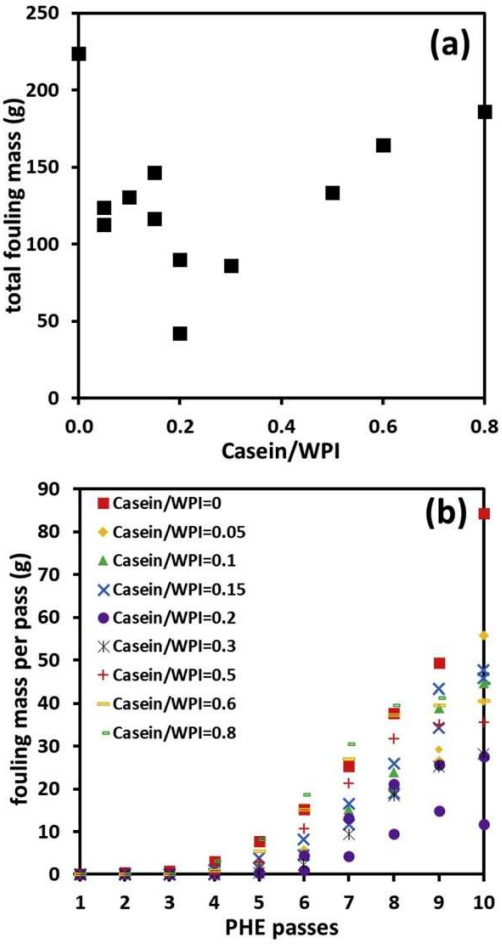

Fig. 4. (a) Effect of Casein/WPI on the total fouling mass inside PHE. (b) Fouling mass distribution in each pass along the PHE at various Casein/WPI ratios. Note that replicated data at Casein/WPI of 0.05, 0.15 and 0.2 were obtained from individual experiments.

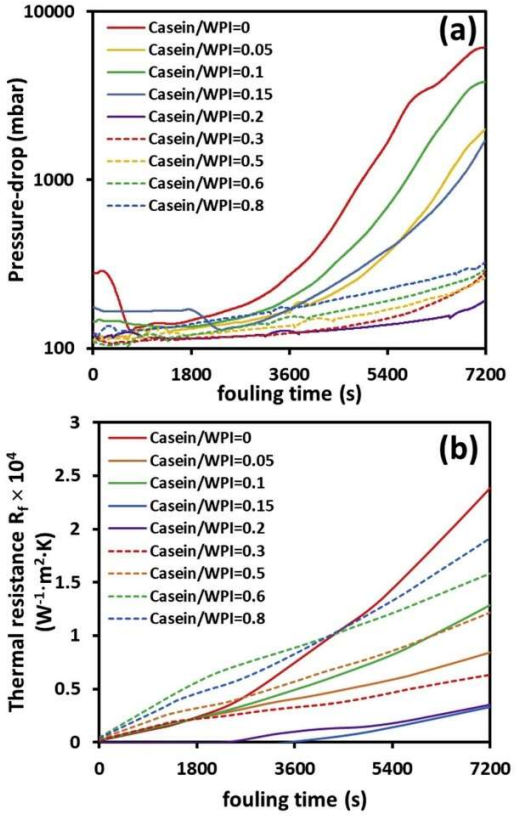

Fig. 5. (a) Pressure-drop and (b) thermal resistance R_f evolution of fouling fluids containing different Casein/WPI within 2 h fouling run. Data at Casein/WPI of 0.05, 0.15 and 0.2 are the average values obtained from two individual experiments. Solid lines represent the results at Casein/WPI≤0.2 and dotted lines refer to that Casein/WPI>0.2. Note that log scale on y-axis on (a).

obtained despite not significantly different values of BLG denaturation level (Fluid#1 compare with Fluid#2 to#12, Table 3). Besides, it is observed that the reduction of fouling mass is not accompanied by less denatured BLG proteins (Fluid#1 to#5, Table 3). On the other hand, the BLG denaturation level is significantly lower at higher Casein/WPI (Fluid#9 to#12, Table 3, although in those conditions more fouling mass was observed.

These facts lead us to conclude that it is hard to correlate the BLG denaturation activity with fouling mass behavior. Thereby, a more systematic study on how casein affects the thermal denaturation kinetics of BLG will be discussed in the following section.

3.3. BLG thermal denaturation kinetics

As mentioned previously, we have observed through heat treatment process within PHE that the denaturation level of BLG is almost unchanged when casein was added to WPI protein (Casein/WPI from 0 to 0.2). Nevertheless, simultaneously a decreasing fouling behavior is observed regarding fouling deposit mass. In order to provide a more exhaustive view on how casein affects the thermal denaturation process of BLG at different temperatures, the thermal denaturation kinetics of BLG were studied at molecular level, using trials at laboratory scale and samples having the same compositions as the fouling fluids applied in the pilot-scale PHE (compositions are shown in Table 1).

Fig. 7(a) is a typical example of the soluble BLG concentration (C_s) evolution with time for a 0.5 wt% WPI solution heat-treated at different holding temperatures (70 °C–90 °C). For a given holding temperature, as expected, C_s decrease with time and for a fixed heating time, C_s decrease sharper with higher holding temperatures. For all the studied conditions, a value of 2 for the reaction order was found to be appropriate. In the literature, the findings for the reaction order for the heat-induced denaturation of BLG commonly varied between 1.5 and 2. For example, several researchers have reported a reaction order of 1.5 (Anema and McKenna, 1996; Dannenberg and Kessler, 1988; Oldfield et al., 1998, 2005), whereas (Hillier and Lyster (1979); Lyster (1970); Manji and Kakuda (1986); Park and Lund (1984)) found that BLG denaturation followed second-order reaction kinetics. This discrepancy among these studies may be explained by the variability of the medium

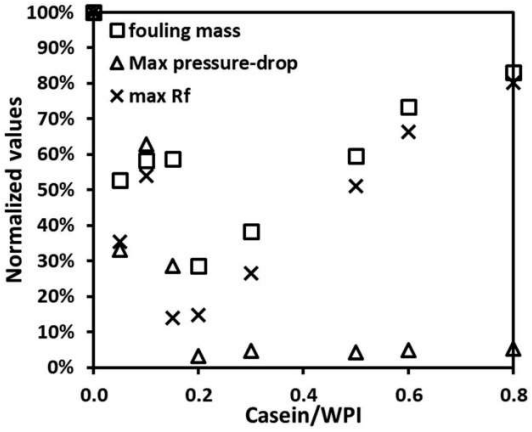

Fig. 6. Effect of Casein/WPI on the normalized total fouling mass and maximum values of pressure-drop and thermal resistance R_f. Notice that the data at Casein/WPI of 0.05, 0.15 and 0.2 are the average values obtained from two individual experiments. Values are normalized by dividing values obtained at Casein/WPI of 0.

of the protein solution (different buffers or simulated milk ultrafiltrate), the heating treatments (direct stream injection or sealed capillary tubes), protein compositions (isolated BLG or whey with or without casein), protein assays or even statistical approaches (Jaskulka et al., 2000).

Giving the best-fit values of k_f, the logarithm can be plotted against the inverse of the holding temperature in the Arrhenius plot as shown in Fig. 7(b). Analysis of Fig. 7(b) shows clearly that, the introduction of both ionic calcium and micellar casein modifies the denaturation rate constant of BLG while maintaining the same shape (broken slope). Inspection of model solutions containing different Casein/WPI ratios reveals a global increase of k_f when Casein/WPI goes up. The positive shift observed in the ordinate axis in Arrhenius plot appears very moderate for Casein/WPI varying from 0 to 0.2, while at high Casein/WPI such as 0.8, the increase of k_f is more remarkable. More precisely, for Casein/WPI ranges from 0 to 0.2 (corresponding to fouling mass decreasing region), increasing Casein/WPI enhances slightly the BLG denaturation constants for the unfolding step, while in the aggregation limited region, the values are overlapping, suggesting a limited effect of casein on the BLG aggregation process. It is difficult to compare our results with those of literature as in this field few kinetic data of dairy solutions exist. Nevertheless, the significant increase of k_f with higher casein content agrees with those reported in Kessler and Beyer (1991), who found increased denaturation constants at elevated casein/whey proportions from sweet whey to skim milk.

Table 4 is another view of the BLG denaturation behavior in the presence of micellar casein, as it summarizes the corresponding activation energies Ea in each denaturation step calculated from the linear regression in the Arrhenius plot. The calculated Ea for unfolding and aggregation for whey protein solutions are 252 and 210 kJ mol^{-1}, respectively. Note that there is no statistical difference between these two values, indicating there is only one dominant reaction at this temperature range, which is unfolding (70–90 °C). These present Ea are comparable to the range of Ea values in skim milk, 265–280 kJ mol^{-1}, reported by (Anema and McKenna (1996); Dannenberg and Kessler (1988); Oldfield et al. (1998)) for temperature lower than 90 °C. The addition of Ca^{2+} resulted in similar values of aggregation Ea at 230 kJ mol^{-1} to the whey protein but a much larger value of 411 kJ mol^{-1} was found for the unfolding Ea. Similar Ea values have been reported for a 0.5 wt% whey protein with an additional 80 ppm Ca^{2+} (Khaldi et al., 2018). These results confirm the opposite binary effect of Ca^{2+} on the BLG unfolding step observed by Petit et al. (2011): on one hand, Ca^{2+} facilitates the BLG unfolding by increasing k_f, while on the other hand, Ca^{2+} limits the process by resulting in larger activation energy.

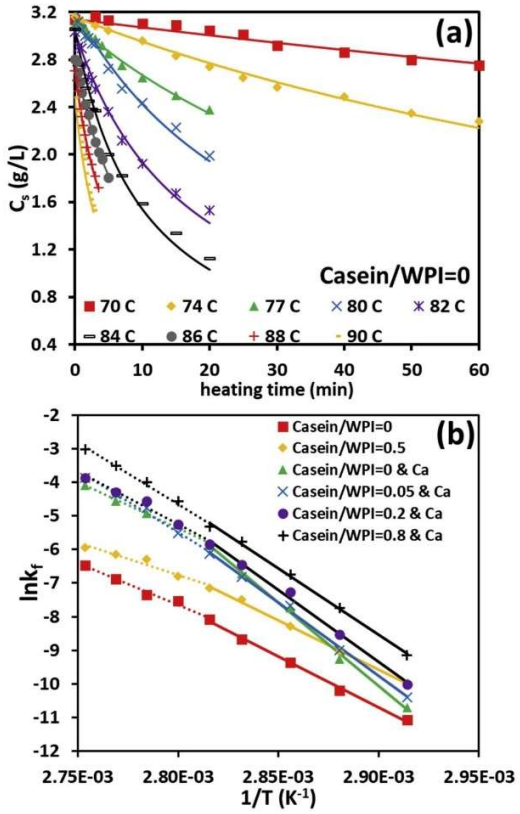

Fig. 7. (a) Evolution of soluble BLG concentration against heating time at various heating temperatures (denote in legend). The solution contains only 0.5 wt% WPI without additional Ca^{2+} (nor casein powder). Solid lines represent best-fit to equation (1) using a reaction order of 2. (b) Arrhenius plot for the BLG denaturation reaction at different protein compositions (shown in Table 1). Solid lines correspond to the linear regressions in the unfolding region while dashed lines refer to the aggregation region.

When analyzing more intimately Table 4 for Casein/WPI solutions (varying from 0 to 0.2), increasing Casein/WPI slightly decreases the activation energy for BLG unfolding. From the thermodynamical point of view, it can be assessed that in the presence of abundant ionic calcium, micellar casein does not represent an obstacle to limit the BLG unfolding. On the contrary, the presence of casein does not seem to strongly affect the activation energy for the aggregation process: a clear trend showing decrease or increase is not obtained for the range of Casein/WPI ratio investigated.

To sum up, from Fig. 7 and Table 4, it appears again that the decreased fouling mass at Casein/WPI from 0 to 0.2 is unlikely to be linked to the minor changes in the BLG denaturation reaction due to introduction of casein. It is more probably due to the change in mineral interactions introduced by casein that affects the origin of fouling build-up. For high Casein/WPI (*e.g.* 0.8), the increase of denaturation of BLG is more significant and this time it is possible that the increase of the

Table 4
Calculated kinetic parameters for BLG denaturation at various Casein/WPI using one-step reaction model. Errors denote standard errors from linear regression.

	Casein/WPI ratios								
	Denaturation parameters	0	0.5	0[a]	0.05[a]	0.2[a]	0.8[a]	4[b]	0[c]
Unfolding	ln (k^0_{unf})	77 ± 3	75.5 ± 1.9	133 ± 5	117 ± 4	114 ± 5	105 ± 3	91.0 ± 10.5	141.8
	Ea_{unf} (kJ/mol)	252 ± 9	243 ± 6	411 ± 13	363 ± 11	354 ± 14	327 ± 9	285.5 ± 30.8	431.6
Aggregation	ln (k^0_{agg})	62 ± 5	47 ± 7	72 ± 5	97 ± 6	83 ± 7	98 ± 6	58.8 ± 5.7	74.1
	Ea_{agg} (kJ/mol)	210 ± 15	160 ± 20	230 ± 15	305 ± 18	260 ± 20	303 ± 16	15.3 ± 1.8	233.5

[a] Solutions contain additional 42 ppm Ca^{2+}.
[b] Kinetic data for skim milk reported by Oldfield et al. (1998), while the unfolding region was recognized between 70 and 90 °C.
[c] Kinetic data for whey proteins reported by Khaldi et al. (2018). Solution contained additional 80 ppm Ca^{2+}.

fouling mass is correlated to an increase of BLG denaturation reaction. This is expected as BLG has a larger opportunity to interact with dissociated casein proteins or κ-casein located at the surface of casein micelle, facilitating the aggregation process (Anema and Li, 2003).

3.4. Element mapping of fouling deposit

In order to further investigate the effect of casein on the fouling, the morphology and chemical composition of the fouling layer was characterized using EPMA. For each fouling experiment, the deposits were collected from two different plates (*i.e.* P_{14} and P_{21}) so as to see the influence of temperature on the build-up of the fouling layer. In each EPMA analysis, Fe (iron), S (sulfur), P (phosphate) and Ca (calcium) were determined in the same area of fouling layer cross-section.

Fig. 8 shows the element mapping results of fouling layers obtained from fouling solutions at four different Casein/WPI ratios collected from P_{14}. Repartition of Ca, P and the characteristic element of the protein (S) of the deposit formed at an average temperature of 78.9 °C without the addition of casein is shown in Fig. 8(a). A compact fouling structure was found in this case with homogenously distributed signals of both Ca and S. The P element inside deposit, however, was negligible as the signal in the deposit is even weaker than the stainless steel substrate. This low P signal can be also found in the fouling deposit formed at low casein concentration (Casein/WPI ≤0.2) or at a higher temperature (84.6 °C, Fig. S6). Moreover, the areas corresponding to Ca and S overlap each other, indicating a co-location of Ca and proteins inside the fouling layer. These results support the idea that in absence of casein and for the range of calcium/BLG ratio investigated (~9), Ca^{2+} acts as binding agents of denatured proteins to co-precipitate upon the hot stainless steel surface (Visser and Jeurnink, 1997). The effect of calcium on the morphology of the fouling layer has been previously reported by Khaldi et al. (2018). These authors demonstrated that the fouling growth mechanism depends and evolve on the increase of Ca/BLG ratios: at low Ca/BLG ratio (2.3), the fouling layer is compact, while in the case of higher Ca/BLG ratio such as 22.9, calcium-based particles act as anchor-points for an arborescent fouling growth.

When casein was present as shown in Fig. 8(b)–(c), heterogenous fouling structures were obtained. In these conditions, the fouling layer was less compact and airier. Moreover, both Ca and S started to be unevenly distributed inside the fouling layer with less intensity of Ca, even though more Ca was present in the fouling fluids (scale bars for each element are identical). Despite this, co-location of Ca and S signals was still apparent in the deposit except at Casein/WPI of 0.8 where P element could no longer be ignored in the fouling layer.

To obtain a deeper insight into the distribution of mineral (Ca, P) in the fouling layer and their interactions with protein (S), overlapped areas of Ca, P and S have been plotted in Fig. 9. It is evidenced that protein favored two types of organization with mineral: either with Ca

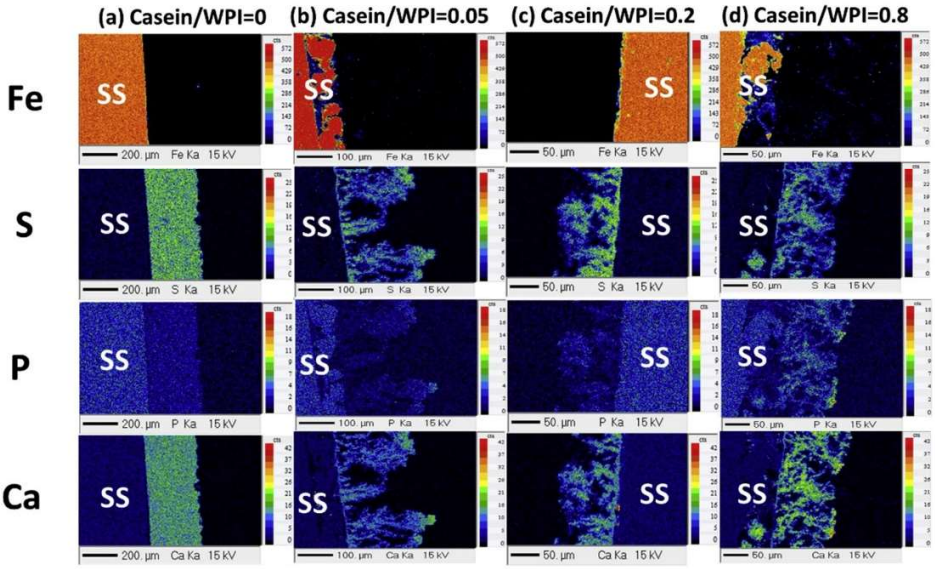

Fig. 8. Fe, S, P and Ca mappings of the cross-section of the fouling layer for fouling fluids at various Casein/WPI ratios of (a) 0 (b) 0.05 (c) 0.2 and (d) 0.8. Deposits were collected from plate P14 with an average temperature of 78.9 °C. SS refers to stainless steel.

alone or with Ca–P as the overlapped area of Ca, P and S (Ca–P–S, green area) differs from that for Ca–S (pink area). Besides, Ca–P–S are more conjugated and act like "tree-trunk" while the Ca–S areas are more scattered around the Ca–P–S. This finding reveals the existence of CaP nanoclusters as Casein/WPI ratio progressively increases, acting as linking agents for fouling build-up. These CaP nanoparticles can be created in the bulk or more possibly introduced from amorphous CaP inside casein micelle (Holt et al., 2013). From this point of view, the increased amount of fouling mass at Casein/WPI from 0.2 to 0.8 could be due to the increased amount of binding agents (CaP). When temperature was higher as shown in Fig. 9(b), the area representing Ca–P–S was relatively smaller but the general trend of CaP surrounding with proteins is consistent. This difference with observation at lower temperature might be caused by the lower level of Ca^{2+} in the bulk (transferred into casein-bound calcium) as Ca^{2+} might also contribute to the formation of CaP nanoclusters.

3.5. SDS-PAGE

To further characterize the fouling deposits, they were analyzed using SDS-PAGE to study the protein composition. Fig. 10 presents the electrophoresis results of eight different fouling deposits formed at four Casein/WPI ratios and collected from two different fouling locations. Pure protein standards were also performed to provide better identification of each protein in the fouling deposits. Results show all fouling deposits are mainly composed of α-casein, β-casein, BLG, and α-la, which is in agreement with those reported for milk fouling (Changani et al., 1997; Jeurnink, 1991). Note that there are few caseins detected even in the condition where casein was not supposed to be present (Casein/WPI of 0). This is probably due to powder elaboration and the difficulty to obtain WPI solutions free of casein during membrane separation process of dairy fractions.

Inspection of casein content in fouling deposits shows a general trend of an increased amount of both α and β-casein in the deposits with higher Casein/WPI ratios. On the other hand, BLG shows similar content inside the deposits for all conditions applied except a significant larger band referring BLG was found for deposits collected from P_{14} at Casein/WPI of 0. Notice that all the fouling deposits were wholly dissolved prior to SDS-PAGE, hence, these results suggest a more proteinaceous deposit formed at a relatively lower temperature with the fouling solution without the addition of casein powder. On the contrary, a more mineral deposit was formed using the same fouling fluid but at a higher temperature condition (*i.e.* P_{21}) as less BLG content was found despite a larger total fouling mass. Notice that the amount of total calcium content for these model fouling fluids is much lower compared to that of normal milk. At this low calcium level, the structure of casein micelle was proposed to swell and individual caseins such as α or β-casein located at the interior of micelle become easier to dissociate into the bulk. Hence, the increased total fouling mass at Casein/WPI from 0.2 to 0.8 might due to the larger participation of α/β-casein or submicelles in the formation of fouling. The absence of κ-casein in the deposit supports the idea that κ-casein prevents BLG from depositing by formation of κ-casein/BLG complexes in the serum phase (Jeurnink and Dekruif, 1995).

4. Conclusions

In this paper, whey protein-based model solutions containing various Casein/WPI ratios were applied in order to study the effect of casein on the fouling behaviors in a pilot-scale PHE applying a pasteurization schedule. It was firstly established that for the WPI powder used, the ionic calcium was a vital element promoting denaturation and fouling mass deposit. Secondly, for the casein-based protein solutions elaborated, the fouling mass dropped dramatically until a minimum value as Casein/WPI increased to 0.2. However, exceeding this critical Casein/WPI ratio, fouling mass increased with elevated Casein/WPI ratios. Casein/WPI ratio also alters the fouling structure: the fouling layer was compact and homogeneous with evenly distributed calcium and proteins when casein was absent, suggesting a binding role of Ca^{2+} between denatured proteins during the build-up of fouling. However, fouling deposits became heterogeneous and less dense: co-located Ca–S elements were scattered around the Ca–P conjugates. This inhomogeneity suggests that CaP nanoclusters, introduced by micellar casein, may act as new linking species between proteins as the fouling grows.

Results from gel electrophoresis revealed a larger participation of α/β-casein in the fouling deposits at higher Casein/WPI conditions. This might explain why fouling mass increased at high Casein/WPI ratios as more dissociated caseins were involved in the formation of fouling. Concerning BLG denaturation, casein seems poorly affect the BLG denaturation process, and it was shown that the fouling behavior was not correlated to the BLG denaturation level at the conditions where fouling mass decreased (Casein/WPI$\leq$0.2) or increased (Casein/WPI>0.2).

It is finally proposed that micellar casein change deeply the calcium balance and the content of CaP nanocluster modifies sharply the interactions which occur between proteins species (BLG, caseins) and mineral element (ionic calcium, Ca–P) thereby affecting the protein denaturation and mineral precipitation.

CRediT authorship contribution statement

Weiji Liu: Conceptualization, Methodology, Investigation, Validation, Writing - original draft. **Xiao Dong Chen:** Supervision, Project administration, Funding acquisition, Writing - review & editing. **Romain Jeantet:** Writing - review & editing, Visualization, Project

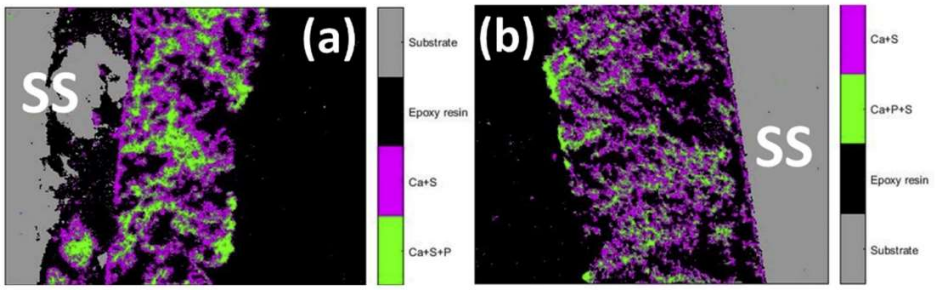

Fig. 9. Overlapped areas of Fe, S, P and Ca elements of the cross-section of the fouling layer. The deposits were collected from the same fouling run using fouling fluid at Casein/WPI of 0.8 but different plates: (a) P_{14} and (b) P_{21} resulting in different fouling temperatures at 78.9 and 84.6 °C, respectively. SS refers to stainless steel. The grey area denotes the SS substrate and the black area refers to the epoxy resin. The area in green corresponds to overlapped signals of Ca, S and P, while the pink area refers to the overlapped Ca and S. (For interpretation of the references to color in this figure legend, the reader is referred to the Web version of this article.)

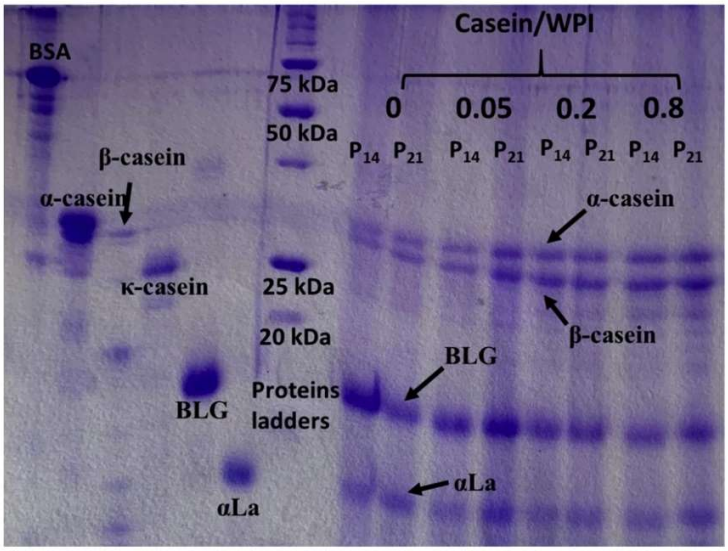

Fig. 10. SDS-PAGE results including pure protein standards, protein ladders, and fouling deposits. Pure proteins are (from left to right) BSA, α-casein, β-casein, κ-casein, BLG, and α-lactalbumin (αLa). Fouling deposits were obtained at different Casein/WPI ratios of 0, 0.05, 0.2 and 0.8; in each condition, deposits were collected from two different plates (P_{14} and P_{21}).

administration. **Christophe André:** Supervision, Software, Writing - review & editing, Project administration. **Severine Bellayer:** Investigation. **Guillaume Delaplace:** Conceptualization, Resources, Writing - review & editing, Supervision, Project administration.

Acknowledgments

This work was supported by project funding from the National Key Research and Development Program of China (International S&T Cooperation Program, ISTCP, Project No. 2016YFE0101200). It was also supported by international joint laboratory FOOD PRINT collaborative project between INRAE, Agrocampus and Soochow University. The authors thank the Hauts-de-France Region and FEDER for their financial support through the ALIBIOTECH program which allows us to buy the HPLC equipment used in these experiments. We also thank INGREDIA who provides us the different types of powders and for the scientific exchange shared with them on this subject through the PROTEINOLAB ANR program.

Appendix A. Supplementary data

Supplementary data to this article can be found online at https://doi.org/10.1016/j.jfoodeng.2020.110175.

Conflict of interest form

- All authors have participated in (a) conception and design, or analysis and interpretation of the data; (b) drafting the article or revising it critically for important intellectual content; and (c) approval of the final version.
- This manuscript has not been submitted to, nor is under review at, another journal or other publishing venue.
- The authors have no affiliation with any organization with a direct or indirect financial interest in the subject matter discussed in the manuscript

References

Anema, S.G., Li, Y., 2003. Association of denatured whey proteins with casein micelles in heated reconstituted skim milk and its effect on casein micelle size. J. Dairy Res. 70 (1), 73–83.
Anema, S.G., McKenna, A.B., 1996. Reaction kinetics of thermal denaturation of whey proteins in heated reconstituted whole milk. J. Agric. Food Chem. 44 (2), 422–428.
Bansal, B., Chen, X.D., 2006. A critical review of milk fouling in heat exchangers. Compr. Rev. Food Sci. Food Saf. 5 (2), 27–33.
Barish, J.A., Goddard, J.M., 2013. Anti-fouling surface modified stainless steel for food processing. Food Bioprod. Process. 91 (4), 352–361.
Bhattacharyya, J., Das, K., 1999. Molecular Chaperone-like Properties of an Unfolded Protein (s-Casein).
Blanpain-Avet, P., Andre, C., Khaldi, M., Bouvier, L., Petit, J., Six, T., Jeantet, R., Croguennec, T., Delaplace, G., 2016. Predicting the distribution of whey protein fouling in a plate heat exchanger using the kinetic parameters of the thermal denaturation reaction of beta-lactoglobulin and the bulk temperature profiles. J. Dairy Sci. 99 (12), 9611–9630.
Boye, J.I., Alli, I., 2000. Thermal denaturation of mixtures of α-lactalbumin and β-lactoglobulin: a differential scanning calorimetric study. Food Res. Int. 33 (8), 673–682.
Broyard, C., Gaucheron, F., 2015. Modifications of structures and functions of caseins: a scientific and technological challenge. Dairy Sci. Technol. 95 (6), 831–862.
Changani, S.D., Belmar-Beiny, M.T., Fryer, P.J., 1997. Engineering and chemical factors associated with fouling and cleaning in milk processing. Exp. Therm. Fluid Sci. 14 (4), 392–406.
Choi, W., Jun, S., Nguyen, L.T., Rungraeng, N., Yi, H., Balasubramanian, S., Puri, V.M., Lee, J., 2013. 3-D milk fouling modeling of plate heat exchangers with different surface finishes using computational fluid dynamics codes. J. Food Process. Eng. 36 (4), 439–449.
Dalgleish, D.G., Corredig, M., 2012. The structure of the casein micelle of milk and its changes during processing. Annual Review of Food Science and Technology 3 (1), 449–467.
Dannenberg, F., Kessler, H.G., 1988. Reaction kinetics of the denaturation of whey proteins in milk. J. Food Sci. 53 (1), 258–263.
Donato, L., Guyomarc'h, F., 2009. Formation and properties of the whey protein/κ-casein complexes in heated skim milk — a review. Dairy Sci. Technol. 89 (1), 3–29.
Farrell Jr., H.M., Jimenez-Flores, R., Bleck, G.T., Brown, E.M., Butler, J.E., Creamer, L.K., Hicks, C.L., Hollar, C.M., Ng-Kwai-Hang, K.F., Swaisgood, H.E., 2004. Nomenclature of the proteins of cows' milk—sixth revision. J. Dairy Sci. 87 (6), 1641–1674.
Fryer, P.J., Christian, G.K., Liu, W., 2006. How hygiene happens: physics and chemistry of cleaning. International Journal of Dairy Technology 59 (2), 76–84.
Grijspeerdt, K., Mortier, L., De Block, J., Van Renterghem, R., 2004. Applications of modelling to optimise ultra high temperature milk heat exchangers with respect to fouling. Food Contr. 15 (2), 117–130.

Guérin, R., Ronse, G., Bouvier, L., Debreyne, P., Delaplace, G., 2007. Structure and rate of growth of whey protein deposit from in situ electrical conductivity during fouling in a plate heat exchanger. Chem. Eng. Sci. 62 (7), 1948–1957.
Haque, Z., Kinsella, J.E., 2009. Interaction between heated κ-casein and β-lactoglobulin: predominance of hydrophobic interactions in the initial stages of complex formation. J. Dairy Res. 55 (1), 67–80.
Hillier, R.M., Lyster, R.L.J., 1979. WHEY-PROTEIN denaturation IN heated milk and cheese whey. J. Dairy Res. 46 (1), 95–102.
Holt, C., Carver, J.A., Ecroyd, H., Thorn, D.C., 2013. Invited review: caseins and the casein micelle: their biological functions, structures, and behavior in foods1. J. Dairy Sci. 96 (10), 6127–6146.
Jang, H.D., Swaisgood, H.E., 1990. Disulfide bond formation between thermally denatured β-lactoglobulin and κ-casein in casein micelles. J. Dairy Sci. 73 (4), 900–904.
Jaskulka, F.J., Smith, D.E., Larntz, K., 2000. Determining the kinetic reaction rate order for the thermal denaturation of β-lactoglobulin using two statistical approaches. Int. Dairy J. 10 (9), 589–595.
Jeurnink, T.J.M., 1991. Effect of proteolysis in milk on fouling in. heat-exchangers Netherlands Milk And Dairy Journal 45 (1), 23–32.
Jeurnink, T.J.M., Dekruif, K.G., 1995. Calcium-concentration in milk in relation to heat stability and fouling. Neth. Milk Dairy J. 49 (2–3), 151–165.
Kehoe, J.J., Wang, L., Morris, E.R., Brodkorb, A., 2011. formation of non-native β-lactoglobulin during heat-induced denaturation. Food Biophys. 6 (4), 487.
Kessler, H.-G., Beyer, H.-J., 1991. Thermal denaturation of whey proteins and its effect in dairy technology. Int. J. Biol. Macromol. 13 (3), 165–173.
Khaldi, M., Blanpain-Avet, P., Guérin, R., Ronse, G., Bouvier, L., André, C., Bornaz, S., Croguennec, T., Jeantet, R., Delaplace, G., 2015. Effect of calcium content and flow regime on whey protein fouling and cleaning in a plate heat exchanger. J. Food Eng. 147, 68–78.
Khaldi, M., Croguennec, T., André, C., Ronse, G., Jimenez, M., Bellayer, S., Blanpain-Avet, P., Bouvier, L., Six, T., Bornaz, S., Jeantet, R., Delaplace, G., 2018. Effect of the calcium/protein molar ratio on β-lactoglobulin denaturation kinetics and fouling phenomena. Int. Dairy J. 78, 1–10.
Lewis, M.J., 2011. The measurement and significance of ionic calcium in milk - a review. International Journal of Dairy Technology 64 (1), 1–13.
Lyster, R.L.J., 1970. The denaturation of α-lactalbumin and β-lactoglobulin in heated milk. J. Dairy Res. 37 (2), 233–243.
Mahdi, Y., Mouheb, A., Oufer, L., 2009. A dynamic model for milk fouling in a plate heat exchanger. Appl. Math. Model. 33 (2), 648–662.
Manji, B., Kakuda, Y., 1986. Thermal denaturation of whey proteins in skim milk. Can. Inst. Food Sci. Technol. J. 19 (4), xxxvii.
Miyawaki, A., Sawano, A., Kogure, T., 2003. Lighting up cells: labelling proteins with fluorophores. Nat. Cell Biol. Suppl, S1–S7.
Morgan, P.E., Treweek, T.M., Lindner, R.A., Price, W.E., Carver, J.A., 2005. Casein proteins as molecular chaperones. J. Agric. Food Chem. 53 (7), 2670–2683.
Oldfield, D.J., Singh, H., Taylor, M.W., 2005. Kinetics of heat-induced whey protein denaturation and aggregation in skim milks with adjusted whey protein concentration. J. Dairy Res. 72 (3), 369–378.
Oldfield, D.J., Singh, H., Taylor, M.W., Pearce, K.N., 1998. Kinetics of denaturation and aggregation of whey proteins in skim milk heated in an ultra-high temperature (UHT) pilot plant. Int. Dairy J. 8 (4), 311–318.
On-Nom, N., Grandison, A.S., Lewis, M.J., 2010. Measurement of ionic calcium, pH, and soluble divalent cations in milk at high temperature. J. Dairy Sci. 93 (2), 515–523.
Park, K.H., Lund, D.B., 1984. Calorimetric study of thermal denaturation of β-lactoglobulin. J. Dairy Sci. 67 (8), 1699–1706.
Patocka, G., Jelen, P., Kalab, M., 1993. Thermostability of skimmilk with modified casein/whey protein content. Int. Dairy J. 3 (1), 35–48.
Paulsson, M., Dejmek, P., 1990. Thermal denaturation of whey proteins in mixtures with caseins studied by differential scanning calorimetry. J. Dairy Sci. 73 (3), 590–600.
Petit, J., Herbig, A.L., Moreau, A., Delaplace, G., 2011. Influence of calcium on β-lactoglobulin denaturation kinetics: implications in unfolding and aggregation mechanisms. J. Dairy Sci. 94 (12), 5794–5810.
Petit, J., Six, T., Moreau, A., Ronse, G., Delaplace, G., 2013. β-lactoglobulin denaturation, aggregation, and fouling in a plate heat exchanger: pilot-scale experiments and dimensional analysis. Chem. Eng. Sci. 101, 432–450.
Price, W.V., 1927. Concerning the addition of calcium chloride to milk for cheese making. J. Dairy Sci. 10 (5), 373–376.
Sadeghinezhad, E., Kazi, S.N., Dahari, M., Safaei, M.R., Sadri, R., Badarudin, A., 2015. A comprehensive review of milk fouling on heated surfaces. Crit. Rev. Food Sci. Nutr. 55 (12), 1724–1743.
Sawyer, W.H., Norton, R.S., Nichol, L.W., McKenzie, G.H., 1971. Thermodenaturation of bovine β-lactoglobulin: kinetics and the introduction of β-structure. Biochim. Biophys. Acta Protein Struct. 243 (1), 19–30.
Shimada, K., Cheftel, J.C., 2002. Sulfhydryl group/disulfide bond interchange reactions during heat-induced gelation of whey protein isolate. J. Agric. Food Chem. 37 (1), 161–168.
Tolkach, A., Kulozik, U., 2007. Reaction kinetic pathway of reversible and irreversible thermal denaturation of beta-lactoglobulin. Lait 87 (4–5), 301–315.
Udabage, P., McKinnon, I.R., Augustin, M.-A., 2000. Mineral and casein equilibria in milk: effects of added salts and calcium-chelating agents. J. Dairy Res. 67 (3), 361–370.
Ven Murthy, M.R., Carrier-Malhotra, L., 1989. Progressive unfolding of the conformational states of transfer RNA and ribosomal 5S RNA by methylene blue binding. In: Vijayalakshmi, M.A., Bertrand, O. (Eds.), Protein-Dye Interactions: Developments and Applications. Springer Netherlands, Dordrecht, pp. 316–330.
Visser, J., Jeurnink, T.J.M., 1997. Fouling of heat exchangers in the dairy industry. Exp. Therm. Fluid Sci. 14 (4), 407–424.
Wijayanti, H.B., Bansal, N., Deeth, H.C., 2014. Stability of whey proteins during thermal processing: a review. Compr. Rev. Food Sci. Food Saf. 13 (6), 1235–1251.
Yong, Y.H., Foegeding, E.A., 2010. Caseins: utilizing molecular chaperone properties to control protein aggregation in foods. J. Agric. Food Chem. 58 (2), 685–693.

ANNEX II-experimental failure on fluorescence

The build-up of a laboratory-scale fouling device (with a transparent cover) was initially designed for monitoring fouling growth *in situ* and in a real-time manner. This can be achieved by performing localized temperature measurements in the microchannel. There are several reported techniques being capable to measure temperature at the microscopic scale (Gosse et al., 2009). They can be divided into three different groups, based on the method of contact between the measuring device and the medium, namely (i) invasive, (ii) semi-invasive and (iii) non-invasive (Childs et al., 2000). The first group mainly consists of micro-thermometer devices. Although rapid and precise, these probes normally require additional fabrications steps and can only perform temperature measurements at discrete points (Aigouy et al., 2011; Barilero et al., 2009). The non-invasive methods comprise the traditional infrared thermometry approach (Roper et al., 2007) or the more advanced spectroscopy methods for probing thermodynamic equilibrium (Kim et al., 2006). Although they directly exploit the bulk properties of the solvent, these techniques lack in reactivity and sensitivity. In semi-invasive methods, a molecular probe that responds to temperature variations is usually introduced to the medium.

Among semi-invasive methods, the fluorescence-based method has received increasing interest due to its high spatial resolution and precision. This approach exploits the temperature dependence of the fluorescence quantum efficiency of the molecular dye. For example, Rhodamine B (RhB) is the most commonly used dye in laser-induced fluorescence thermometry for microfluidic systems (Day and Gu, 2010; Williams et al., 2010). The emission quantum yield of RhB drops with increasing temperature, a consequence of the rotation of diethylamino groups on the xanthene ring (Casey and Quitevis, 1988; Onganer and Quitevis, 1992). Unfortunately, RhB was ruled out in our case as RhB has been reported to have strong dye-protein interactions (Feng et al., 2021). These dye-protein interactions might bring unpredicted disturbance on the fluorescence performance of RhB during fouling growth, and therefore is undesired. Instead of RhB, the dye Pyrromethene 556 (PM556) has been screened to be a suitable fluorescent candidate for our application by showing temperature dependence without external interactions with whey proteins (Feng, 2019).

Figure A1 illustrates the cross-section of the microchannel in the laboratory-scale fouling device with fouling growth. A plate heater providing the constant surface temperature is mounted below

the device. A fluorescence dye is introduced into the fouling solution which acts as a temperature indicator. As aforementioned in section 4.3 (Chapter Four), the fluorescence intensity of the dye solution in a heated channel with a clean surface is described as follows:

$$I_{\text{flu}} = I_0 \hat{A} \varepsilon [Dye] \int_0^{\delta_0} \Phi_\delta d\delta \quad \text{(eq. A1)}$$

where I_0 is the excitation light intensity, $\hat{A}$ is the emitted light collection fraction, Φ_δ refers to the quantum yield of dye at tunnel height of δ, ε is extinction coefficient of the dye at the excited wavelength ($m^2 \cdot mol^{-1}$), δ_0 is the solution thickness (m), and [Dye] is the concentration of the dye ($mol \cdot m^{-3}$). Equation A1 is modified if fouling deposit occurs with a thickness δ_x:

$$I_{\text{flu}} = I_0 \hat{A} \varepsilon [Dye] \int_{\delta_x}^{\delta_0} \Phi_\delta d\delta \quad \text{(eq. A2)}$$

From equations A1-A2, it is clear that, as fouling proceeds, a thicker fouling layer would lead to lower fluorescence intensity of the channel. Meanwhile, the solution temperature might decrease as a consequence of increased thermal resistance, resulting in higher fluorescence intensity. Nevertheless, since the overall fouling is not severe, the impact of deposit thickness on the fluorescence signal could be ignored. In this case, the fluorescence intensity of the channel has a positive correlation to the thermal resistance of the fouling deposit.

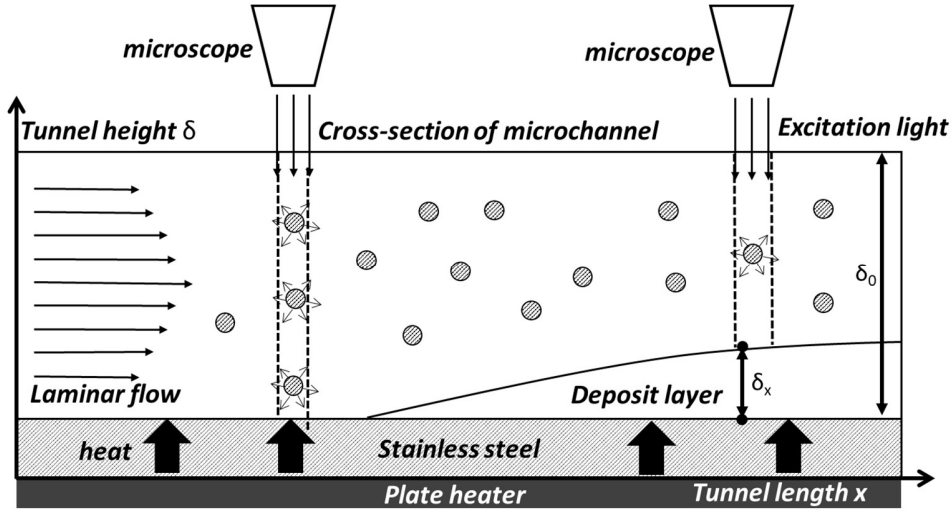

Figure A1. Cross-section of the microchannel in the benchtop fouling rig mounted upon a plate heater during fouling growth. The device was placed under a microscopy system for fluorescence measurement. For comparison, the objective of the microscope is targeted at the location where

the stainless steel surface is clean or with the formation of fouling deposit. Circles denote fluorescent probes homogeneously distributed in the channel, while those with arrows represent excited fluorescent molecules.

Fouling fluids were prepared as described previously in section 4.2.1 (Chapter Four) but with the presence of 10 μM PM556. Additional ionic calcium was achieved by adding $CaCl_2$. Fouling set-up is the same as shown in Figure 4.1(c) in Chapter Four. There are two critical reasons that lead to the failure of this methodology. The first disturbing factor came from the turbidity of the solution after heating. If the solution contains only fluorescence dyes (without proteins), a smoothly decreasing trend of solution fluorescence was obtained as shown in Fig. A2(a). This decreasing fluorescence intensity is a consequence of increasing solution temperature as illustrated in Fig. A2(b). However, when the solution contains both dye and proteins, abnormal data were observed: the fluorescence intensities were much higher at tunnel length larger than ~40 mm even though no fouling has yet started. Because of this, the calculated solution temperatures are much lower which cannot be true. These abnormal data were obtained once the solution temperature is higher than 70 °C (Fig. A2(b)) which is exactly the critical temperature when thermal denaturation and aggregation of proteins starts. The thermal aggregation of proteins in the bulk fluid led to the increased turbidity of the solution and thus disturbed the fluorescence measurement as can be visualized by eyes.

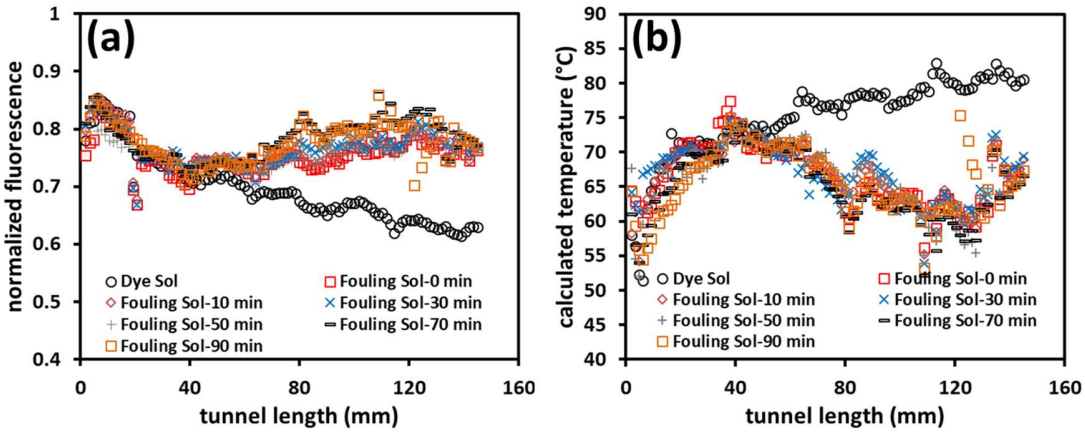

Figure A2. (a) Normalized fluorescence intensity profiles of fouling solutions along the microchannel in the benchtop fouling device at different fouling times. Fouling solutions contain 0.5 wt% WPI, 50 ppm Ca^{2+} as well as 10 μM PM556. Note that data obtained using only dye

solutions were shown for comparison. The corresponding calculated temperatures using fluorescence are shown in (b).

To get rid of the turbidity issue, it was decided to pump separately the dye solutions (10 μM PM556) and the protein solutions (0.5 wt% WPI with added calcium). The protein solution was firstly subjected into the fouling rig; after appropriate running time, MilliQ water was pumped into the channel to remove the fouling solutions before switching to dye solutions. In this way, the fluorescence measurement was performed with the absence of proteins in the bulk fluid. However, problematic results were obtained again as shown in Fig. A3(a). This is due to the formation of fouling deposits formed at the bottom surface of the PMMA cover which dramatically disrupt the fluorescence signals (Fig. A3(b)).

In conclusion, both the turbidity of the heated solution due to thermal aggregation of whey proteins and the occurrence of fouling upon the PMMA cover induce significant interference on the fluorescence measurement of the channel. Solving these issues is very tricky or rather impossible, therefore, it was finally decided to use this methodology solely on temperature mapping of the solution in the microchannel. The calculated temperatures were applied to compare with the CFD simulated values for validation of the numerical model.

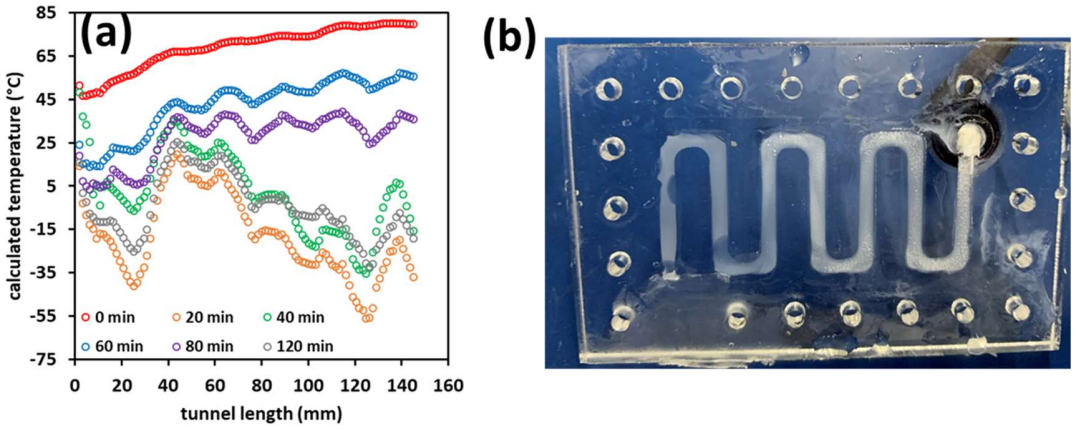

Figure A3. (a) Problematic temperature profiles of PM556 solution in the microchannel of the fouling rig after different fouling times. Note that in this scenario, fouling solution containing only protein and calcium content was firstly subjected into the tunnel. After different running times, the protein solution was replaced by PM556 solution for fluorescence measurement. (b) shows the

picture with fouling occurred at the bottom surface of the PMMA cover (or upper surface of the channel).

ANNEX III-numerical modeling of milk fouling

When the 3D CFD model was built based on the realistic geometry of the benchtop fouling device, a preliminary trial was performed to simulate milk fouling in such a device based on the method adopted from Pan et al. (2019). The main idea is to verify the necessity considering the dynamic evolution of fouling layer structure on the fouling progress (*e.g.* mass/heat transfer and bulk reactions). Briefly, the same governing equations of momentum (eq. 4.4-4.5), heat (eq. 4.6-4.7), mass transfer (eq. 4.15-4.18) and surface reaction (4.19-4.20) as described in Chapter Four were used. The fouling model was used as reported by De Jong (1997) such that the fouling of the milk in the stainless steel surface is wholly caused by the denaturation of BLG during the thermal process. The reaction pathway from native BLG to fouling deposit is shown in Figure A4. In this case, the thermal denaturation reaction of BLG is described using a two-step denaturation scheme (equation 1.22, Chapter One). The corresponding reaction rate constant k_i can be described by the Arrhenius equation:

$$k_i = k_{i0} \exp\left(-\frac{Ea_i}{RT}\right), i = U, A, D \quad \text{(eq. A3)}$$

In order to verify whether or not the fluid mechanic on the fouling removal can be ignored in the laminar regime, the effect of local flow velocity on fouling deposition rate was also considered in the deposition pre-exponential factor k_{D0} as reported by Choi et al. (2013) as:

$$k_{D0} = -407.663 v_L + 5.286 \quad \text{(eq. A4)}$$

where v_L is the longitudinal mean velocity of the fluid above the fouling layer, which varies with the height of the deposit (δ) (see Figure A5). The parameters for BLG denaturation kinetics as well as the deposition reaction are summarized in Table A1. The boundary conditions are similar as described in Chapter Four while parameters for fouling solutions were modified to represent milk as shown in Table A2. The physical properties of milk and fouling deposit layer are summarized in Table A3 while those for solid materials are the same as shown in Table 4.2 (Chapter Four).

The dynamic growth of fouling deposit is achieved using a pseudo-dynamic approach developed by Zhang et al. (2015) as illustrated in Figure A6. In the milk fouling process, the growth rate of fouling layer is much smaller than the rate of mass, heat and momentum transfer and rate of fouling reactions. Therefore, the dynamic growth of fouling layer can be approximated as a set of

sequential steady-state processes taking place in a continuously-changing geometric domain. The procedure taken to implement fouling layer growth is described as follows:

Step 1. At $t_0 = 0$ h, equations governing the mass/heat transfer and thermal denaturation of BLG are solved to obtain the spatial distribution of the fluid velocity, temperature and concentration of different BLG species under the steady-state conditions with the initial geometry (*i.e.* without deposition layer domain). Localized deposition rate r_D can be calculated using the localized variables as mentioned above.

Step 2. At $t_1 = \Delta t$ h, localized fouling deposition thickness is obtained using the localized deposition rate calculated at t_0. Reconstruct the model geometry by updating the fouling layer height. This new model geometry contains a new domain, namely fouling layer domain. Solve the steady-state model again at the current time to obtain an updated localized deposition rate at t_1.

Step 3. At $t_i \leq t_{end}$, update t by $t+\Delta t$. Repeat step 2 to rebuild the geometry and solve the steady-state models until the simulation can be terminated at $t = t_{end}$.

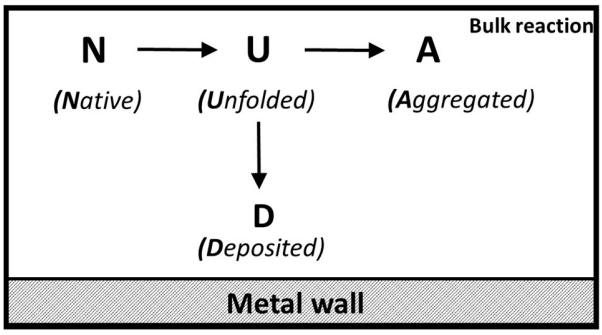

Figure A4. Reaction pathway from native BLG to deposit as reported by De Jong (1996).

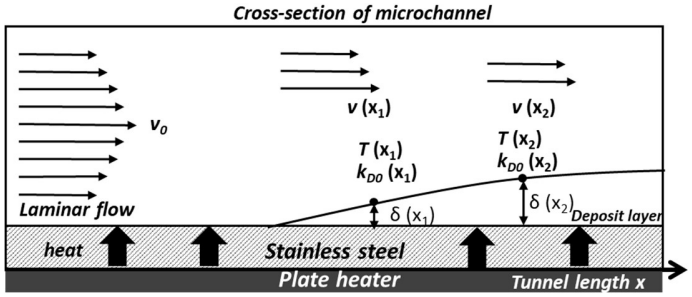

Figure A5. Illustration of the effect of dynamic formation of fouling deposit layer on the localized variables including temperature, velocity and deposition rate.

Table A1. The parameter values of reaction kinetics (Choi et al., 2013; De Jong, 1996)

Reactions	Variables	Values	Units
Unfolding	Ea_U	261.4	$kJ \cdot mol^{-1}$
	k_{U0}	3.368E37	s^{-1}
Aggregation	Ea_A	288.5	$kJ \cdot mol^{-1}$
	k_{A0}	4.568E39	$m^3 \cdot kg^{-1} \cdot s^{-1}$
Deposition	Ea_D	45.1	$kJ \cdot mol^{-1}$
	k_{D0}	$-407.663v+5.286$	s^{-1}

Table A2. Simulation parameters for boundary and initial conditions (Pan et al., 2019)

Variables	Values	Units
Initial solid temperature	25	°C
Inlet fluid temperature, T_{in}	25	°C
Inlet fluid velocity, v_{in}	0.0106	$m \cdot s^{-1}$
Inlet native BLG concentration, Cs_0	5	$kg \cdot m^{-3}$
Inlet unfolded BLG concentration	1×10^{-20}	$kg \cdot m^{-3}$
Inlet aggregated BLG concentration	1×10^{-20}	$kg \cdot m^{-3}$
Bottom surface temperature	87.5	°C
Air temperature	25	°C

Table A3. Physical properties of the fouling fluid and deposit (Choi et al., 2013)

Materials	Variables	Value	Units
Milk	Specific heat, $C_{p,m}$	3831	$J \cdot kg^{-1} \cdot K^{-1}$
	Density, ρ_m	1027	$kg \cdot m^{-3}$
	Thermal conductivity, k_m	0.53	$W \cdot m^{-1} \cdot K^{-1}$
	Viscosity, μ_m	7.75E-3	Pa·s
Deposit	Specific heat, $C_{p,d}$	3400	$J \cdot kg^{-1} \cdot K^{-1}$
	Density, ρ_d	1030	$kg \cdot m^{-3}$
	Thermal conductivity, k_d	0.37	$W \cdot m^{-1} \cdot K^{-1}$

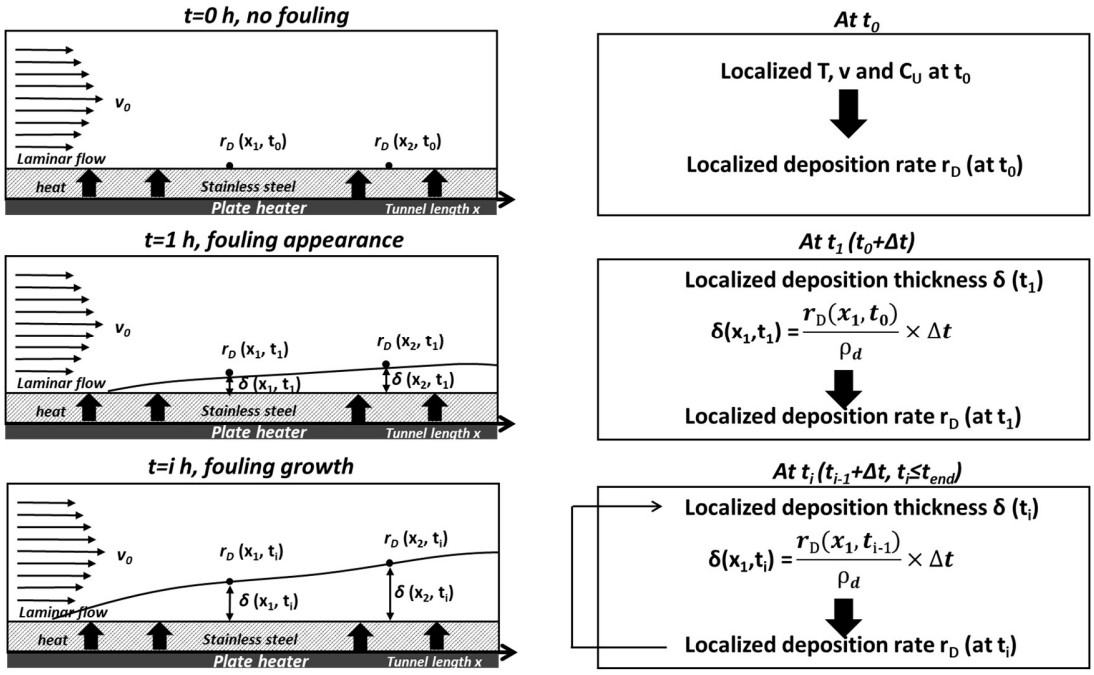

Figure A6. The pseudo-dynamic approach to simulate fouling layer growth.

In this trial, a 10-h fouling process was simulated with a time step of 1 h. CFD provides comprehensive spatial distribution data at any time instant, which can be used to quantify the effect of the dynamic evolution of fouling layer formation on the momentum, heat and mass transfer processes. Figure A7 shows the initial steady-state CFD simulation results in the u-shape microchannel of the benchtop fouling rig, including velocity field, temperature profile and BLG denaturation progress. As expected, the milk fouling is mild and therefore presents little effect on the fluid velocity or the temperature as depicted in Figure A8. At a specific time instant, the fouling rate increases along the tunnel, resulting in the maximum values found at the outlet of the device. This result correlates well with the thermal denaturation progress of BLG as the amount of fouling precursor (*i.e*. unfolded BLG) keeps increasing along the tunnel length (Fig. A7(f)). The maximum fouling deposit thickness is about 0.3 mm located at the outlet of the device after 10-h fouling; this layer compared to the tunnel thickness (3.5 mm) is very thin, therefore, the formation of the deposit layer is not considered to significantly affect the momentum, heat/mass transfer or the bulk reactions. Because of this, it is not surprising to see the milk fouling follows a linear fouling pattern with almost a constant deposition rate as shown in Figure A9. This deposition rate is in the same

magnitude as those performed milk fouling in a simplified 2D heat exchanger (Pan et al., 2019) or whey protein fouling as described in Chapter Four.

In conclusion, in this trial, a 10-h milk fouling was simulated in the custom-built laboratory-scale fouling device using a 3D CFD model. Results confirm that if the fouling is mild, the formation of a thin deposit layer does not lead to a significant change of the momentum, heat/mass transfer or the thermal denaturation of BLG in the bulk fluid. Based on this finding, the dynamic evolution of the deposit layer during fouling was not taken into account as described in Chapter Four.

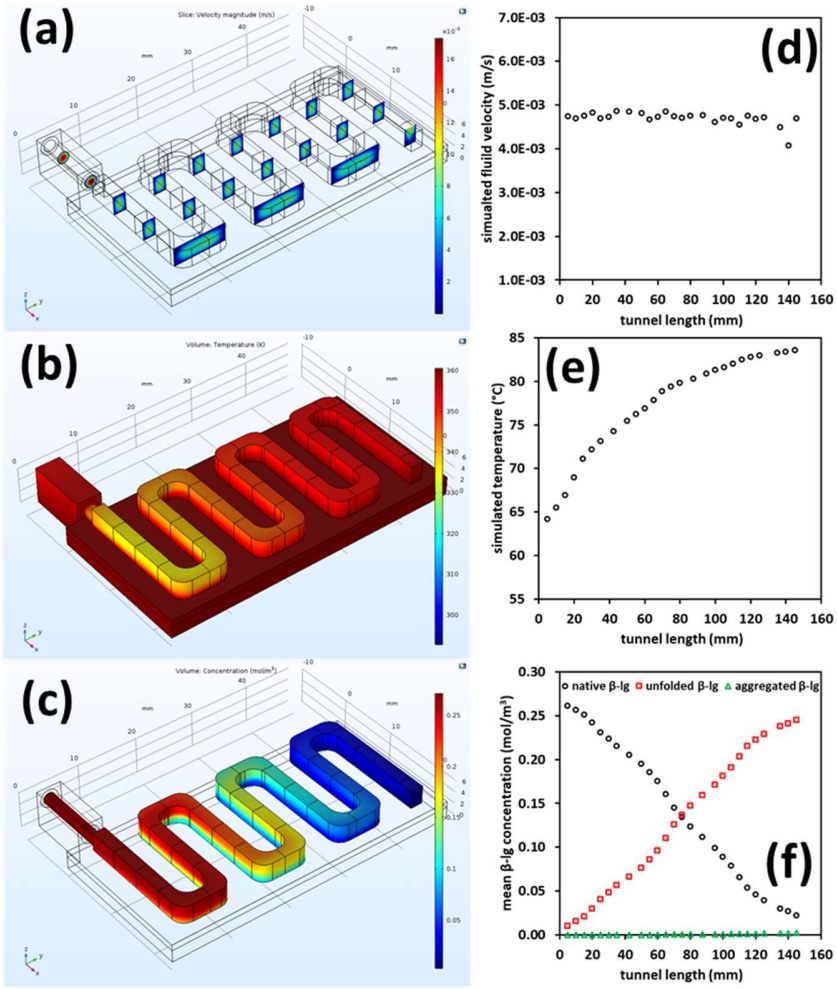

Figure A7. 3D CFD simulation results in the fluid domain at t = 0 h with a clean surface (a) fluid velocity field, (b) temperature field and (c) native BLG concentration distribution. (d) to (f) present corresponding mean values along the u-shape tunnel length.

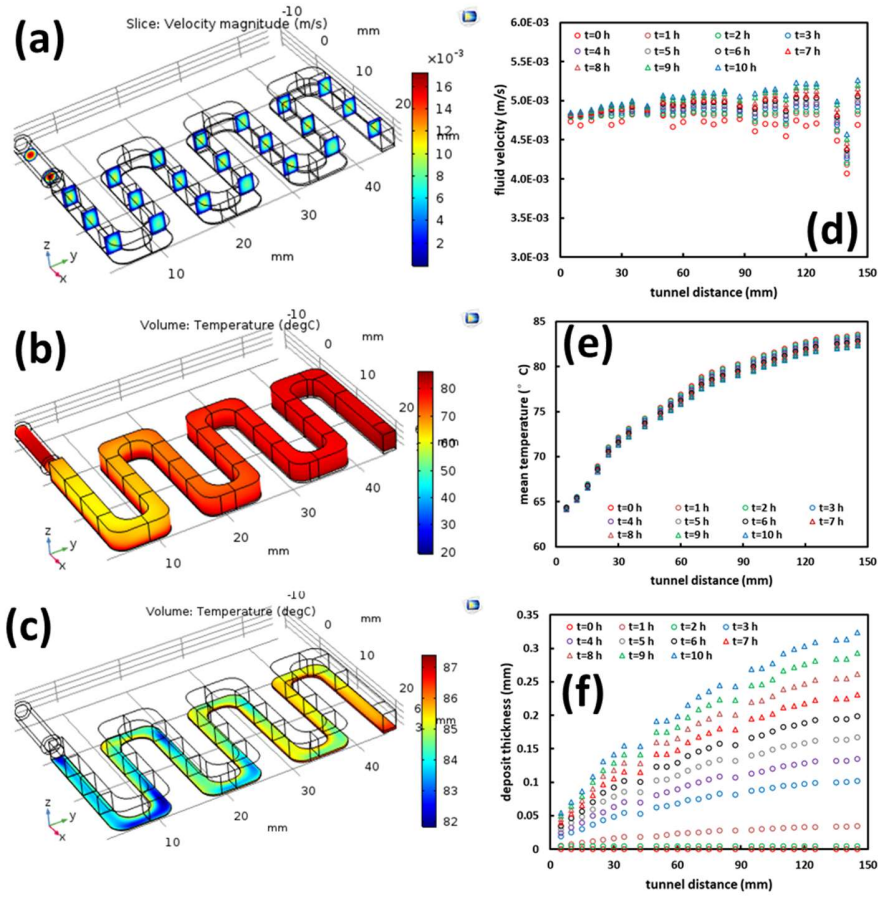

Figure A8. 3D CFD simulation results in the fluid domain at t = 10 h: (a) fluid velocity field, (b) temperature field. Note (c) presents the temperature distribution in the deposit domain at 10 h. (d)-(f) shows the dynamic evolution of velocity, temperature profiles and deposit thickness along the u-shape tunnel during 10 h fouling run.

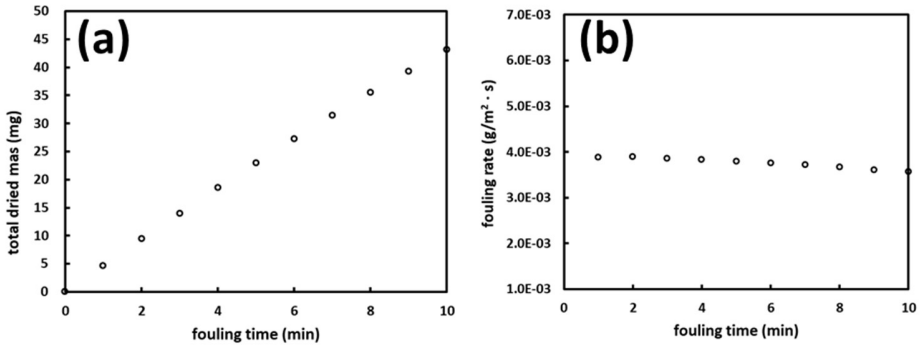

Figure A9. Simulated evolution of (a) total dried deposit mass (b) overall deposition rate in the benchtop fouling device during 10 h fouling run.

ANNEX IV-poor rehydration of casein powder

Blocking issue in the laboratory-scale fouling device

Preliminary experiments tried to use protein powders as similar as possible to those performed in the pilot-scale PHEs. Both whey and casein protein powders were supplied from the same manufacturer (Ingredia, France) which has almost the same characteristics from previous pilot plant experiments. They were Prodiet 90 S for whey protein isolate (WPI) and Promilk 872 B for whole casein powder, respectively. The rehydration protocol used to prepare fouling solution was similar to those used in pilot plant (*i.e*. 50 °C, 1 h). However, this methodology seems insufficient to fully rehydrate the protein powders, especially for caseins which induced blocking issues in the microchannel in the fouling rig as shown in Figure A10. The casein powder might have better rehydration conditions in the pilot-scale experiments due to the big impeller used for mixing or turbulent flow scheme that might help the beak-down of powder aggregates and thus towards better rehydration. This blocking issue undoubtfully disturbed the fouling experiments such that the total fouling mass cannot be accurately measured. Therefore, full rehydration of the casein powder was necessary to ensure a proper experimental condition.

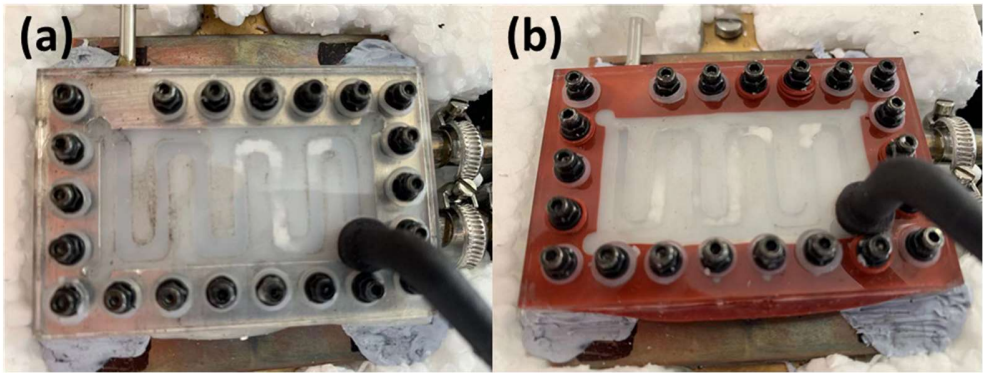

Figure A10. Fouling experiment pictures presenting blocking issues in the microchannel. (a) and (b) shows fouling run performed with fouling solutions at Casein/WPI of 2 and 1, respectively.

Rehydration experiments and particle size measurements

As mentioned in the last section, the rehydration of the protein powder is needed to be improved to ensure a formal experiment. The rehydration experiments were carried out in a 500 mL glass bottle with magnetic stirring at a constant speed set at 350 rpm. The MilliQ water was firstly heated to 50 °C prior to adding whey and casein protein powders to reach different Casein/WPI ratios at 1, 2 and 4, respectively. Concentrated sodium azide stock was added to reach a final concentration of 0.03% (w/v) to prohibit bacterial growth. $CaCl_2$ stock was either added before the rehydration experiment or not to investigate the effect of additional ionic calcium on the rehydration performance of the powder (for fouling experiments, a constant amount of ionic calcium is required to obtain fouling, Chapter Two).

The particle size of the powder was monitored as reported by Jeantet et al. (2010). Briefly, the granulometric distribution of the powder was determined by laser light scattering using a MasterSizer 2000 (Malvern Instruments, Malvern, UK) equipped with a 5 mW He-Ne laser operating at a wavelength of 633 nm. The samples were diluted into the Malvern cell (volume 100 mL) with distilled water in order to reach the correct obscuration (25%). Refractive index taken for solvent, particle and adsorption was 1.33, 1.57 and 0.1, respectively. The granulometric distribution was measured at different rehydration times with minimum time interval at one hour. For comparison purpose, rehydration experiment at Casein/WPI of 2 was also performed in a 3.5 L jacketed glass vessel equipped with a vertically and centrally mounted six-pitched blade impeller as reported in (Richard et al., 2013).

Rehydration results: effect of protein batch and addition of Ca^{2+}

Since fouling solutions contain both whey and casein, all the solutions used for rehydration tests were reconstituted from both whey and casein powders. However, only casein powders have rehydration difficulties as whey protein podwer can always be rehydrated completely. Poor and often inconsistent rehydration properties of micellar casein-dominant powder, specifically their low dispersibility and solubility has remained a significant challenge in the manufacturing of dairy protein-based food and beverages (McSweeney et al., 2021). For many applications, rehydration of a powder in water or an aqueous medium is required for complete expression of protein functionality. If the powder is not completely dissolved, engineering issues could occur as

previously observed in our case, blocking the microchannel in the laboratory-scale fouling device. The spray drying process and the storage strategies are all responsible for the development of insolubility. According to Anema et al. (2006b), a network of casein micelles at the powder particle surface was formed by non-covalent bonding (*e.g.* hydrophobic interactions and/or hydrogen bonds). These interactions increase with increasing storage time and temperature which might accelerate this deterioration in powder solubility.

A clear view of rehydration can be seen in Figure A11 by showing particle size evolution during rehydration process. Two different combinations of whey and casein powders were compared for their rehydration performances. Fig. A11(a)-(c) present results that reconstituted from the protein powders that cause blocking issues in the microchannel as shown in Fig. A10. It is evident that even after 92 h rehydration, large powder aggregates remained despite different processing strategies (*e.g.* in a 3.5 L jacketed glass vessel equipped with a six-pitched blade impeller, Fig. A11(c)). Fig. A11(d)-(f) show better rehydration performance when using another casein powder; the peaks corresponding to large particles are significantly smaller especially after 1 h rehydration. However, it seems that rehydration profiles after 24 h when using powders that caused blocking issues are not so different from those obtained for new powders.

These poor rehydration performances could be attributed to the addition of calcium ions. In fact, the rehydration of the casein powder was significantly improved (as far as disappearance of large powder aggregates and appearance of individual casein micelle) without supplementary $CaCl_2$ as shown in Fig. A11 (g)-(i). It can be seen that after 24 rehydration, all powders were almost completely dissolved particularly at high casein concentrations (Casein/WPI = 4 corresponding to 2 wt% casein, Fig. A11(i)). This negative effect of adding a low amount of calcium on the micellar casein rehydration has also been observed in (Hussain et al., 2011), where two rehydration behaviors were established depending on the calcium concentration. When additional $CaCl_2$ was low (< 0.75%), the wetting and swelling stage of the powder particle was longer, and the total rehydration was not complete even after 500 min. But if the calcium concentration was augmented (*e.g.* from 1.5% to 12%), the swelling stage was not observed and the total rehydration time was significantly shortened. For this reason, to prepare fouling solutions, calcium was only added after complete rehydration of the powder has been achieved (*i.e.* after 24 h rehydration at 50 °C).

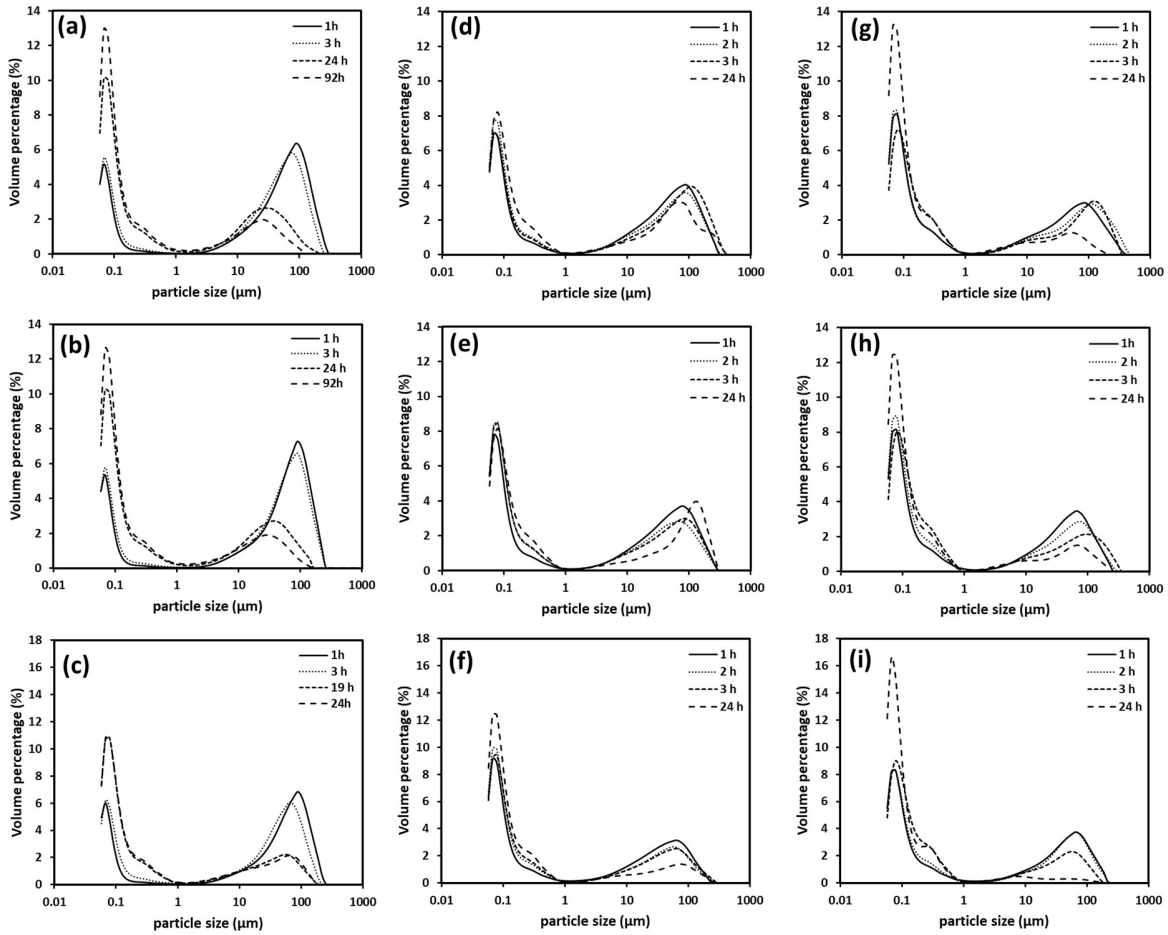

Figure A11. Particle size evolutions of different fouling solutions at various Casein/WPI ratios using two different whey and casein powders. (a)-(c) used protein powders that caused blocking issues in the microchannel (*i.e*. Prodiet 90 S for whey protein isolate (WPI) and Promilk 872 B for whole casein powder, respectively) at Casein/WPI ratios of (a) 1 and (b) 2. Notice that (c) was carried out in a 3.5 L jacketed glass vessel at Casein/WPI of 2. While (d)-(i) used new powders from the same supplier (*i.e*. Promilk 852 FB1 for WPI and Promilk 852 B for casein) at Casein/WPI ratios of (d, g) 1, (e, h) 2 and (f, i) 4. (d)-(f) present results when a constant amount of $CaCl_2$ was added before the rehydration while no calcium was added in (g)-(i).

Thesis outputs

Oral presentations:

Liu W., Chen X.D, Jeantet R., André C., Bellayer S., Delaplace G., Role of casein on the heat-induced denaturation of whey proteins and subsequent fouling in plate heat exchanger. *Proceeding of Heat Exchanger Fouling & Cleaning conference XIII 2019*, Jozefow, Poland, June 2-7.

Liu W., Role of casein on the heat-induced denaturation of whey proteins and its fouling behavior in a pilot-scale plate heat exchanger, *FOODPRINT SYMPOSIUM*, Soochow University, Suzhou, China, October 8th, 2019.

Liu W., Chen X.D., Jeantet R., André C., Delaplace G., Effect of calcium on the thermal denaturation of whey proteins and subsequent fouling in a bench-scale fouling rig: A 3D computational modeling, *Fouling and Cleaning in Food Processing conference 2022*, Lille, France, March 28-30, 2022.

Liu W., Chen X.D., Jeantet R., André C., Delaplace G., Role of casein micelle on the whey protein fouling in a bench-scale fouling device. *Heat Exchanger & Cleaning conference XIV-2022*, Wagrain, Austria, June 5-10, 2022.

Publications:

Liu, W., Chen, X. D., Jeantet, R., André, C., Bellayer, S., Delaplace, G. (2021). Effect of casein/whey ratio on the thermal denaturation of whey proteins and subsequent fouling in a plate heat exchanger. *Journal of Food Engineering*, 289, 110175. IF: 5.354, Q1.

Liu, W., Feng Y., Delaplace, G., André, C., Chen, X.D. (2022). Effect of calcium on the reversible and irreversible thermal denaturation pathway of β-lactoglobulin. Food Hydrocolloids (Under revision).

Liu, W., Feng, Y., Pan, F., Jeantet, R., André, C., Chen, X.D., Delaplace, G., (2022). Effect of calcium on the thermal denaturation of whey proteins and subsequent fouling in a benchtop fouling device: an experimental and numerical approach. *Food and Bioproducts Processing* (Special Issue) (Submitted).

Liu, W., Feng, Y., Jeantet, R., André, C., Chen, X.D., Delaplace, G., (2022). Effect of casein on the thermal denaturation of whey proteins and subsequent fouling in a laboratory-scale fouling device (Manuscript).

Unrelated publications:

Feng, Y., **Liu, W**., Mercadé-Prieto, R., Chen, X. D. (2021). Dye-protein interactions between Rhodamine B and whey proteins that affect the photoproperties of the dye. *Journal of Photochemistry and Photobiology A: Chemistry*, 408, 113092. IF: 4.291. Q1.

Sun, R., **Liu, W**., Kirk, T.V., & Chen, X. D. (2021). A Dual-labeled fluorescent probe for visualization of enzyme activity in simulated food digestion system. *Food Chemistry* (Submitted).

Role of casein micelle on the thermal denaturation of whey protein solutions and fouling mechanisms

Abstract: The present work is a contribution to better understanding the influence of casein micelles on the fouling of serum whey protein solutions. In particular, various experimental and numerical approaches have been carried out both at laboratory and pilot scales (meanwhile new tools have been progressively set up, namely, development of a new kinetic model describing thermal denaturation of β-lactoglobulin (BLG), installation of an experimental laboratory-scale fouling device and a 3D kinetic-based fouling model simulating deposit formation onto surface into the microchannel) to describe denaturation phenomena and better understand the role of casein micelle and calcium in whey fouling mechanisms. Precisely, the addition of casein micelle was found to significantly suppress whey protein fouling both in pilot-scale plate heat exchanger (PHE) as well as the benchtop fouling device. It was concluded that casein micelle acts as a natural calcium chelator during thermal processing and therefore mitigates whey protein fouling. This fouling mitigation effect of casein micelle retains especially at pH conditions close to neutral, resulting in more dissociated caseins into the serum phase which might be sufficient to perform chaperone-like functions. In parallel, a novel kinetic model was developed to describe the thermal denaturation pathway of BLG, providing a mathematical interpretation on the break-slope behavior in the Arrhenius plot and also detailed thermodynamic information for both unfolding and aggregation processes. Results revealed a protective role of calcium ions on the unfolding of BLG while facilitating the aggregation step. On the contrary, caseins favor the unfolding process while limiting the aggregation. This model was subsequently utilized to numerically simulate the denaturation of BLG in the microchannel in the benchtop device. By coupling CFD in a 3D environment, results suggested that fouling is built in such a pattern that for each BLG deposited, one calcium ion is involved.

Keywords: Thermal denaturation; Whey protein fouling; Casein micelle; Kinetic model; CFD modeling

Rôle de la micelle de caséine sur la dénaturation thermique des solutions de protéines de lactosérum et les mécanismes d'encrassement

Résumé: Le présent travail est une contribution à une meilleure compréhension de l'influence des micelles de caséine sur l'encrassement des solutions sériques de protéines de lactosérum. En particulier, diverses approches expérimentales et numériques ont été menées à l'échelle laboratoire et pilote (de nouveaux outils ont été progressivement mis en place, notamment, le développement d'un nouveau modèle cinétique décrivant la dénaturation thermique de la β-lactoglobuline (BLG), la mise au point d'un dispositif experimental d'encrassement à l'échelle du laboratoire et une simulation numérique 3D des d'encrassements de surface) pour décrire les phénomènes de dénaturation et mieux comprendre le rôle des micelles de caséine et du calcium dans les mécanismes d'encrassement des solutions sériques. Précisément, l'ajout de micelle de caséine s'est avéré supprimer de manière significative l'encrassement des protéines de lactosérum à la fois dans l'échangeur de chaleur à plaques à l'échelle pilote (PHE) ainsi que dans le dispositif d'encrassement de paillasse. Il a été conclu que la micelle de caséine agit comme un chélateur de calcium naturel pendant le traitement thermique et atténue donc l'encrassement des protéines de lactosérum. Cet effet d'atténuation de l'encrassement de la micelle de caséine se conserve en particulier dans des conditions de pH proches de la neutralité, ce qui entraîne des caséines plus dissociées dans la phase sérique qui pourraient être suffisantes pour remplir des fonctions de type chaperon. En parallèle, un nouveau modèle cinétique a été développé pour décrire le schéma de dénaturation thermique du BLG, fournissant une interprétation mathématique du comportement de rupture de pente dans le diagramme d'Arrhenius ainsi que des informations thermodynamiques détaillées pour les processus de dépliement et d'agrégation. Les résultats ont révélé un rôle protecteur des ions calcium sur le dépliement du BLG tout en facilitant l'étape d'agrégation. Au contraire, les caséines favorisent le processus de déploiement de BLG tout en limitant l'agrégation. Ce modèle a ensuite été utilisé pour simuler numériquement la dénaturation de BLG dans le microcanal de l'appareil de paillasse. En couplant la CFD dans un environnement 3D, les résultats suggèrent que l'encrassement est construit selon un schéma tel que pour chaque BLG déposé, un ion calcium est impliqué.

Mots clés: Dénaturation thermique; Encrassement des protéines de lactosérum; Micelle de caséine; Modèle cinétique; Simulation CFD